MODELLING OF AN ELECTRO-HYDRAULIC SERVO-SYSTEM

by

K. CANEY B.Sc.(Eng.)

A thesis submitted for the degree of Master of Engineering Science in the Faculty of Engineering, University of Tasmania, Hobart.

- FEBRUARY 1977 -

I agree that, if this thesis is accepted for a degree of the University of Tasmania, it may then be available for loan and copying.

(signed) .....K Caney.....

date ...22/3/77.

TO AVRIL

who moves freely in the worlds of Tolstoy and
C.S. Lewis but is ill at ease in the Orwellian
world of computers.

* * * * * * *

- - I said 'I am resolved to be wise', but this wisdom was beyond my grasp - whatever has happened lies beyond our grasp, deep down, deeper than man can fathom. - -

This alone have I found, that God, when he made man, made him straightforward, but man invents endless subtleties of his own. - -

New English Bible

Ecclesiastes chapter 7.

ACKNOWLEDGEMENTS

The work described in this thesis was carried out at the University of Tasmania during 1975 and 1976 under the supervision of Mr. E. Middleton whose guidance and encouragement is deeply appreciated.

The author also wishes to thank the Department of Science & Technology of the TCAE., Hobart, for use of college computing facilities.

Thanks are also due to the following persons:-

- Mr. A. Christian, Mr. B. Stiberc, Mr. T. McNicol of the University of Tasmania for their assistance with experimental work.

- Mr. K.N. Toms formerly Head of the Department of Surveying, TCAE., Hobart, for strongly encouraging the author to undertake this work.

- Mrs. A. Williams for typing this thesis.

- Staff at the University and TCAE for their interest, advice and assistance.

I hereby declare that, except as stated herein, this thesis contains no material which has been accepted for the award of any other degree or diploma in any University, and that to the best of my knowledge or belief, this thesis contains no copy or paraphrase of material previously published or written by any other person except when due reference is made in the text of the thesis.

K Caney

K.Caney.

CONTENTS

CHAPTER 8 - GENERAL CONCLUSIONS

PREFACE

Many theoretical models have been developed to simulate the performance of hydraulic control components and systems, but all are limited by the assumptions involved and uncertain factors associated with practical hydraulic systems.

Authors warn that seal compressibility, inertia of oil in lines, mounting compliance, structural damping, friction and cavitation may each be significant in appropriate circumstances,and even the bulk modulus of hydraulic oil is difficult to predict for practical systems. Manufacturers may reject theoretically predictable designs because they are prone to wear or expensive to make. For instance sharp edged orifices are replaced by the short tube type and oil passages consist of drilled holes intersecting at angles with frequent changes in section.

The prospect of obtaining a comprehensive mathematical model applicable to manufactured components is therefore remote due to the uncertainties and complexities involved but the designer will require models and methods of solution sufficient for his purposes which are to obtain a reasonable prediction of performance at the design stage.

'Design' may mean the design of a hydraulic circuit component, such a pump or relief valve, or may involve matching standard components to form a system. Ideally the designer requires a model of each system component which can be assembled with all other component models to form a comprehensive system model which can be solved mathematically. If linear models are possible an exact final solution may be feasible but when non-linearities are present, a digital simulation of the model giving a time response to defined inputs may be the only practical method of solution and, inevitably, the designer is involved with the problems of computation.

Computers are now commonplace in design offices. Small computer installations offer a hands-on facility which is flexible and versatile whilst large installations offer enormous capacity and capability but are often remotely located with inflexible management procedures ill-suited to the trial and error design techniques often required for component design optimisation. As such,a small computer may offer the most efficient means of solving these design problems.

This thesis is concerned with methods of modelling hydraulic components and systems with particular emphasis placed on the use of a small computer installation for digital simulation of models, and for other tasks related to laboratory testing of actual systems. The basic aims are to obtain physical and mathematical models of an existing electro-hydraulic two-stage servo-valve, to use a small computer to predict open and closed-loop responses, to obtain actual system responses for comparison with those predicted, and to examine non-linearities encountered.

The thesis is set out in the order in which the work was done. Initially similar work was studied and extended after which the servo-valve was measured and tests were conducted to ascertain physical constants required for the system equations. A linear model was then simulated and actual system responses were obtained for comparison with the first linear model. After this the linear model was slightly modified and other more advanced non-linear models developed.

NOTATION

Symbols are defined when they are introduced and a comprehensive table of symbols appears in section A3.1 in Appendix 3. Commonly used servo-valve variables are defined on figure (2-4) in chapter 2.

SUMMARY OF CONTENTS

CHAPTER I

The extension of previous work by others to prove methods of formulating system equations, digital simulation techniques, and methods of building system block diagrams.

CHAPTER 2

A physical description of the servo-valve and ram unit used in subsequent theoretical and experimental work.

CHAPTER 3

The determination of servo-valve physical constants required for the small perturbation technique.

CHAPTER 4

Development of the first linear model and block diagram and prediction of servo-valve response.

CHAPTER 5

A description of measurement and control techniques developed to obtain servo-valve open and closed-loop responses.

CHAPTER 6

A description and analysis of servo-valve open and closed-loop responses and a study of system models to ascertain the system order of best fit with measured responses.

CHAPTER 7

A review of the first linear model in the light of experimental results, a revision of that model, the development of a non-linear model and an investigation of non-linear parameter coupling.

CHAPTER 8

A modified flapper valve design and a general purpose digital model is proposed and general conclusions are drawn from the entire thesis.

CHAPTER I

1.1 Introduction

The analysis of electro-hydraulic control systems involves four principal activities as follows:

1. Development of physical models that adequately describe the mechanical behaviour of the hardware involved.
2. Description of the physical model in mathematical terms.
3. Analysis of the mathematical model to qualitatively describe the performance of the system.
4. Instrumentation of the actual system and comparison of the actual performance with that predicted by the mathematical model.

While the primary aim of the work described in this thesis was the detailed study of the Vickers SR-4 servo valve and cylinder, in the first instance it was decided to make a critical survey of the published work of Green and Crossley[1] in which the stability of three-way and four-way servo pumps was compared. This work was later commented upon by Dransfield, et al [2], with a view to pointing out the advantage of power-port modelling as a convenient means of arriving at mathematical formulations, and recommending the use of an advanced digital situation language such as Mimic to solve the mathematical model. Having no convenient access to Mimic it was decided to develop computing techniques suited to a small computing facility.

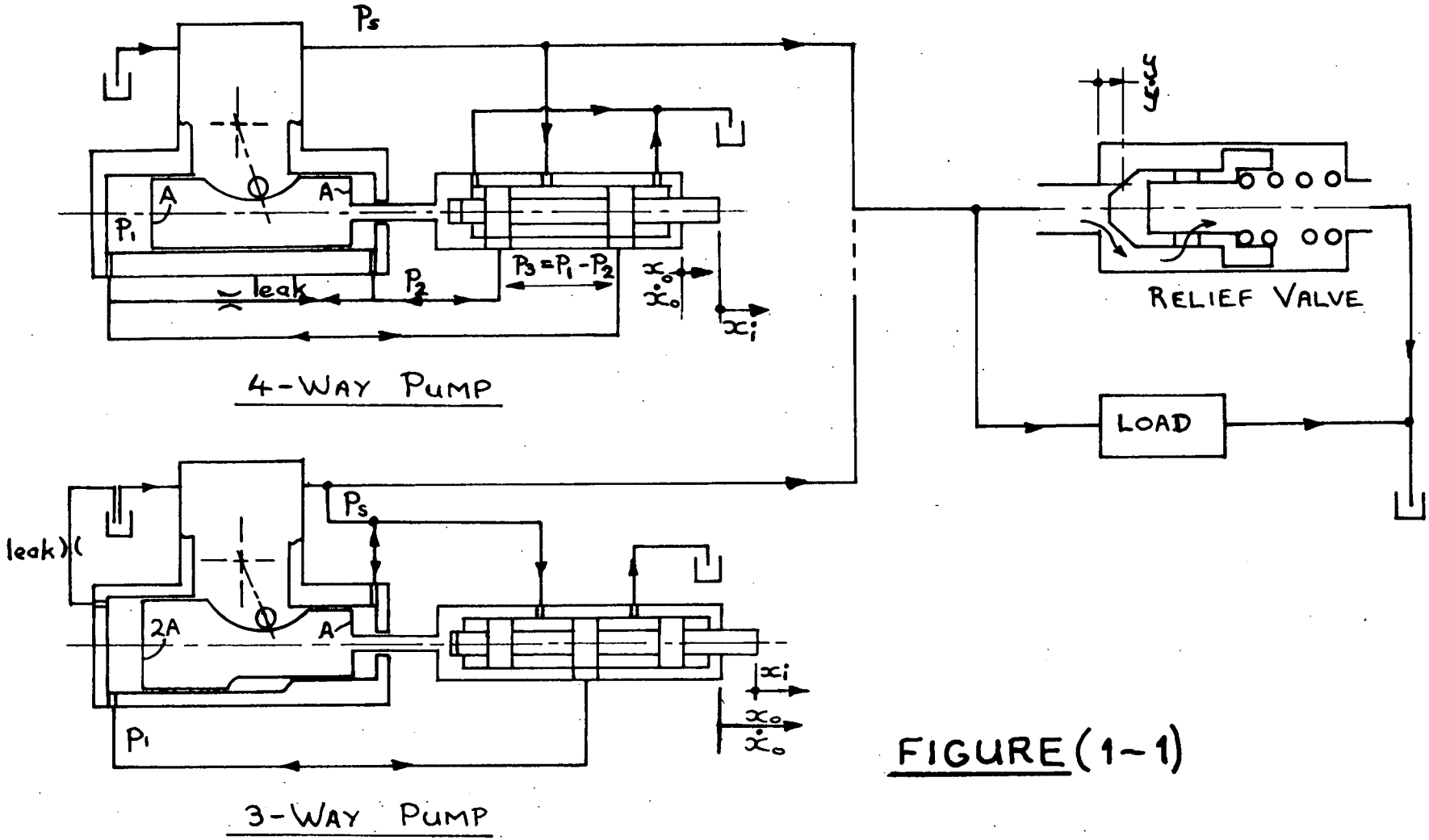

FIGURE (1-1)

SCHEMATIC SYSTEM DIAGRAMS

1.2 Physical Model of Servo-pumps

Physical models of the two pumps described by Green and Crossley are shown schematically in Figure (1-1). Ideally the objective of both systems is to provide a constant pump discharge rate at constant delivery pressure and independant of load characteristics. Alternative servo-valves of the three-way and four-way variety together with a direct acting poppet type relief valve installed across the load comprise the system.

The figure shows the four-way valve to be external for clarity, but in practice the valve is inside the pump and integral with the swash-plate jacking cylinder. External spool input signals (x_i) are transmitted by an external spool shaft which passes through the pump casing. Oil at supply pressure is transferred to the spool centre via a series of drilled holes and is metered to either end of the jacking cylinder by one of two variable orifices, while return flow to the tank is metered by the other. Effective pressure areas at opposite ends of the jacking cylinder are equal and forces generated by the differential pressure p_3 are used to position the swash plate.

The three-way valve is internal with the jacking cylinder but has only one variable orifice which meters flow to and from the large diameter jack end at pressure p_1. Jacking cylinder effective pressure areas are in the ratio 2:1 with the smaller area held at supply pressure so that the jack positioning force is generated by variation in p_1 and p_s.

The nature of the load is not defined but in practice it is likely to be a hydraulic ram or motor operated by a control valve. Green and Crossley assumed the load to be absent in their work.

1.3 Mathematical Models of Servo-pumps

Sets of simultaneous ordinary differential equations are conveniently solved by standard computing techniques when expressed in state-variable form as follows:

$$\dot{X} = A\,X + B\,U$$
$$Y = C\,X + D\,U \qquad \ldots\ldots\ldots \quad (1)$$

where X = vector of state-variable

Y = vector of outputs

U = vector of inputs

A,B,C,D = system matrices relative to the above variable vectors.

1.3.1 Selection of state-variables

For each moveable mass in the system, the velocity and position are the corresponding state variables while for each separate volume of oil the instantaneous pressure is a convenient state variable.

However, it is important to realize that a system can be over-defined in such a way that the matrix A is singular and no solution possible. This situation arises in the case of the four-way servo which has three separate entrapped oil masses subject to pressures p_1, p_2 and p_s making these logical choices as state variables. However the relationship between p_1 and p_2 is not time dependant being given by $p_3 = p_1 - p_2$ and the load pressure p_3 is thus used as the state variable reducing the apparent order of the system by one.

1.3.2 Selection of Inputs

The valve spool position (x_i) is an obvious choice but in practice this is used as a setting and system disturbances are load induced such as a ram force or motor torque. Such inputs give rise to a load flow q_L which changes system equilibrium. In the absence of a specified load, q_L is used as an input on the grounds that it can be independantly specified and imposed on the system.

1.3.3 Equations for four-way Servo-pump

Appendix 1 details the original equations derived by Green and Crossley (including some minor corrections) and these reduce to state-variable form as follows

$$\{\dot{X}\} = [A]\{X\} + [B]\{U\}$$

where

$$\{X\}^T = \{x_o \; \dot{x}_o \; y \; \dot{y} \; P_3 \; P_s\}$$

$$\{U\}^T = \{x_i \; q_L\}$$

For extension i.e. when $x_i > x_o$

$$[A]_{ext} = \begin{bmatrix} 0 & 1 & 0 & 0 & 0 & 0 \\ 0 & 0 & 0 & 0 & \frac{A}{M} & -\frac{\emptyset}{M} \\ 0 & 0 & 0 & 1 & 0 & 0 \\ 0 & 0 & -\frac{k'}{m} & -\frac{C}{M} & 0 & \frac{a'}{m} \\ \frac{-4C_E N}{V_4} & \frac{-4AN}{V_4} & 0 & 0 & \frac{-4C_{L4} N}{V_4} & 0 \\ \frac{N(K+C_E)}{v} & 0 & \frac{-NC_y}{v} & \frac{-Na}{v} & 0 & \frac{-NC_R}{v} \end{bmatrix}$$

For retraction when $x_i < x_o$ the matrix is identical except for one entry in the first column of the bottom row which becomes:

$$a_{61} = \frac{N}{v}(K - C_E)$$

$$[B]_{ext} = \begin{bmatrix} 0 & 0 \\ 0 & 0 \\ 0 & 0 \\ 0 & 0 \\ \frac{4C_E N}{V_4} & 0 \\ -\frac{C_E N}{v} & -\frac{N}{v} \end{bmatrix}$$

For retraction when $x_i < x_o$ the B matrix is identical except for the first entry in the sixth row which becomes:

$$b_{61} = + \frac{C_E N}{v}$$

1.3.4 Equations for three-way Servo-pump

Similarly, Appendix 2 shows the state variable equations to be

$$\{\dot{X}\}^T = \{x_o \; \dot{x}_o \; y \; \dot{y} \; p_1 \; p_s\}$$

$$\{U\}^T = \{x_i \; q_L\}$$

For extension when $x_i > x_o$

$$[A]_{ext} = \begin{bmatrix} 0 & 1 & 0 & 0 & 0 & 0 \\ 0 & 0 & 0 & 0 & \frac{2A}{M} & -\frac{(\emptyset+A)}{M} \\ 0 & 0 & 0 & 1 & 0 & 0 \\ 0 & 0 & -\frac{k'}{m} & -\frac{C}{m} & 0 & \frac{a'}{m} \\ -\frac{NC_E}{V_3} & -\frac{2AN}{V_3} & 0 & 0 & -\frac{NC_{L3}}{V_3} & 0 \\ \frac{N(K+C_E)}{v} & \frac{NA}{v} & -\frac{C_y N}{v} & -\frac{aN}{v} & 0 & -\frac{NC_R}{v} \end{bmatrix}$$

When $x_i < x_o$ the bottom row alters and the first entry becomes

$$a_{61} = \frac{NK}{v}$$

$$[B]_{ext} = \begin{bmatrix} 0 & 0 \\ 0 & 0 \\ 0 & 0 \\ 0 & 0 \\ \frac{C_E N}{V_3} & 0 \\ -\frac{C_E N}{v} & -\frac{N}{v} \end{bmatrix} \quad \text{and} \quad [B]_{ret} = \begin{bmatrix} 0 & 0 \\ 0 & 0 \\ 0 & 0 \\ 0 & 0 \\ \frac{C_E N}{V_3} & 0 \\ 0 & -\frac{N}{v} \end{bmatrix}$$

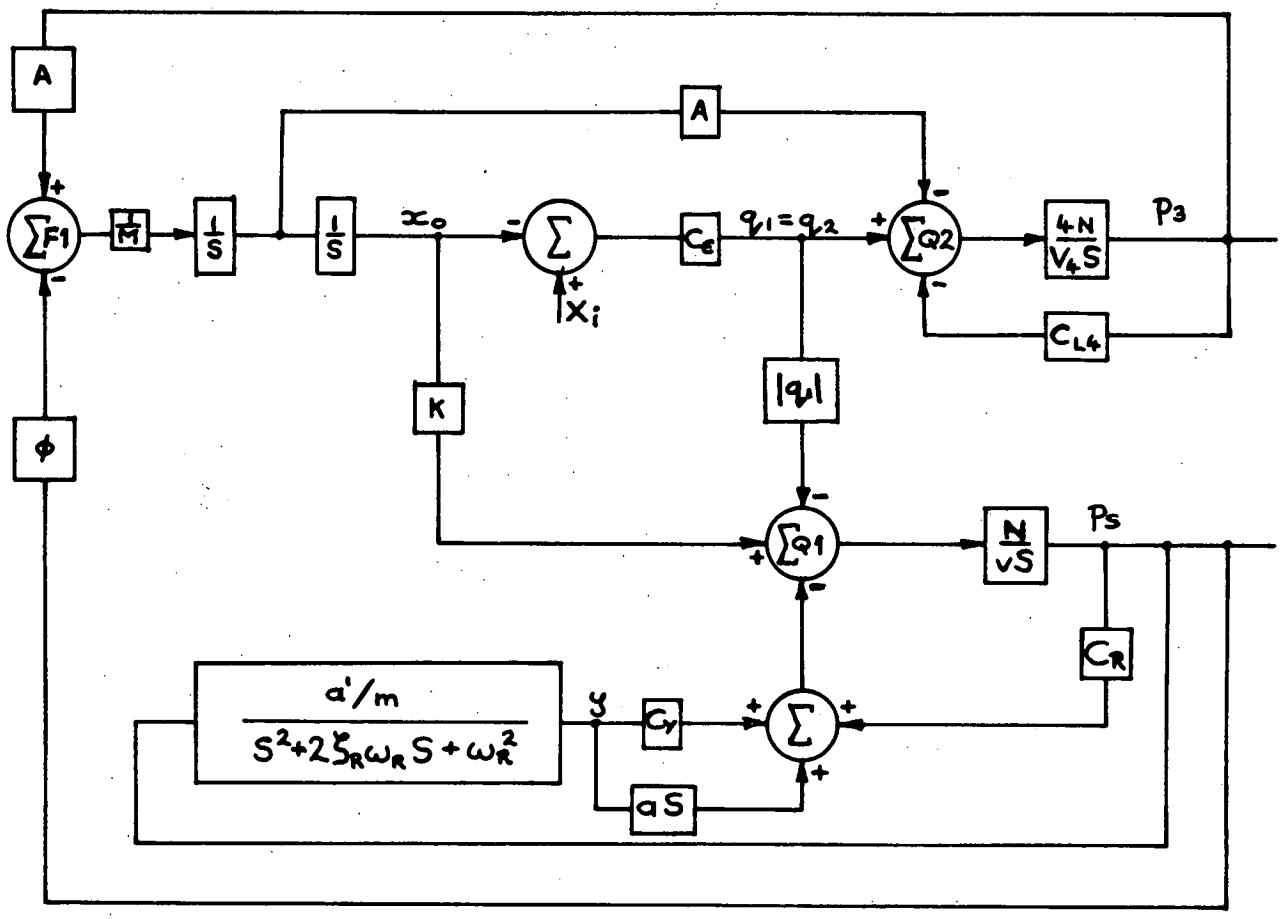

SYSTEM BLOCK DIAGRAM
FIGURE (1-2)

1.3.5 System block diagram for four-way Servo-pump

Figure (1-2) depicts the functional relationship expressed by the system equations in section 1.3.3 and is a modified form of that given by Dransfield, et al[2]. It is useful because it relates the physical system by the mathematical model in a readily understood and simple manner.

The servo-pump comprises three basic component systems, namely the swash-plate and pump, the four-way valve and jack together with the relief valve. All these are linked by a flow summing junction $\Sigma Q1$ at pressure p_s, which forms the main oil reservoir from which the load flow is taken. In addition, the swash plate and jacking systems are linked by a force summing junction $\Sigma F1$ with feedback from p_3 and p_s, and also a flow summing junction $\Sigma Q2$ at pressure p_3.

At first sight it may appear surprising that no direct feedback exists between p_s and the control valve flow q, but C_p for this valve was assumed to be zero for small disturbances. Figure (1-2) is very comprehensive but also cumbersome for general use when matching standard system components. It is more useful to represent each component by transfer functions which can be used to build a system block diagram from the physical system. Since separate components are physically linked by pipes which act as flow summing junctions at points of common pressure it is suggested that each standard component be represented by transfer functions relating pressure, flow and input terms.

For an unspecified load the systems shown in Fig. (1-1) have two inputs (q_L, x_i) and three basic components namely; pump, relief valve, and delivery line volume. q_L is preferred as a system input under these conditions for two reasons. Firstly x_i is a set point on the pump during operation and q_L is likely to be the input which physically causes a disturbance. Secondly the equations given in 1.3.3and 1.3.4are non-linear a..., whereas a linear system can be disturbed at any point when assessing stability, it is better to use the physical disturbance as an input to a non-linear system because response curves so obtained will have most practical significance.

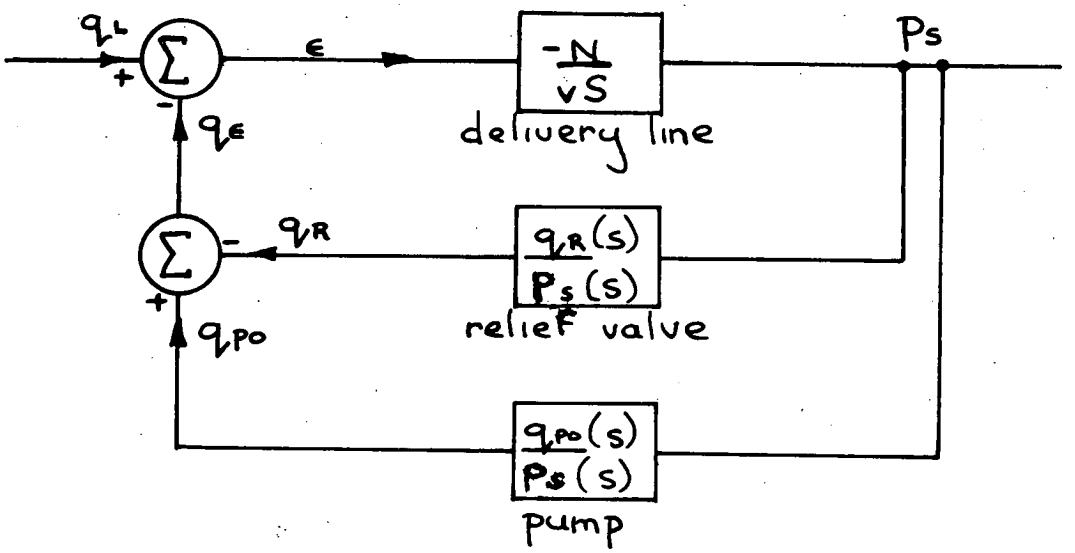

SYSTEM BLOCK DIAGRAM
FIGURE (1-3)

The pump is therefore represented by a transfer function, relating output flow q_{po} to output pressure p_s where $q_{po} = q_p - q_l$ and the relief valve is similarly represented by a transfer function relating q_R to p_S. The delivery line acts a flow summing junction and has a transfer function relating the error flow q_E to pressure p_S and q_L is the only input.

Figure (1-3) becomes a system block diagram specifically intended for investigating system stability when the load is undefined and Appendix 3 shows the transfer functions just discussed to be given by;

$$\frac{q_{po}(S)}{p_s(S)} = - \frac{(\frac{V_4 S^2}{4N} + C_{L4})(K \pm C_E)\frac{\emptyset}{M}}{(S^2(\frac{V_4 S^2}{4N} + C_{L4}) - (C_E + AS)\frac{A}{M})}$$

where the numerator contains the term $(K - C_E)$ when $x_1 > x_o$ and $(K + C_E)$ when $x_i < x_o$.

$$\frac{q_R(S)}{p_s(S)} = \frac{(C_y + aS)\frac{a'}{m} + C_R(S^2 + 2\zeta_R\omega_R S + \omega_R^2)}{(S^2 + 2\zeta_R\omega_R S + \omega_R^2)}$$

$$\frac{p_{s(S)}}{q_E(S)} = \frac{-N}{vS}$$

Using the above transfer functions, the simple and effective system block diagram depicted in Figure (1-3) is easily developed where q_L is an input flow and q_E is the negative feed-back error. Additional system components can be readily added using the flow summing junctions.

For example the load may consist of a ram producing an instantaneous force F_L.

The system input now becomes F_L and the load flow equation is

$$q_L = \frac{A_1(p_s A_1 - F_L)}{(m_1 S + C_1)}$$

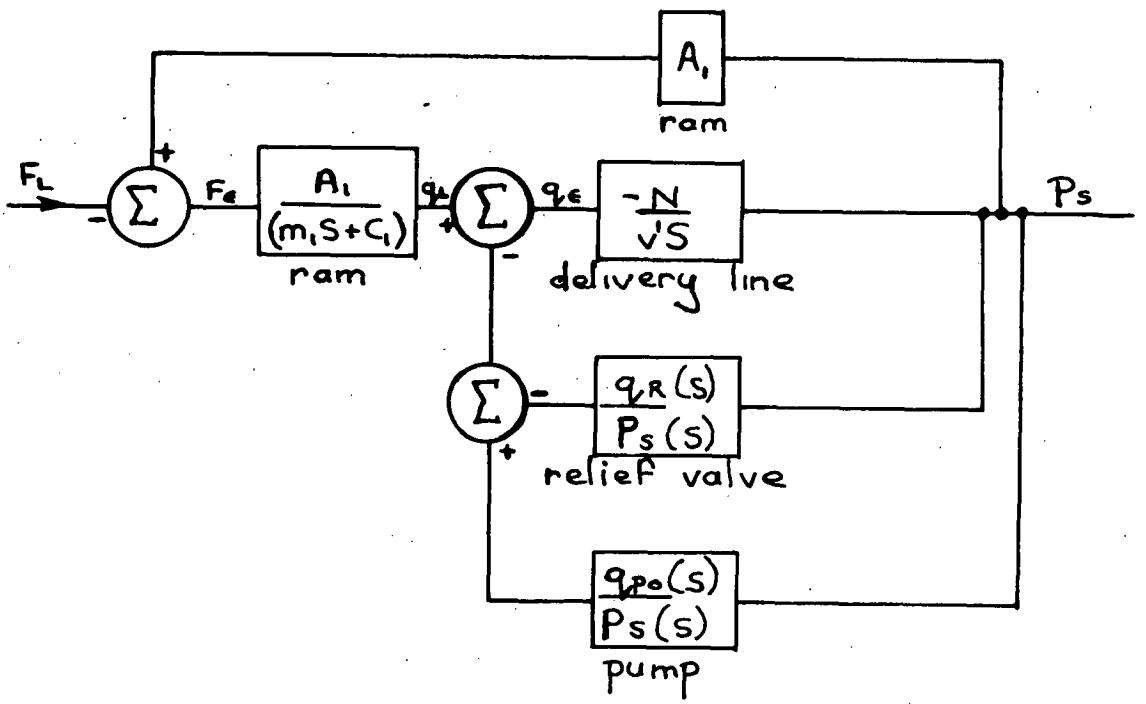

EXTENDED BLOCK DIAGRAM
FIGURE (1-4)

where A_1 is the ram area, m_1 is the ram mass and C_1 is the ram damping constant. The ram increases delivery line volume from v to v'.

Fig. (1-4) becomes the system block diagram.

This suggests that the best systems approach would be to specify all circuit components by transfer functions relating flow, pressure and inputs so that block diagrams of the above type can be readily constructed.

This approach differs from that of Green & Crossley[1] who set up transfer functions relating supply pressure p_1 to jack displacement x_o and while their technique appears to be accurate for the closed loop condition it does not offer a systematic approach which is easily expanded to include other system components.

1.4 Analysis of Mathematical Models

Two commonly used methods of analysis of equations of motion are discussed below.

1.4.1 Steady-state response

The steady-state response technique is applicable to linear systems and entails the calculation of the gain and phase shift over a given frequency range, the dual concepts of phase and gain margin being used to yield a universally qualitative assessment of the stability or otherwise of the system.

Many inherently non-linear systems can be studied by this method by considering small perturbations about some known equilibrium positions. Non-linear expressions such as $\sqrt{(p_1 - p_2)}$ are replaced by a first order truncation of a Taylor series but expressions such as $|q_1|$ present difficulties that are not easy to overcome.

An error found in Reference (1) is of the latter type and renders the steady-state performance described there open to some question as to its validity and meaning. Equations (43) and (48a) of that work both contain a term q_1 representing the flow from the system delivery to servo valve, and is therefore positive at all times. Hence the q_1 of equation (43) is the same as q_1 in equation (13) during extension when $x_o < x_i$, but when $x_o > x_i$ the valve performs a switching operation in which the valve supply is redirected to flow q_2. Hence q_1 in equation (43) should read $|q_1|$.

A similar condition is applied to q_1 in equation (48a) which has the value $q_1 = C_E(x_i - x_o)$ when $x_i > x_o$ and is zero otherwise.

It is the opinion of this author, that more realistic response characteristics are obtained by the analysis of the step perturbations.

1.4.2 Step Perturbation Technique

The step perturbation technique is applicable to both linear and non-linear systems, and entails calculation of the time response of all system variables to a step input, or alternatively, to an imposed initial condition on one or more state-variables. System stability is assessed by consideration of the A matrix eigenvalues and by inspection of the time response data to obtain information about rise time percentage overshoot and settling time for each variable, so that qualitative assessment procedures can be applied.

The response of a system can often be approximated to an 'equivalent second order system' and stability is then measured qualitatively in terms of equivalent damping ratio and natural frequency.

1.5 Four-way Servo-system Approximate steady-state Response

The steady-state response technique is not applicable to the non-linear equations given in Appendix 1 unless approximations are made. It is assumed that non-linear effects are small and that the matrices A and B for extension only govern the system equations.

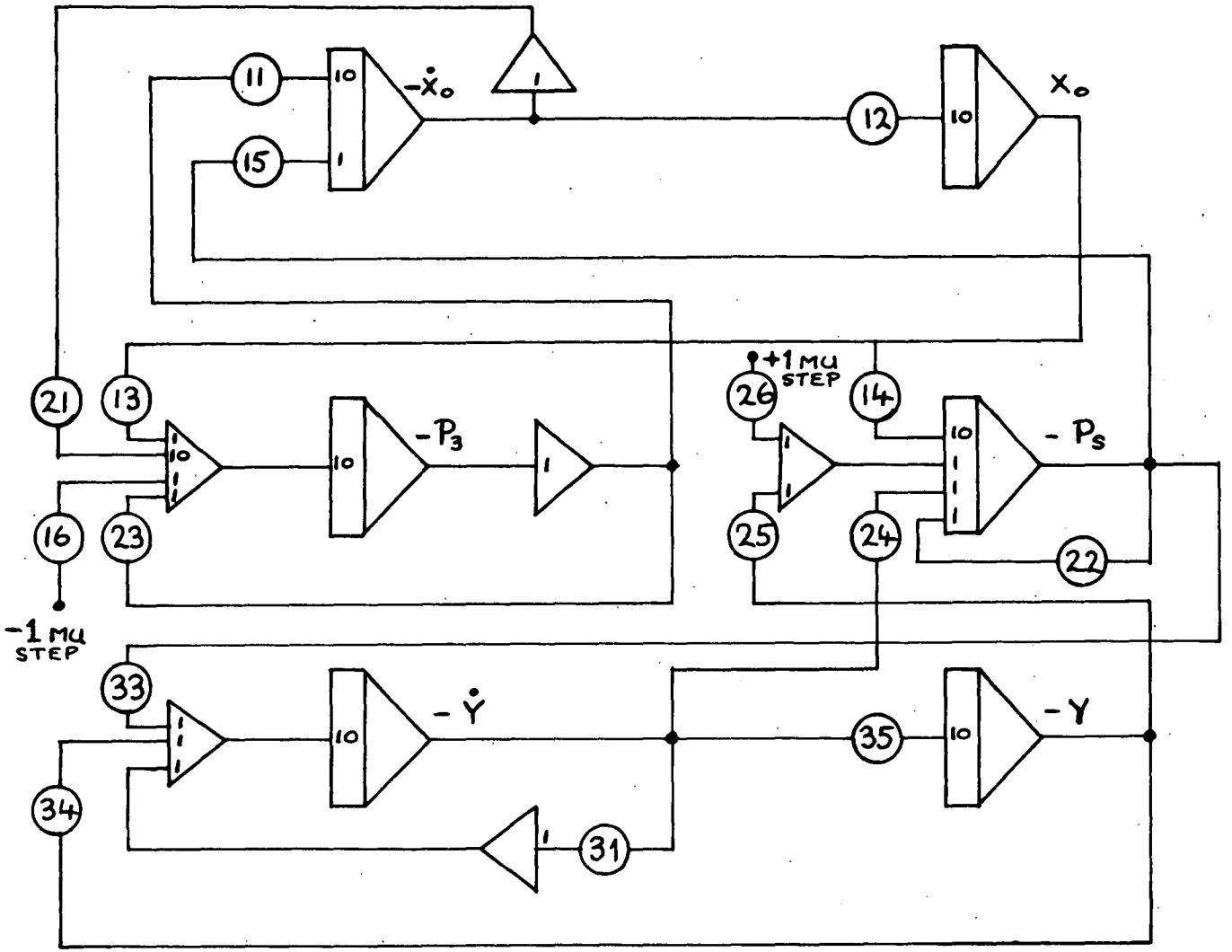

ANALOG SIMULATION DIAGRAM

Pot Settings No.	Value
11	·160
12	·333
13	·601
14	·031
15	·019
16	·601
21	·100
22	·021
23	·560
24	·009
25	·352
26	·294
31	·388
32	—
33	·781
34	·639
35	·120

FIGURE(1-5)

Using the analog scaled equations a frequency response is obtained by the method detailed in Appendix 1.

1.6 Analog Simulation

Analog simulation of the four-way servo-system is done using a step input x_i and using approximate equations which assume the A and B matrices to be those for extension only.

Appendix 1 sets out the technique for time and amplitude scaling of the equations and fig. (1-5) shows the analog circuit built directly from the scaled equations without further reference to the physical system.

Amplitude scaling problems are reduced by this method because $\{\dot{X}\}$ variables are not explicitly generated and amplitude estimates are required for state-variables only.

Simultaneous step inputs of plus and minus one machine unit are applied to pots 16 and 26 respectively, and state-variable responses are measured at the integrator outputs suitably time scaled for a plotter.

1.7 Digital Simulation

Two algorithms are evaluated below:

1.7.1 First Algorith

This is taken from reference (3)

If $X = A X + B U$ and if $U(t) = U(KT)$

for $K T \leqslant t < \overline{K + 1}\ T$ then

$$X(\overline{K + 1}\ T) = \emptyset\ (T)\ X\ (KT) + \Delta\ (T)\ U(KT)$$

where

$$\emptyset(T) = \varepsilon^{AT} + I + A\ T + \frac{A^2T^2}{2!} + \ldots\ldots$$

and

$$\Delta(T) = \varepsilon^{AT} \int_o^T -\varepsilon^{At}\ dt\ B$$

$$= [I\ T + \frac{AT^2}{2!} + \frac{A^2T^3}{3!} \ldots\ldots]B$$

Program 1 uses this algorithm and gives verified results. It is particularly suitable for linear problems where A and B are matrices of constants only so that $\emptyset(T)$ and $\Delta(T)$ are evaluated once only.

Numerical instabilities due to truncation errors occur if the time interval T is too large, and the present equations require T to be about 10^{-4} secs or less. Convergence of the series is rapid and it is sufficient to sum about ten terms.

The non-linearities encountered require that $\Delta(T)$ and $\emptyset(T)$ be evaluated twice and the alternative values are used where $x_o > x_i$ and when $x_o < x_i$.

This algorithm is therefore suited to the present equations but is too slow when non-linearities requiring repetitive calculation of $\Delta(T)$ and $\emptyset(T)$ are encountered.

1.7.2 Second Algorithm

Programs 2 and 3 use the Runge-Kutta method as described by reference (4).

This algorithm is susceptible to truncation errors and induced instabilities of several types, but these are overcome by using sufficiently small time intervals.

The maximum allowable time interval is given by $2.7/\max|\lambda|$ where λ is the largest real negative eigenvalue of A, but this interval may be too large where oscillatory solutions are involved. If A has eigenvalues $(-\lambda \mp \mu\, i)$ where λ is large and positive the algebraic solution oscillates with increasing amplitude for intervals greater than some critical size. Reference (4) therefore recommends computational care with this method. In practice over-sized time intervals cause incoherent outputs which effectively indicate the presence of an instability. Intervals of 10^{-4} seconds are used in both programs.

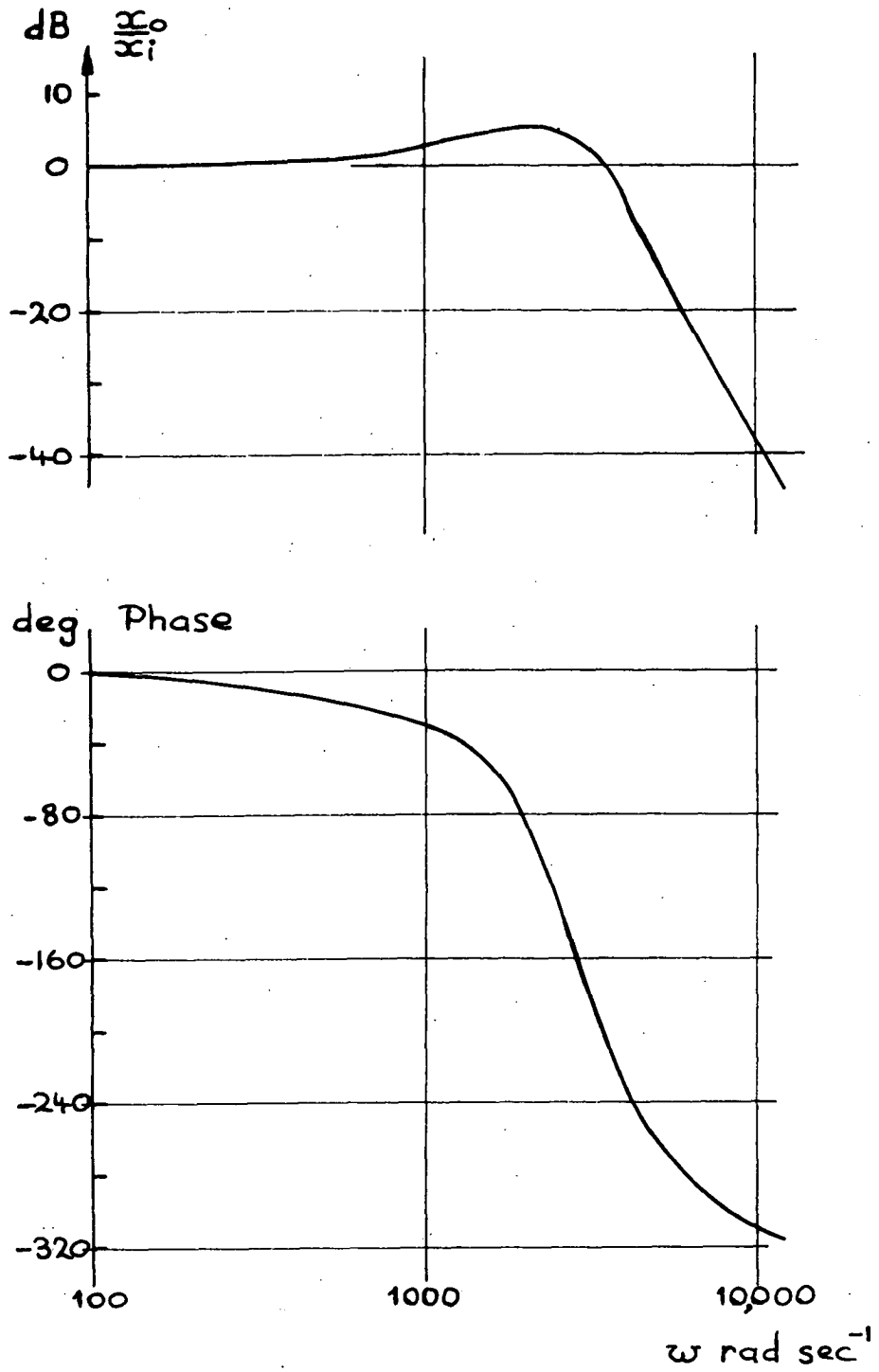

Frequency response of the approximated four-way servo-system.

figure (1 - 6)

Small time intervals must be maintained throughout the solution which extends program run time, but non-linearities involving frequent changes to A can be included with an insignificant additional run-time penalty.

The Runge-Kutta algorithm is therefore preferred because it offers ready inclusion of non-linearities, acceptable run time, and requires less program space.

1.8 Matrix Scaling for Digital Computation

Previous experience shows that unscaled problems sometimes produce completely wrong results due to truncation errors in computation. OS8 BASIC is accurate to about seven digits (23 bits) so that significant errors may occur if ill-matched numbers are added.

Appendix 1 shows the scaled and unscaled A matrix with numbers ranging from 0.009 to 10 in the former and $1.77E^{5}$ to $1.8E^{14}$ in the latter case.

Despite the ill-conditioned appearance of the unscaled A matrix it does not induce errors and Programs 1 to 3 do not therefore employ scaling. However the A matrix scaled for analog computation can be used with more confidence and is recommended for general use.

The relative insensitivity of digital solutions to amplitude scaling is a major advantage in sharp contrast to analog solution where amplitude scaling is a difficult problem, especially with high order systems.

1.9 Approximated Four-way servo-system steady-state results

Figure (1-6) records the gain and phase of x_o when a sinusoidal signal x_i is applied to the pump servo-valve spindle.

The system behaves as a high frequency filter above 6000 rad/sec and has a positive gain up to 4000 rad/sec. It is very stable over the entire frequency range,

RESPONSES OF THE APPROXIMATED FOUR-WAY SERVO-SYSTEM TO A STEP PERTURBATION x_i

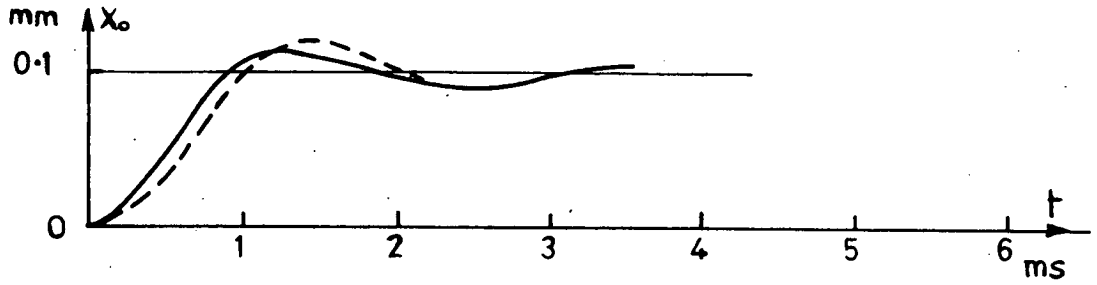

Cylinder Displacement figure (1 - 7)

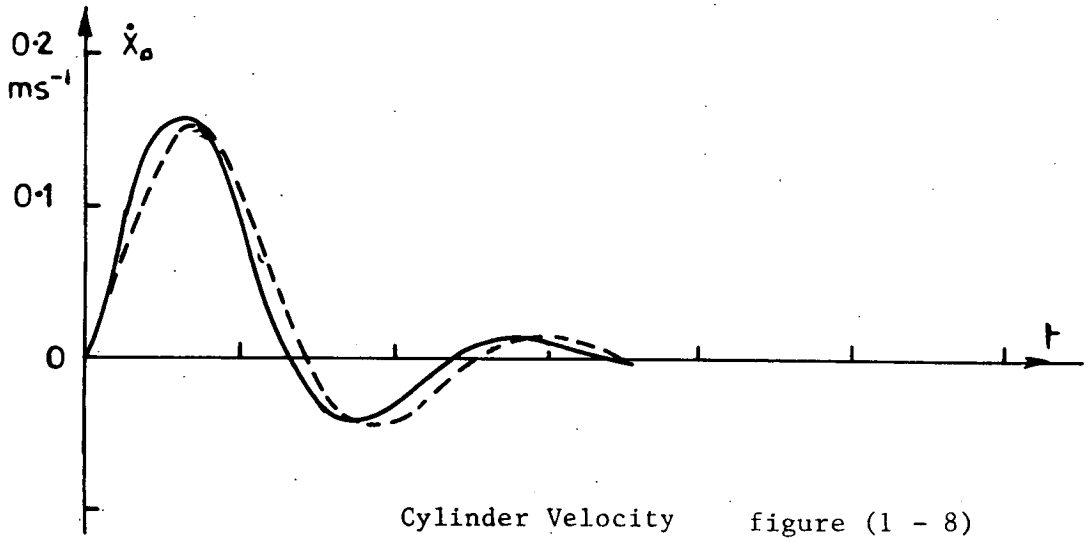

Cylinder Velocity figure (1 - 8)

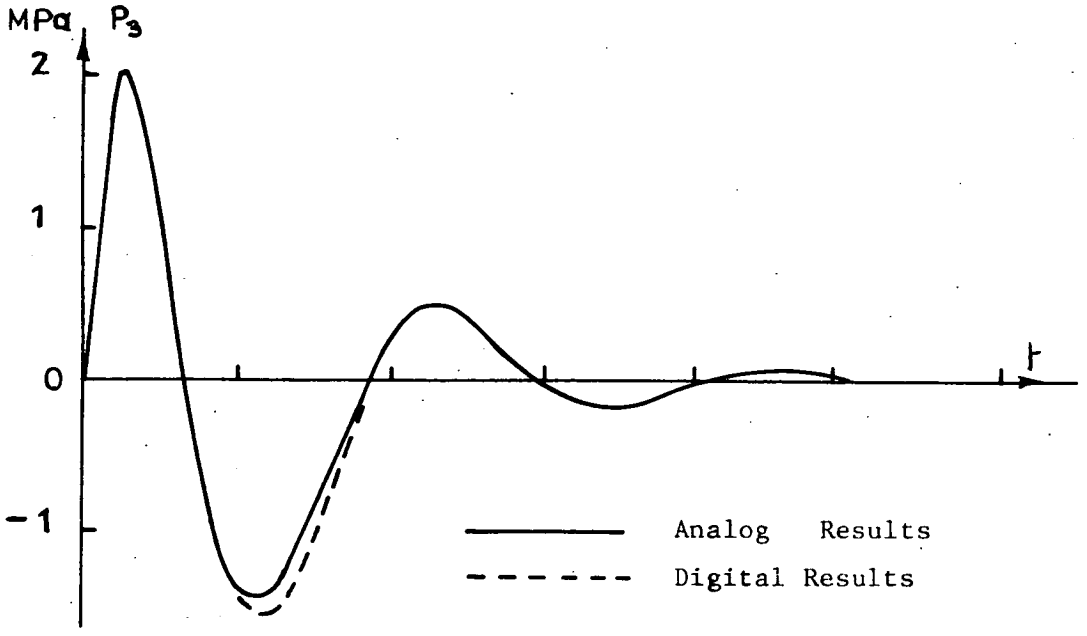

Jacking Cylinder Pressure figure (1 - 9)

but x_o has maximum excitation at 2,000 rad/sec and is least stable when disturbed by that frequency.

1.10 Approximated Four-way servo-system step perturbation response

This system is analysed by Dransfield et al[2] and present results may be compared with those previously published.

Results shown in figs. (1-7) to (1-12) are obtained by analog and digital simulation.

1.10.1 Analog Simulation

These results are in general agreement with the digital results except that y and p_s drift to final values higher than the scaled equations predict. This error probably results from unbalanced effects within the analog computer.

1.10.2 Digital Simulation

Digital results are obtained from Program 2 in slightly modified form. These results are verified to the extent that they are given by two separate programs and all long term final values converge toward values predicted from the state-variable equations.

The match with previously published results[2] is very good bearing in mind that several system constants are estimated from Green and Crossley's work, and such values may differ slightly causing minor discrepancies. The effect of such differences on the general shape and scale of the curves is insignificant.

1.11 Non-linear four-way servo-system step perturbation response

Results are obtained from Program 2 in two ways discussed below.

RESPONSES OF THE APPROXIMATED FOUR-WAY SERVO-SYSTEM TO A STEP PERTURBATION x_i

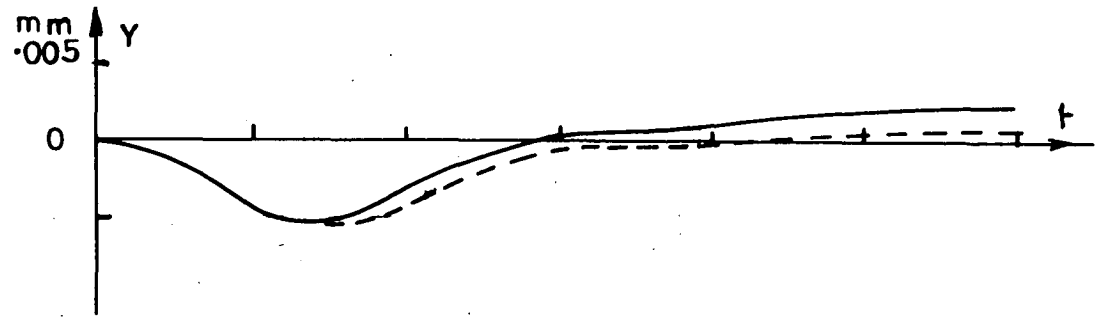

Relief Valve Position figure (1 - 10)

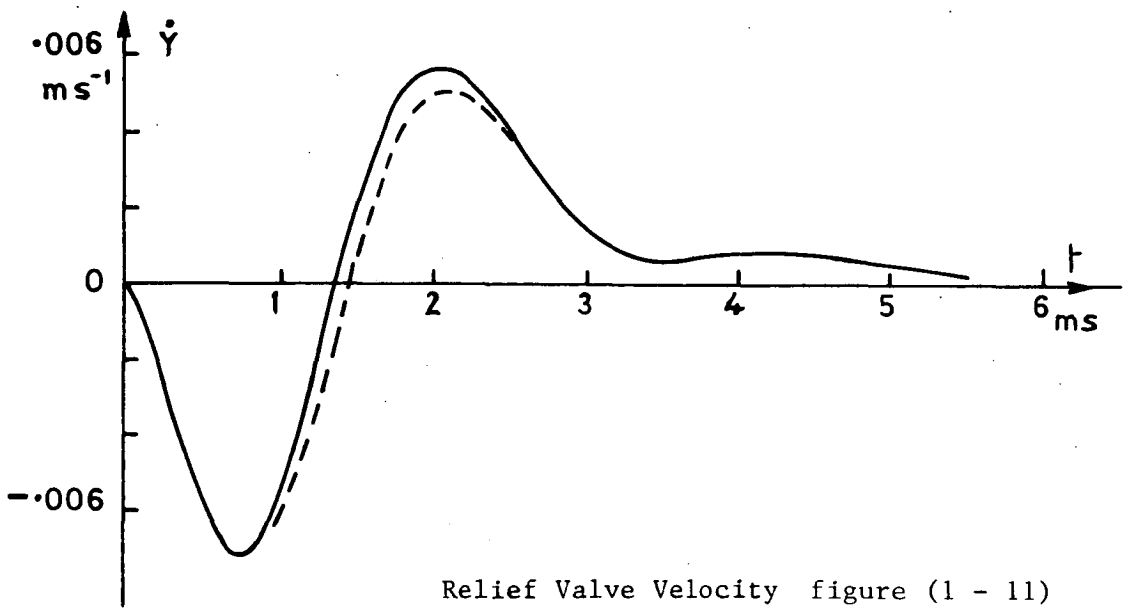

Relief Valve Velocity figure (1 - 11)

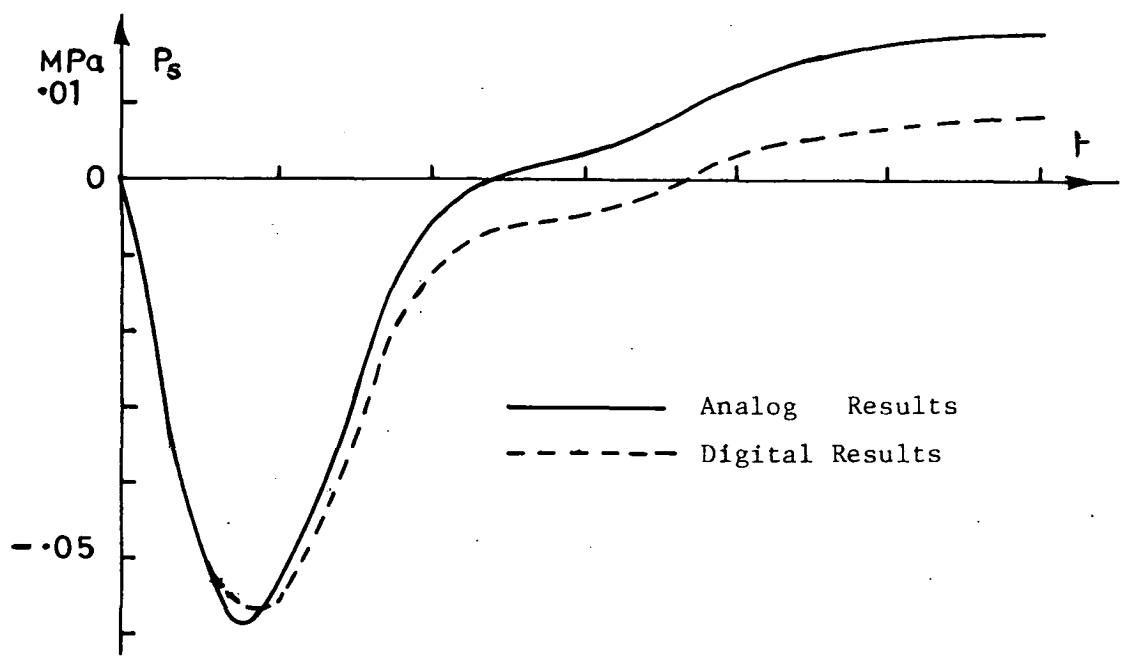

Supply Pressure figure (1 - 12)

1.11.1 Step perturbation applied to x_i

Figures (1-13) to (1-18) show the results obtained for both positive and negative spool input perturbations (x_i).

Eigenvalues for the two A matrices governing extension and retraction are given in Appendix 1 and it is interesting to note their effect on the time solution which has the general form

$$x = A_1\epsilon^{\lambda_1 t} + A_2\epsilon^{\lambda_2 t} \cdots A_n\epsilon^{\lambda_n t}$$

for each state-variable. All eigenvalues affect the individual state-variable responses depending on the excitation amplitudes A_1 to A_n. The smallest negative real eigenvalue and the least damped complex conjugate pair are likely to dominate the later stages of the solution and other more rapidly decaying transients affect the early stages when variables are being excited following the step input. The non-linearities involve periodic switching between two sets of equations which complicates the above picture because a particular transient may be excited at alternate switching points and will therefore have a small intermittent effect on an oscillatory solution. Magnitudes of A_n depend upon the method of perturbing the system. Amplitudes directly linked with the physical disturbance tend to be most excited and those indirectly linked tend to be least excited, hence it is possible to get some idea of the relative values of A_n without excessive calculation. Using x_i as a step input there is a chain effect where one component excites another. The step opens the servo-valve which draws flow so that p_3 rapidly increases and p_s rapidly decreases. p_3 then excites the jacking cylinder (x_o) and p_s excites the relief valve (y). In subsequent motion p_3 and x_o are heavily inter dependant as are p_s and y

RESPONSES OF THE NON-LINEAR FOUR-WAY AND THREE-WAY SERVO-SYSTEMS TO A STEP PERTURBATION x_i

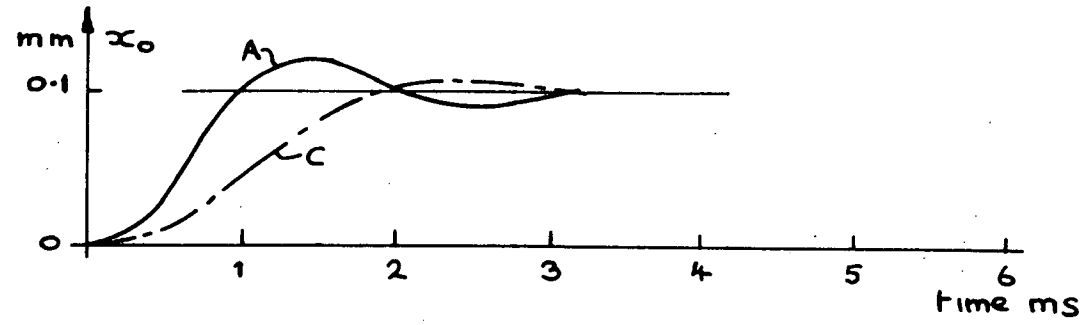

Cylinder Displacement figure (1 - 13)

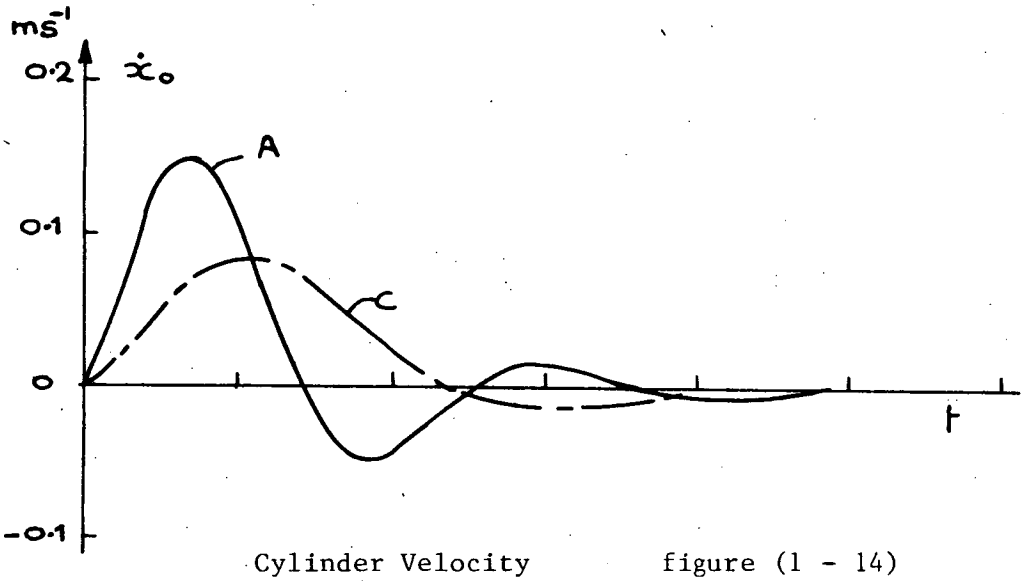

Cylinder Velocity figure (1 - 14)

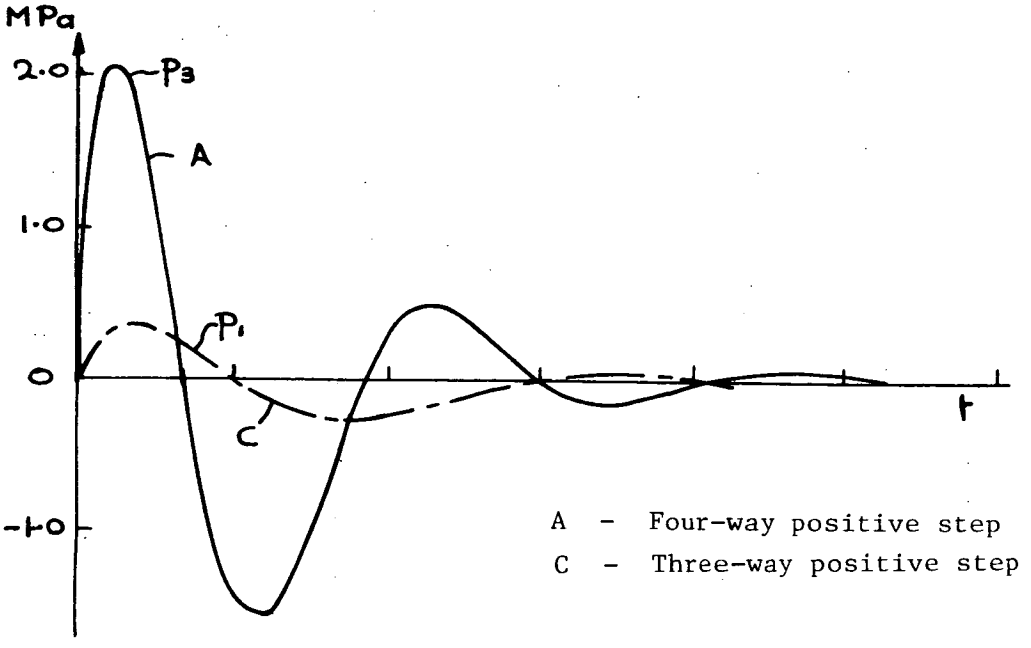

Jacking Cylinder Pressure figure (1 - 15)

hence specific eigenvalues tend to influence specific responses as in the table below.

Eigenvalue	State-variable	Extension	Retraction
λ_1	p_s y $\dot{y}$	-595	-585
λ_2	p_s p_3	-3622	-3624
λ_{34}	y $\dot{y}$	-1654 ± 1770 i	-1656 ± 1769 i
λ_{56}	$x_o \dot{x}_o$ p_3	-987 ± 2804 i	-990 ± 2804 i

Fortunately the values differ only slightly between extension and retraction indicating no drastic change in the response at switching points.

λ_1 is the dominant real eigenvalue and it dominates the long term response of p_s y and $\dot{y}$. λ_2 is responsible for the rapid initial rise of p_3 and the rapid initial fall of p_s. λ_{34} creates heavily damped relief valve oscillations which are only slightly excited and λ_{56} is the dominant complex conjugate pair giving rise to damped oscillations of x_o $\dot{x}_o$ and p_3. Broadly speaking figures (1-13) and (1-14) are functions of λ_{56}, figure (1-15) is a function of λ_2 up to about 0.5 ms and then a function of λ_{56}, figures (1-16) and (1-17) are functions of λ_1 with some small influence from λ_{34} and figure (1-18) is dominated by λ_2 up to about 0.5 ms after which λ_1 becomes dominant.

State-variable responses to a positive and negative input contrast sharply in some cases. 'Pump' state-variables (x_o $\dot{x}_o$ p_3) respond almost identically to figures (1-13) (1-14) and (1-15) but in a negative sense for a negative step. 'System' state-variables (p_s y $\dot{y}$) respond in the same sense for positive and negative inputs as shown in figures (1-16) to (1-18).

RESPONSES OF THE NON-LINEAR FOUR-WAY AND THREE-WAY SERVO-SYSTEMS TO A STEP PERTURBATION x_i

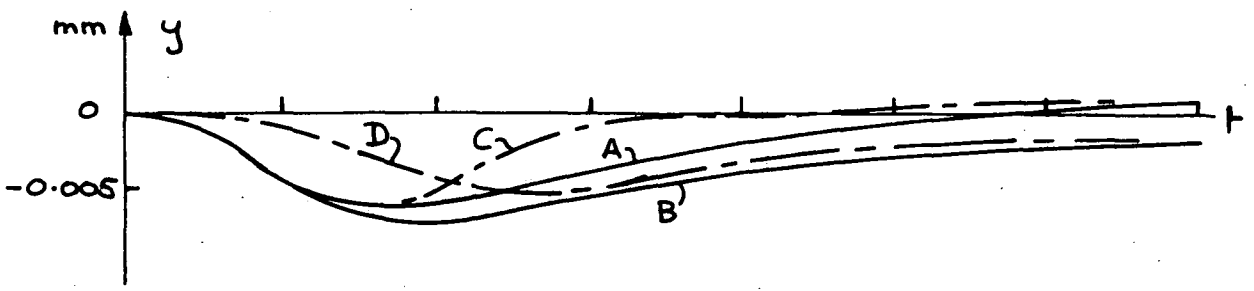

Relief Valve Position figure (1 - 16)

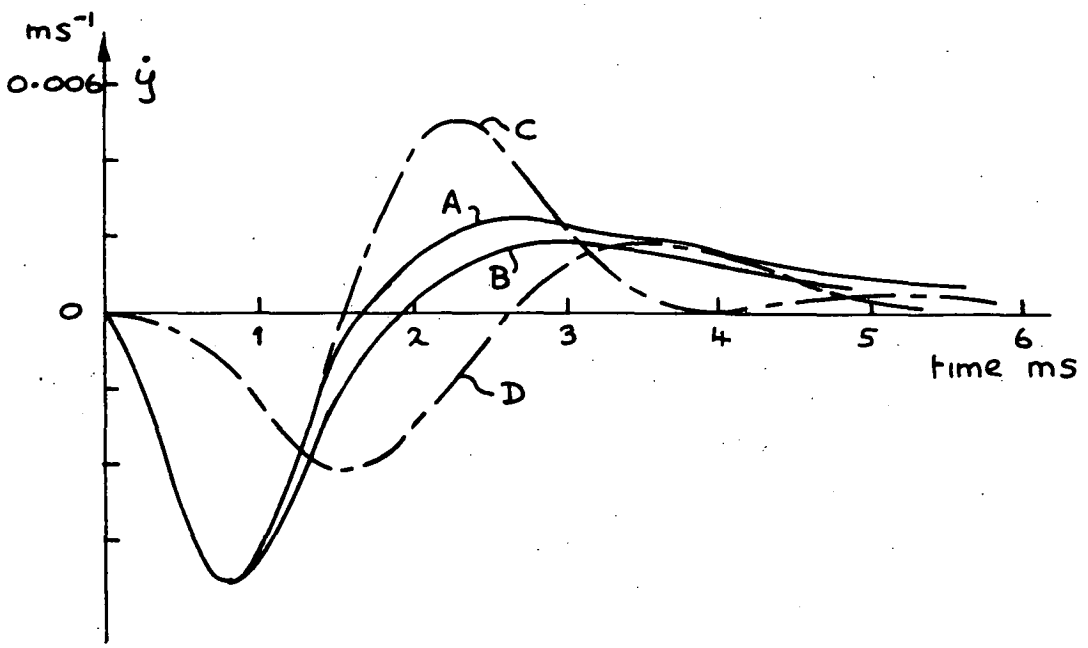

Relief Valve Velocity figure (1 - 17)

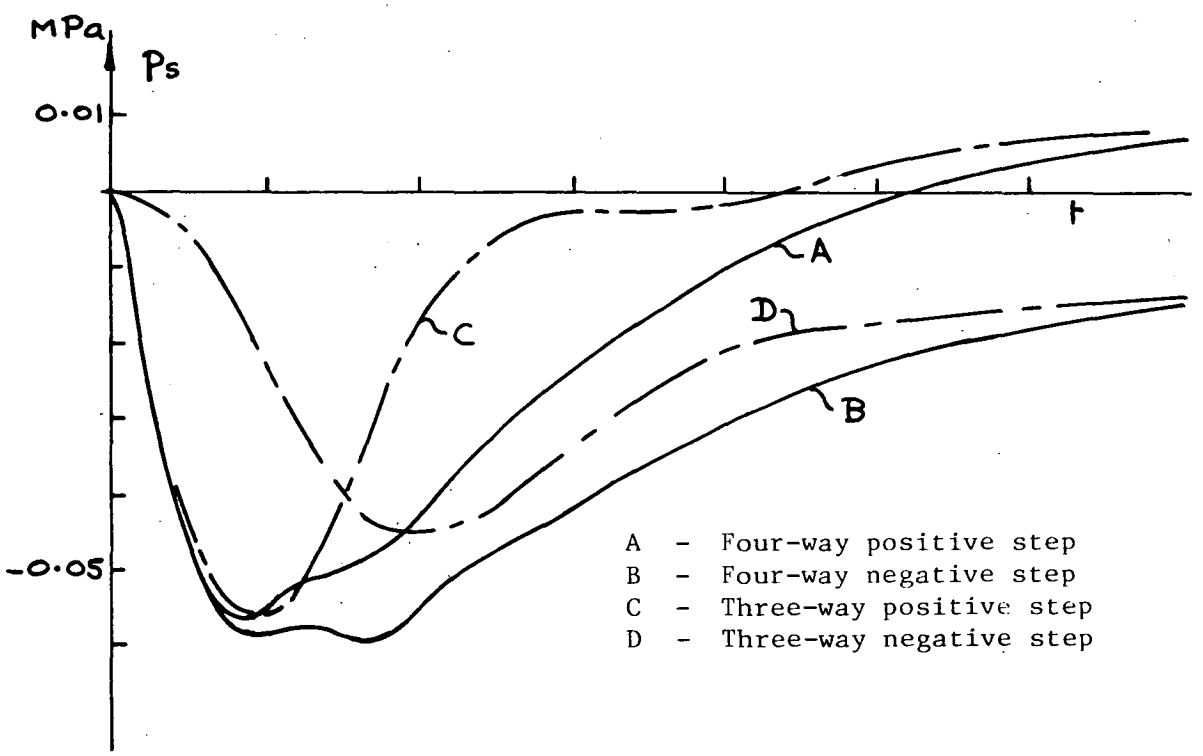

Supply Pressure figure (1 - 18)

This latter effect is explained by detailed study of figure (1-18). For a positive step the initial tendency is for p_s to fall because oil is taken from the pump delivery for control purposes, that is to build up p_3 and to begin jacking cylinder movement x_o. Control flow is proportional to $(x_i - x_o)$ and pump output flow to x_o, hence as x_o increases control flow decreases whilst pump output increases and these effects combine to arrest the fall of p_s. At 1.0 ms $x_o = x_i$ and the pump first passes its final equilibrium position where no control flow is drawn, but subsequently oscillations of x_o cause control flow to be taken whenever x_o is different from x_i in either a positive or negative sense. The fall in p_s causes the relief valve to close slightly so that it passes flow below its original value. After 1.0 ms x_o overshoots and produces more flow, some of which is taken for control purposes but there is a surplus and p_s rises. After 2 ms the pump has virtually settled at its new equilibrium position and has little further effect so that p_s and y increase toward their final positive values.

For a negative step input p_s also has an initial fall off as control flow is taken from the pump delivery and as x_o is reduced the pump output also reduces so that at 1.0 ms, when the pump first passes its final equilibrium position, p_s is more negative than for the positive step input. The overshoot of x_o further reduces pump output flow and causes control flow to be drawn but the relief valve has closed slightly and passes less flow so p_s remains nearly constant between 1.0 and 2.0 ms. After 2.0 ms the pump has largely settled down so that p_s and y can move to their final negative values.

1.11.2 Initial condition applied to p_s

Figure (1-19) records the system response to an initial condition applied to p_s with no other inputs.

In this case the pump jack (x_o) can only be excited by force feedback from p_s to the jack which is very small, and x_o is scarcely excited. This confirms that there is very little coupling between x_o and p_s and indicates that

RESPONSES OF THE NON-LINEAR FOUR-WAY AND THREE-WAY SERVO-SYSTEMS TO AN INITIAL CONDITION IMPOSED ON THE SUPPLY PRESSURE

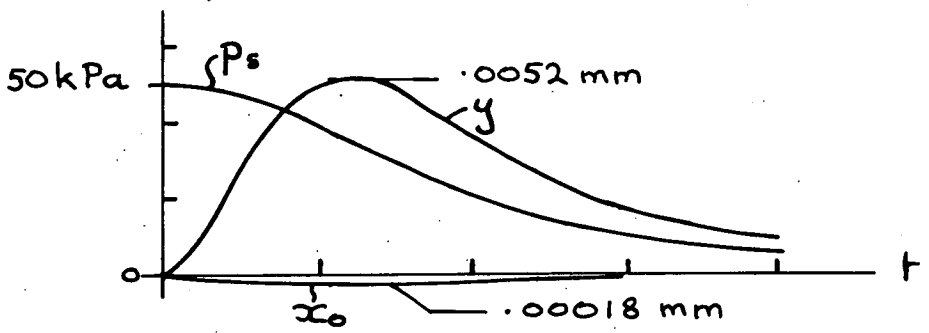

Four-way servo-system response figure (1 - 19)

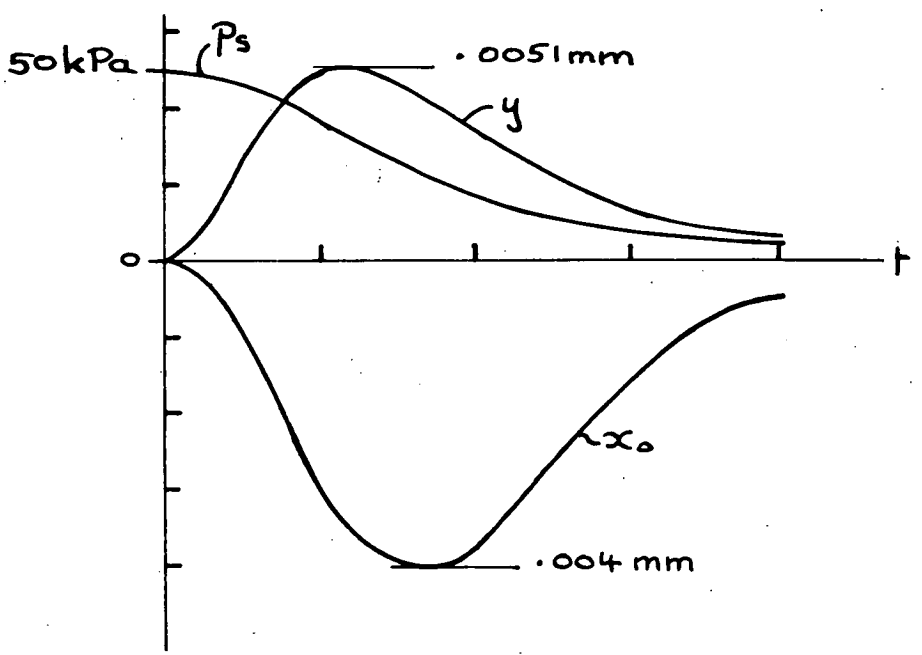

Three-way servo-system response figure (1 - 20)

load induced disturbances have little effect on the four-way servo-pump. The response of this system approximates to the response of the delivery line and relief valve, and is quite linear. A negative initial condition similarly applied has an almost identical response but in the opposite sense.

No oscillatory effects appear in the solution which is largely dominated by λ_1 although λ_{34} would be expected to play a minor role since it is connected with the relief valve. λ_{56} is not excited because it is associated with the pump.

In contrast with section 1.11.1 which shows a non-linear response of 'system' state-variables the present method of perturbing the system produces linear results. This highlights the need to select the perturbed variable carefully if conclusions are being reached regarding system stability.

1.12 Non-linear three-way servo-system step perturbation response

Results are obtained from Program 3 in two ways discussed below.

1.12.1 Step perturbation applied to x_i

As for the four-way case eigenvalues for the A matrices have particular significance for specific state-variables

Eigenvalue	State-variable	Extension	Retraction
λ_1	$p_s y \dot{y}$	-432	-661
λ_2	$P_1 (p_s)_{ext}$	-1976	-1710
λ_{34}	$y \dot{y}$	$-1673 \pm 1732\ i$	$-1615 \pm 1712\ i$
λ_{56}	$x_o \dot{x}_o p_1$	$-1054 \pm 1854\ i$	$-1130 \pm 1765\ i$

λ_2 affects the response of p_2 during extension but not in retraction because control flow is not then drawn from the delivery line. By comparison with the four-way servo results in section 1.11.1 λ_1 is significantly less during ram extension and slightly greater during retraction. λ_2 is almost halved, λ_{34} remains little altered and λ_{56} has a lower natural frequency and higher damping ratio. λ_1 indicates that p_s, y and $\dot{y}$ are likely to decay more rapidly during retraction. λ_2 indicates that a rapidly decaying initial transient will be present in the responses of p_1 and p_s during extension but not in p_s during retraction. This transient will not be as severe as for the four-way system. λ_{56} indicates that x_o and p_1 will oscillate slower and overshoot less.

Figures (1-13) to (1-15) show the responses of x_o $\dot{x}_o$ and p_1 to a positive step perturbation x_i. A negative step produces almost identical results in the opposite sense.

x_o rises at about half the rate of the four-way case and oscillation is at the frequency predicted by λ_{56}.

p_1 cannot be directly compared to p_3 but a comparison can be made on the basis of generated forces which are Ap_3 in one case and $A(2p_1 - p_s)$ in the other. p_s is small compared to p_1 hence the force accelerating the jacking cylinder is approximately $2Ap_1$ in this case and Ap_3 in the four-way case. Comparing $2p_1$ to p_3 indicates a much lower force and accounts for the slower response of x_o.

Figures (1-16) to (1-18) show the responses of y $\dot{y}$ and p_s to positive and negative step perturbations.

In response to a positive step p_s falls initially as control flow is drawn from pump delivery to build up p_1 and begin movement of the jack. As the jacking ram moves control flow continues to be drawn in proportion to $(x_i - x_o)$,

and therefore in decreasing quantities, until $x_o = x_i$ at about 2 ms, but pump output simultaneously increases in proportion to x_o, and flow is also fed back to the delivery line from the high pressure end of the jacking ram in proportion to $\dot{x}_o$. These three effects combine to minimise p_s at 1.0 ms and to make it rise thereafter. At 2.0 ms x_o overshoots and control flow then ceases to be drawn but the resulting tendency for p_s to rise is arrested because $\dot{x}_o$ becomes negative after 2.3 ms and oil is drawn from the supply line to the high pressure side of the jacking ram. Beyond 4 ms the pump has settled and p_s rises to its final positive value.

The response of p_s to a negative step x_i differs from other p_s responses because no control flow is taken during the first 2 ms. As the step is applied the equilibrium leakage flow is abruptly cut off and there is a momentary tendency for p_s to become slightly positive, but p_s falls as x_o becomes negative and delivery flow is diverted to the jacking ram, whilst concurrently the pump output reduces in proportion to x_o. p_s is minisised at 2 ms because the relief valve has closed a little and passes less flow and x_o is becoming less negative. After 2 ms x_o overshoots and control flow is taken from the delivery for the first time which retards the rise of p_2, but this is offset when $\dot{x}_o$ becomes positive after 2.3 ms. As the pump settles p_s rises to its final negative value as does y.

1.12.2 Initial condition applied to p_s

Figure (1-20) records the system response to an initial condition applied to p_s with no other inputs.

p_s and y respond as in the four-way case but x_o is excited to an amplitude twenty times greater, indicating that there is far more coupling between x_o and p_s in the three-way servo-pump.

A negative initial condition similarly applied produces almost identical results but in the opposite sense indicating that this system behaves in a linear manner when perturbations are load induced and should remain linear unless the amplitude of x_o is allowed to become significant.

1.13 Assessment of System Stability

Green and Crossley concluded that 'the three-way servo-valve is inherently less stable . . . .'

The scope of this work is limited to considering one damping ratio for each pump jacking ram and one damping ratio for the system relief valve. Results indicate that the three-way servo-system has more inherent damping characteristics as evidenced by the system eigenvalues which in turn suggests it is more stable mathematically. Figure (1-13) supports this argument by showing the sluggish response of the three-way servo-system by comparison with the four-way when perturbed by a step input x_i. When the perturbation is load induced as in figures (1-19) and (1-20), a different picture emerges because x_o is excited to much larger amplitudes in the three-way servo-system. This can also be shown by using q_L as in input as discussed earlier in this chapter. In this case x_o may reach unacceptably large amplitudes which invalidate assumptions made in the small perturbation analysis or exceed physically imposed limits, and the system may become physically unstable whilst remaining'mathematically' stable.

Clearly system stability must be assessed using both criteria. Green and Crossley reached their conclusion by evaluating the transfer function coupling p_s and x_o and noting that x_o is larger for the three-way case, but this could be a cumbersome and indecisive method to apply if it entails examination of coupling between an input and several output variables.

The step perturbation technique can be used to assess the magnitude of all coupling terms by stepping an input and observing the time response of all system variables. The step must be applied to an input or state-variable which causes the physical disturbance of the system, as in figures (1-19) and (1-20), otherwise coupling terms which have most practical significance may not be apparent. For example the coupling between p_s and x_o is not important when x_i is used as an input. It is therefore concluded that both 'mathematical' and 'physical' stability can be assessed by the step perturbation technique providing the step is applied at the correct position within the system.

The relative stability between the three-way and four-way servo-systems can be assessed as follows;

The three-way servo-system is inherently more damped and is more stable when fitted to a system disturbed by perturbations of x_i, but it is less stable when subjected to load induced perturbations.

1.14 Summary of computing facilities

Analog simulation was disgarded in favour of digital simulation because all types of non-linearities are easily included in the latter method, although the speed of analog simulation suits it to problems involving parameter changes to optimise system response.

Digital simulation was performed on a hands-on system available in the form of a PDP-8E or PDP-8F computer with 16K of core and having disc and magnetic tape data storage facilities. Output was on teletype or line-printer and input by teletype or high speed paper tape reader.

Programs were written in OS8 BASIC which was found to have all necessary language features. Early eigenvalue and state-variable programs were checked out on an ELLIOT 503 using standard ALGOL programs and were found to be accurate.

The following programs were written;

(a) Matrix characteristic polynomial by Krylov's method (5).

(b) Polynomial solution.

(c) (a) and (b) were combined to form a matrix eigen value program.

(d) Runge-Kutta solution of differential equations.

Using these programs the available computing facility was highly flexible and well suited to the work undertaken. Lack of access to MIMIC was not a serious disadvantage and the hands-on nature of the facility allowed on-line editing of the programs which gave a high degree of control not always available to users of advanced languages.

1.15 Summary of Chapter I

The original objectives set out in section 1.1 were achieved. System equations were methodically manipulated into state-variable form and analog and digital solution techniques were developed and evaluated. Digital solution was preferred for the non-linear equations encountered and programs suited to a small computer were written and proved. From these programs system responses were found and system stability was assessed. A technique for specifying component transfer functions and building flexible block diagrams which physically identify with system components was also developed.

The techniques developed in this chapter are applied to a Vickers SR-4 Servo-valve in the following work.

REFERENCES

(1) Green, W.L. and Crossley, T.R.
An analysis of the control Mechanism used in variable-delivery hydraulic pumps.
Proc. Instn. of Mech. Engrs. Vol. 185 6/71.

(2) Dransfield, P., Barnard, B.W., Rogers, K. and Young, M.
On prediction at the design stage, of hydraulic control system dynamic performance.
The second international JSME symposium fluid machinery and fluidics, Tokyo, Sept., 1972.

(3) Ward, J.R. and Strum, R.D.
State Variable Analysis.
Prentice-Hall, N.J.

(4) Fox, L., and Mayers, D.F.
Computing methods for scientists and engineers.
Clarendon Press, Oxford.

(5) Anthony Ralston.
A first course in numerical analysis.
McGraw-Hill.

(6) Peter Dransfield
Engineering systems and automatic control
Prentice-Hall.

(7) P. Atkinson
Feedback control theory for Engineers
Heineman.

(8) F.H. Raven
Automatic control engineering
McGraw-Hill Kogakusha.

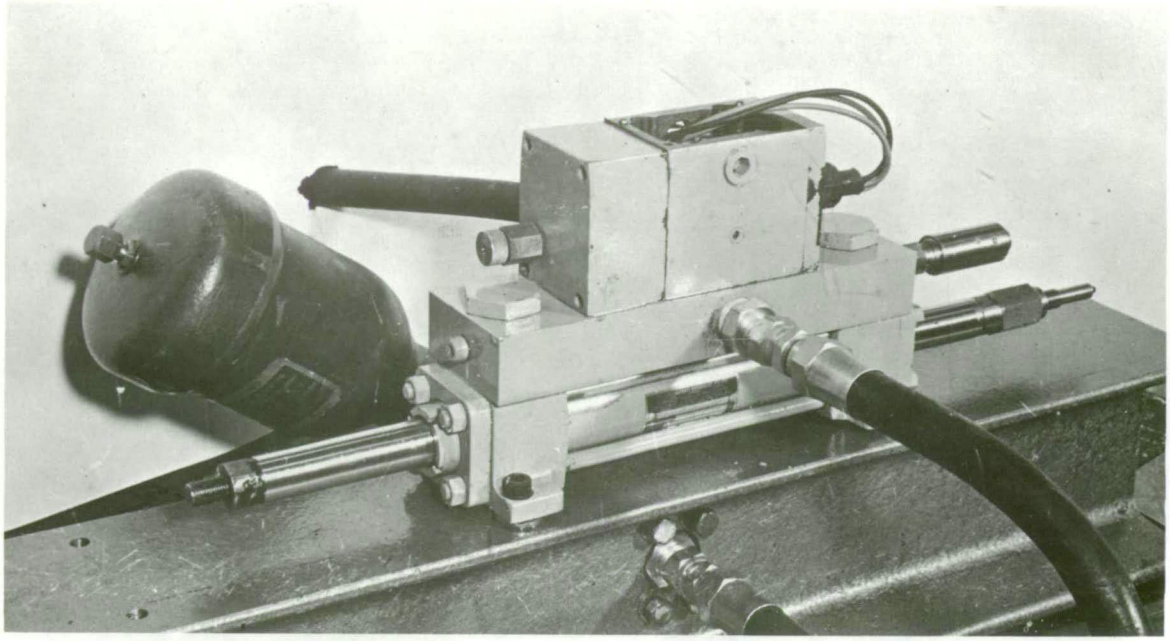

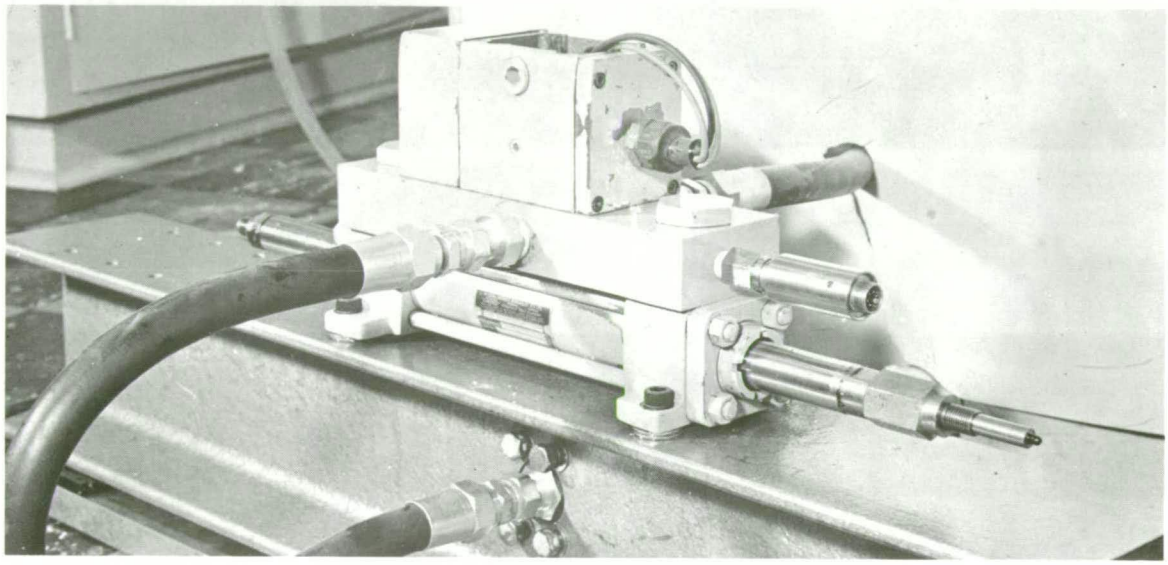

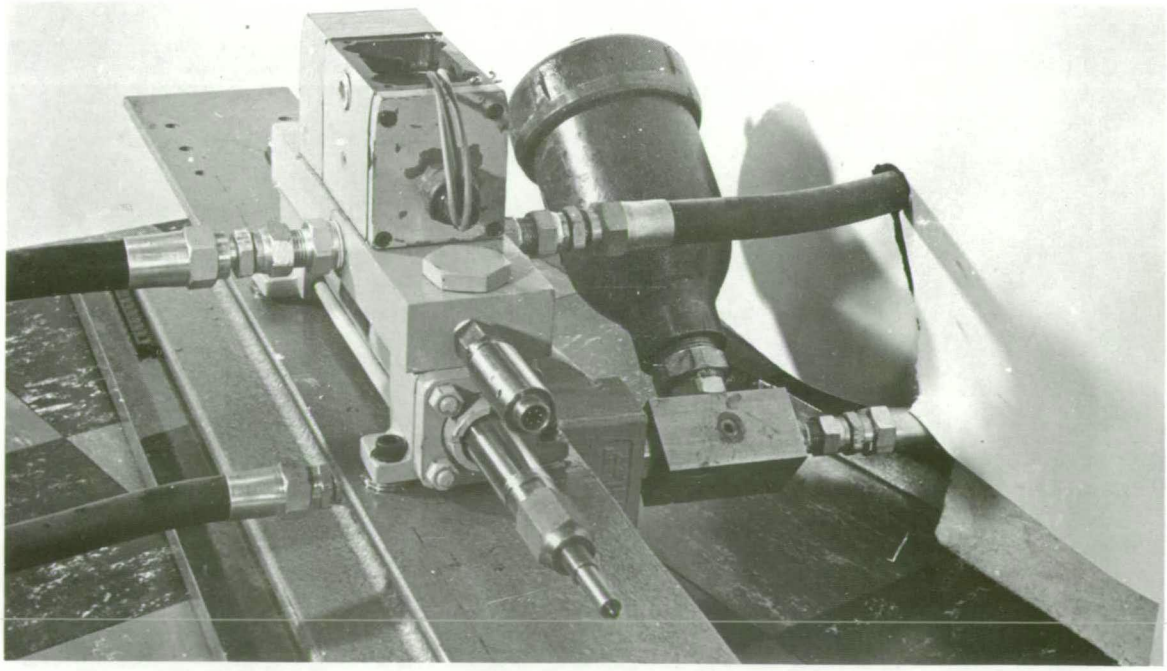

Figure (2-1)

CHAPTER 2

2.1 Introduction

This chapter contains a physical description of the servo-valve and ram unit which is used in subsequent theoretical and experimental work.

2.2 Description of Components

Ths unit shown in figure (2-1) comprises three basic component parts described below.

2.2.1 Hydraulic Ram

Vickers Model W30-FL-NC-HH-FT-IR-5H-2

The ram is a standard double shafted model with 1.50 in. dia. bore, 1.00 in. dia. shafts, 6 in. stroke and 3000 p.s.i. pressure capability. It comprises a cylindrical centre section clamped between two end caps by four tie bolts and sealed with 0 rings. Each end cap houses a shaft seal, shaft bearing bush and port connection. The ram piston is attached at the shaft centre and runs inside the cylinder sealed by one 0 ring with two backing rings, and the shaft is located and sealed by the two end caps.

2.2.2 Subplate

The subplate acts as an interface between the servo-valve and ram, and also houses the supply and return line connections to the pump unit. It comprises a steel block 1.5 in. thick with drilled oil transfer passages. The servo-valve is mounted on the subplate with four set screws and there are five interconnecting ports sandwiched between these items each sealed by an 0 ring. Of these ports one is blanked off, two service the ram, one is supply, and one is to drain. The subplate is attached to the ram by two sturdy set screws which locate in the ram port connections.

VICKERS ELECTRO-HYDRAULIC SERVO VALVE

Model No SF4-100-30-002-10

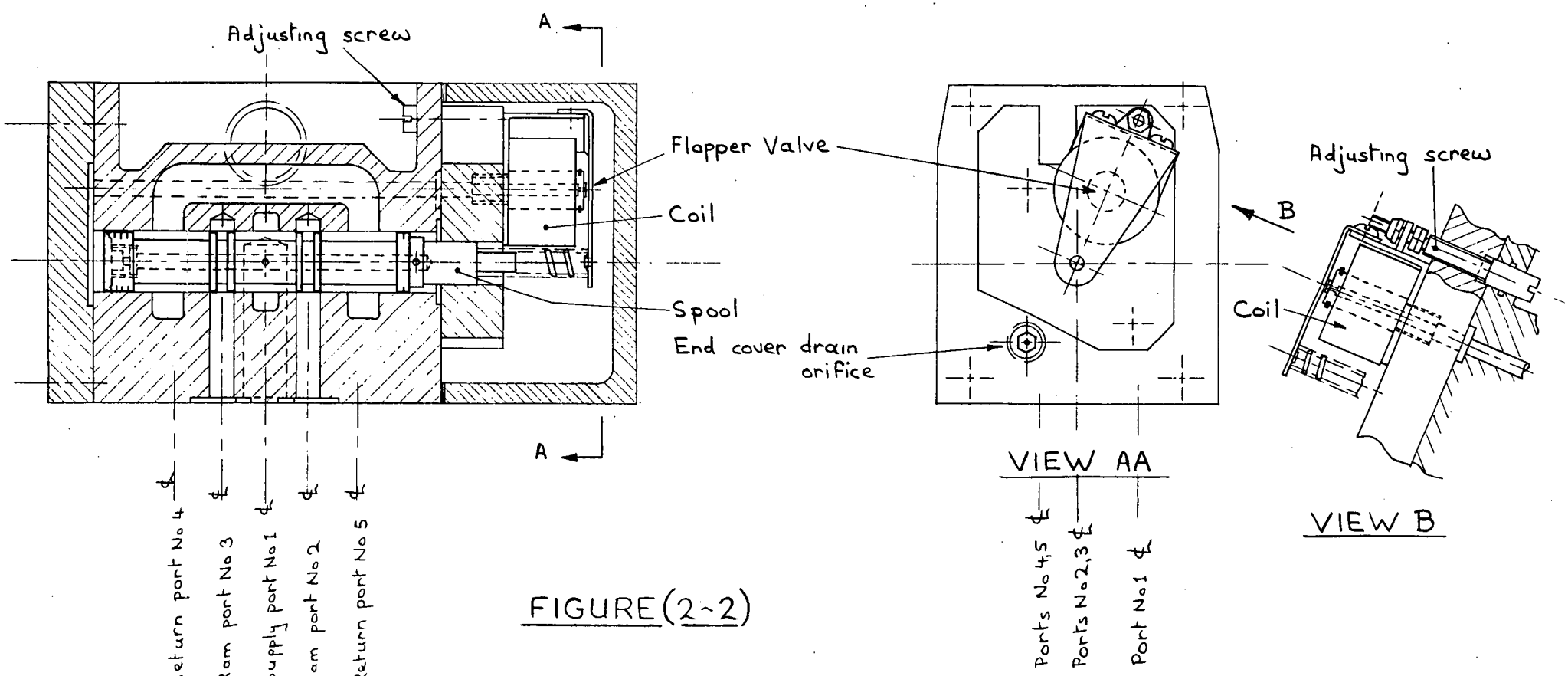

FIGURE (2-2)

These screws have drilled oil passages and are sealed by 0 rings as required to prevent leakage.

2.2.3 Servo-valve

Model code SF4-30-002-10

The Vickers two stage SF-4 servo-valve is shown in figure (2-2) and some critical component parts are detailed in figure (2-3).

Figure (2-2) shows the valve at its zero flow position with both ram ports sealed by the spool and figure (2-4) schematically shows the control circuit which uses a flapper valve to balance the spool.

Oil at supply pressure is ducted to the annular section surrounding the spool centre where it is available for control purposes or to power the ram.

Control flow passes through an orifice drilled in the side of the spool at centre position and into a drilled hole on the spool centre-line. From here the main control flow passes through a second orifice at the open end of the spool, but if the spool is moving this flow may be supplemented or depleted by flow from an annular section between the right hand spool land and the spool end bearing adjacent to the spring. There is a drilled hole in the spool connecting this latter volume to the spool centre-line drilling.

After passing the second orifice control flow is again supplemented or depleted because the spool end acts as a moving piston, and remaining flow is ducted through the flapper valve to the end cover and then through a drain orifice to the tank return port.

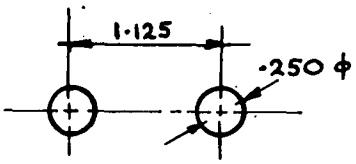

ORIFICE SPACING

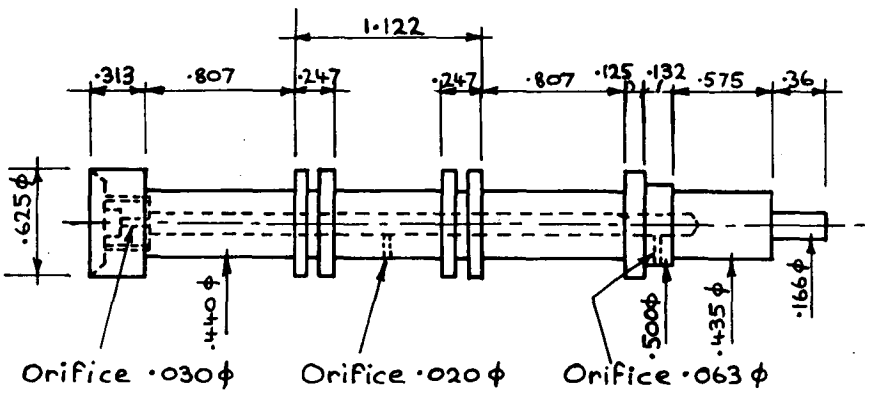

All dimensions in inches as measured

VALVE SPOOL

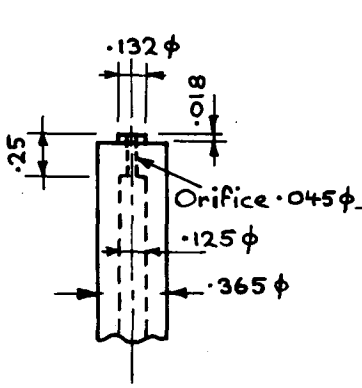

FLAPPER NOZZLE

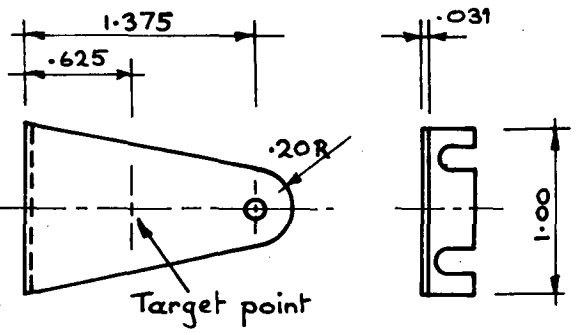

FLAPPER ~ Soft Iron

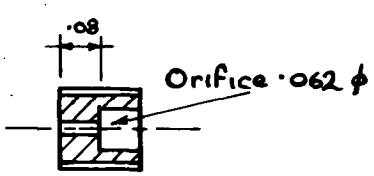

END COVER DRAIN ORIFICE

FLAPPER VALVE DETAILS - FIGURE (2~3)

The control flow gives rise to pressures p_2, p_3 and p_4 acting on the spool as defined by figure (2-4). p_3 and p_4 act over circular areas and p_2 acts over an annular area.

When the spool is displaced from central position it uncovers orifices which meter flow to and from the ram. These orifices are formed by stopped holes drilled through the valve base and piercing the spool locating bore at both bottom and top, as shown on figure (2-2). The spool land pertaining to each hole is divided so flow can pass through the orifice area exposed on the top side, into the stopped end of the hole and then through the divided land to the port. Flow is therefore metered at both top and bottom of the spool bore and flow forces thus generated cancel out perpendicular to the spool centre-line and do not tend to jam the spool. Figure (2-3) indicates a small underlap between the spool lands and orifice holes.

The spool is mainly located by its lands having largest diameter but there is a further locating bearing at the spring end machined in a separate component. These two bores must be concentric to avoid jamming and the right hand spool land is probably made narrow because otherwise it would tend to jam more easily for small misalignments.

The flapper valve design is best seen in view B of figure (2-2). Oil passes through the nozzle and impinges on the flapper target area as detailed in figure (2-3). The flapper acts as a spring which is attracted by an electro-magnet to vary the gap between the nozzle end and the flapper target enabling flow to be controlled by coil current. There is an external adjusting screw which loads a tag on the flapper support

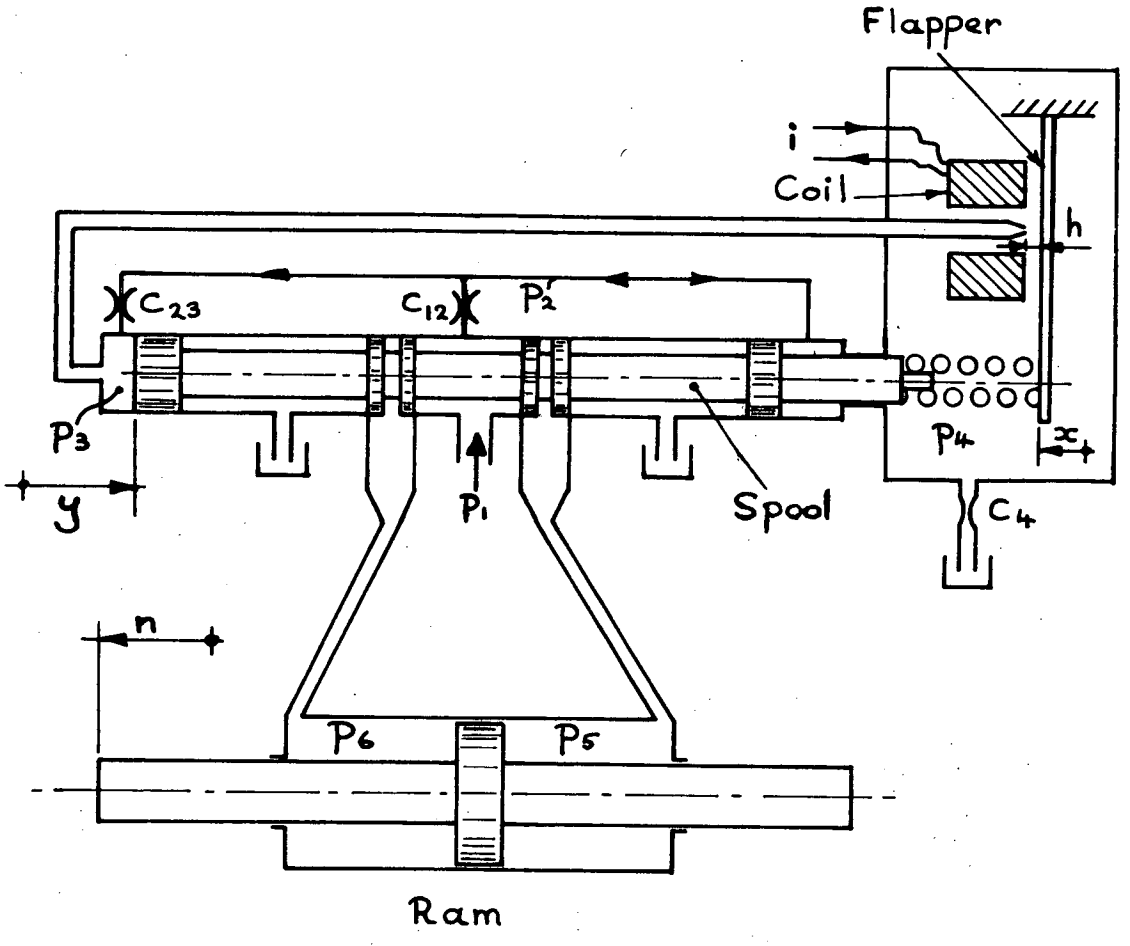

SERVO-VALVE SCHEMATIC DIAGRAM

FIGURE (2~4)

bracket to adjust the gap for setting up purposes. This screw is adjusted to obtain a correct equilibrium coil current. Feedback between the flapper position and spool is achieved by a coil spring which locates on both items.

O rings are used throughout the valve to seal pressure between components with the exception of the flapper valve end cover which utilises a gasket.

CHAPTER 3

3.1 Introduction

The objectives of this chapter are as follows:

(1) To establish equilibrium conditions of the servo-system shown in figure (2-4).

(2) To experimentally determine coefficients describing the dynamic variation of certain system variables, as required in the perturbed equations, where theoretical estimates are unreliable.

(3) To compare experimental results with theoretical estimates wherever possible.

Sections included are:

3.2 Measurement of system equilibrium conditions.
3.3 Estimation of oil viscosity.
3.4 Fixed orifice flow coefficients.
3.5 Flapper spring constants.
3.6 Flapper valve magnetic force.
3.7 Flapper valve flow characteristics.
3.8 Estimation of spool underlap

3.2 Measurement of system equilibrium conditions

With reference to figure (2-4) the system is in equilibrium when ram position n is constant. This is achieved by applying a constant supply pressure p_1 to the valve and adjusting coil current i until the flapper valve balances the spool at its null position. Control flow then passes in series through fixed orifice C_{12}, fixed orifice C_{23}, the flapper valve, and fixed orifice C_4.

Pressures p_1, p_2, p_4, p_5 and p_6 are readily measured but p_2, h, and control flow q are internal and must either be estimated, or measured by modifying the valve body in some way.

3.2.1 Measurements recorded

It was not considered practical to measure either p_2 or h, but q was measured by modifying the flapper valve end cover to redirect control flow externally. The internal drain orifice hole was plugged and the orifice relocated in an external drain line, where oil flow was timed into a measuring jar. Pressure transducers were positioned at appropriate locations to monitor p_1, p_3, p_4, p_5 and p_6, and a temperature transducer was fitted into the flapper valve end cover to record oil temperature. The valve and oil lines were warmed up to an average operating temperature of $50^{o}C$ by reciprocating the ram rapidly to allow high oil flow. The ram was then stopped and a test made immediately, before the reduced oil flow could cool significantly. A temperature rise of about $4^{o}C$ was observed between control flow inlet and outlet ports, so tests were run with an outlet temperature of $52^{o}C$. Average results recorded from a series of tests were:

p_1	= 6.895 MPa	p_1	= 13.79 MPa
p_3	= 0.827 MPa	p_3	= 1.565 MPa
q	= 16.5 mls^{-1}	q	= 23.4 mls^{-1}
T_{oil}	= $50^{o}C$	T_{oil}	= $50^{o}C$

3.3 Estimation of oil viscosity

The hydraulic oil used was HLP65 which has viscosities of 34.3 cs at $100^{o}F$ and 5.5 cs at $210^{o}F$ (taken from BP literature). Merritt[1] gives an approximate viscosity conversion equation as

$$\mu = \mu_o \varepsilon^{-\lambda(T - T_o)}$$

where λ is a constant for the particular oil and μ_o is the absolute viscosity at temperature T_o.

From the above information λ and μ_o are calculated from the known viscosities at two temperatures, hence;

$$\mu = 0.0303 \epsilon^{-0.0301(T - 37.8)} \text{ Nsm}^{-2}$$

where T is in degrees centigrade

T^oC	μ Nsm^{-2}	
25	0.0651	
50	0.0210	Operating range
55	0.0181	recommended by
60	0.0156	Vickers
65	0.0134	

3.4 Fixed orifice flow coefficients

To estimate flow coefficients for orifices C_{12}, C_{23} and C_4 the nominal diameters were measured by inserting standard twist drills to find a fit.

Orifice number	Pass drill diameter inches	No pass drill diameter inches	Nominal diameter inches
C_{12}	0.020	0.021	0.020
C_{23}	0.0292	0.031	0.030
C_4	0.062	0.0635	0.0625

Nominal diameters appear in figure (2-3) but are not sufficiently accurate for present purposes because small measurement errors have a large influence on orifice flow coefficients at diameters of this order.

Orifice C_{23} was not unscrewed from the spool because there was a risk of damage;consequently tube length measurements for both C_{12} and C_{23} were not taken. C_4 was measured in detail and found to have chamfered tube ends with a tapered bore 0.064 inches in diameter at the discharge end. As such it did not conform with standard sharp edged designs considered in texts.

Experimental determination was the only possible way of obtaining flow coefficients for the three orifices.

3.4.1 Flow coefficients for orifices C_{12} and C_{23}

Estimates of coefficients are based on nominal diameters using experimental data obtained at equilibrium conditions.

Spool forces

The valve spool is acted upon by four forces in its equilibrium position such that

$$p_3A_3 = p_2A_2 + p_4A_4 + F$$

where A_n is an effective area, p_n is a pressure, and F is the spring force.

Control Flow

The equations governing control flow are:

$$q = C_{12} \pi d_{12}^2 \sqrt{((p_1 - p_2)/\rho)}$$

$$q = C_{23} \pi d_{23}^2 \sqrt{((p_2 - p_3)/\rho)}$$

Equilibrium conditions

Taking the following data from section 3.2.1 and spool measurements

d_{12} = 0.508 mm dia $\quad A_2 = 1.020 \times 10^{-4}$ m^2

d_{23} = 0.762 mm dia $\quad A_3 = 1.979 \times 10^{-4}$ m^2

d_4 = 1.588 mm dia $\quad A_4 = 0.959 \times 10^{-4}$ m^2

ρ at 50°C = 854 kg m^{-3} F = 8.85 N

p_1 = 6.895 MPa p_3 = 0.827 MPa

p_4 = 0.051 MPa q = 16.5 mls^{-1}

Substituting in the three equations above and solving gives

C_{12} = 0.722

C_{23} = 0.932

p_2 = 1.471 MPa

By comparison with published information for short tubed orifices (figure 2.18 of reference [2]) the value of C_{12} is close to that anticipated but, C_{23} is about 25% higher, probably due to under-estimation of the nominal diameter coupled with the effect of rounded, rather than sharp, edges.

3.4.2 Flow coefficient for orifice C_4

The test rig in figure (3-6) was modified by removing the nozzle and vernier assembly and replacing them with an adapter containing orifice C_4. Oil was passed through the orifice and allowed to impinge on a horizontal surface placed 25mm from the discharge, and measurements of flow rate and pressure drop were recorded at 50°C.

Results

The discharge coefficient is given by

$$C_Q = 4q/(\pi d_4^2 \sqrt{(2\Delta p/\rho)})$$

Results give a value of 0.82 at the working flow rate, rising to 0.84 when the flow rate is doubled. C_4 is therefore assigned the value 0.82 based on nominal diameter d_4.

This value is higher than anticipated from published information but the discrepancy is readily explained by tube taper and the effect of chamfered tube ends.

3.5 Flapper spring constants

Details of the flapper valve design appear in figures (2-2) and (2-3). The flapper is attached to its support bracket by two screws and forces are applied by the coil spring at position 1, and by the oil jet and magnetic effects at position 2, which is the target point. For analytical purposes it is sufficient to obtain influence coefficients governing absolute and relative deflections between points 1 and 2.

3.5.1 Experimental determination of spring constants

The complete flapper valve assembly was removed from the valve and set up so that loads could be applied at positions 1 and 2, and respective deflections were measured by a dial gauge with negligible contact force. Loads were applied separately at the two positions and values of the influence coefficients were determined graphically as:

$$a_{11} = 1.1 \times 10^{-4} \text{ m N}^{-1}$$

$$a_{22} = 0.11 \times 10^{-4} \text{ m N}^{-1}$$

$$a_{21} = a_{12} = .293 \times 10^{-4} \text{ m N}^{-1}$$

3.6 Flapper valve magnetic force

The instantaneous magnetic force exerted on the flapper depends upon coil current i and orifice gap h. Coil inductance has no effect if a current driving source is employed to power the coil.

3.6.1 Theoretical magnetic force

Magnetic force is proportional to the square of the flux $\emptyset$ which in turn depends upon coil current i and circuit reluctance R.

At currents below onset of saturation the force is governed by the equation

$$F \propto \phi^2 \propto \frac{i^2}{(R_I + R_A)^2}$$

where R_I and R_A are iron and air reluctances. R_I is constant and R_A is proportional to h hence:

$$F = \frac{K\, i^2}{(1 + bh)^2}$$

where K and b are constants.

At higher currents the onset of saturation occurs and force increases at a slower rate because ϕ is no longer proportional to i and R_I also increases in value. Neglecting this latter effect

$$F = \frac{K\, f(i)}{(1 + bh)^2}$$

In practice the air gap usually becomes dominant when h exceeds about two thousandth of the magnetic circuit length, which is 0.15 mm in this case, consequently the value of bh in the denominator is expected to be about 1 in the working range when $h \doteq 0.13$ mm.

Experimental work is required to establish which of the above equations is applicable.

3.6.2 Experimental determination of magnetic force

The flapper valve assembly was removed from the servo-valve and set up without the feed back coil spring, and a dial gauge with negligible contact force was used to measure flapper deflection. A series of tests were conducted with different initial gaps (h_o) and the target point deflection was recorded for varying coil current. All tests were run with air in the gap on the assumption that substitution of oil would make little difference.

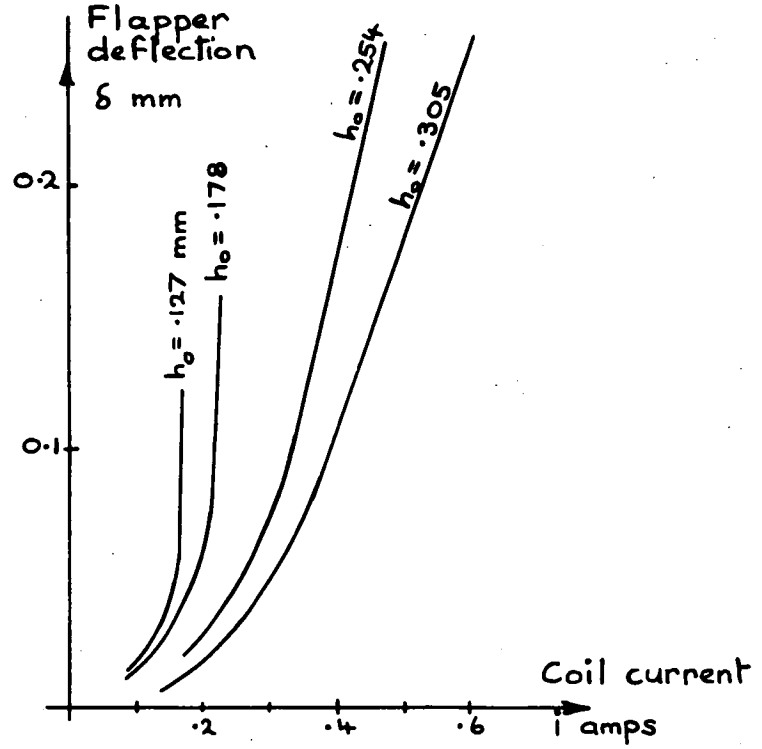

Flapper deflection versus coil current

Figure (3-1)

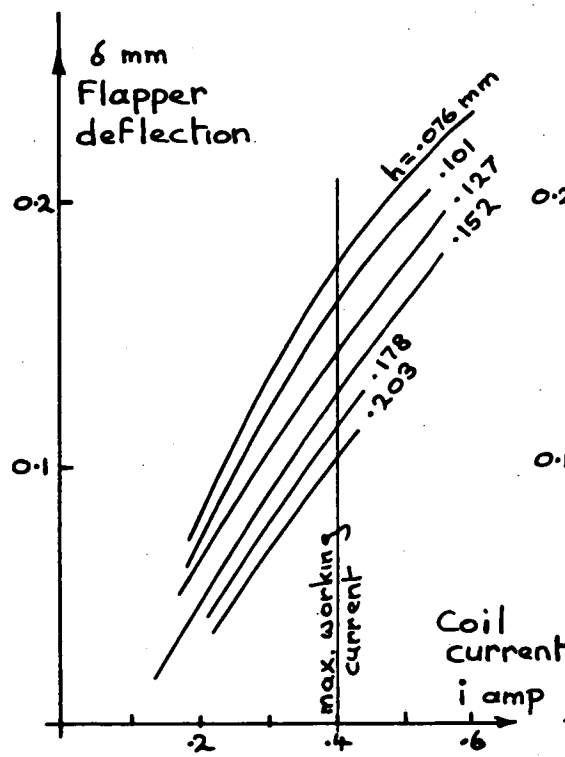

Flapper deflection versus coil current at constant gap

Figure (3-2)

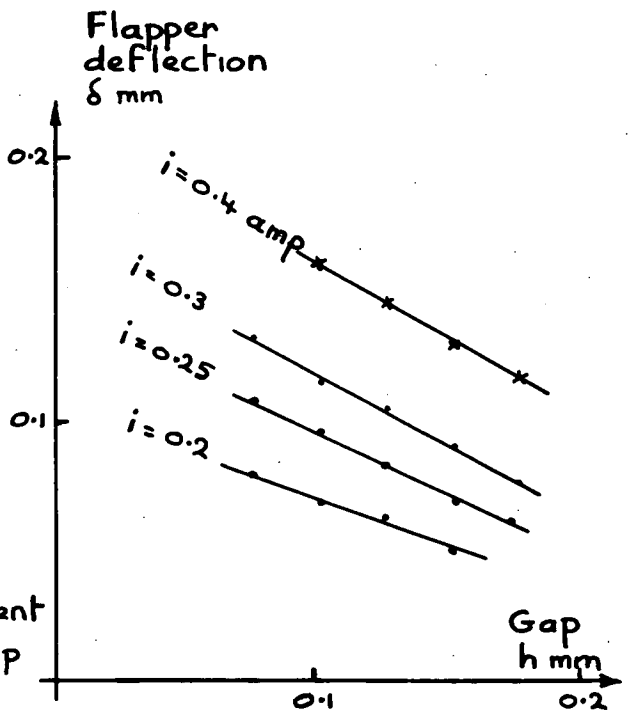

Flapper deflection versus gap at constant coil current

Figure (3-3)

3.6.3 Experimental Results

Results are recorded in figure (3-1) where the deflection δ is plotted against coil current i. δ is the deflection of the target point and is related to the magnetic force F by;

$$F = \delta/a_{22}$$

where a_{22} is the influence coefficient representing flapper stiffness at the target point. Alternatively

$$F = (h_o - h)/a_{22}$$

where h_o is the initial gap setting and h is the actual gap length.

Since F depends upon both i and h the perturbed equation is

$$F_{PERT.} = \left(\frac{\partial F}{\partial i}\right)_{const.h} i_{PERT.} + \left(\frac{\partial F}{\partial h}\right)_{const.i} h_{PERT}$$

The results are therefore reorganised in figures (3-2) and (3-3) to show the variation of δ with i at constant h, and the variation of δ with h at constant i.

Figure (3-2) indicates that saturation effects occur above 0.1 amp coil current. Curves are not defined near the origin but from theoretical considerations they should start at the origin and increase as i^2. Above 0.15 amps curve slope is fairly constant which suggests that working values of i should be restricted between 0.15 and 0.4 amps, the latter being the maximum recommended by the manufacturer. In this case all curves are approximated to straight lines converging at i = 0.05 amps, and

$$\delta \alpha (i - 0.05) \text{ at constant h.}$$

From theoretical considerations the curves in figure (3-3) should start at some value δ_o when h = 0 and reduce in proportion to $(1 + bh)^{-2}$. The figure shows that when δ is plotted against h there is a linear relationship over the range considered. Curve fitting to the theoretical equation gives

$$f(i) = (i - 0.05$$

and $$\delta = \frac{1.05\ (i - 0.05)}{(1 + 3.81)^2}$$ in the working range

where δ and h are in mm and i is in amps.
At equilibrium when i = 0.25 amps and h = 0.13 mm

$$\left(\frac{\partial \delta}{\partial i}\right)_{\text{const.h}} = 0.47 \text{ mm/amp}$$

$$\left(\frac{\partial \delta}{\partial h}\right)_{\text{const.i}} = -0.45$$

These two values compare favourably with those scaled from figures (3-2) and (3-3).

Since $F = \delta / a_{22}$ the perturbed equation becomes

$$F_{PERT} = 42.5\ i_{PERT} - 40818\ h_{PERT}$$

where F is in newtons, i is in amps, and h is in metres.

3.7 Flapper valve flow characteristics

Flapper valve flow characteristics are mentioned by Merritt [1] in section 5-9 and by McCloy and Martin [2] in section 2.10.

Merritt bases his analysis on reference (3) and states that flow is governed by the equation

$$q = C_Q\ \pi\ dh\ \sqrt{(2\Delta\ p/\rho)}$$

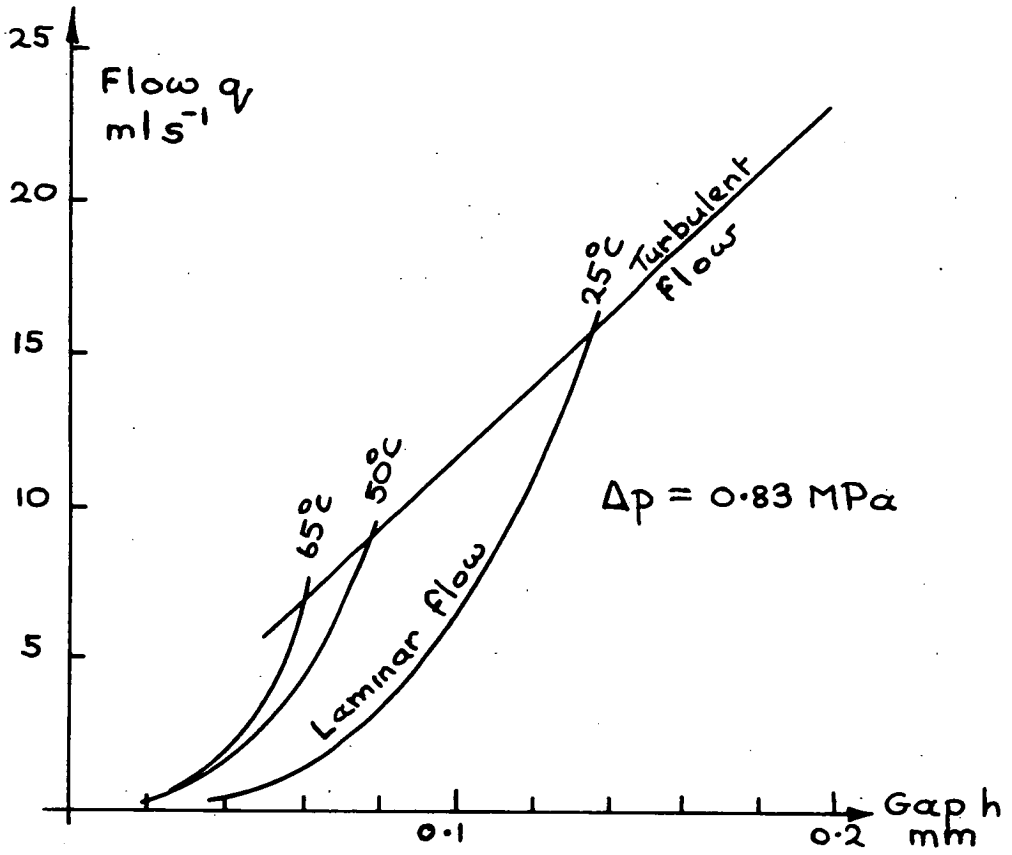

Estimated Flapper valve Flow at const. pressure

Figure (3-4)

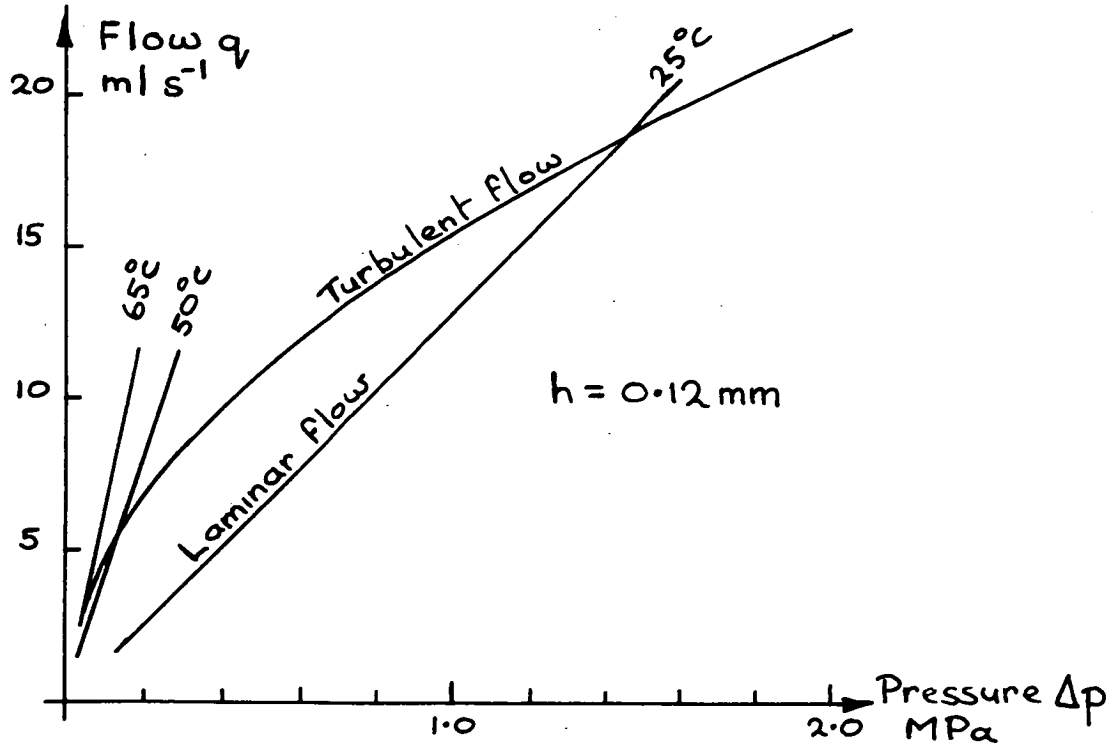

Estimated Flapper valve Flow at const. gap

Figure (3-5)

where C_Q is the flow coefficient, d is the orifice diameter, h is the gap, Δp is the pressure drop and ρ is the oil density. C_Q is expected to be about 0.6 provided land length beside the orifice hole is less than twice the gap, but C_Q increases for greater land lengths and can exceed 0.9 at high Reynolds numbers. The Vickers nozzle shown in figure (2-3) has a flat end 3.35 mm dia. terminated by a step 0.45 mm high and then a further flat surface 9.27 mm dia. with two spanner flats cut into it. This design does not conform to standard designs considered in the references but approximates to a flat ended nozzle of 3.35 mm diameter.

McCloy and Martin note that laminar flow prevails at low Reynolds numbers and Feng's[4] results support this point. Under these conditions for a standard flat ended nozzle

$$q = \frac{\pi h^3 \Delta p}{6 \mu \log(D/d)}$$

where D is the outer diameter, d is the nozzle diameter, μ is the absolute viscosity, h is the gap length and Δp is the pressure drop.

This equation is likely to apply at low flow rates where flow will become temperature dependant because μ appears in the denominator. Under these conditions the effective value of D is likely to be 3.35 mm since the nozzle face step is large in relation to an anticipated gap length of 0.13 mm.

3.7.1 Theoretical flapper valve oil flow

The two equations in section 3.7 apply at high and low flow rates respectively and a transition point or area is anticipated at some intermediate flow rate.

C_Q in the first equation must be estimated from sparce information. Merritt's comments indicate a value above 0.6 because orifice land length exceeds twice the gap, (it is about nine times gap length), but Reynold's numbers are low and the high value of 0.9 is not therefore expected. A value of 0.75 is possible and is assumed here for theoretical purposes.

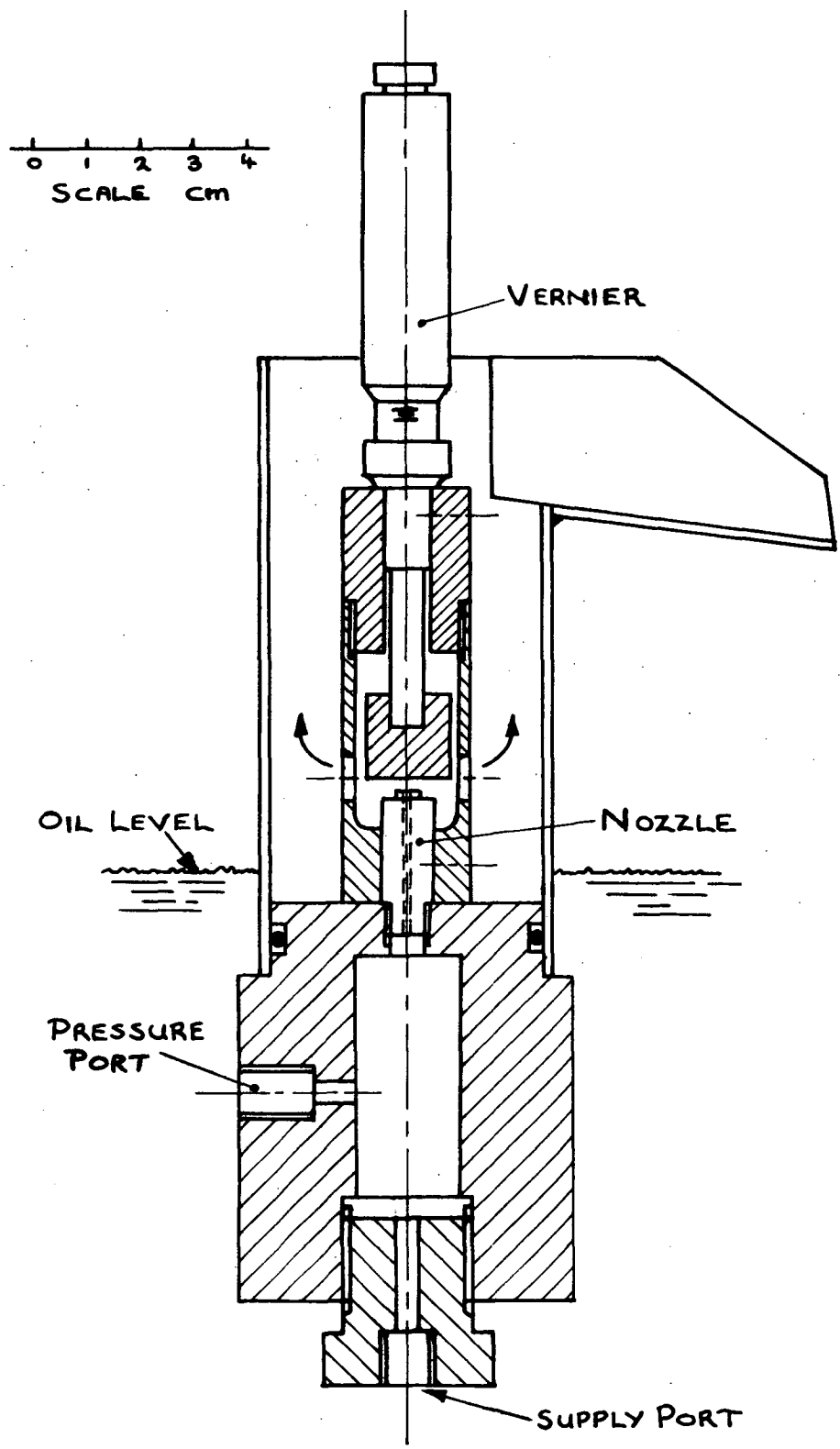

Flapper valve Flow characteristics

Test rig

Figure (3-6)

hence assuming;

$\rho = 854 \text{ kg m}^{-3}$ $\quad d = 1.143$ mm

$C_Q = 0.75$ $\quad D = 3.35$ mm

For Turbulent flow

$$q = 130.4\ h \sqrt{\Delta p} \quad \text{mls}^{-1}$$

For laminar Flow

$$q = 486.9\ h^3\ \Delta p/\mu \quad \text{mls}^{-1}$$

where h is in mm, ΔP is in MPa, and μ is in Nsm^{-2}.

Figures (3-4) and (3-5) show the theoretical characteristic flow curves at known equilibrium conditions for three oil temperatures ranging from 25°C to 65°C, which is the maximum recommended.

Figure (3-4) predicts the transition point location when Δp is held constant and h is varying. It indicates that flow is laminar below 10 mls^{-1} at an oil temperature of 50°C. At equilibrium flow of 16.5 mls^{-1} the predicted gap is 0.14 mm.

Figure (3-5) predicts the transition point location when h is held constant and Δp is varying. It occurs at flows less than 6 mls^{-1} provided the oil has warmed up to 50°C. Equilibrium pressure is about 0.83 MPa which is remote from the transition point.

The above figures indicate that the flapper valve will operate above transition point provided oil temperature exceeds 50°C.

3.7.2 Experimental flapper valve oil flow characteristics

The nozzle was removed from the servo-valve and mounted as shown in figure (3-6) so that nozzle flow impinged on a flat target surface which could be accurately positioned by a vernier with 0.01 mm graduations. Oil pressure was measured by a semi-conductor transducer attached to the pressure port and oil flow rate was measured by timing flow into a measuring jar. In order to maintain oil temperature constant the brass mounting block was immersed in hot oil contained in the 100 litre pump supply tank and, in addition, supply oil was passed through a small bore copper coil,

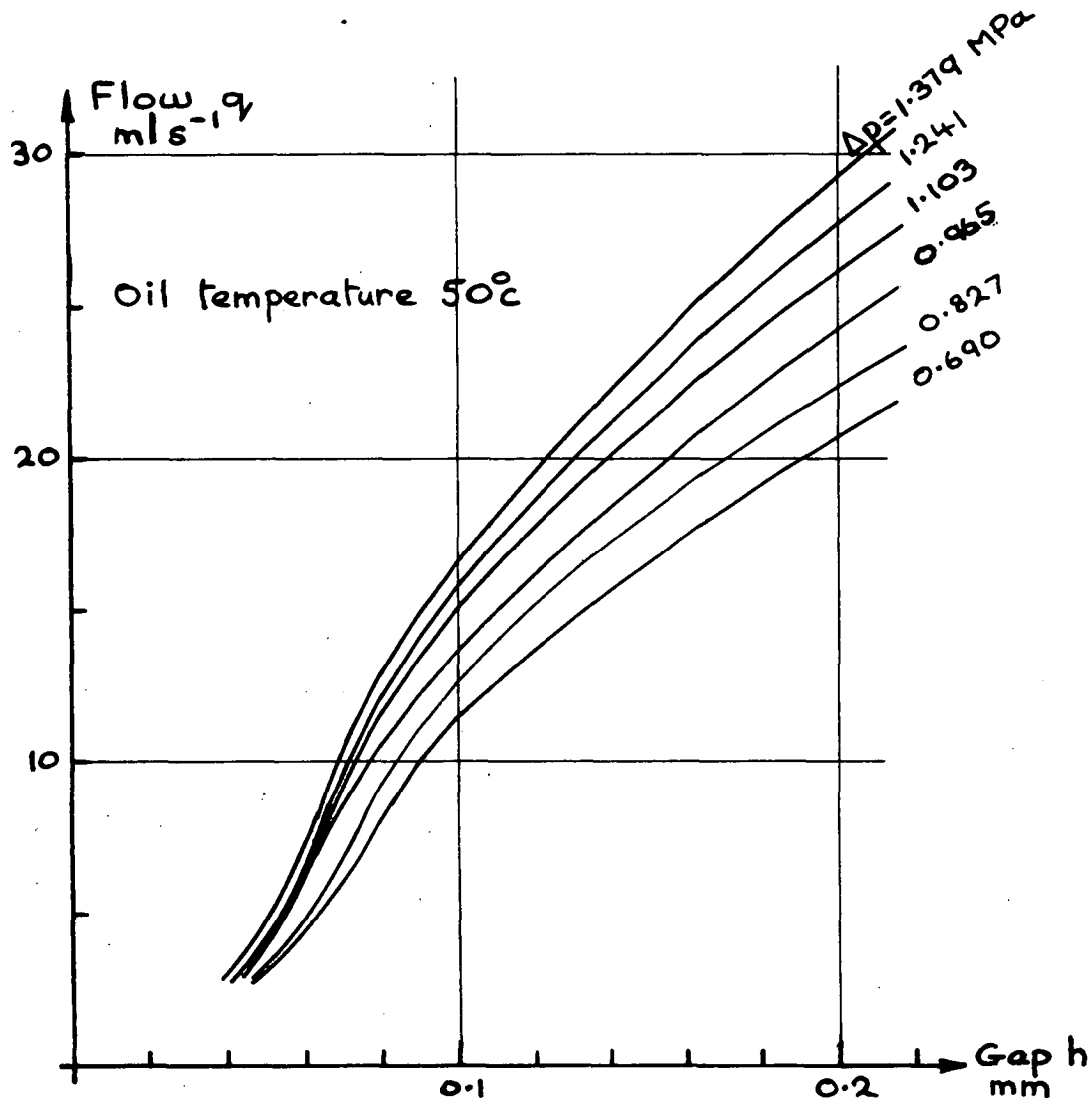

Flapper valve oil flow versus gap at constant pressure drop Figure (3-7)

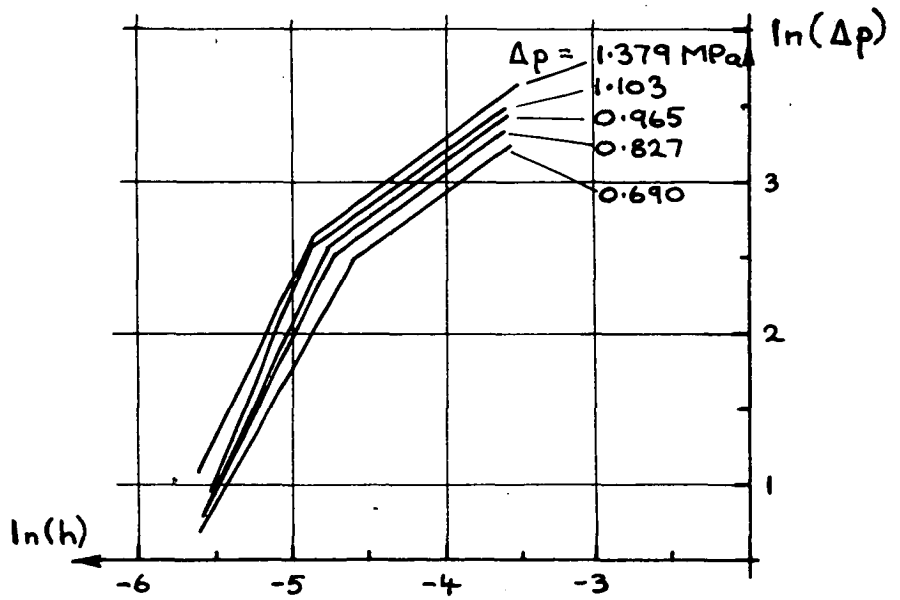

Log(q) versus log(h) at constant Δp
Figure (3-8)

also immersed in the supply tank, before being connected to the supply port.

Oil temperature in the supply tank was maintained constant by placing a water cooled heat exchanger in the pump relief valve return line so that surplus heat could be removed from the system. Tank oil was stirred to ensure adequate circulation and oil temperature was measured by thermometers placed in the tank, and in the nozzle outlet flow. In this manner oil temperature was controlled to within $1\frac{1}{2}^{o}C$.

A series of tests were run at $50^{o}C$ oil temperature to measure the flow rate at constant pressure drop for varying gap length, and also to measure the flow rate at constant gap for varying pressure drop.

At gaps below 0.07 mm it was difficult to obtain repeatable flow measurements and results were slightly scattered but larger gaps gave repeatable results.

3.7.3 Experimental Results

Experimental results are recorded in figures (3-7) and (3-9).

Figure (3-7) clearly shows the two flow patterns expected before and after the transition point which occurs at about 12 mls^{-1}. Below this figure q increases to a power of h greater than 1, but above it q clearly increases at some power of h which is less than 1. The above results are plotted on a logarithmic scale in figure (3-8) to find the powers of h mentioned above. Below the transition point the curves have an average slope varying between 2 and 3 due to scattered results obtained at gap measurements below 0.7 mm, but above the transition point all curves closely approximate to straight lines with a slope of 0.7. From figure (3-8) it is concluded that $q \propto h^{0.7}$.

Figure (3-9) shows the results of tests conducted at gap lengths above 0.09 mm, and consequently at flows beyond the

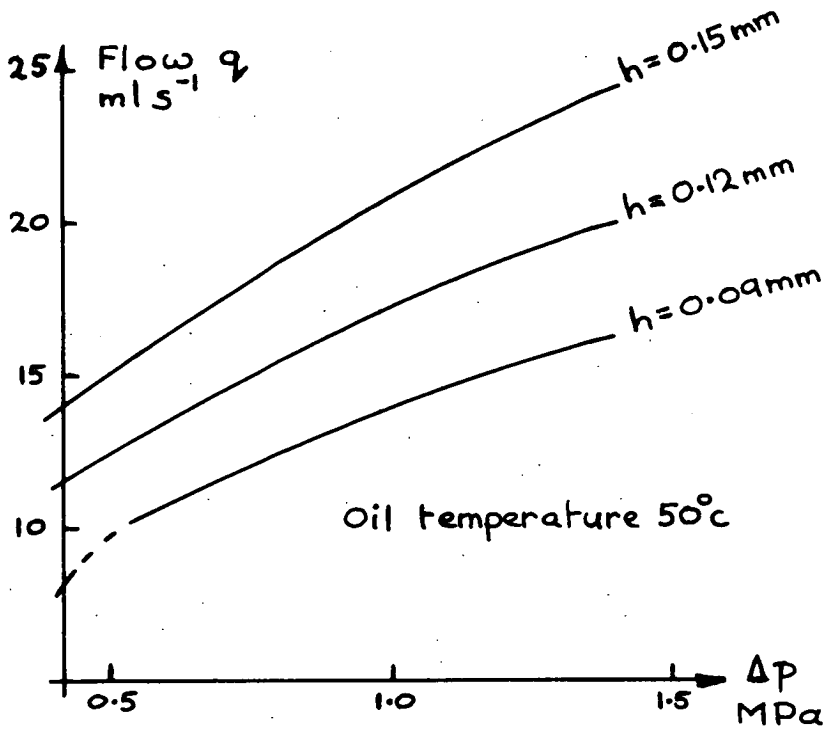

Flapper valve oil flow versus pressure drop at constant gap

Figure (3-9)

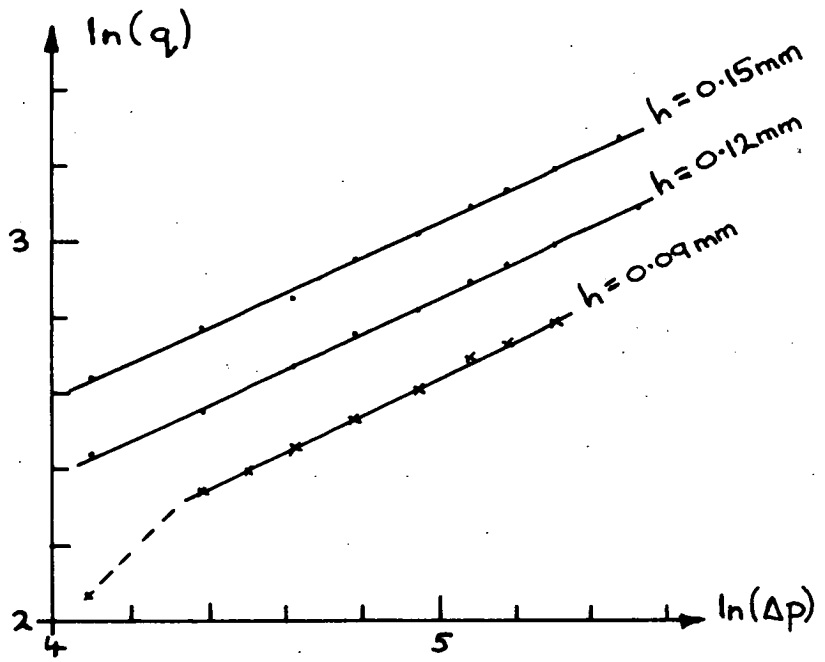

Log (q) versus log (Δp) at constant h

Figure (3-10)

transition value. The transition point is not in evidence except at the dashed end of the curve for h = 0.09 mm. Plotted on logarithmic scales as in figure (3-10) the results are excellent approximations to straight lines in all three cases, the respective slopes being:

h	slope
.09 mm	0.480
.012 mm	0.472
.015 mm	0.480

Equilibrium conditions given in section 3.2.1 indicate that $q = 16.5$ mls^{-1} and $\Delta p = 0.82$ MPa which enables the equilibrium gap length h_o to be estimated from figure (3-7) as $h_o = 0.13$ mm. Hence the slope values above are interpolated to give a mean slope of

$$0.472 + (0.480 - 0.472)/3 = 0.4747$$

and it is concluded that $q \propto (\Delta_p)^{0.475}$ in the working region.

3.7.4 Experimental Flapper valve Flow equation

From the previous section

$$q = (\text{Constant}) h^{0.7} (\Delta p)^{0.475}$$

and at equilibrium condition

$$q = 75.624\ h^{0.7} (\Delta p)^{0.475} \text{ mls}^{-1}$$

when h is in mm and Δp is in MPa.

3.7.5 Experimental flow coefficient

Reynolds number for a flat ended nozzle is

$$R = \frac{2\ q\ \rho}{\pi\ d\ \mu}$$ which becomes

$$R = 22.65\ q \quad \text{at } 50^{\circ}C$$

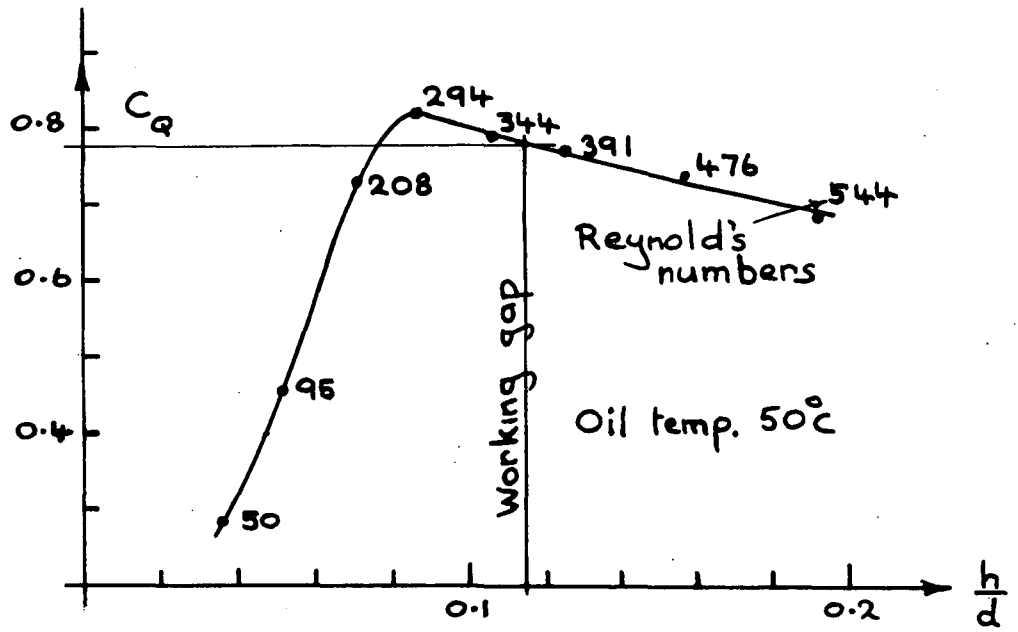

Variation of flapper valve flow coefficient with gap ratio Figure(3-11)

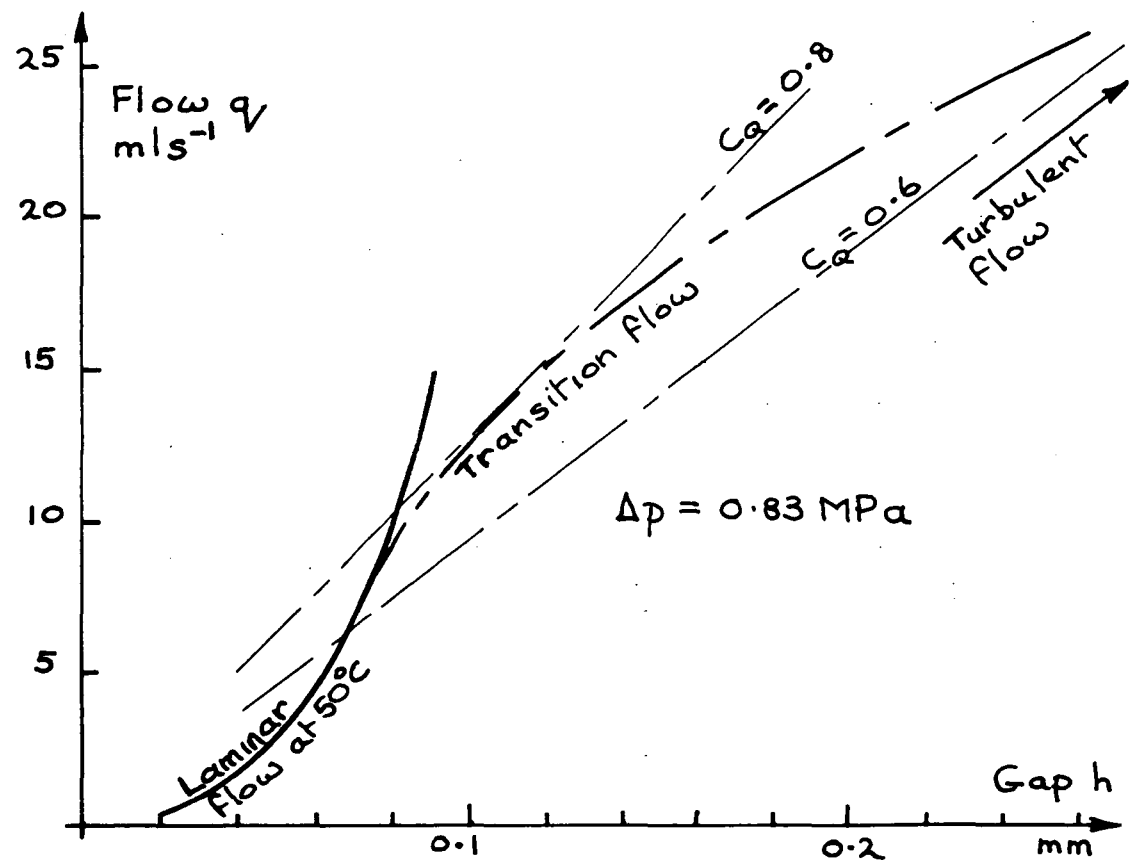

Method of approximating the flapper valve flow characteristic in the transition region Figure (3-12)

when ρ = 854 kgm^{-3}, μ = 0.021 Nsm^{-2}, d = 1.143 mm and q is in mls^{-1}.

Working from the curve for h = 0.827 MPa in figure (3-7) and using the equation

$$C_Q = q/(\pi dh \quad (2\Delta p/\rho))$$

Figure (3-11) shows the variation of C_Q with gap h and with Reynold's number.

Feng's results indicate that C_Q tends to a value of 0.6 at ratios of h/d greater than 0.2 when using a flapper nozzle with diameter ratio D/d = 3.42, and figure (3-11) shows the same trend although h/d is higher and D/d is 2.93. It is clearly an advantage to predict C_Q accurately without experimental tests and the figure suggests that nozzles should be designed to operate at Reynold's numbers above 700 and h/d ratios above 0.25 in which case C_Q is close to 0.6.

Figure (3-12) is a development from the theoretical curve in figure (3-4) which is oversimplified because the transition flow region is not included. Laminar flow prevails at low flow rates and turbulent flow occurs at high flow rates when C_Q is 0.6. For nozzles with a diameter ratio D/d of about 3 the maximum value of C_Q should be around 0.8. Turbulent flow lines are drawn corresponding to C_Q = 0.6 and 0.8 and the laminar flow curve is also drawn at the anticipated oil temperature. The transition flow curve is then sketched in as a natural extension of the laminar flow curve which touches the upper turbulent flow line and merges with the lower turbulent flow line at h/d > 0.25.

For present purposes the nozzle operates in the transition region where C_Q is a variable and the flow equation in section 3.7.4 is therefore used because it can be perturbed more accurately than an equation involving C_Q.

3.8 Estimation of spool underlap

Measurements of spool underlap were difficult to obtain accurately due to inaccessibility of the circular orifices and bye-pass flow tests were conducted to provide further information.

The servo-system was stabilised at equilibrium condition and total bye-pass flow in the tank return line was measured at two supply pressures. Results were:

p_1 = 6.895 MPa $\quad\quad$ q_L = 26.8 mls^{-1}

p_1 = 13.79 MPa $\quad\quad$ q_L = 39.9 mls^{-1}

When the spool is at centre position small segmental orifices are exposed at either side of the spool lands allowing flow to bye-pass. The first orifice throttles flow from supply pressure to one half of supply pressure, and the second orifice then throttles it to tank return pressure. There are four such leakage paths and calculations show that the orifice segmental height required for the measured flows is 0.1 mm assuming a flow discharge coefficient of 0.75. Reference (2) states that small openings give rise to lower discharge coefficients at low Reynold's numbers where oil viscosity becomes more significant, but the results indicate turbulent flow because q_L is proportional to the square root of P_1 consequently the orifice flow coefficient should be similar to the assumed value in section A3.4.5.

By comparison with measured underlap of 0.045 mm the discrepancy appears too large to be explained by measurement errors and is probably due to rounded orifice edges, in which case orifice area may be significantly increased at small openings but the effect is likely to be less significant at large openings.

In the absence of more preçise information 'effective' orifice underlap is assumed to be 0.075 mm at this stage.

REFERENCES

(1) Merritt, Herbert E.
Hydraulic Control Systems
John Wiley & Sons. Inc.

(2) McCloy, D. and Martin, H.R.
The Control of Fluid Power.
Longman.

(3) Lichtarowicz, A. and Markland, E.
Journal of Fluid Mechanics
vol. 17, Pt. 4, December 1963, C.U.P., England.

(4) Feng, T.Y.
Static and dynamic control characteristics of flapper nozzle valves.
Trans. ASME (1959) 81, Series D.

CHAPTER 4

4.1 Introduction

In this chapter a linear mathematical model of the servo-system shown in figure (2-4) is developed and solved by digital simulation.

4.2 Selection of state-variables

Selection is made with reference to section 1.3.1 and figure (2-4).

4.2.1 Mass position state-variables

Spool y and $\dot{y}$

Ram $\dot{n}$

n would also be chosen if there were any ram forces proportional to it (i.e. a spring load).

Flapper

Movement of the flapper mass is small and is neglected in this analysis.

4.2.2 Pressure state-variables

Pressure P_1

P_1 is constant in this analysis.

Pressures P_2 and P_3

P_2 and P_3 apply to small oil volumes which are regarded as incompressible.

Pressure P_4

The volume of oil at P_4 is significant but P_4 is small and has little effect on system performance. This oil volume is regarded as incompressible.

Pressures P_5 and P_6

P_5 and P_6 are combined to form the load pressure $P_L = P_5 - P_6$, which is a state-variable.

4.2.3 Selected state-variables

$\dot{y}$ y P_L $\dot{n}$

4.3 System equations

Appendix 3 records the detailed derivation of the perturbed system equations (A3-1) to (A3-12).

In order to linearise the equations, significant assumptions are made in the sections discussed below.

4.3.1 Section A3.4.5

The value assigned to C_Q is very important because valve flow, and consequently the system gain, is proportional to C_Q. Published data is fairly precise and the value of 0.75 should be accurate to within 5% provided the orifice opening is large enough to establish turbulent flow. At very small orifice openings C_Q decreases with Reynolds number.

Values assigned to C_C and θ are not readily determined from published data and are estimated from data relating to linear spool valve orifices. Both vary with orifice opening. At very small openings viscous effects dominate and flow adheres to the orifice edge in which case θ is 90° and jet forces are zero. At an opening of approximately three times spool radial clearance flow breaks away and θ increases with orifice opening from 21° to 69° at large openings. The assumed value of θ is not therefore valid at very small orifice openings but resulting errors should be insignificant.

The equation describing jet flow force is perturbed assuming a light ram load when pressure drop across the valve is constant. For a step input the Δp transient is maximum early in the time response when orifice area is small, and becomes small when orifice area is maximum. The term neglected is the product of area and Δp which is therefore small at both extremes of the

time response.

The term A' is linearised by calculating the average value required to give a correct orifice area at maximum opening. This overestimates orifice area at all openings below maximum with a corresponding influence on system response.

4.3.2 Section A3.4.6

A destabilising transient spool force exists having a value $\rho L\dot{q}$ for each damping length considered. Calculations indicate that the resultant force is less than 1.0 $\dot{y}$ and has no significant effect on the equations.

4.3.3 Sections A3.6.2 and A3.6.3

The segmental orifice flow equation is linearised as above.

4.3.4 Section A3.6.4

Oil volumes at pressures p_5 and p_6 are assumed equal and the ram operates close to its central position. This enables the equations for $\dot{p}_5$ and $\dot{p}_6$ to be combined into an equation for $\dot{p}_L$ and reduces the number of state-variables by one.

4.4 Digital solution of the system equations

Program SERVOI.BA was developed to solve the system equations for a step input coil current. It is divided into sections each headed by a REMARK statement.

Spool static condition - line 1015

Using the method described in chapter 3 equilibrium condition of the system is computed for any supply pressure.

Perturbation constants - lines 1105 and 1140

In these sections equilibrium conditions calculated above are substituted into the perturbed equations.

Scaling constants - line 1225

Matrix amplitude scaling constants are defined here as required. Amplitude scaling is not necessary in this program and may be omitted.

Set up equation matrix - line 1260

Equations (A3-1) to (A3-10) contain thirteen variables, nine of which can be eliminated. The ten equations are defined in a two dimensional array which is reduced to a single equation in $\ddot{y}$ $\dot{y}$ y and i.

Rate of change of orifice area - line 1574

The term A' is linearised by calculating the average value required to give correct orifice area at maximum opening, and spool underlap u has a significant influence. Underlap increases orifice area at all openings and introduces a null position gain which is otherwise absent. At equilibrium condition underlap at each end of the spool lands allows flow to pass from supply pressure to ram line pressure, whilst an equal flow passes from the ram line to tank return. Positive spool movement causes an increase in one flow and a corresponding decrease in the other, resulting in a flow gain. This effect continues until spool position y = u when bye-pass flow ceases and orifice area corresponds to an opening of 2u. In the program orifice area is assumed linear from y = 0 to y = u after which the true area is calculated for opening y + u. A trial value of y_m is used to estimate A' by the method in section A3.4.5 and these values are substituted into the equation in $\ddot{y}$ $\dot{y}$ y and i (obtained above) to give the estimated current step. y_m is iterated to give the specified current step.

Figure (4-1) details the orifice area characteristic and demonstrates the strong linearising effect due to valve underlap.

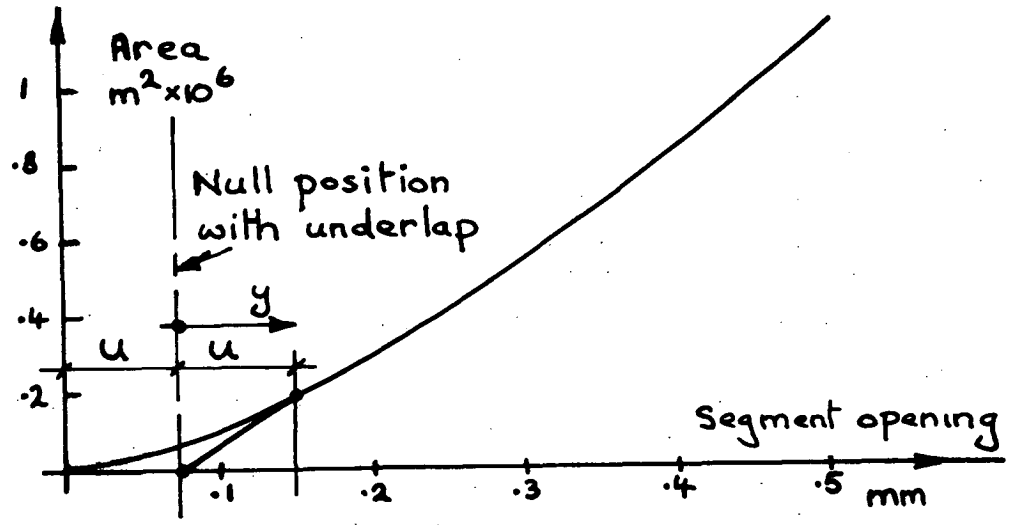

Figure (4-1)

Set up A matrix - line 1602

System equations are assembled into a (4 x 4) A matrix and a (4 x 1) B matrix.

Runge Kutta routine - line 1639

Using the A and B matrices this routine solves the equations by a fourth order method and prints out results.

4.5 Typical system equations

System equations depend upon supply pressure P_1.

P_1 = 6.895 MPa

$$\dot{X} = \begin{bmatrix} -22486 & -.103E7 & 0 & 0 \\ 1 & 0 & 0 & 0 \\ 0 & .507E13 & 0 & -.965E10 \\ 0 & 0 & .288E-3 & -333 \end{bmatrix} \begin{Bmatrix} y \\ y \\ P_L \\ n \end{Bmatrix} + \begin{bmatrix} 6984 \\ 0 \\ 0 \\ 0 \end{bmatrix} \{i\}$$

Eigenvalues are

X1 = -45.93
X2 = -166.6 + 1658 i
X3 = -166.6 - 1658 i
X4 = -2240

P_1 = 13.79 MPa

$$\dot{X} = \begin{bmatrix} -29178 & -.178E7 & 0 & 0 \\ 1 & 0 & 0 & 0 \\ 0 & .711E13 & 0 & -.965E10 \\ 0 & 0 & .288E-3 & -333 \end{bmatrix} \begin{Bmatrix} y \\ y \\ P_L \\ n \end{Bmatrix} + \begin{bmatrix} 11513 \\ 0 \\ 0 \\ 0 \end{bmatrix} \{i\}$$

Eigenvalues are

X1 = -61.3
X2 = -166.6 + 1658 i
X3 = -166.6 - 1658 i
X4 = -29117

4.5.1 An analysis of matrix elements

The A matrix eigenvalues are easily determined because A can be reduced to two (2 x 2) matrices on the leading diagonal coupled by entry A (3,2). Eigenvalues are not affected by A(3.2) and can be obtained directly from the reduced matrices.

The real negative eigenvalues are approximately equal to A(1,1) and -A(1,2)/A(1,2) and derive from the servo-valve, whilst the complex conjugate pair relates to lightly damped oscillations of the ram and oil lines.

Element A(1,1) derives from the damping areas in equations (A3-5) to (A3-7) and the damping constant in (A3-10). This latter equation contributes only -31 to the total and clearly has negligible effect. In fact this element is largely dominated by equations (A3-6) and (A3-4) containing constant K_3 which is the most significant factor in determining its value. A(1,1) sets the maximum allowable Runge Kutta time interval which is 2.7/22486 = 0.00012s when P_1 = 6895 MPa.

Element A(1,2) is influenced by entries proportional to y in equations (A3-8) to (A3-10) which are spring and pressure feedback forces in the first two equations and jet reaction forces in the third equation. When supply pressure is 6.895 MPa the jet force accounts for about 30% of the value of this element.

Element A(3,2) is a coupling term directly proportional to $A'\sqrt{P_1}$ and since A' is fairly constant at approximately 0.0025 this element is dominated by a P_1 influence.

Elements A(3,4) and A(4,3) are constants and element A(4,4) is a ram damping term directly proportional to the ram damping ratio.

4.6 Performance prediction from system eigenvalues

The two sets of eigenvalues given in section 4.5 indicate there will be a dominant eigenvalue varying between -46 and -61 as supply pressure rises from 7 to 14 MPa. A lightly damped complex conjugate pair exists at 264 Hz, corresponding to the natural frequency of the ram and its oil supply passages, but this is not expected to be significant when the system is excited under light or no-load conditions and at low frequencies. The large negative eigen values should have little effect on system response.

Non-linearities associated with the segmental orifices are expected to influence performance but this effect appears in the coupling term A(3,2) and does not alter the eigenvalues.

4.7 System block diagram

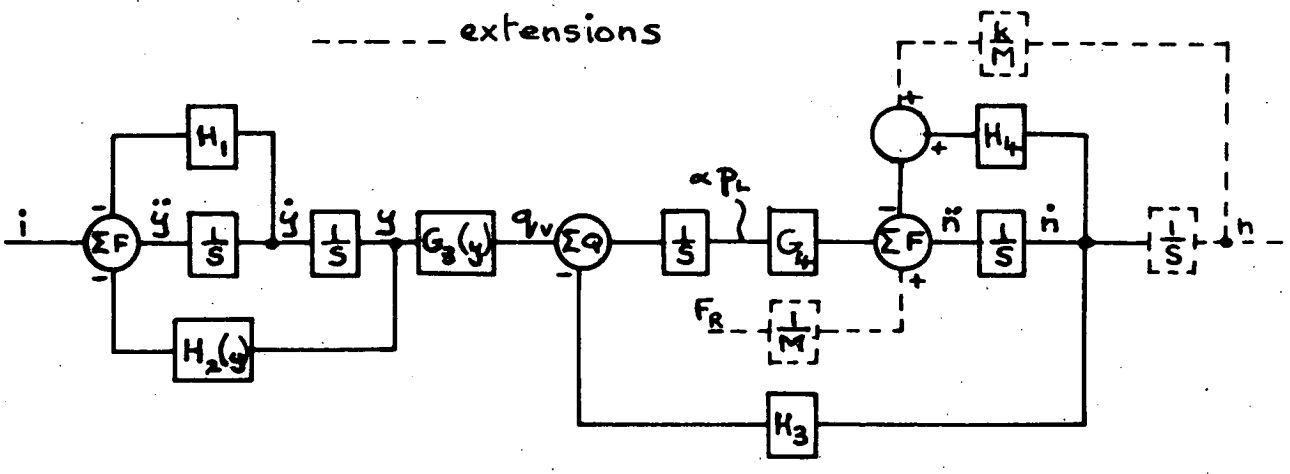

System block diagram Figure (4-2)

Figure (4-2) is the block diagram constructed from the equations in section 4.5.

There are two coupled systems in series represented by the transfer functions

$$\frac{q_v(S)}{i(S)} \quad \text{and} \quad \frac{n(S)}{q_v(S)}$$

which are identified as the servo-valve and the ram and oil lines respectively. Non-linearities exist in the functions $H_2(y)$ and $G_3(y)$ both of which have been linearised in program SERVO1.BA to make these terms constant. This is most easily achieved for $H_2(y)$, which represents force feedback on the valve spool due to ram oil flow, because it is 70% constant with only 30% dependance upon A' (and hence y). $G_3(y)$ represents the segmental orifices which set the ram oil flow and is directly proportional to A'.

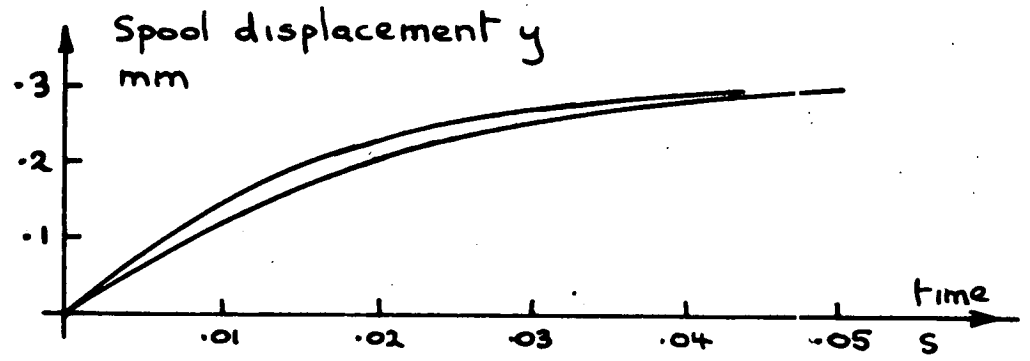

Valve spool response to a current step Figure (4-3)

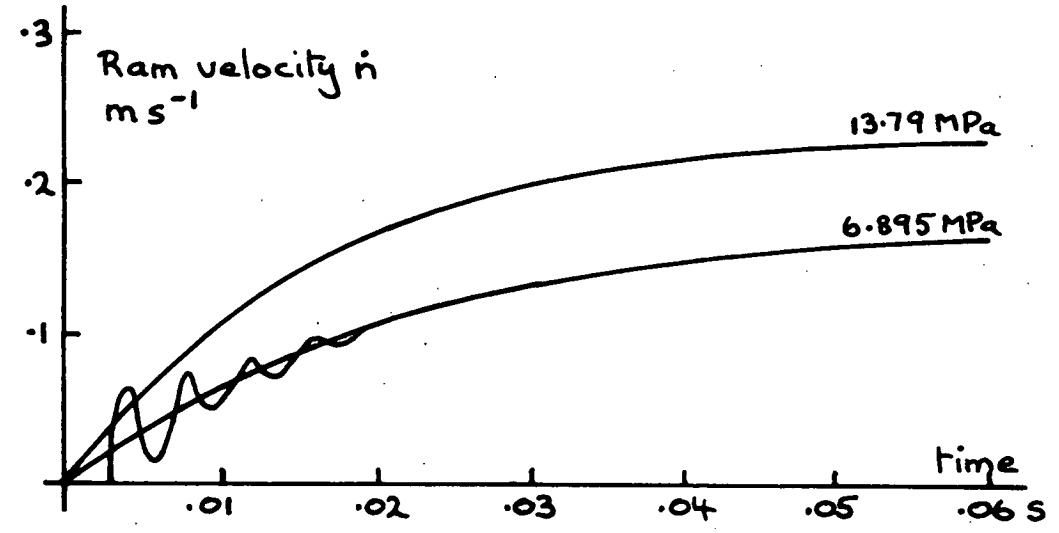

Ram velocity response to a current step Figure (4-4)

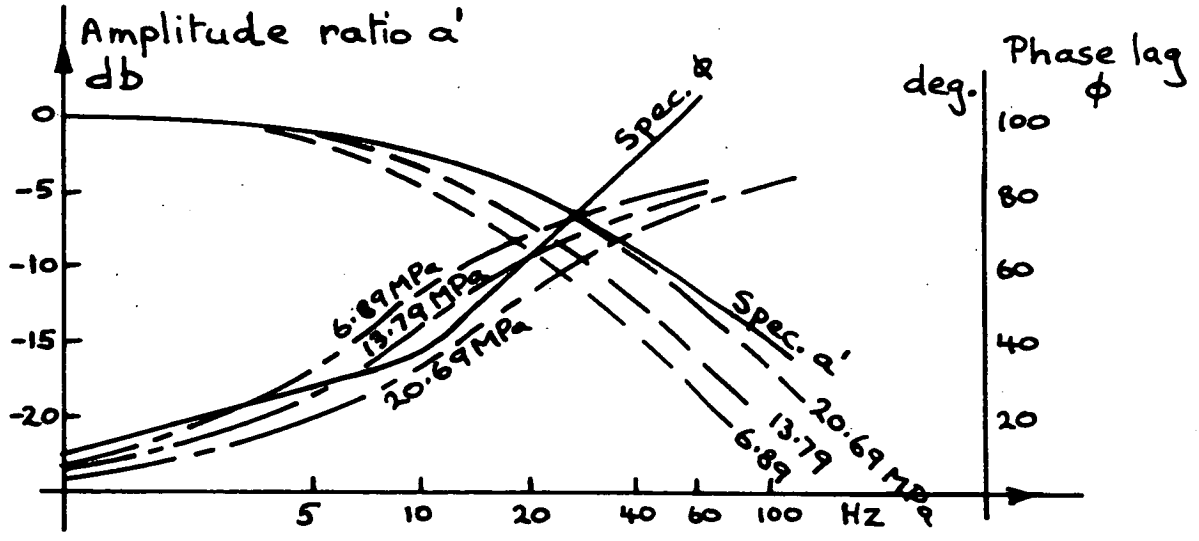

Frequency response Figure (4-5)

The overall transfer function is;

$$\frac{n(S)}{i(S)} = \frac{G_3}{(S^2 + H_1 S + H_2)} \times \frac{G_4}{(S^2 + H_4 S + G_4 H_3)}$$

Figure (4-2) does not include feedback from P_L which exists as a minor effect provided the load pressure perturbation is small. If included there is feedback from P_L to both q_v and the input force summing junction, the former being most significant.

4.7.1 Extended block diagram

Extensions to figure (4-2) are shown in dashed lines and allow for a ram force perturbation F_R and a spring load proportional to ram displacement m. System order is increased from 4 to 5 which is inevitable in any case since positional feedback from n to i must be included eventually.

4.8 Servo-valve frequency response

Figure (4-5) shows frequency responses for the servo-valve only based on the transfer function in section 4.7.

Results are compared with the manufacturer's 'typical response curve' (at unspecified pressure). Predicted response is very similar at P_1 = 21 MPa which is the maximum valve pressure rating. The program predicts a maximum phase lag of 90^o at high frequency whereas the specification indicates larger phase lags above 30 Hz but there is a good match over the normal operating range of the servo-valve.

4.9 System response to a step input

The results shown in figures (4-3) and (4-4) are obtained from program SERVO1.BA using a time increment of 0.5×10^{-4} seconds.

The program gives equilibrium conditions as follows:

P_1 MPa	P_2 MPa	P_3 MPa	P_4 MPa	q mls^{-1}	h mm
6.895	1.467	0.824	0.044	16.49	0.1344
13.789	2.860	1.565	0.088	23.40	0.1437
20.684	4.254	2.306	0.134	28.69	0.1479

As anticipated time responses are dominated by one real negative eigenvalue and the oscillation is not in evidence unless specifically excited. This latter effect is achieved in figure (4-4) by inserting a program statement to hold the ram stationary for 0.003s after the current step is applied.

4.10 Concluding comments

The linearised program gives reasonable results but the major linearising assumptions are made when dealing with the segmental orifices which control system gain. A non-linear program is developed later paying particular attention to these orifices.

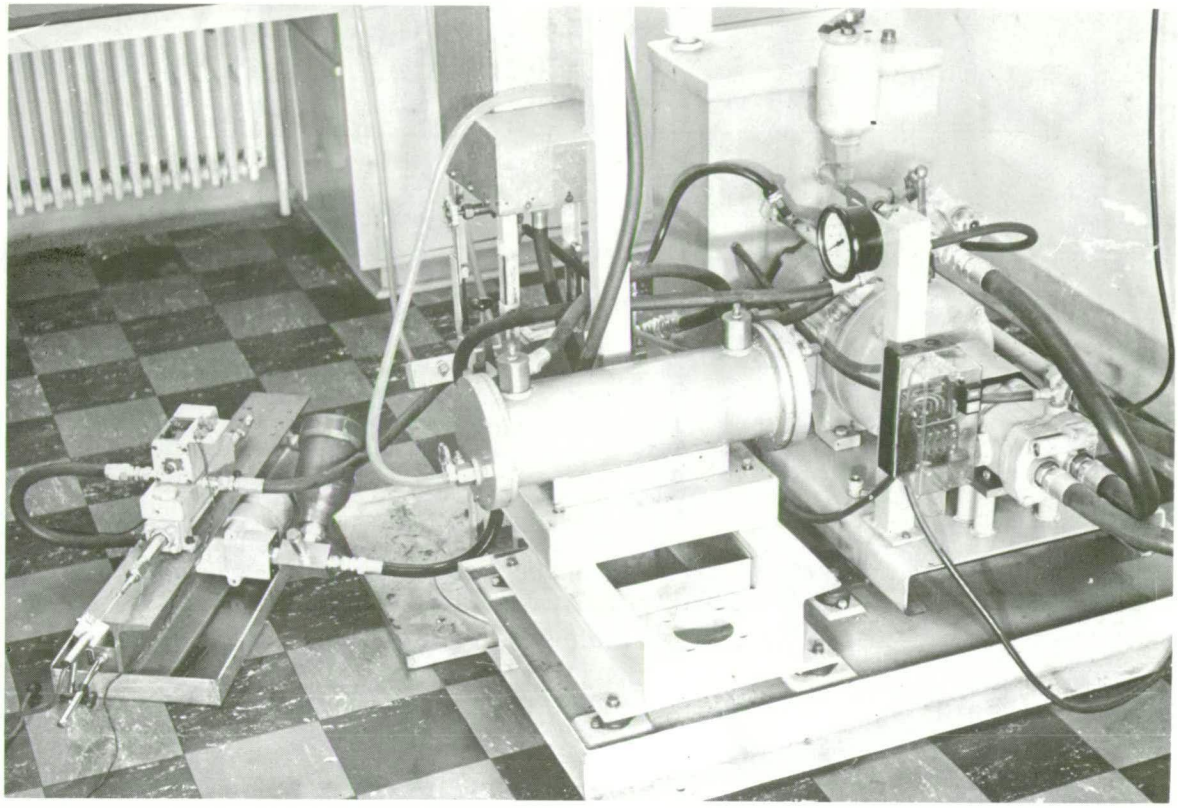

CHAPTER 5

5.1 Introduction

This chapter contains a description of the hydraulic circuit, instrumentation and experimental procedures employed to obtain dynamic responses of the servo-system.

5.2 Hydraulic Circuit

All tests were conducted on an existing hydraulic test facility previously described in reference (1) but modified slightly as required for present purposes.

The circuit, shown in figure (5-1), employs a variable displacement pressure compensated pump and an adjustable pressure relief valve, either of which can be used to control delivery pressure. Two accumulators minimise pressure pulsations in the delivery line one being located close to the servo-system to maintain constant supply pressure at that point under variable flow test conditions. Pump flow is much larger than system requirement at all times allowing a large flow of excess oil through the heat exchanger which is cooled to control oil temperature. Fine and coarse mesh filters are fitted in the 'system' supply and return lines respectively and shut off values are conveniently located to isolate the 'system'. All circuit components are rated at 21 MPa except the pump and relief valve which have a 14 MPa rating.

Major circuit component specifications are listed below:

Pump - Vickers type PVB-10-RSY-20-CM-10
Relief valve - Vickers CT-06-C
Servo valve - Vickers SF4-100-30-002-10
Ram - Vickers W30-FL-NC-HH-FT-IR-5H-2
Motor - 10HP/1440 RPM
Accumulators - Greer Mercier, size 1 quart

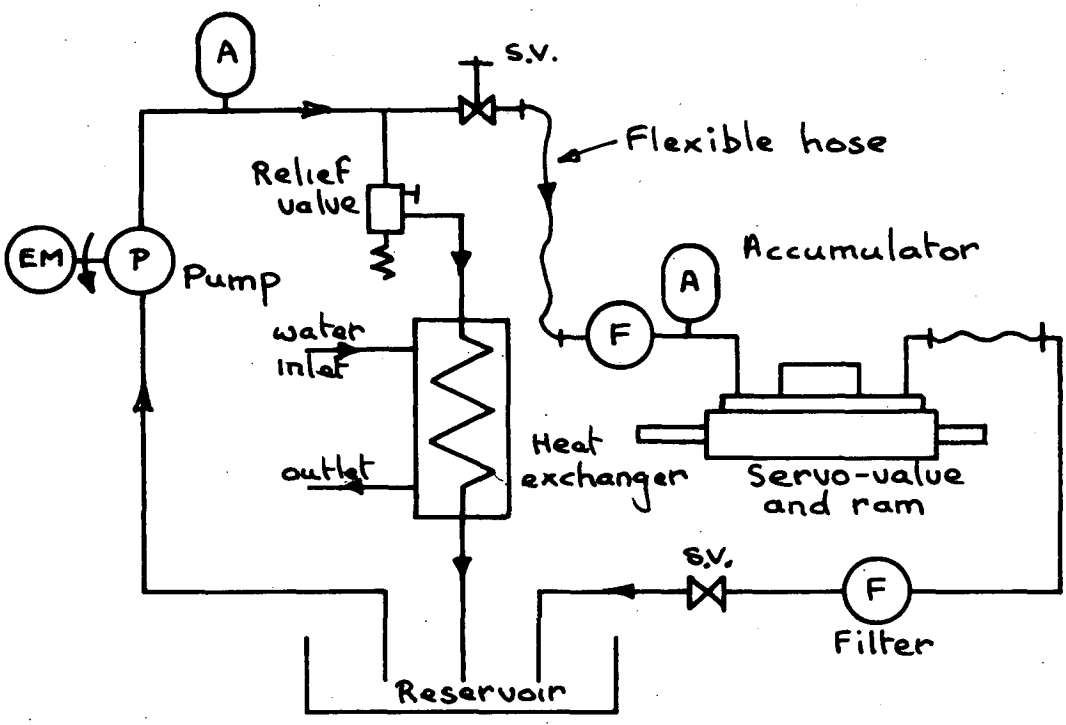

Hydraulic circuit - Figure (5-1)

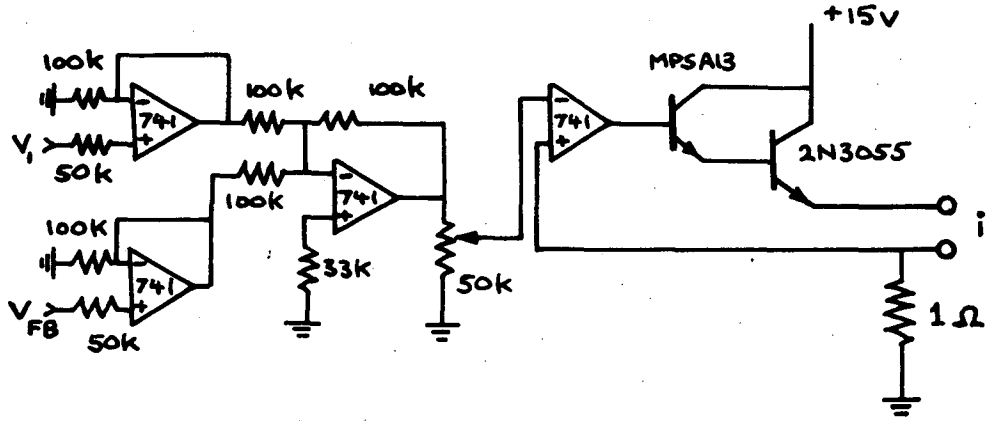

Precision current source - Figure (5-2)

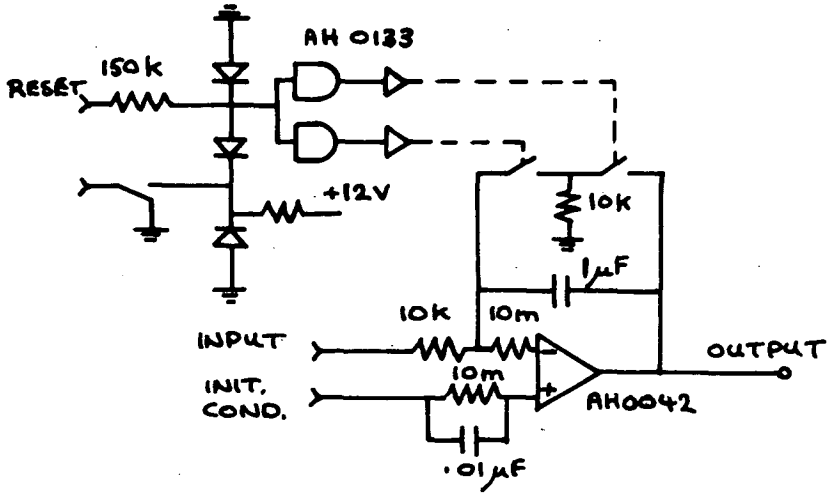

Active integrator Figure (5-3)

The above circuit proved satisfactory for the work undertaken, supply pressure fluctuations being very small and oil temperature being the only variable requiring attention during operation. Reservoir temperature was readily controlled by the heat exchanger but it tended to alter quite rapidly at high delivery pressure (high heat input) and needed constant correction. Automatic control of oil temperature would have been an asset for the tests undertaken, and would be essential for long run testing, but no suitable control equipment was readily available at the time. There was also a tendency for oil to cool in the servo-valve supply lines due to low flow rates when the valve was stabilised at centre position prior to a step input test. This was not too serious because spool underlap bye-pass flows were significant (see section 3.8) but the problem was overcome by oscillating the ram for some time immediately prior to a test in order to circulate a large flow of hot oil. In retrospect the circuit could have been fitted with a bye-pass line across the servo-valve controlled by a needle valve, to increase flow through 'system' supply lines.

5.3 Experimental control and measurement techniques

Control and measurement techniques were developed for tests to determine open and closed-loop dynamic responses of the servo-system to stepped and sinusoidal inputs. Specific items are described in the following sections.

5.3.1 Precision current source

This was developed to power the servo-valve coil to eliminate phase shifts encountered using a voltage source, and was designed to produce an output current proportional to the sum of two input voltage signals with negligible phase error. The current source was designed to be controlled by the computer and was constructed as a plug board for the computer I/O bus.

With reference to figure (5-2) two input signals V_1 and V_{FB} are summed and fed through an inverting amplifier to a calibration resistor. V_1 is programmed to vary between 0 and -10V and V_{FB} is an external signal from the ram position feedback amplifier. The calibrated voltage signal controls an operational amplifier which drives the heavy output transducer to control voltage drop across a precision one ohm resistor in such a manner that both amplifier inputs are at the same voltage potential. Output current is therefore proportional to the sum of V_1 and V_{FB} and is independent of load impedance, provided the load is sufficiently low to pass the current from a 15V supply. In practice the servo-valve coil has 20 ohms resistance and the circuit is calibrated at 20V/amp to a maximum of 0.5 amps.

Tests were conducted on the current board to check its response to stepped and sinusoidal inputs under operating conditions. Input voltage signals were applied by a signal generator and output current was measured as a voltage drop across a known resistor. Using the sampling program later described both input and output voltages were sampled and plotted to give the results in Appendix 4, figures (A4-1) to (A4-3).

These results show negligible relative phase shift but indicate the presence of a high frequency output ripple and some slight wave distortion. The ripple frequency is deceptive in the results due to periodic sampling and it is best measured from the step response where it is above 3KHz and too high to be significant. Wave distortion probably results from board design layout. The board has three grounded points which return to a single terminal and it is thought that some small voltage feedback could result and cause distortion. A better design would be to run an independent earth wire for the main current path through the one ohm resistor. However the response distortion was small and the current board was regarded as acceptable and used in all subsequent tests.

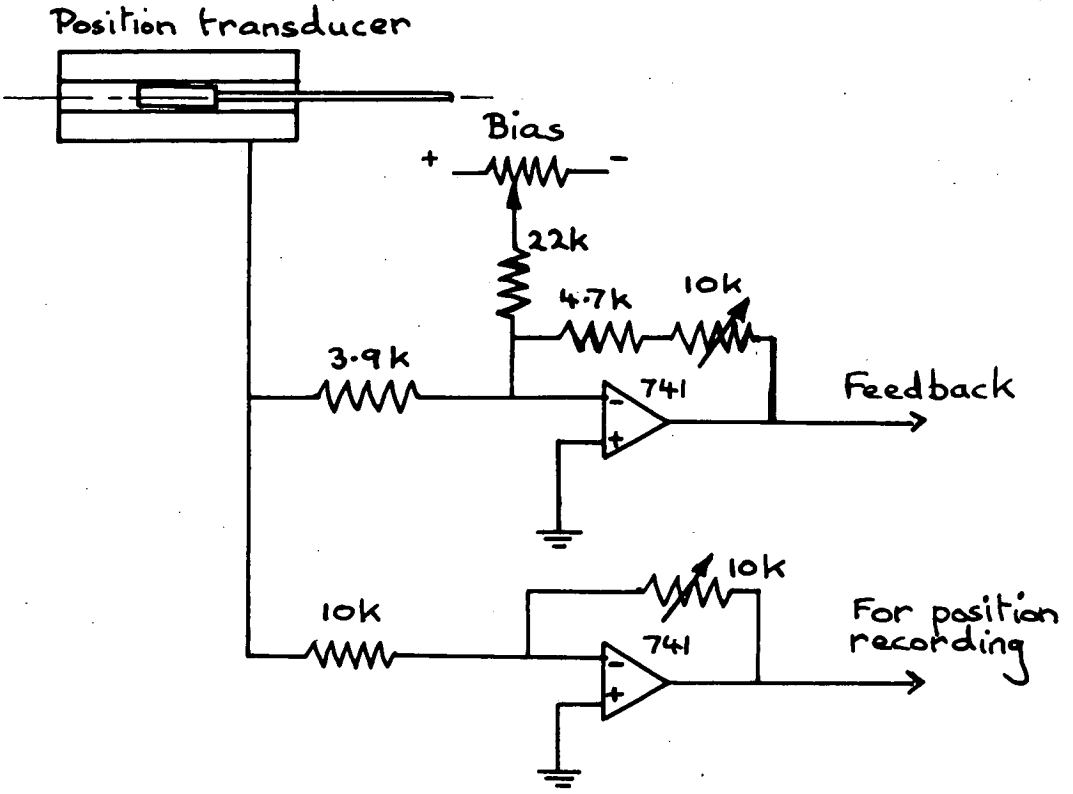

Feedback amplifier - Figure (5-4)

5.3.2 Ram velocity measurement

No suitable velocity transducer was available and ram velocity had to be measured indirectly. The signals encountered were basically low frequency (up to 40 Hz) with high frequency (250 Hz) inertia bounce superimposed, and it was decided to attach an accelerometer to the ram shaft and integrate its output to obtain velocity. There was some doubt as to the low frequency response with this technique, since accelerometers are normally high frequency devices, but alternative methods would have involved the use of a position trandsucer with doubtful high frequency response, and since a good quality high impedance charge amplifier was available it was decided to use the technique. Low frequency response was later checked against the position transducer at frequencies down to 5 Hz and found to be quite satisfactory.

Figure (5-3) details the active integrator used in conjunction with a Bruel & Kjaer type 2626 conditioning charge amplifier. The integrator is initialised by an analog switch operated by an external signal.

This arrangement proved satisfactory but difficult to set up and stabilise. The operational amplifier was very stable with virtually no drift but the B&K charge amplifier had a small D.C. voltage on 'direct' output which had to be offset, and even on 'transformer' output it was still difficult to stabilise. It was often necessary to make several test runs before a stable set of results could be recorded.

5.3.3 Ram position measurement

Ram position was measured by a Hewlett Packard 24DCDT 1000 displacement transducer directly coupled to the ram shaft which was used in conjunction with the feedback amplifier in figure (5-4), to provide a closed loop feedback signal and a position signal for data logging. This unit has infinite resolution and provides a signal of

18V/inch over a range of $\pm$ 1 inch with superimposed high frequency ripple. Output is frequency dependant and it has a transfer function of the form

$$\frac{V(S)}{x(S)} = \frac{K}{(S + 628} \quad \text{(from Maker's literature)}$$

Ripple measurements showed a wave form sketched below at a frequency of 3333Hz.

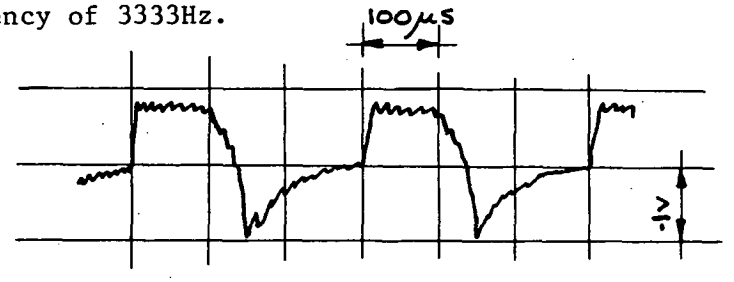

The ripple was amplified by the precision current source and produced voltage swings of 3V amplitude at the output current transducer. Some thought was given to filtering it out, but this could not be done easily without introducing an unwelcome phase shift in the main feedback signal. Checks indicated that all operational amplifiers were working below saturation at ripple peaks, and the ripple was then tolerated because it could be handled normally by the electrical circuit and was too high in frequency to interfere with the servo-valve response. This highlights the need for low ripple levels in feedback loops.

The other problem encountered with position measurement was the range of amplitudes needing to be measured within one test which varied from say, 10 mm at 3Hz to perhaps 0.75 mm at 40 Hz and necessitated use of the transducer at a small percentage of span. Work of this nature is obviously best conducted with a range of transducers better suited to test conditions.

5.3.4 Pressure Measurement

Three types of pressure transducer were employed,these being:

Type (a) National Semiconductor type LX1440 with piezoresistive strain sensor.

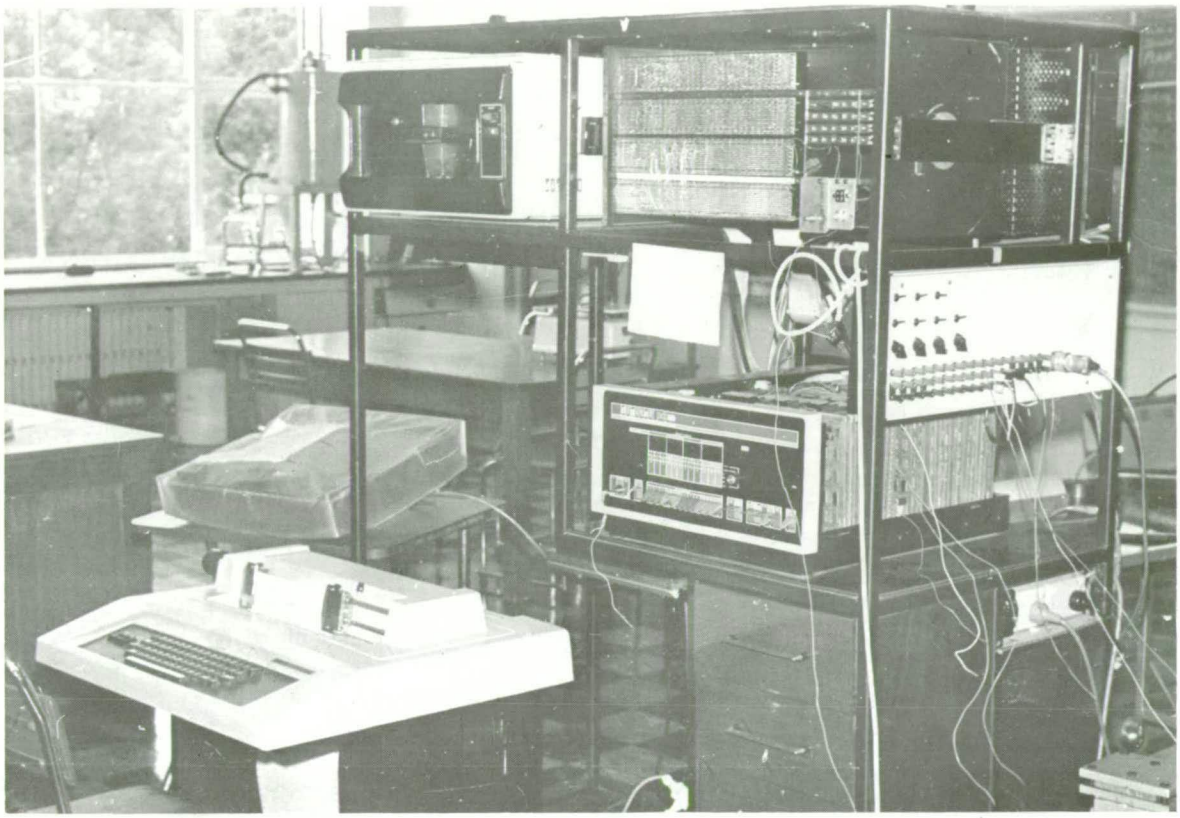

Type (b) M.B. Electronics series 500 with metal diaphragm and strain gauges.

Type (c) Robinson Halpern type 155A with metal diaphragm and LVDT position sensor.

Type (a) proved unreliable under test conditions and too little was known about the frequency response of types (b) and (c) to use them quantitatively under dynamic conditions. (b) and (c) were used qualitatively to check the logical consistency of other data and for constant pressure tests.

5.3.5 Computing facility

A PDP8-E computer was available for control and data logging purposes featuring:

16 K Core
I/O external bus
AM8-EA eight channel analog multiplexer
AD8-EA A/D converter
3- A/D converters
Real time clock
Decwriter
H.S. paper tape punch
H.S. paper tape reader.

5.3.6 Control program

Test control, data logging and recording were all affected by program SAMP3.PA written in PAL8 machine code for this purpose. The program naturally divides into sections as follows:

Pointer address 00200 to 00377

This section is the main control routine. The real time clock is set up and there is a delay loop where the equilibrium

coil current can be adjusted by the switch register setting. When key 'G' is depressed the program initialises the integrator, steps current, starts the clock, and stores data from four multiplexer channels in fields 2 and 3. When all samples are stored it stops the clock and halts pending direction to one of the data handling routines.

Pointer address 00400 to 00577

In this routine data can be continuously displayed on a CRO screen one section at a time by depressing Key 'N'. The data section is endlessly circulated and displayed as a series of dots on the screen to give the appearance of a continuous trace. This routine is used to check data before plotting.

Pointer address 00600 to 00777

In this plotter routine any data section can be permanently recorded on an XY plotter.

Pointer address 01200 to 01377

This service routine is required to service keyboard interrupt requests,and sense timing errors for the real time clock.

5.4 Experimental procedures

In the following tests oil temperature was standardised at $50^{o}C$ and responses were obtained at supply pressures of 6.895 and 13.79 MPa with a coil current perturbation of 0.05 amps and an equilibrium coil current of approximately 0.235 amps. Checks confirmed that supply pressure perturbations were very small.

5.4.1 Open-loop step responses

These were obtained using SAMP3.PA exactly as listed. The servo-system was set up complete with accelerometer and active integrator and the program was started at address 00200. The switch register was then adjusted to allow very slow ram creep in the required direction with the ram 1.5 cm from centre, but moving towards centre. Key 'G' initiated a coil current step and the ram moved to one end of its travel although data sampling occurred near centre position. It was necessary to have initial ram creep because of a dead band up to 30 ma wide in which the ram was likely to be stationary, making it difficult to determine step size without creep.

Sampled ram velocity data was displayed on the CRO to ascertain that the integrator was stable and to determine signal magnitude, after which the step response was plotted via the plotter routine.

5.4.2 Open-loop frequency responses

The servo-system was set with a signal generator connected to the current source feedback input and SAMP3.PA was modified to remove the current stepping statement and to sample at intervals consistent with the applied frequency. As above the program was started at line 00200 and the switch register adjusted manually until the ram was performing stable oscillations about its central position. Key 'G' then initiated sampling of the input and integrator signals both of which were displayed and plotted.

5.4.3 Closed-loop step responses

The servo-system was set up with the position transduced and feedback amplifier linked to the current source to produce a stable system. Utilising SAMP3.PA as in section 5.4.1 step inputs were applied for various feedback gains and ram position measurements were recorded from the feedback amplifier output conditioned for that purpose.

5.4.4 Closed-loop frequency responses

These responses were obtained using a signal generator to drive the current source. The driving and feedback position signals were both sampled and plotted for a range of frequencies at one feedback gain setting and supply pressures of 6.895 and 13.79MPa.

REFERENCES

1. Jones, I.F.
Development and analysis of a fluid power test facility.
University of Tasmania.

CHAPTER 6

6.1 Introduction

In this chapter open and closed-loop servo-system responses are recorded and analysed. System models up to fifth order are constructed and compared with the actual results by curve fitting techniques to ascertain the order of the best model.

6.2 Experimental Results

All experimental results associated with the tests in section 5.4 are recorded in Appendix 4.

6.2.1 Open-loop step responses

Three typical results are recorded in figures (A4-4) to (A4-6).

Figures (A4-4) and (A4-5) exhibit a 'standard' form consisting of a 3ms delay time after which the ram velocity decays exponentially towards its final value which it reaches in about 40 ms. Following the initial delay there is a lightly damped oscillation at about 400 Hz, superimposed on the basic response, which normally disappears within 25 ms and sometimes shows first peak amplitudes up to one half of the final value. Final ram velocity for a 50 ma step varies from test to test between 0.17 ms^{-1} and 0.2 ms^{-1} being up to 15% greater for the negative step. An average value of 0.185 ms^{-1} is representative of normal performance.

Negative current steps sometimes give rise to the form shown in figure (A4-6), but never positive steps. This form exhibits a similar initial pattern to that described above but then settles into a sometimes prolonged oscillation having a frequency between 220 and 250 Hz depending on supply pressure. Final velocity for this response is also higher.

Each of the result patterns detailed above is highly repeatable enabling successive tests to produce virtually identical results.

It is suggested that the initial time delay and transient oscillation indicate stiction because there is a sudden release of energy consistent with a build up of pressure which, when released, causes the initial overshoot and subsequent damped oscillation. Light ram damping is indicated by a decay over several cycles.

The pattern shown in figure (A4-6) shows oscillations at or slightly below the inertia bounce frequency predicted in section 4.5 and the fact that this effect occurs for negative steps when the flapper gap is enlarged suggests an unstable flow pattern in the flapper valve, i.e. a tendency to become fully turbulent.

Assuming velocity obeys the equation

$$V = V_{max} (1 - e^{-kt})$$

where k is the dominant system eigenvalue, it is possible to estimate k by plotting $-\ln(1-V/V_{max})$ versus time to give a straight line of slope k. This has been done on figures (A4-4) and (A4-5) by drawing an average line through the oscillating parts of the curves and results show straight lines which intersect the time axis between zero and 5 ms. The k values from these results are typical of those obtained from a number of tests, varying between 55 and 75 when P_1 = 6,895 MPa and between 75 and 95 when P_1 = 13.79 MPa.

Final velocity is pressure dependant and varies as $\sqrt{P_1}$.

Results suggest the following transfer functions relating ram velocity n and coil current 1.

P_1 = 6,895 MPa

$$\frac{n(s)}{i(s)} = \frac{.185\ k}{(s + k).05}$$

P_1 = 13.79 MPa

Servo-valve open loop response

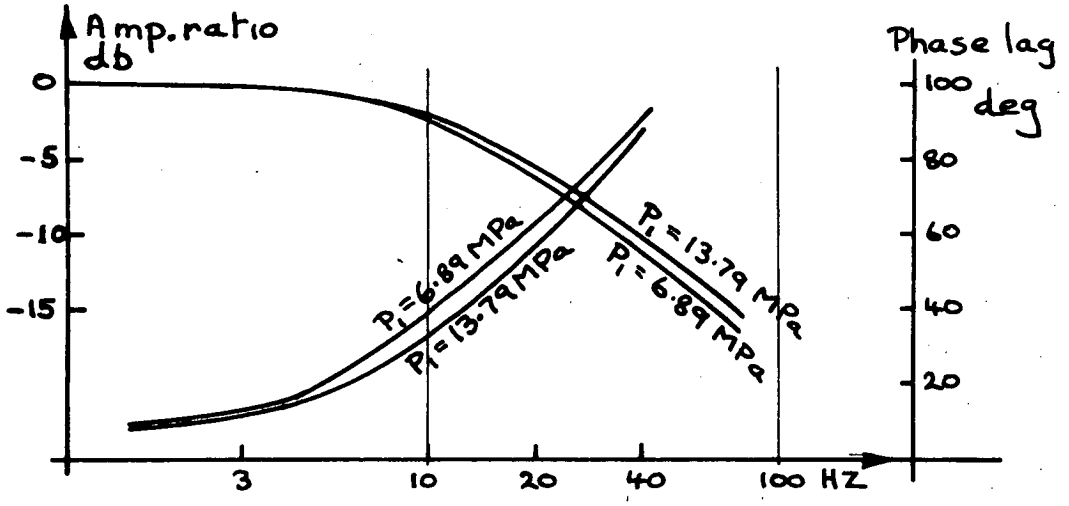

Experimental Frequency response - Figure (6-1)

$$\frac{n(s)}{i(s)} = \frac{.185\ \sqrt{2}\ k}{(s + k).05}$$

where k is within the above limits.

6.2.2 Open-loop frequency response

Two result sets recorded for supply pressures of 6.89 and 13.79 MPa appear in appendix 4 in figures (A4-7) to (A4-14).

The results indicate a ram velocity waveform which is generally sinusoidal but sometimes corrupted by seal stiction and inertia bounce.

At 3Hz the waveform looks good in figures (A4-7) and (A4-11) although the latter result has severe 'noise' superimposed which is due to the recording technique. For this result only the charge amplifier overloaded at its normal setting and signal gain to the multiplexer had to be reduced by a factor of 10 with a corresponding increase in plotter gain. The 10 bit A/D converter had insufficient resolution for such a small signal and conversion errors became amplified, resulting in the 'noise'.

At 10 Hz the inertia bounce is clearly excited each time the velocity changes sign indicating that either the valve gain varies sharply at this point or, more likely, that the ram seals need time to establish themselves. This effect becomes more significant as the frequency increases particularly at the higher supply pressure where, for instance, at 20 Hz there appears to be a strong stiction tendency at the null position followed naturally by excitation of the inertia bounce transient.

The above result sets give a frequency response in figure (6-1) which is similar to the manufacturer's specification and program results from the chapter 4. These curves indicate corner frequencies at about 10 and 12 Hz for the low and high pressures respectively which corresponds to the lower end of the range of k values in section 5.5.1.

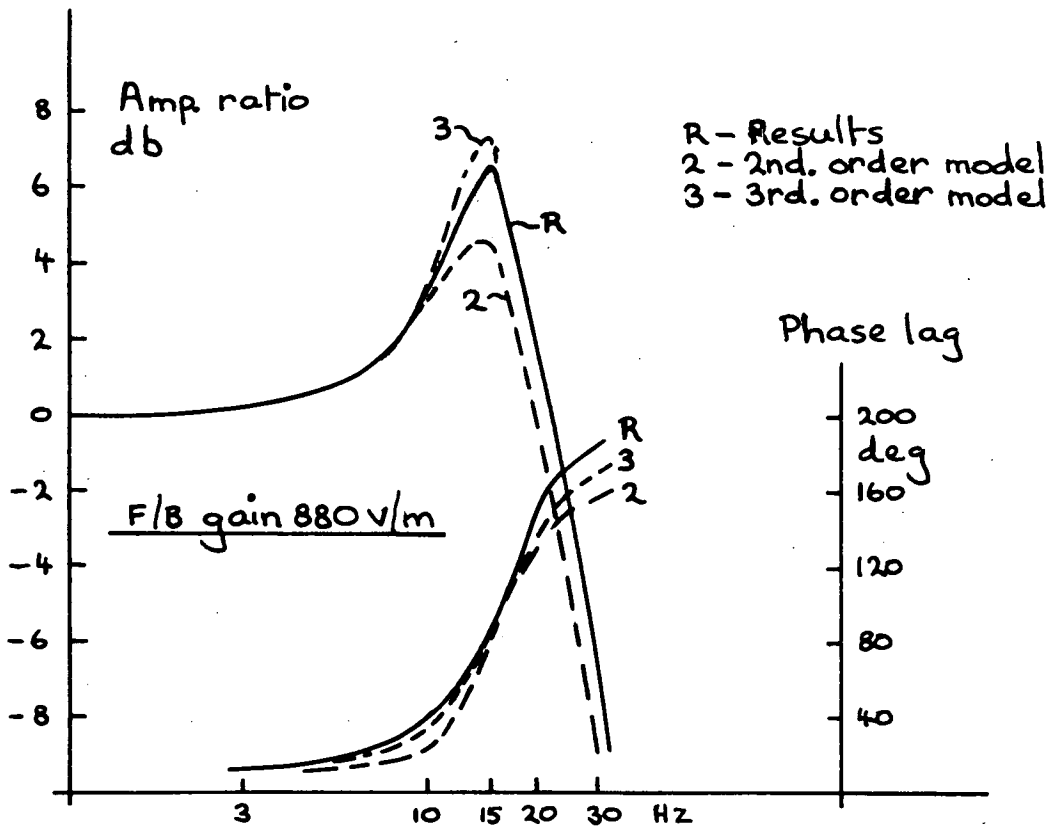

Closed-loop system Frequency response Figure (6-2)

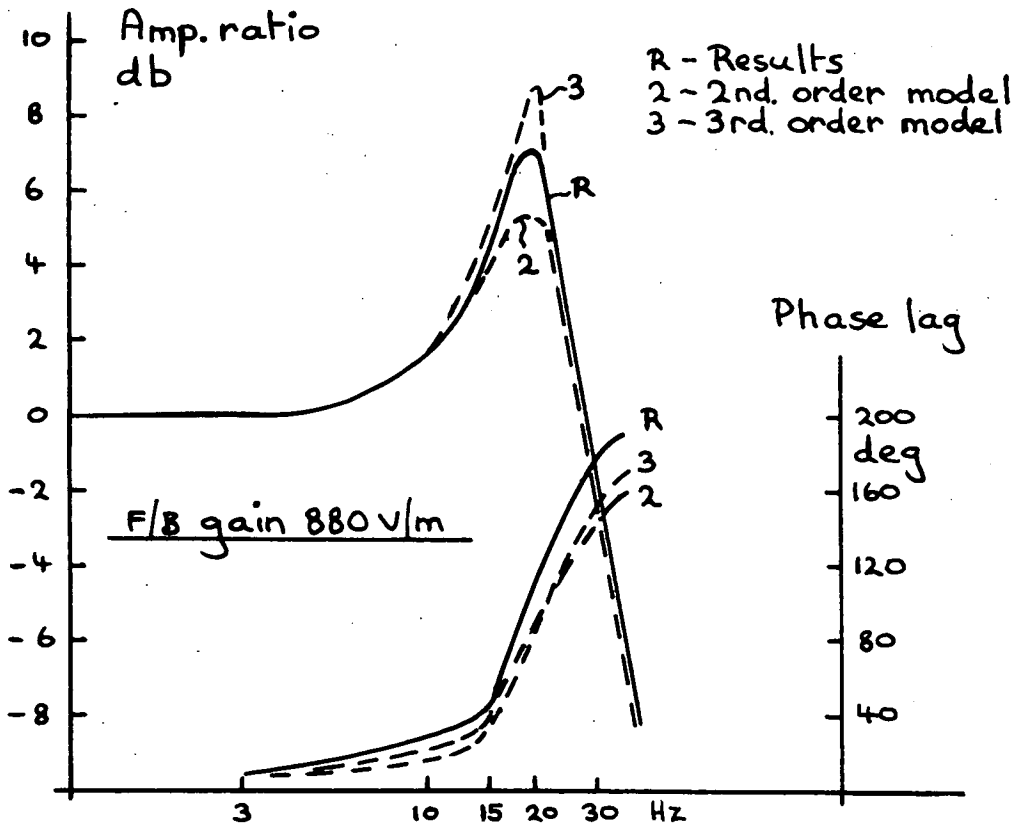

Closed-loop system Frequency response Figure (6-3)

6.2.3 Closed-loop frequency response

Two result sets recorded for supply pressures of 6.89 and 13.79 MPa with a feedback gain of 880 V/m appear in appendix 4 in figures (A4-15) to (A4-27). These results show ram position as measured by the position transducer and differ from those in section 5.5.2 because maximum ram velocity occurs at the central position.

It is evident that the response curves are distorted from their basic sinusoidal shape wherever ram velocities are low. For instance figure (A4-15) suggests that the ram seals do not stabilise at the sliding velocities encountered and move intermittently giving rise to a non-linear oscillation superimposed upon a basically sinusoidal response. This effect is also observed in figure (A4-21) where it is much more irregular. At higher sliding velocities as in figures (A4-16), (A4-17),(A4-22) and (A4-23) the irregular effect is observed near extreme amplitude positions but is less evident near the centre where sliding velocity is higher. Frequencies above 20Hz appear to excite the inertia bounce frequency which is evident in figures (A4-18), (A4-19), (A4-20), (A4-25), (A4-26) and (A4-27) at a frequency close to 250 Hz.

Figures (6-2) and (6-3) show the closed-loop frequency response derived from the above result sets.

6.2.4 Closed-loop step responses

Figures (A4-28) and (A4-29) show system responses to a step input as recorded by the position transducer. High frequency low amplitude transducer noise is evident in these curves and may be disregarded since it does not derive from the ram itself. The responses assume an expected form with an initial fast decaying transient forming a short time delay followed by a rapid rise with a subsequent overshoot and damped oscillating motion. As feedback gain increases, the positional change is decreased, oscillation frequency increases, and the oscillation becomes less damped with greater percentage overshoot.

These effects could all be predicted from the root locus plot of a second order system.

Seal stiction is evidenced by the appearance of pulses which are first seen when the direction of motion reverses and subsequently observed at irregular intervals as the motion settles. A slow low amplitude oscillation occurs about the new equilibrium position, probably resulting from the dead band noted in section 5.4.1.

6.3 Open-loop system order

The servo-valve open-loop response is adequately described by a first order transfer function of the form suggested in section 6.2.1 with k values of 60 and 75 applicable for pressures P_1 = 6.89 and 13.79 MPa respectively. These k values are correct for frequency responses and are at the lower end of the suggested range for step responses.

If the servo-system response is to be investigated an additional transfer function from section 4.7 must be included if the inertia bounce effect is required, making the system third order. The third order open-loop model is used later in section 6.4.4 where feedback is also included to give a fifth order closed-loop model. However for most purposes it is doubtful whether the additional complexity caused by an increase of two in system order is worthwhile.

6.4 Closed-loop system order

Using the block diagram below the system can be from second to fifth order depending on the assumptions made.

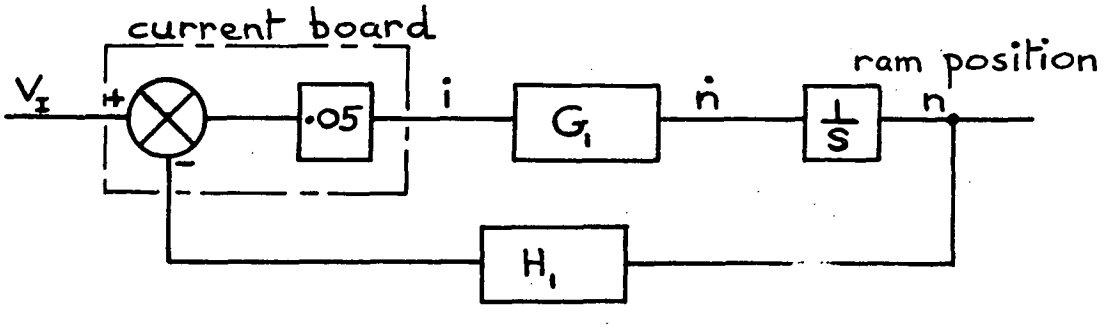

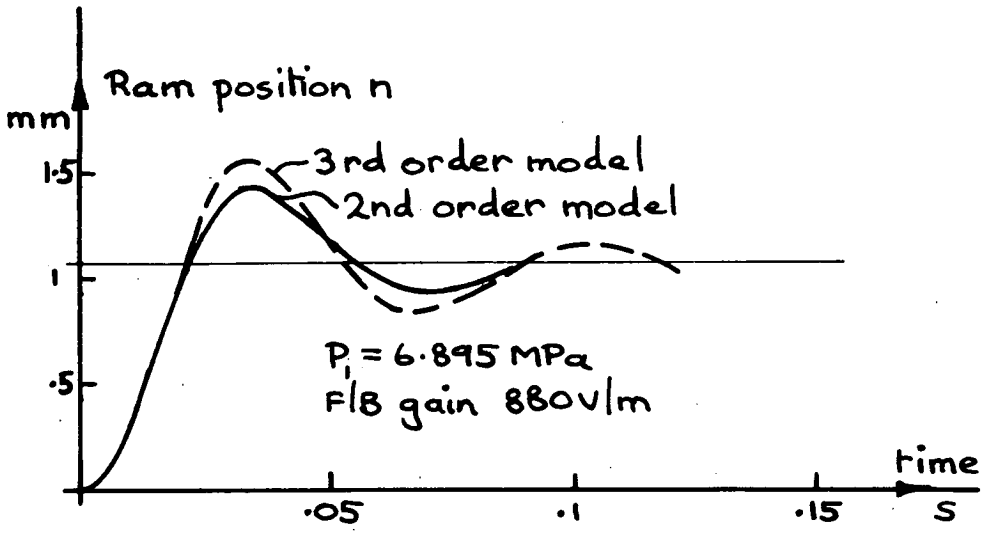

Closed-loop step response Figure(6-4)

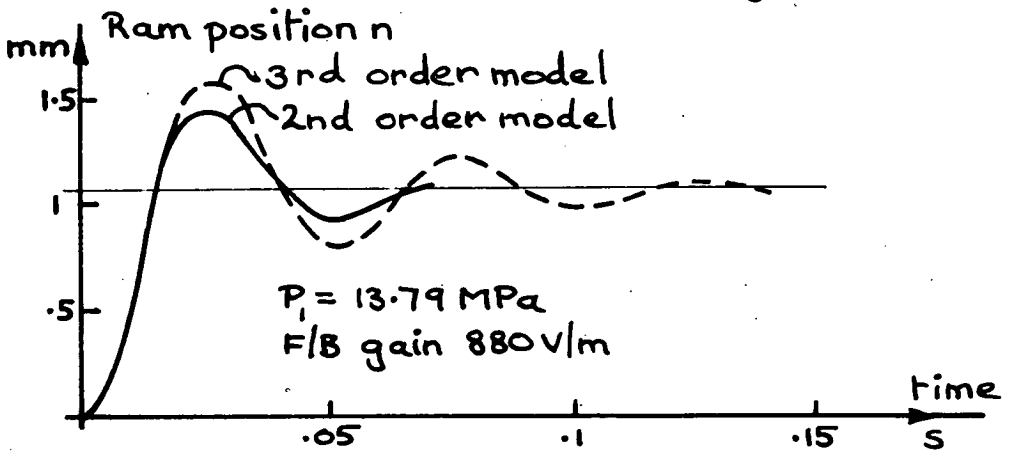

Closed-loop step response Figure(6-5)

These systems are investigated below at two supply pressures and one feedback gain by curve fitting to experimental results.

6.4.1 Second order system

Using the transfer functions suggested in section 6.2.1 with k values of 60 and 75 assumed for the two pressures, and assuming proportional feedback;

$H_1 = 880$ V/m

$G_1 = \frac{222}{(S + 60)}$ at $P_1 = 6.89$ MPa.

$G_1 = \frac{392}{(S + 75)}$ at $P_1 = 13.79$ MPa

The transfer functions are:

$$\frac{n(S)}{V(S)} = \frac{11.1}{S^2 + 60S + 9768} \quad \text{at } P_1 = 6.89 \text{ MPa}$$

with poles at $-30 \pm 94\,i$ corresponding to a damping ratio of 0.3 and a damped natural frequency of 15 Hz.

$$\frac{n(S)}{V(S)} = \frac{19.6}{S^2 + 75S + 17248} \quad \text{at } P_1 = 13.79 \text{ MPa}$$

with poles at $-37.5 \pm 125.9\,i$ corresponding to a damping ratio of 0.29 and a damped natural frequency 20Hz. Frequency responses for these transfer functions are given in figures (6-2) and (6-3) and indicate that, by comparison with recorded results, true responses are less damped. This fact is confirmed in figures (A4-28) and (A4-29) where the oscillation decays much too slowly for the damping ratios predicted giving the step responses in figures (6-4) and (6-5). Predicted oscillation frequency agrees with the results.

6.4.2 Third order system

Assuming the position transducer has the transfer function stated by its manufacturer

$$H_1 = \frac{880 \times 628}{(S + 628)}$$

$P_1 = 6.89$ MPa and G_1 as above.

$$\frac{n(s)}{V(s)} = \frac{11.1\ (S + 628)}{S^3 + 688\ S^2 + 3760S + 6134304}$$

with poles at $-21.9 \pm 95.1\ i$ and -644.3 corresponding to a damping ratio of 0.22 and a damped natural frequency of 15.1 Hz.

$P_1 = 13.79$ MPa and G_1 as above

$$\frac{n(S)}{V(S)} = \frac{19.6\ (S + 628)}{S^3 + 703\ S^2 + 47100S + 10831744}$$

with poles at $-23.3 \pm 126.3\ 1$ and -656.4 corresponding to a damping ratio of 0.18 and a damped natural frequency of 20.1 Hz.

By comparison with measured responses in figures (6-2) and (6-3) the third order system gives a close approximation to the actual system with assumed K values of 60 and 75.

Figures (6-4) and (6-5) show step responses using the above transfer functions with the same scales as figures (A4-28) and (A4-29) for comparison purposes. Actual response has a slightly higher initial overshoot but otherwise there is good similarity. It appears that step inputs give rise to higher k values than do sinusoidal inputs, probably because the flapper valve flow pattern alters from its 'constant gap' characteristic pattern to a dynamic one during the step. The higher k value results in a faster rise time which causes higher initial overshoot.

The damping ratio is sensitive to phase delay in the feedback loop there being a reduction from 0.3 to 0.2 due to the modified H_1.

The third order closed-loop system is considered to give an excellent match with measured results and should be suitable for most analytical purposes.

6.4.3 Fourth order system

The linear program in chapter 4 indicates a servo-valve pole at about -22500 and this can be included into the third order system by altering G_1.

$$G_1 = \frac{222 \times 22500}{(S + 60)(S + 22500)} \qquad \text{when } P_1 = 6.89 \text{ MPa}$$

in which case

$$\frac{n(S)}{V(S)} = \frac{11.1 \times 22500\ (S + 628)}{S^4 + 23188S^3 + 15.518E^6S^2 + 8.478E^8S + 1.38E^{11}}$$

with poles at $-21.63 \pm 95.1\ i$, -644.8, and -22500 corresponding to a damping ratio of 0.22 and a damped natural frequency of 15.1 Hz. This transfer function gives a frequency response almost exactly the same as the third order system and therefore offers no analytical advantage.

6.4.4 Fifth order system

A fifth order system can be constructed by inclusion of the ram and oil lines transfer function from section 4.7. Using the third order system and including this additional term in G_1 a fifth order system results. The additional term is;

$$\frac{G_4 H_3}{S^2 + H_4 S + H_3 G_4}$$

Values for G_4, H_3, and H_4 are taken from the program A matrix in chapter 4. The resulting transfer function has poles at $-21.3 \pm 95.3\ i$, -643, and $-167.7 \pm 16582\ i$. It produces results basically similar to

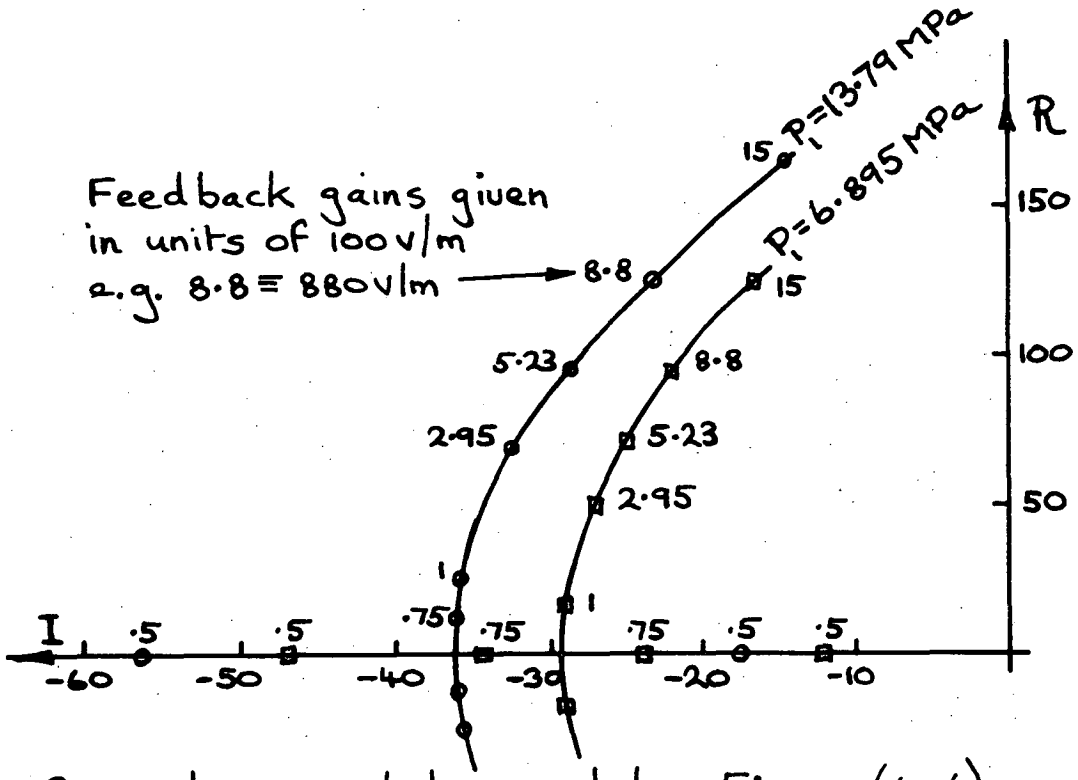

Open-loop root locus plot Figure (6-6)

the third order system but with the inertia bounce in evidence and offers little analytical advantage for the increase in system order.

6.5 Closed loop root locus plot

This is given in figure (6-6) for the third order model at two supply pressures. Gains in the range 295 to 880 V/m were available during tests. The system was stable at these gains and the plot predicts eventual instability at higher feedback gains.

6.6 Chapter Summary

Experimental data in this chapter indicates that the servo-valve has a frequency response very similar to the manufacturer's specification but falling away at lower supply pressures as predicted in chapter 4. Dominant poles are located at -60 and -75 radians/sec for supply pressures of 6.89 and 13.79 MPa respectively and ram velocity is proportional to $\sqrt{P_1}$ with an average value of 0.185 m/s for a 500 ma current step when P_1 = 6.89MPa. Within the frequency range investigated servo-valve response can be described by a first order transfer function and the closed-loop system is best regarded as third order, bearing in mind that inertia bounce may also be superimposed on results. Response waveforms are distorted from their basic sinusoidal shape both by inertia bounce and, more severely, by seal compliance when ram velocity is low or changes sign.

Dominant poles for step responses tend to be more negative than those stated above suggesting different flow patterns in the flapper valve nozzle under 'dynamic' and 'equilibrium' conditions. It is possible that the introduction of flapper dither could eliminate this latter effect.

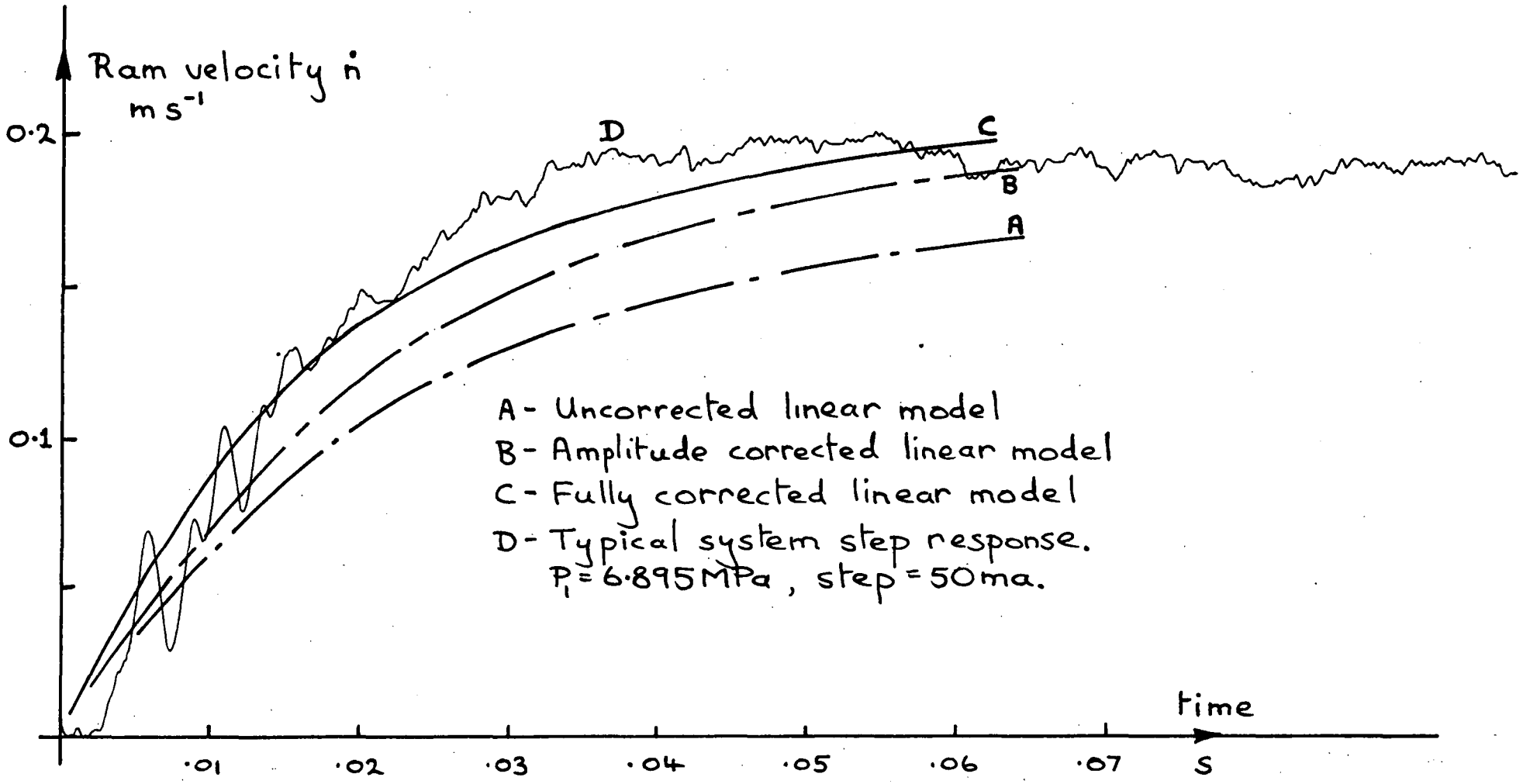

Corrected linear model open-loop step response Figure (7-1)

CHAPTER 7

7.1 Introduction

In this chapter the linear model SERVO1.BA is reviewed in the light of experimental data from chapter 6 and a non-linear program is developed and used to investigate parameter coupling.

7.2 Linear model review

A comparison of experimental and linear model results indicates that predicted ram velocities are 20% low and the dominant pole is 25% low. Figure (7-1) compares an actual response curve with model results and shows response curves when certain corrections are included. Curve A is for the unmodified model which has a dominant pole at -45.8 and curve B retains the same pole but is amplitude corrected. Curve C has the dominant pole of -60 suggested in chapter 6 and is also amplitude corrected. It is apparent that the model must give responses as for curve C if accurate results are sought although amplitude correction alone gives a good approximation to the negative step response shown, and an even better approximation to a positive step response. Possible sources of the discrepancies are discussed below.

Valve underlap

With reference to section 3.8 valve underlap was assigned an average value because measurements and flow experiments could not be simply reconciled. Underlap has a large effect on flow gain and could account for the amplitude error encountered if enlarged to the upper limit considered (0.1mm), although this appears unrealistic. This modification has the secondary influence of increasing the dominant A matrix negative eigenvalue slightly, but not to the required value of -60.

Valve spool jet reaction forces

These forces were originally calculated assuming fully established jets at an angle of 65^{o} tending to resist spool opening.

Any reduction in jet force allows more spool movement and therefore more valve flow which increases ram velocity. It could be argued that jets adhere to one or other surface and jet forces are either zero or reduced in value. If so element A(1, 2) could be reduced by up to 30% which has the effect of increasing valve opening by 43% and also altering the dominant pole from -45.8 to -32, i.e. in the wrong sense. This latter fact tends to support the initial assumptions.

Leakage within the servo-valve

Leakage paths were again examined to ascertain their likely influence. The possibility of leakage from pressure p_2 past the narrow spool land was checked out by careful measurements and by inclusion of program statements to allow a small leakage flow, but no significant effects were encountered. Theoretical leakage flows were minute and, even when increased by a factor of 10, had little influence on results. It was concluded that leakage effects were unlikely to cause the errors under investigation.

Orifice discharge coefficients

Coefficient C_{23} was assigned a high value in section 3.4.1 and checks were made to see whether this exerted a large influence. Values of C_{12} and C_{23} were therefore reduced by the same proportion which in turn reduced the control flow predicted, but the program was insensitive to such changes.

Magnetic force and flapper influence coefficients

The experimental procedure employed to obtain magnetic force necessitated use of the measured influence coefficients making these two items interdependant.

The flapper valve is set up by an external adjusting screw which applies force to a tensioning tag, and this arrangement is theoretically suspect because applied forces may alter the bending

characteristics of the flapper support bracket. Influence coefficients were originally determined by applying loads to the flapper and measuring deflections, and theoretical checks indicated that the flapper support bracket was bending significantly because calculated coefficients were some 65% of actual results. It was therefore possible that the coefficients varied according to the tensioning force applied to the tag.

To check this out a series of tests were run as follows. The servo-valve was set up as for a normal test run and adjusted to give correct null-position coil current, after which the valve end covers were removed without altering the flapper valve setting. The flapper was found to be in contact with the nozzle when no coil spring force was present. The flapper was loaded by means of a vernier gauge which positioned the spool and applied a force via the coil spring. Light touch dial gauges were then set up to measure flapper movement at positions 1 and 2 (section A3.3.2).

Using this arrangement influence coefficients a_{11} and a_{12} were measured directly by applying forces to the flapper via the coil spring at position 1. Results were about 10% less than previous results.

Influence coefficient a_{22} and magnetic force were checked by applying coil current at constant gap settings and using the coil spring tension to maintain the gap. Flapper force equilibrium equations similar to those in equations (A3-8) and (A3-9) were written and solved. These results supported the magnetic force equations previously obtained by another method but indicated a lower value of coefficient a_{22}.

It was finally concluded from the checks that influence coefficients varied according to the set up of the flapper valve and no reliable coefficient values could be estimated. Values used in the programs must therefore be regarded as typical only, and it is considered that some portion of the program discrepancies under

discussion stem from this source.

Flapper valve flow characteristics

Perturbation constants K_3 and K_5 were obtained from the equation describing steady state flow of the flapper valve in section A3.2.4. This flow is in the transition region and is proportional to $P^{0.475}\ H^{0.7}$. In the fully turbulent region flow could be expected to be proportional to H/P. There is a real possibility that the flow tends to obey the latter assumption under dynamic conditions in which case perturbation constants alter, depending on the discharge coefficient then applicable. If C_Q is taken as 0.6 then K_3 and K_5 are very similar but the equilibrium gap is enlarged to .17 mm and magnetic force is correspondingly reduced. In this case program amplitudes reduce and the dominant pole is unaltered. If C_Q is higher, say 0.75, then K_3 increases by 25% and the equilibrium gap is unaltered. In this case both amplitude and dominant pole move significantly in the required sense. In fact the program is highly sensitive to the value of K_3, more so than any other perturbation constant. An increase of 40% in K_3 gives all required corrections to the program and brings the dominant pole to within 2.5% of the experimental value from chapter 6.

7.2.1 Linear model modifications

From the above discussion it is concluded that linear model discrepancies stem from a combination of effects, the most significant being, underlap, flapper influence coefficients, and flapper valve flow coefficients. It is not possible to pin-point precise causes of the error, but either K_3 must be increased by 40% or a_{22} similarly increased to make the required corrections.

The linear program is corrected by increasing K_3 by 40% in all further work including the non-linear program later developed.

7.2.2 Revised system equations

Using the above modification;

P_1 = 6.895 MPa

$$\dot{X} = \begin{bmatrix} -21817 & -.127E^{7} & 0 & 0 \\ 1 & 0 & 0 & 0 \\ 0 & .5158E^{13} & 0 & -.9468E^{10} \\ 0 & 0 & .000288 & -333 \end{bmatrix} \begin{Bmatrix} y \\ y \\ p_L \\ n \end{Bmatrix} + \begin{bmatrix} 9319 \\ 0 \\ 0 \\ 0 \end{bmatrix} \{i\}$$

$\lambda 1 = -58.45$

$\lambda 2 = -166.6 + 1658\ i$

$\lambda 3 = -166.6 - 1658\ i$

$\lambda 4 = -21758$

P_1 = 13.79 MPa

$$\dot{X} = \begin{bmatrix} -27892 & -.2127E^{7} & 0 & 0 \\ 0 & 0 & 0 & 0 \\ 0 & .7215E^{13} & 0 & -.9648E^{10} \\ 0 & 0 & .000288 & -333 \end{bmatrix} \begin{Bmatrix} y \\ y \\ p_L \\ n \end{Bmatrix} + \begin{bmatrix} 14808 \\ 0 \\ 0 \\ 0 \end{bmatrix} \{i\}$$

$\lambda 1 = -76.46$

$\lambda 2 = -166.6 + 1658\ i$

$\lambda 3 = -166.6 - 1658\ i$

$\lambda 4 = -27815$

7.3 Reduced order linear systems

The A matrices in section 7.2.2 (and chapter 1) have a large eigenvalue $\lambda 4$ which is a nuisance because it restricts the Runge Kutta time interval to very small values. $\lambda 4$ has virtually no effect on the time response at low frequencies but the small time interval must be maintained throughout computation to avoid numerical instabilities and run-time becomes very extended. For example when feedback is included the equations can be fifth order and a typical run is over 0.1s at intervals of 5×10^{-5}s with print-outs at 1ms each taking fifty seconds.

Physically $\lambda 4$ exists because valve spool mass gives rise to an inertia force during acceleration and $\lambda 4$ can be eliminated by assuming a light spool when investigating low frequency response. Row 1 of the matrix equation is divided by A(1,1) and y is eliminated to give a third order system.

For example when P_1 = 6.895 MPa

$$\dot{X} = \begin{bmatrix} -58.29 & 0 & 0 \\ .5158E^{13} & 0 & -.9648E^{10} \\ 0 & .000288 & -333 \end{bmatrix} \begin{Bmatrix} y \\ p_L \\ n \end{Bmatrix} + \begin{bmatrix} .427 \\ 0 \\ 0 \end{bmatrix} \{i\}$$

There is now a dominant pole at -58.29 and a complex pole at $-166.6 \pm 1658\,i$. Maximum time interval for the fourth order model was $2.1/|\lambda_{MAX}|$ = .124ms using the rule from section 1.7.2 but it is not possible to increase the interval to 2.7/166.6 = 16 ms because the complex pole introduces a high frequency oscillation with a period of 3.8 ms which obviously limits the interval increase. As a 'rule of thumb' a practical time interval was found to be the smaller of $1.5/|\lambda_{MAX}|$ or one twentieth of the period of the highest frequency oscillation. In the present case the actual time interval may be increased by a factor of four from .05 ms to .2 ms and this, coupled with a reduction in system order, results in a considerable saving in computer run-time.

System order can be further reduced by eliminating p_L as a state variable. Physically this assumes the oil to be inelastic and system response becomes that of the servo-valve only. All ram inertia and load effects are eliminated and ram velocity is directly proportional to y making the system first order.

$$\dot{y} = -58.29\ y + .427\ i$$

$$n = 534.6\ y$$

The first order approximation is useful for block diagram system analysis because it is simple and low order but the third order system is more accurate and can be solved with modest run-times.

7.4 Non-linear model development

The Runge-Kutta method requires the function to be evaluated four times for each time interval and the form of the equations, i.e. linear or non-linear, is of no consequence. Linear equations are most convenient because they can be evaluated using standard matrix multiplication routines, but other terms may be included as desired. Where equations are difficult to perturb, such as $Q = K\ A(y)\ P$ for the segemntal orifices, it is possible to circumvent the problem by calculating the actual flow perturbation from two conditions of the equation for Q, rather than resorting to a perturbed flow q with two component terms.

Two equations relating to the segmental orifices can be handled in this way.

Spool jet reactions in equation (A3-10)

Here the term in y becomes

$$\ldots\ +1700\ y + 1.25A(y)(P_1 - p_L)$$

Main row flow in equation (A3-12)

Here the term in y becomes

$$+ .1027 \sqrt{(P_1 - p_L)} \times A(y)$$

These modified equations introduce switching type non-linearities due to the valve spool which directs flow to alternate sides of the ram piston depending on the sign of spool displacement y. The load pressure perturbation p_L can be either positive or negative with a corresponding influence on ram force, but whenever y changes sign the spool switches valve flow and p_L then acts in the opposite sense. p_L is therefore positive in these two equations when y is positive and changes sign when y does.

Since some terms remain linear and others become non-linear the simplest method of altering the linear program is to retain basic matrix handling routines and introduce a third term R such that;

$$\dot{X} = A\,X + B\,U + R$$

where R is a matrix of non-linear forcing terms which are functions of y and p_L.

The spool jet reaction force terms become divided between A and R so that the linear term 1700y contributes to element A(1, 2) and the non-linear part appears as R(1). Element A(3, 2) becomes zero and the main ram flow term appears as entry R(3).

Using this algorithm it is no longer necessary to estimate A' and the program is suited to larger perturbations without loss of accuracy because all load pressure and spool position feedback terms are fully included.

The non-linear program SERV08.BA appears in Appendix 5. It is a modified form of the linear program SERV01.BA with the routine for estimating R included. SERV08.BA incurs a small run-time penalty

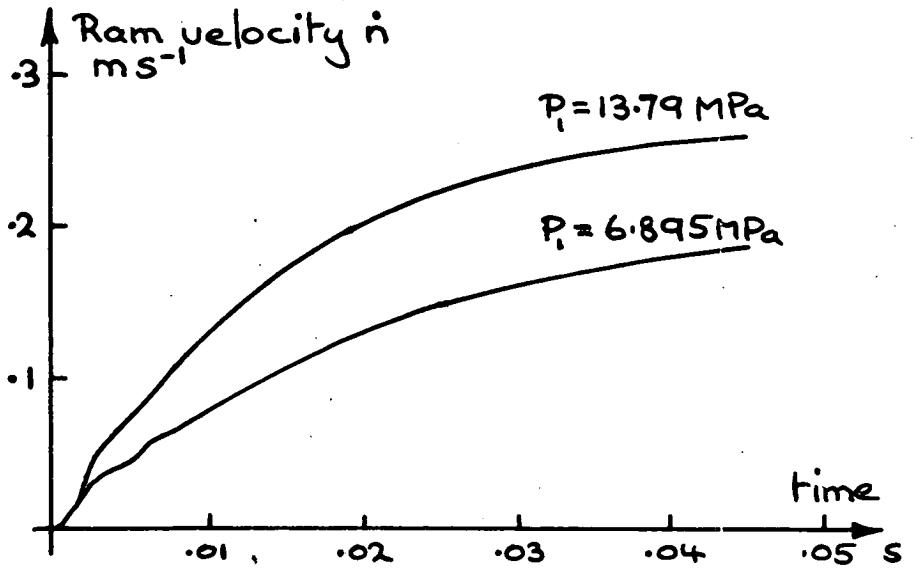

Non-linear model open-loop step-response

Figure (7-2)

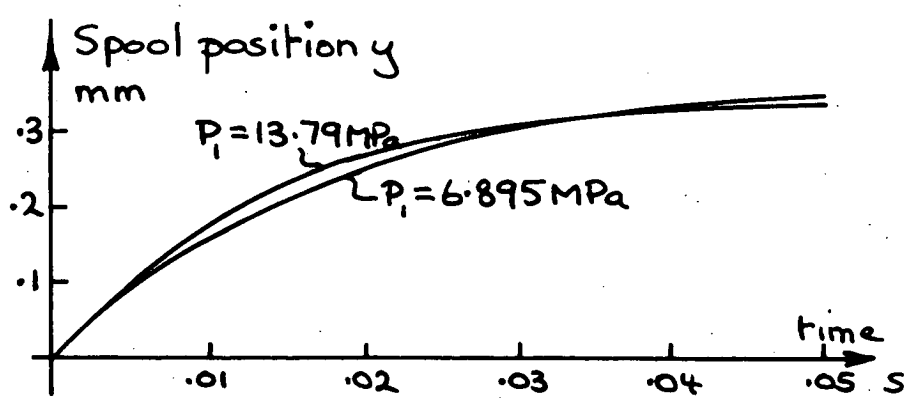

Non-linear model open-loop step response

Figure (7-3)

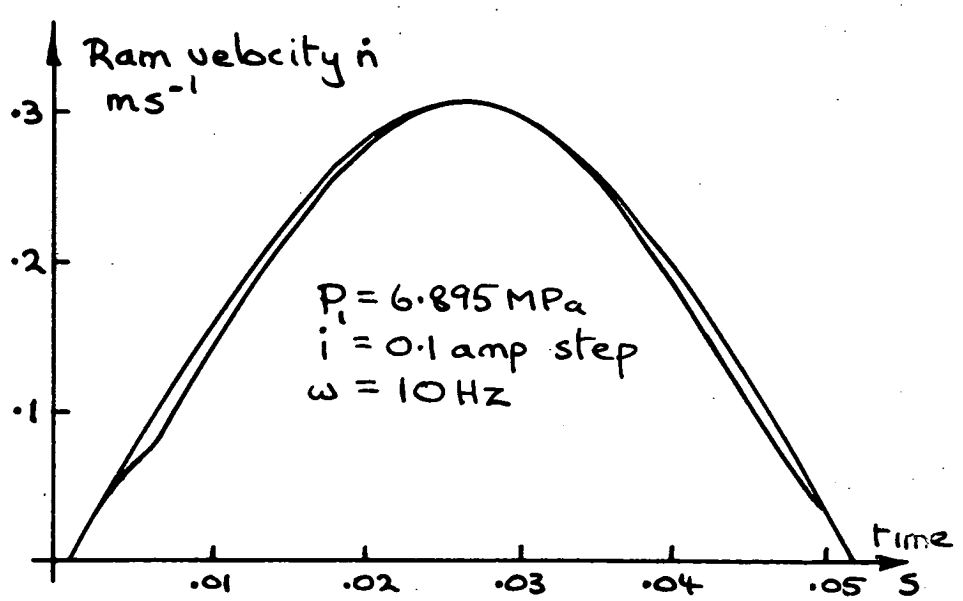

Non-linear model open-loop Frequency response

Figure (7-4)

because of this additional subroutine which has to perform orifice area calculations frequently.

7.5 Non-linear model responses

Figures (7-2) to (7-3) show responses obtained from SERVO8.BA.

7.5.1 Step response

The open-loop step response in figures (7-2) and (7-3) are similar to those obtained from the linear model in chapter 4 but with ram inertia bounce slightly in evidence between 0 and 0.1s. Spool displacement rises quicker at the higher pressure but tends to a slightly lower terminal value than at the lower pressure, which accounts for the different dominant poles at these pressures and for the fact that ram velocity varies as $\sqrt{P_1}$ (since spool openings are similar).

7.5.2 Sinusoidal response

Figure (7-4) demonstrates the response error to a 10 Hz sinusoidal input which has twice the amplitude previously used. There is again some evidence of inertia bounce excitation and the response waveform has a negative error making it slimmer than a true sine wave of the same amplitude. This error decreases at smaller current perturbations and the inertia bounce becomes more pronounced at higher frequencies.

7.6 Parameter coupling

Coupling between coil current i and ram velocity $\dot{n}$ has been dealt with for the linearised system, but additional effects derive from supply and load pressure perturbations and from non-linear terms.

Supply and load pressure perturbations (p_1 and p_L) affect three basic equations from appendix 3 the first of which involves perturbing P_1 in equation (A3-1) to give the control flow as

$$q_1 = K_1 p_1 - K_1 p_2$$

which can be included with other system equations to give an additional linear forcing term in the spool motion equation which becomes;

$$y + 58.29\ y = .427\ i - 3.25\ E^{-10}\ p_1$$

when spool mass is neglected and P_1 = 6.895 MPa.

Secondly jet reaction force feedback results from an equation in section A3-4 which can be perturbed in the form

$$1.25\ A_y(P_1 + p_1 - p_L)$$

where A_y is the instantaneous segmental orifice area, p_1 is the supply pressure perturbation, and p_L is the load pressure perturbation which is subject to switching type non-linearities (see section 7.4). In expanded form this jet reaction is

$$1.25\ P_1\ A'y + 1.25\ A_y(p_1 - p_L)$$

but since the system is perturbed at y = 0 when A_y = 0 the second term is zero for linear analysis. However in a dynamic situation some feedback from p_1 and p_L will occur when A_y is not zero, resulting in a slightly modified linear response.

Thirdly the valve flow equation (A3-12) is altered to contain the term

$$-.1027\ A_y \sqrt{(P_1 + p_1 - p_2)}$$

from which p_1 and p_L are normally eliminated by linear analysis as above, and p_L is again non-linear due to spool switching.

It is possible that some or all of these three new terms may be significant under some conditions and a revised servo-valve block diagram is shown below to study these effects when P_1 = 6.89 MPa. This diagram is of reduced order and the servo-valve model is first order as in section 7.3.

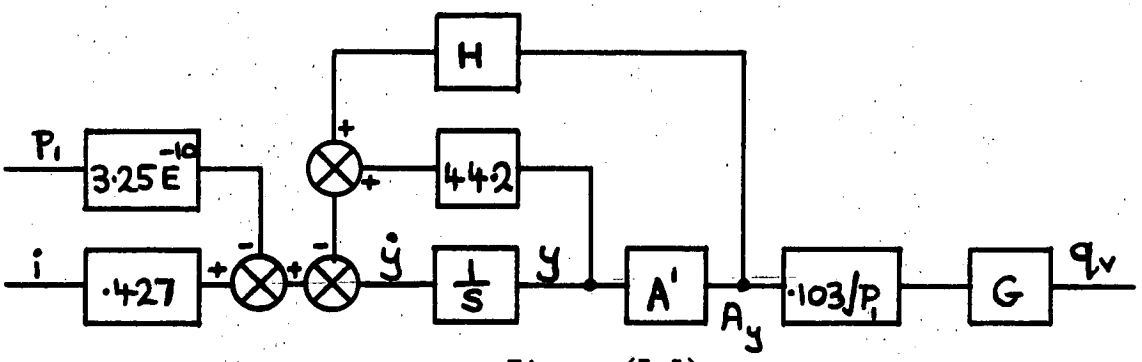

Figure (7-5)

$$H = 14.08(1 + (p_1 - p_L)/P_1)/A'$$

$$G = \sqrt{(1 + (p_1 - p_L)/P_1)} = 1 + .5(p_1 - p_L)/P_1$$

$$A' = f(y) = 0.0025$$

The servo-valve has three inputs i, p_1, p_L and one output q_v. Non-linear terms G and H in valve terms where input variables are multiplied and it is therefore impossible to discuss input/output coupling for each separate input because there is a complex interdependance where, for instance, the effect of p_L depends on the level of i. The block diagram is best discussed in terms of its basic linear response as modified by non-linear terms.

Since coupling is complex the likely magnitudes of input signals must be taken into account. p_1 is a supply pressure perturbation and most hydraulic systems are designed to control supply pressure using either a relief valve or pressure compensated pump. Either device requires a supply pressure perturbation to operate it but pump gain should be high enough to minimise p_1, provided there is adequate pump capacity. The present valve drives

a double acting ram which draws two pulses of oil from supply for one ram cycle which is likely to cause a supply pressure perturbation of the form

$$p_1 = - |A \sin\omega t|$$

where A/P_1 is small and ω is the ram frequency. Delivery line oil capacity and line elasticity are likely to round off these pulses to give an offset and frequency of 2ω so that

$$p_1 = - B + C \sin 2\omega t$$

where both B and C are small in relation to P_1.

By contrast p_L cycles at ram frequency and may be large in relation to P_1 with the basic form

$$p_L = D \sin\omega t$$

where $D < P_1$ and p_L assumes the same sign as spool position y in the block diagram functions H and G.

Coil current perturbation i is also at ram frequency with typical amplitudes below 100 ma.

7.6.1 Supply pressure coupling

This stems from three sources namely the separate p_1 input, H and G.

The separate p_1 input produces a linear forcing term which is coupled to q_v by a transfer function similar in form to the one applicable to i. With typical input levels of i = .05 amps and $p_1 = .05\ P_1$ these two terms may be compared and they produce forcing terms with respective magnitudes of .021 and .0011 m s^{-1}, indicating that supply pressure coupling with q_v deriving from this particular input is very small, and almost certainly negligible.

Feedback from A_y to y is determined by H which has a second constant feedback term (44.2) in parallel which is dominant and therefore tends to cushion non-linear effects deriving from H and A'. With small i and p_1 perturbations these effects can be disregarded and the feedback constant from y to y becomes 44.2 + 14.08 = 58.28 as in the previous linear analysis.

The product of G and A' remains as the dominant non-linear term. Assuming there is a small coil current perturbation at frequency then A' is nearly linear and the valve spool position is given by $y = Y \sin \omega t$ with the basic linear output flow $q_v = Q \sin\omega t$ and an induced supply pressure perturbation p_1 in which case

$$q_v = Q \sin \omega t(1 + .5(-B + C \sin(2\omega t - \phi))/P_1))$$

If B and C are small, say less than 5% P_1 then the harmonic amplitude is less than 2.5% Q and has little significance.

It is concluded that coupling between p_1 and valve flow q_v is likely to be weak under normal conditions and may cause slight harmonic distortion of the output flow but is unlikely to cause instability.

7.6.2 Load pressure coupling

Load pressure perturbations are likely to be much larger than supply pressure perturbations and are difficult to analyse mathematically due to the condition governing the sign of p_L in the system equations. Coupling magnitude is therefore demonstrated by using the non-linear model in modified form.

SERV08.BA was modified to eliminate $\dot{y}$ as a state-variable (as in section 7.3) and ram position n was introduced to replace it making the model fourth order with y p_L $\dot{n}$ and n as state-variables. A ram load was introduced by means of a stiff sprin[illegible]n the ram

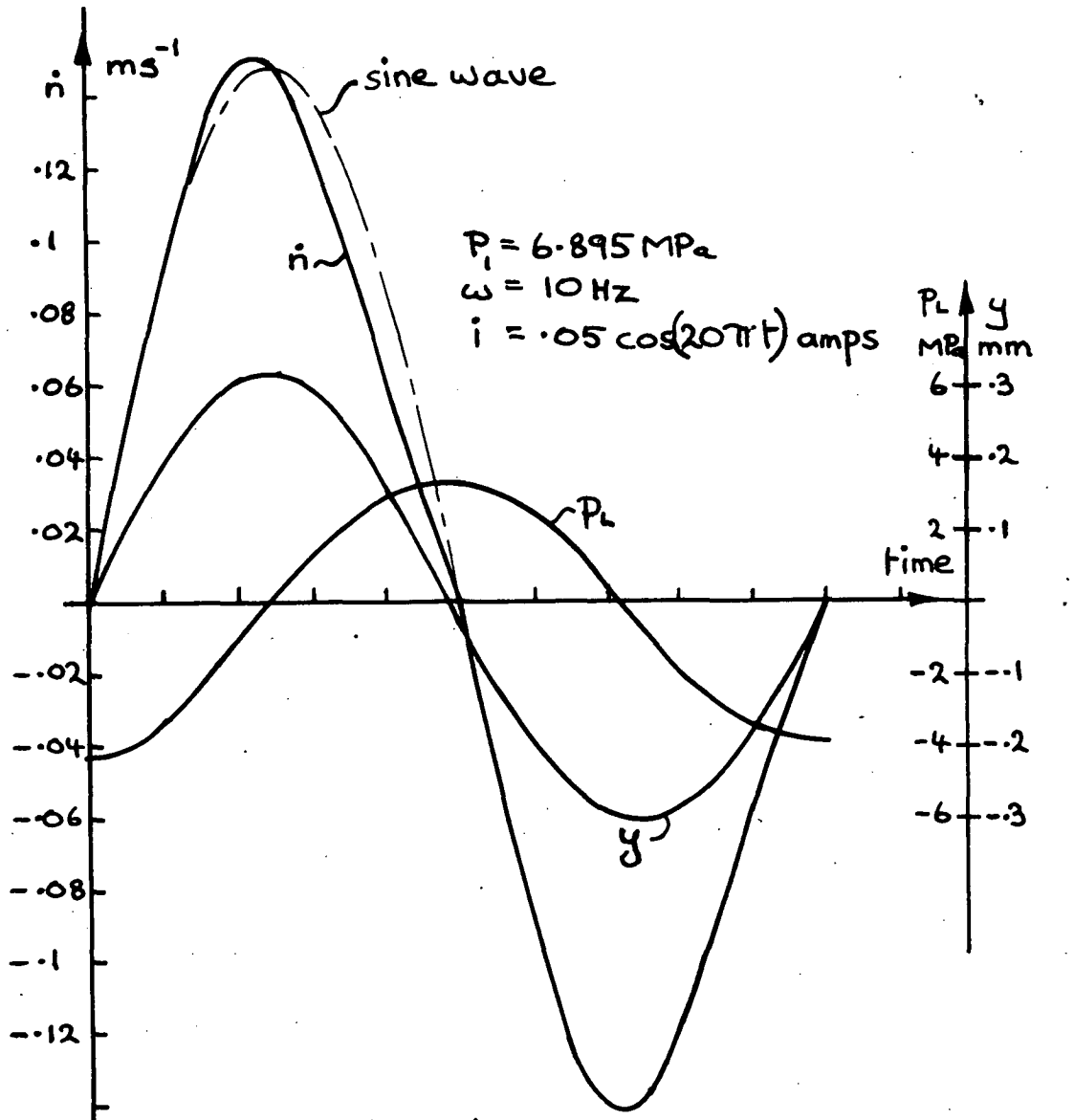

Spring loaded non-linear servo-system
Closed-loop response Figure(7-6)

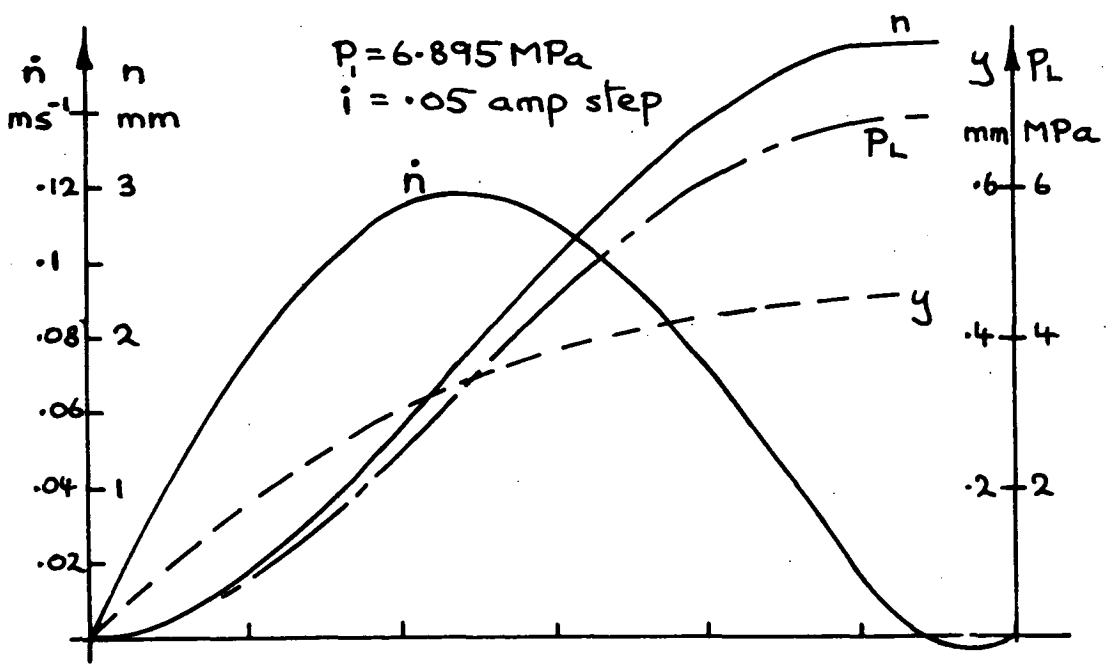

Spring loaded non-linear servo-system
Closed-loop step response Figure(7-7)

shaft so that large load pressures would result at small amplitudes. The model therefore simulated an open-loop servo-system consisting of the servo-valve and ram with a spring load and coil current input. Responses were obtained for stepped and sinusoidal inputs as shown in figures (7-6) and (7-7).

Figure (7-6) shows a steady-state response for a coil current input $i = .05 \sin 20\pi t$ with a load spring rate of 500 kN/m and a supply pressure $P_1 = 6.895$ MPa. Ram velocity $\dot{n}$ is directly proportional to valve flow q_v.

Spool displacement y has a sinusoidal form indicating that non-linear terms in H are not significant and the spool responds in a linear manner almost regardless of load pressure perturbation levels. $\dot{n}$ and p_L show a basic response pattern from 0 to 50 ms, when y is positive, which is repeated in a negative sense from 50 to 100 ms when y is negative. As $\dot{n}$ rises from 0 the ram is at an extreme position where spring load is maximum and during the first 25 ms the spring assists ram movement and causes $\dot{n}$ to overshoot by comparison with a sinusoidal response. From 25 to 50 ms the spring is loading the ram and $\dot{n}$ is less than the sinusoidal response value giving rise to second harmonic distortion during the first half of the response. A similar pattern is repeated during the second half of the response but in a negative sense. The load pressure response lags 90° behind y and suffers similar distortion to $\dot{n}$ with p_L values up to $60\%P_1$.

Figure (7-7) shows a response of the same model to a step input i = 50 ma. Load pressure rises until it equals supply pressure by which time the ram has reached equilibrium at a new position. No meaningful result for this case could be obtained from a linear analysis neglecting p_L because final equilibrium depends on the fact that $p_L = P_1$.

It is concluded that coupling between p_L and q_v results in non-linear output wave distortion which tends to straighten the wave edges and advance wave peaks on the time axis. The extent of distortion depends upon the magnitude of the load pressure perturbation and it is obviously desirable to use the ram well below its maximum capacity to obtain good wave forms.

7.7 Chapter Summary

The linear program in chapter 4 gave results with 20-25% amplitude and dominant pole errors which were investigated and thought to originate mainly from the flapper valve theoretical analysis. Flapper influence coefficients and flow perturbation constant K_3 were both suspect quantities due to the flapper valve design. The program was corrected by increasing K_3 by 40% after which it produced results giving an excellent match with measured responses.

System order was reduced from four to three with negligible low frequency error by assuming the valve spool to be light and a significant computer run-time saving resulted.

A non-linear program was developed for detailed response analysis, and this was used to investigate parameter coupling effects due to load and supply pressure perturbations.

CHAPTER 8

8.1 Introduction

In this chapter a modified flapper valve design and general purpose digital model are proposed and general conclusions are drawn from the entire thesis.

8.2 Flapper valve design

The flapper valve design is criticised because stiffness coefficients vary according to the adjusting screw load and there is no accurate means of aligning the flapper to ensure that it is parallel with the jet nozzle end in a plane perpendicular to the axis of bending. As such, the design is not amenable to theoretical bending analysis which seriously hinders any simulation attempt. Whilst this may not be a problem from the manufacturer's point of view it compels the designer to rely on experimental data and defeats the object of performance prediction by accurate simulation at the design drawing stage of development. An alternative design is proposed in figure (8-1) in the belief that it overcomes the above problems with negligible increase in cost or complexity.

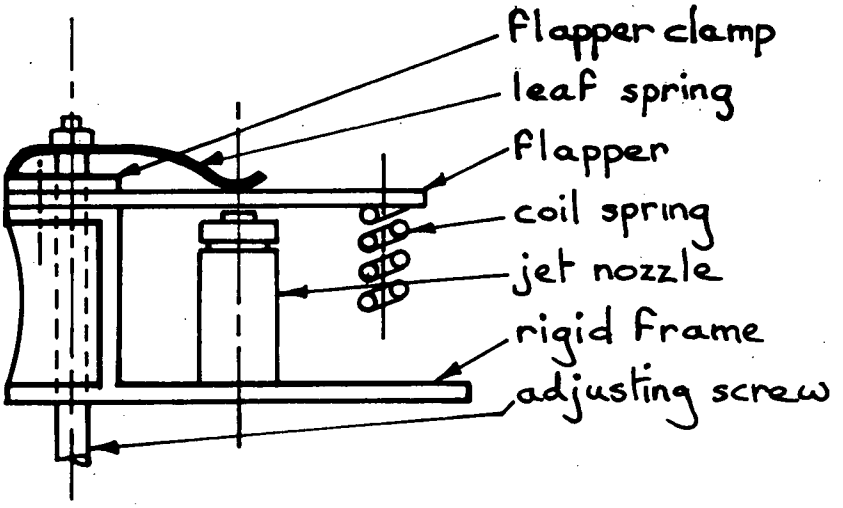

Figure (8-1)

In this design the flapper cantilevers from a rigid base and both initial gap setting and flapper alignment are accurately defined. Null position gap is set by an adjusting screw which tensions a leaf spring to bear on the flapper. This arrangement retains the present basic layout and could be incorporated into the existing valve with minor modifications.

8.3 General purpose digital model

The modelling technique used throughout this thesis involved formulation of system equations, manipulation of equations into state-variable form, and solution by the fourth order Runge-Kutta technique.

System equations were formulated using the small perturbation technique by identifying force and flow summing junctions throughout the system and writing equations which summed to zero at those points. Force equations normally related to a moving mass and flow equations related to any enclosed oil volumes subjected to varying pressure. State-variables then became mass positions, mass velocities, and enclosed volume pressures. This equation formulation technique was found convenient for system analysis because separate components, e.g. pump, relief valve, ram etc., are always coupled by oil lines which form flow summing junctions at some pressure and, in effect, the technique amounts to power bonding. System inputs are naturally accommodated in the equation formulation and result in the B matrix of forcing terms.

Solution of the state-variable equation is possible in a variety of ways if it is linear but for a general purpose model the Runge-Kutta technique was found attractive because non-linear terms could be incoporated with ease and it was numerically stable provided the time interval was sufficiently small. The time interval was determined with reference to A matrix eigenvalues by consideration of the maximum real negative root and the highest oscillation frequency (see section 7.3). Eigenvalues were also indispensible for performance and stability prediction and, in addition, were used to indicate whether the system order could be reduced.

The two criteria used to estimate a Runge Kutta time interval were also found useful to indicate the possibility of system order reduction. The presence of a disproportionately large real negative A matrix eignevalue, which would affect system response at frequencies well beyond the normal range of interest, resulted because moving mass inertia forces were dominated by other forces. Order reduction was accomplished by ignoring the mass in which case mass position remained as a state-variable and mass velocity was removed to the time derivative vector to replace mass acceleration. Order reduction was also suggested by the presence of a high frequency complex conjugate pair which resulted when small oil volumes were regarded as compressible and the oil pressure included as a state-variable. In this case order reduction was accomplished by neglecting oil compressibility and the oil pressure was eliminated as a state-variable. Normally this procedure would be expected to introduce one real negative eigenvalue to replace the complex conjugate pair although in section 7.3 a zero resulted due to the nature of the system being investigated. It is also possible that oil compressibility may be considered in a situation where damping is high enough to inhibit oscillatory transients in which case real negative eigenvalues will result from this source, but this would only be possible at very low frequencies since the damping ratio must be greater than the oscillation frequency which would rarely be the case in 'normal' systems.

A general purpose digital model is proposed below. A small computer may not have sufficient capacity to handle the entire model as one comprehensive program and it may be necessary to chain two or three smaller programs if tape or disc storage is available, or otherwise use separate component programs.

8.3.1 Digital model flow chart

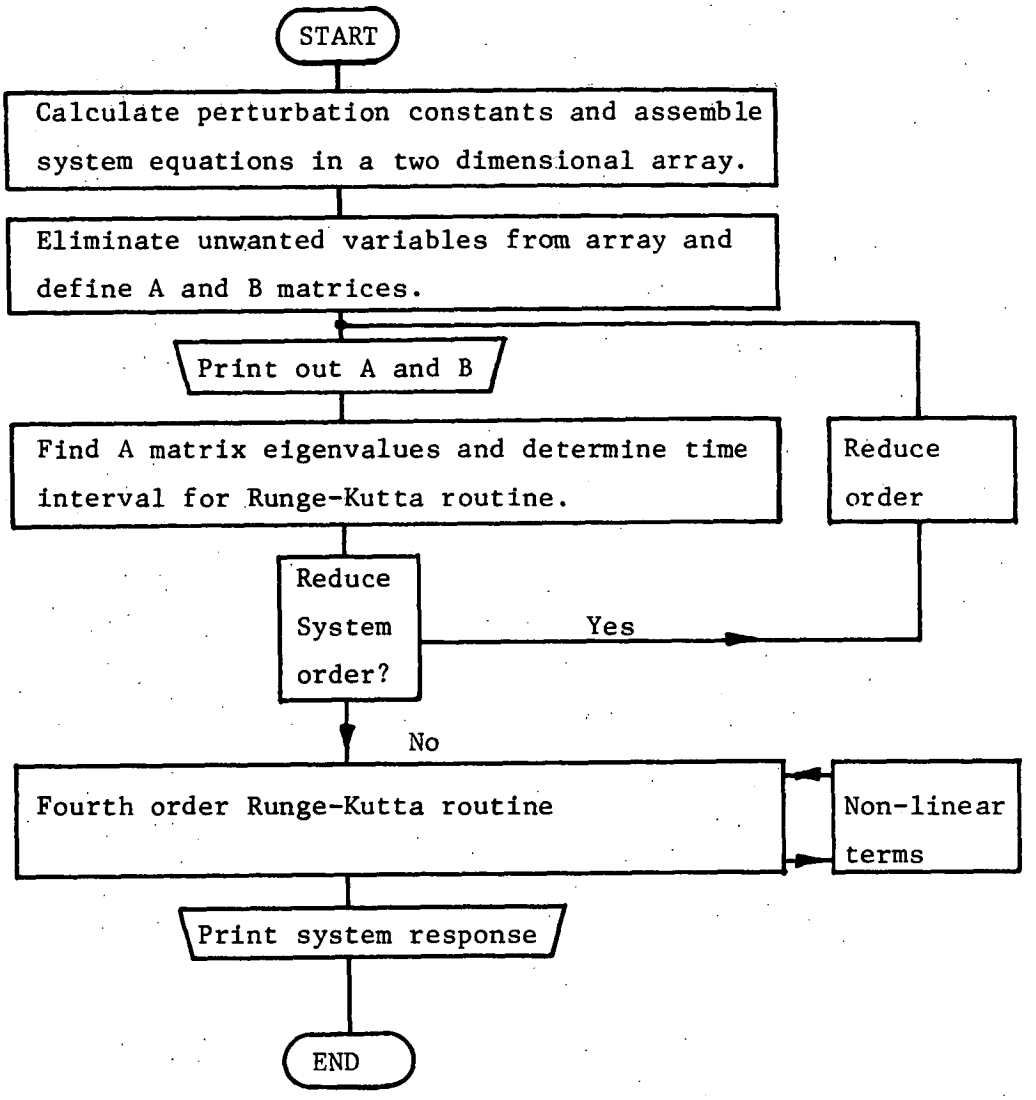

8.4 Servo-system model order

The system modelled comprised a servo-valve directly coupled to a hydraulic ram. It was found that the servo-valve could be modelled as a first order system provided all perturbations were small. The ram and associated oil lines were modelled as a second order system but with small load pressure perturbations the effect of this system was small enough to be neglected in which case the ram acted as a simple flow integrator and the combined system linear model became second order in the open-loop condition and third order in the closed-loop condition (using the specified position transducer as a feed back device).

Large perturbations in either coil current or load pressure necessitated the use of non-linear models tailored to the particular application. For instance, with large coil current perturbations and light load conditions,the servo-valve would be a first order non-linear model and the ram a simple integrator, but with large load perturbations the ram would be a second order model.

8.5 Correlation of model with test results

The original digital model developed in chapter 4 gave a good indication of system performance by comparison with test results. A subsequent modification was included in chapter 7 in the light of experimental results and the eventual model then accurately predicted light load open-loop system response over the normal operating range for which tests were conducted. Above 35Hz both the manufacturer's specification and the extrapolated test results indicated a larger phase lag than the model, as in figure (4-5), but thi frequency range has little practical significance and was not investigated. The final open-loop model was used as the basis for a closed-loop system model (section 8.4.4) which also gave a very reliable prediction of system response.

In general, it is concluded that the digital models developed gave a fair description of the systems described and that the validity of the modelling technique has been demonstrated.

8.6 Review of basic objectives

The basic aims of this thesis, as set out in the preface, were achieved. Methods were proved for formulating system equations, manipulating them into state-variable form, reducing system order if required, and solving the system model by digital simulation. An existing servo-valve was modelled with reasonable accuracy and the versatility of a small computer for modelling, control, interfacing and data logging was demonstrated. System block diagrams were constructed and used to investigate linear and non-linear responses including parameter coupling deriving from non-linear effects.

In conclusion,the thesis has demonstrated the validity of the analytical techniques proposed and the application of a small computer, such as may be available in design offices, to digital simulation of systems of sixth order or more.

APPENDIX 1

A1-1

Table of Green and Crossley's Constants

A	$3.225E^{-4}$	m^2
a	$4.923E^{-5}$	m^2
a'	$4.923E^{-5}$	m^2
C_E	0.646	m^2S^{-1}
K	0.0322	m^2S^{-1}
k	$2.802E^{5}$	Nm^{-1}
k'	$4.1067E^{5}$	Nm^{-1}
M	1.817	Kg
m	0.0536	Kg
N	$6.895E^{8}$	Nm^{-2}
v	$4.332E^{-4}$	m^3
δ	45	degrees
ζ_R	0.7	
ζ_3	$0.7/\sqrt{2}$	
ζ_4	0.7	
τ_3	0.001	S
τ_4	0.0005	S
ϕ	$3.225E^{-5}$	m^2
ω_{n3}	2830	rad S^{-1}
ω_{n4}	4000	rad S^{-1}
C_{L4}	$8.597E^{-12}$	m^5N^{-1}
C_{L3}	$1.340E^{-10}$	m^5N^{-1}
C_R	$1.301E^{-11}$	$m^5N^{-1}S^{-1}$
C_y	2.322	m^2S^{-1}

A1-2 Four-way servo-system equations

Using the equations from Green & Crossley. From equations 10 to 14 setting $C_p = 0$

$$q_1 = q_2 = C_E(x_1 - x_o)$$

Let $p_3 = p_1 - p_2$

Adding equations 13 and 14

$$\frac{V_4}{2N}\dot{p}_3 = -2C_E x_o - 2A\dot{x}_o - 2C_{L4} p_3 + 2C_E x_i \quad \ldots\ldots\ldots \text{A4}$$

From equation 17

$$M\ddot{x}_o = A p_3 - \emptyset p_s \quad \ldots\ldots\ldots \text{B4}$$

From equations 38 to 41

$$m\ddot{y} = -k' y - C\dot{y} + a' p_s \quad \ldots\ldots\ldots \text{C4}$$

From equations 43 to 46b and 10 to 13

q_1 in equation 43 should read $|q_1|$

For extension only when $x_i > x_o$

$$\frac{V}{N}\dot{p}_s = (K + C_E)x_o - C_y y - a\dot{y} - C_R p_s - C_E x_i - q_L \quad \ldots\ldots \text{D4(a)}$$

For retraction only when $x_i < x_o$

$$\frac{V}{N}\dot{p}_s = (K - C_E)x_o - C_y y - a\dot{y} - C_R p_s + C_E x_i - q_L \quad \ldots\ldots \text{D4(b)}$$

also $\dot{x}_o = \frac{d}{dt} x_o \quad \ldots\ldots\ldots \text{E4}$

and $\dot{y} = \frac{d}{dt} y \quad \ldots\ldots\ldots \text{F4}$

State-variables are:

$$x_o \quad \dot{x}_o \quad y \quad \dot{y} \quad p_3 \quad p_s$$

Inputs are:

$$x_i \quad \text{and} \quad q_L$$

Equations A4 to F4 are assembled to the standard state-variable form

$$\{\dot{X}\} = [A]\{X\} + [B]\{U\}$$

where $\{X\}^T = \{x_o \quad \dot{x}_o \quad y \quad \dot{y} \quad p_3 \quad p_s\}$

$$\{\dot{X}\}^T = \{\dot{x}_o \quad \ddot{x}_o \quad \dot{y} \quad \ddot{y} \quad \dot{p}_3 \quad \dot{p}_s\}$$

$$\{U\} = \{x_i \quad q_L\}$$

Substituting values given in section A1-1 the A matrix becomes:

$$\begin{bmatrix} 0 & 1 & 0 & 0 & 0 & 0 \\ 0 & 0 & 0 & 0 & 1.777E^{-4} & -1.777E^{-5} \\ 0 & 0 & 0 & 1 & 0 & 0 \\ 0 & 0 & -7.668E^{6} & -3878 & 0 & 8.926E^{-4} \\ -1.803E^{14} & -9.006E^{10} & 0 & 0 & -5600 & 0 \\ a_{61} & 0 & -3697E^{12} & -7.837E^{7} & 0 & -20.706 \end{bmatrix}$$

where $a_{61} = 1.079E^{12}$ during extension, $x_i > x_o$

$a_{61} = -.976E^{12}$ during retraction, $x_i < x_o$

The B matrix becomes:

$$\begin{bmatrix} 0 & 0 \\ 0 & 0 \\ 0 & 0 \\ 0 & 0 \\ 1.803E^{14} & 0 \\ b_{61} & -1.592E^{12} \end{bmatrix}$$

where $b_{61} = -1.028E^{12}$ during extension, $x_i > x_o$

$b_{61} = +1.028E^{12}$ during retraction, $x_i < x_o$

A1-3- Equation scaling for analog computation

Maximum amplitudes for state-variables are estimated below and used to obtain computer scaled variables.

Variable	Max. Value	Computer Scaled Variable
x_o	10^{-4}m	$[1.0E^4 x_o] = X_o$
$\dot{x}_o$	$.37ms^{-1}$	$[3 \dot{x}_o] = \dot{X}_o$
y	$3E^{-5}$m	$[3E^4 y] = Y$
$\dot{y}$	.037 m	$[25\dot{y}] = \dot{Y}$
P_3	$3E^6$ Pa	$[P_3/3E^6] = P_3$
P_s	$3.5E^5$Pa	$[P_2/3.5E^5] = P_s$

Amplitude and time scaling

Equation A4 is scaled as an example using the computer scaled variables given above allowing a time factor $\beta = 1000$, $x_i = .0001$m and $q_L = 0$.

$$\dot{p}_3 = -1.803E^{14}\, x_o - 9.006E^{10}\, \dot{x}_o - 5600\, p_3 + 1.803E^{14}\, x_i$$

$$\dot{p}_3 = \frac{d}{dt}\, p_3$$

$$\frac{d}{dt}\left[\frac{p_3}{3E^6}\right] = \frac{1.803E^{14}[1.0E^4 x_o]}{3E^6 \times \beta \times 1.0E^4} - \frac{9.006E^{10}[3\dot{x}_o]}{3E^6 \times \beta \times 3} -$$

$$\frac{-5600}{\beta}\,[p_3/3E^6] \qquad + \frac{1.803E^{14} \times .0001}{3E^6\ \beta}$$

$$\frac{d}{dt}\,[P_3] = -6.01\,[X_o] - 10.006[X_o] - 5.6[P_3] + 6.01$$

Matrix A scaled becomes

$$\begin{bmatrix} 0 & 3.333 & 0 & 0 & 0 & 0 \\ 0 & 0 & 0 & 0 & 1.60 & -.019 \\ 0 & 0 & 0 & 1.2 & 0 & 0 \\ 0 & 0 & -6.39 & -3.878 & 0 & 7.81 \\ -6.01 & -10.006 & 0 & 0 & -5.6 & 0 \\ a_{61} & 0 & -.352 & -.009 & 0 & -.021 \end{bmatrix}$$

$a_{61} = 0.308$ during extension

$a_{61} = -.279$ during retraction.

Matrix B becomes

$$\begin{bmatrix} 0 & 0 \\ 0 & 0 \\ 0 & 0 \\ 0 & 0 \\ 6.01 & 0 \\ b_{61} & 0 \end{bmatrix}$$

$b_{61} = -.294$ during extension

$b_{61} = +.294$ during retraction

A1-4 - Steady-state values for a step input

In the steady-state condition following a step input x_i the values of $\{\dot{X}\}$ will all be zero.

Solving the equations for final values gives:

$y = 0.0013$ mm

$p_3 = 0.0011$ MPa

$p_2 = 0.011$ MPa

$x_o \doteqdot 0.0001$ m

$x_o \neq x_i$ because the step input causes a slight change in the equilibrium leakage flow.

A1-5 Scaled matrix eigen values

Extension	Retraction
-0.595	-0.585
-3.622	-3.624
$-1.654 \pm 1.770\ i$	$-1.656 \pm 1.769\ i$
$-0.987 \pm 2.804\ i$	$-0.990 \pm 2.804\ i$

The above eigenvalues must be multiplied by $\beta = 1000$ to convert to real time. The two complex conjugate pairs give rise to oscillations of 281 and 446 cps with damping ratios of 0.68 and 0.33 respectively. These values suggest that system repsonse will be dominated by the smallest negative real root and the least damped complex conjugate pair.

A1-6 Steady-state response

$$X = A\,X + B\,U$$

$$(SI-A)\,X = B\,U$$

$$X = (SI - A)^{-1}\,U$$

and $$U = x_i \cos\ \omega t$$

Substitution in the above equation gives the maximum amplitude of x_o to be:

$$x_o max = \sqrt{\frac{R_N^2 + I_N^2}{R_D^2 + I_D^2}} \times x_{imax}.$$

and phase lag ϕ is given by:

$$\phi = \tan^{-1} \frac{I_D}{R_D} - \tan^{-1} \frac{I_N}{R_N} .$$

where $R_N = -111.7 + 125.14\ \omega^2$

$I_N = -251.2\omega + 32.07\ \omega^3$

$R_D = 111.7 - 269.7\ \omega^2 + 45.7\ \omega^4 - \omega^6$

$I_D = 306.6\omega - 141.7\ \omega^3 + 9.50\ \omega^5$

where ω is the real time frequency divided by 1000.

APPENDIX 2

A2-1 Three-way servo-system equations

From equation 27

$$\dot{x}_o = \frac{2A}{M} p_1 - \frac{(\phi + A)}{M} p_s \quad \ldots\ldots\ldots \text{A3}$$

also $$\frac{d}{dt}(x_o) = \dot{x}_o \quad \ldots\ldots\ldots \text{B3}$$

and $$\frac{d}{dt}(y) = \dot{y} \quad \ldots\ldots\ldots \text{C3}$$

From equations 38-41

$$m\ddot{y} = -k'y - c\dot{y} + a' p_s \quad \ldots\ldots\ldots \text{D4}$$

Setting $C_p = 0$ gives $q_1 = C_E(x_i - x_o)$

and from equation 25

$$q_1 = C_E(x_i - x_o) = \frac{V_3}{N} \dot{p}_1 + 2A \dot{x}_o + C_{L3} p_1$$

$$\frac{V_3}{N} \dot{p}_1 = -C_E x_o - 2A \dot{x}_o - C_{L3} p_1 + C_E x_i \quad \ldots\ldots\ldots \text{E3}$$

From equations 43 to 48b

For ram extension

$$\frac{v}{N} \dot{p}_s = (K + C_E)x_o + A \dot{x}_o - C_y y - a\dot{y} - C_R p_s - C_E x_i - q_L \quad \ldots \text{F3(a)}$$

For ram retraction

$$\frac{v}{N} \dot{p}_s = Kx_o + A\dot{x}_o - C_y y - a\dot{y} - C_R p_s - q_L \quad \ldots\ldots\ldots \text{F3(b)}$$

State-variables are

$x_o \; \dot{x}_o \; y \; \dot{y} \; p_1 \; p_s$

Inputs are

x_i only - q_L is set at zero.

As in Appendix 1 the A and B matrices are evaluated below.

The A matrix becomes:

$$\begin{bmatrix} 0 & 1 & 0 & 0 & 0 & 0 \\ 0 & 0 & 0 & 0 & 3.554E^{-4} & -1.955E^{-4} \\ 0 & 0 & 0 & 1 & 0 & 0 \\ 0 & 0 & -7.668E^{6} & -3878 & 0 & 8.926E^{-4} \\ -2.256E^{13} & -2.254E^{10} & 0 & 0 & -3962 & 0 \\ a_{61} & 5.134E^{8} & -3.697E^{12} & -7.837E^{7} & 0 & -20.706 \end{bmatrix}$$

$a_{61} = 1.0789E^{12}$ during extension when $x_i > x_o$

$a_{61} = 5.1308E^{10}$ during retraction when $x_i < x_o$

and the B matrix becomes

$$\begin{bmatrix} 0 \\ 0 \\ 0 \\ 0 \\ 2.256E^{13} \\ b_{61} \end{bmatrix}$$

where $b_{61} = -1.028E^{12}$ during extension

$b_{61} = 0$ during retraction

A2-2 Scaled Equations for the Analog Computer

Using $\beta = 1000$ and the same scaled variables as for the four-way valve the A matrix is:-

$$\begin{bmatrix} 0 & 3.333 & 0 & 0 & 0 & 0 \\ 0 & 0 & 0 & 0 & 3.199 & -.2053 \\ 0 & 0 & 0 & 1.2 & 0 & 0 \\ 0 & 0 & -6.39 & -3.878 & 0 & 7.81 \\ -.752 & -2.504 & 0 & 0 & -3.962 & .462 \\ a_{61} & .489 & -.352 & -.009 & 0 & -.021 \end{bmatrix}$$

and the B matrix is:-

$$\begin{bmatrix} 0 \\ 0 \\ 0 \\ 0 \\ .752 \\ b_{61} \end{bmatrix}$$

where

$a_{61} = 0.308$ during extension

$a_{61} = 0.0146$ during retraction

$b_{61} = -0.294$ during extension

$b_{61} = 0$ during retraction.

A2-3 Scaled Matrix Eigenvalues

Allowing for the time factor $\beta = 1000$ the eigenvalues for the extension matrix are

-432

-1976

$-1054 \pm 1,854\, i$

$-1673 \pm 1,732\, i$

and for the retraction matrix:-

$$-661$$

$$-1710$$

$$-1130 \pm 1765\,i$$

$$-1615 \pm 1712\,i$$

In both cases the complex conjugate pairs are similar yielding oscillations with a period of approximately 0.0035 sec and damping ratios of about 0.5 and 0.69 but the dominant real negative roots of -661 and -432 differ significantly between extension and retraction.

APPENDIX 3

A3.1 Table of symbols and constants

Where variables are perturbed the symbols are upper case for the actual value, and lower case for the perturbed value.

All units used throughout this chapter are standard S.I.

Symbol	Definition	Value	Units
a_{11}	Flapper influence coefficient	1.1E-4	mN^{-1}
a_{12}	"	.293E-4	"
a_{22}	"	.11E-4	
A_{12}	Orifice area (nominal)	2.027E-7	m^2
A_{23}	"	4.56E-7	"
A_{34}	"	1.026E-6	"
A_{40}	"	1.979E-6	"
A_R	Ram pressure area	.6334E-3	"
A'	Perturbed segmental area		
A_2	Spool pressure area	1.02E-4	m^2
A_3	"	1.979E-4	"
A_4	"	0.959E-4	"
C_C	Flow contraction coefficient		
C_Q	Orifice flow coefficient		
C_{12}	"	0.722	
C_{23}	"	0.932	
C_4	"	0.820	
d	diameter		
F, f	Force, actual and perturbed		
F_{MAG}	Flapper magnetic force		
F_{j3}	Jet force on flapper		
F_j	Jet force on spool		
F_{sp}	Coil spring force		

H, h	Flapper valve gap, actual and perturbed		
i	Perturbed coil current		
K	Coil spring rate	1700	Nm^{-1}
M	Ram mass with attachments	2.2	Kg
m	spool mass	0.0705	Kg
N	Bulk modulus of oil	690E6	Nm^{-2}
n	Ram position		
P, p	Pressure, actual and perturbed		
ΔP, Δp	Pressure differential, actual and pert.		
Q, q	Flow rate, actual and perturbed		
ρ	Oil mass density	854	Kg m^{-2}
V_5	Ram supply line volume	.906E-4	m^3
V_6	Ram return line volume	.906E-4	m^3
x	Flapper end position		
y	Spool position		

A3.2 Control flow equations

The perturbed flow equation for a fixed area orifice is

$$q = \frac{C_0 A \ \Delta p}{\sqrt{(2\rho \ \Delta P)}}$$

A3.2.1 Flow q_1 through orifice C_{12}

$$\Delta P = P_1 - P_2$$

$$\Delta p = -p_2$$

$$q_1 = \frac{-C_{12}A_{12}p_2}{\sqrt{(2\rho(P_1 - P_2))}} \qquad \ldots\ldots \quad (A3\text{-}1)$$

or $q_1 = - K_1 p_2$

A3.2.2 Flow q_2 through orifice C_{23}

$$\Delta p = (p_2 - p_3)$$

$$q_2 = \frac{C_{23}A_{23}(p_2 - p_3)}{\sqrt{(2\rho(P_2 - P_3))}} \qquad \ldots\ldots \quad (A3\text{-}2)$$

or $q_2 = K_2(p_2 - p_3)$

A3.2.3 Flow q_4 through orifice C_4

Allowing for a back pressure of 7kPa

$$\Delta p = p_4$$

$$q_4 = \frac{C_4 A_4 p_4}{\sqrt{(2\rho(P_4 - 7000))}} \qquad \ldots\ldots \quad (A3\text{-}3)$$

or $q_4 = K_4 \ p_4$

A3.2.4 Flapper valve flow q_3

From chapter 3

$$Q_3 = 13.45 \times 10^{-6} H^{0.7} \Delta P^{0.475} \quad \text{in consistent SI units}$$

$$\Delta P = P_3 - P_4$$

In perturbed form

$$q_3 = 13.45 \times 10^{-6} ((P_3-P_4)^{0.475} \times 0.7H^{-0.3}h + H^{0.7} \times 0.475(P_3 - P_4)^{-0.525}(p_3-p_4)) \quad \text{(A3-4)}$$

or $q_3 = K_3 h + K_5(p_3 - p_4)$

A3.2.5 Division of flow q_1

At spool velocity $\dot{y}$ the flow q_1 supplies orifice C_{23} and the annular area A_2

$$q_1 = q_2 - A_2 \dot{y} \quad \text{. . . .} \quad \text{(A3-5)}$$

A3.2.6 Division of flow q_2

At spool velocity $\dot{y}$ the flow q_2 supplies the flapper valve and the annular area A_3

$$q_2 = q_3 + A_3 \dot{y} \quad \text{. . . . .} \quad \text{(A3-6)}$$

A3.2.7 Division of flow q_3

Flapper valve flow to the end cover is supplemented by flow from the spool end movement.

$$q_4 = q_3 + A_4 \dot{y} \quad \text{. . . . .} \quad \text{(A3-7)}$$

A3.3 Flapper force equilibrium

The flapper is acted upon by three forces.

Spring force F_{sp}

Magnetic force F_{MAG} refer to chapter 3

Oil jet force F_{j3}

F_{j3} remains to be determined.

A3.3.1 Oil jet force on the Flapper

Using equation (4.21) from McCloy and Martin in modified form

$$F_{j3} = A_{34}(P_3 - P_4) + \rho Q^2/A_{34}$$

where

$$Q = 13.45 \times 10^{-6} H^{0.7} (P_3 - P_4)^{0.475} \text{ from section A3.1.5}$$

$$F_{j3} = 1.0261 \times 10^{-6}(P_3 - P_4) + 0.15056 H^{1.4}(P_3 - P_4)^{0.95}$$

and in perturbed form

$$f_{j3} = (1.0261 \times 10^{-6} + .15056 H^{1.4}(P_3 - P_4)^{-0.05} x.95)(p_3 - p_4)$$

$$+ .15056(P_3 - P_4)^{0.95} \times 1.4H^{0.4}(h)$$

reducing to

$$f_{j3} = K_6 h + K_7(p_3 - p_4)$$

A3.3.2 Flapper force equations

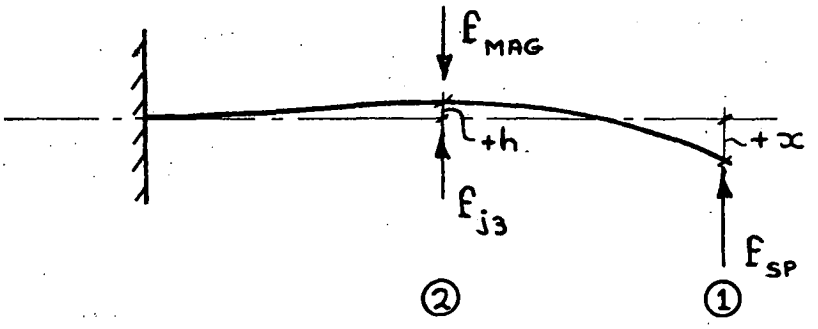

Assuming negligible mass and damping the perturbed flapper force equation is;

$$(f_{j3} - f_{MAG})a_{12} + f_{sp}\, a_{11} = - x$$

$$(f_{j3} - f_{MAG})a_{22} + f_{sp}\, a_{21} = h$$

$$f_{sp} = K(x + y)$$

$$f_{MAG} = 42.51 - 40818h$$

Substitution yields two equations

$$(40818 + K_6)h + K_7(p_3 - p_4) + 26606x + 4724.3y - 42.51 = 0 \quad ..(A3-8)$$

$$(K_6 - 50091)h + K_7(p_3 - p_4) + 4528(x + y) - 42.51 = 0 \quad ..(A3-9)$$

A3.4 Dynamic equilibrium of the spool

Given a time dependant displacement y as defined by figure (2-4) the spool is subjected to the following forces

A3.4.1 Inertia force

$$m\ddot{y} = .0705\ \ddot{y}$$

A3.4.2 Damping force

Spool natural frequency = $\sqrt{(K/m)}$

$= \sqrt{(1700/.0705)}$

$=$ 155.2 radians/sec

Assuming a damping ratio of 0.1 the damping constant C is

$$C = 2 \times 0.1 \times 155.2 \times .0705 = 2.19 \text{ Nsm}^{-1}$$

therefore

damping force = $2.19\ \dot{y}$

A3.4.3 Spring force

$$k(x + y) = 1700\ (x + y)$$

A3.4.4 Pressure forces

$$p_2A_2 + p_4A_4 - p_3A_3$$

A3.4.5 Oil jet forces

From Merritt equation (5-86) the steady state flow force resulting from flow Q is

$$F_j = \frac{\rho Q^2 \cos\theta}{C_c A}$$

where ρ is the mass density, C_c is the contraction coefficient, A is the flow area and θ is the jet angle.

Since $Q = C_Q A\sqrt{(2\Delta P/\rho)}$

$$F_j = 2C_Q^2\ A \cos\theta\ \ \Delta P/C_c$$

The orifice is segmental and Mcloy & Martin predict a discharge coefficient C_D of 0.7 from their figure (2.10) provided the opening is not very small. C_Q is expected to be slightly larger than C_D hence a value of 0.75 is assumed.

C_c depends on the orifice opening and varies between about 0.7 at small openings and 1.0 at large openings. Using Mcloy & Martin's figure (2.6) a value of 0.72 is assumed.

The jet angle θ also depends upon the orifice opening as in Mcloy & Martin's figure (2.5). Allowing a typical spool radial clearance of 0.004mm and spool openings up to 0.5 mm the jet angle varies between 64 and 67.5°, hence $\cos\theta$ is assumed to be 0.4.

Substituting these values gives

$$F_j = 0.625\ A\ \Delta P$$

This equation cannot be used in the standard perturbed form because it reduces at zero to the equilibrium point when both A and $(\partial A/\partial y)$ are zero. The perturbed equation is therefore simplified as follows:

$$f_j = 0.625\ (\Delta P(\frac{\partial A}{\partial y})\ y + A\ \Delta p)$$

The second term is neglected because A is generally small and an average value for $(\partial A/\partial y)$ is calculated so that the orifice area is correct at maximum opening.

For a segmental orifice of diameter D and opening y the opening area is given by

$$A_y = D^2/4(\cos^{-1}\ (1-2y/D)-2(1-2y/D)\sqrt{(y/D-\ (y/D)^2)})$$

At maximum opening y_m the orifice area is

$$(\frac{\partial A}{\partial y})' y_m = A_{ym}$$

$$A' = (\frac{\partial A}{\partial y})' = A_{ym}/y_m$$

Four jets act on the spool due to two orifices at each of the throttling positions metering flows to and from the ram. In each case ΔP is half the supply pressure and all reactions tend to close the valve. Hence the resultant jet force is:

$$f_j = 4 \times 0.625 \times (.5P_1) \times A' \times y$$

$$f_j = 1.25\ P_1\ A'y$$

A3.4.6 Transient flow force

With reference to Mcloy & Martin section 4.4 a transient flow force exists due to the rate of change of momentum of oil within the annular chambers surrounding the spool. This force is considered later but it is noted that the damping lengths associated with the force are L_1 = 7.94mm and L_2 = 11.11mm, and since $L_2 > L_1$ the force is a destabilising transient.

A3.4.7 Resultant spool force equation

From the component equations developed in the preceding sections;

$$m\ddot{y} + 2.19\dot{y} + kx + A_2p_2 + A_4p_4 - A_3p_3$$

$$+ (1.25\ P_1A' + 1700)y = 0 \qquad \ldots\ldots \quad (A3\text{-}10)$$

A3.5 Dynamic equilibrium of the ram

With reference to figure (2-4) the ram is acted upon by the following forces.

A3.5.1 Inertia force

$M\ddot{n}$

A3.5.2 Ram damping force

Ram damping forces derive from two shaft seals and the ram piston seal. Damping is expected to be light and a damping ratio of 0.1 is assumed. The natural frequency of the ram is 1666 radians/second and the ram mass is 2.2 kg.

$$\text{Ram damping constant} = 2 \times 0.1 \times 1666 \times 2.2$$

$$= 733\ \text{Nsm}^{-1}$$

$$\text{Damping force} = 733\dot{n}$$

A3.5.3 Pressure forces

Pressures p_5 and p_6 act over an annular area $1\frac{1}{2}$ x 1 inches diameter to give a force

$$A_R (p_6 - p_5)$$

A3.5.4 Resultant ram force equation

$$P_L = (p_5 - p_6)$$

$$M\ddot{n} + 733 \dot{n} - A_R p_L = 0 \qquad \ldots . \quad (A3\text{-}11)$$

A3.6 Flow equilibrium in the oil passages between valve and ram

There are two oil passages at pressures p_5 and p_6 and for each one there is a dynamic flow equilibrium for volume changes resulting from the following factors.

A3.6.1 Ram velocity flow

This is the product of the ram annular area and ram velocity $\dot{n}$ and it is equal and opposite for the two volumes considered.

Volume at p_5 $\quad - A_R \dot{n}$

Volume at p_6 $\quad + A_R \dot{n}$

A3.6.2 Supply line metered flow

With reference to section A3.4.5 the flow through each segmental orifice area is

$$Q = C_Q A\sqrt{(2\Delta P/\rho)}$$

where $\Delta P = (P_1 - P_5)$ which is $0.05P_1$ at equilibrium.
In perturbed form

$$q = C_Q\sqrt{(2/\rho)}\,(0.5A(\Delta P)^{-.5}(-p_5) + (\Delta P)^{.5}\,(\tfrac{\partial A}{\partial y})y)$$

As in section A3.4.5 this equation is difficult to use and is linearised by neglecting the first term, which should be small, and assuming that $(\partial A/\partial y)$ can be linearised as previously.

Hence for two orifices in parallel

$$q = 2C_Q \sqrt{(2/\rho)} \sqrt{(P_1 - P_5)} \times A' \times y$$

$$q = 0.05133 \sqrt{P_1}\, A'\, y$$ which is the supply line flow perturbation.

A3.6.3 Return line metered flow

As in the previous section except that $\Delta P = (P_6 - 0)$ which is also $0.5\, P_1$ and the flow is an output.

hence

$$q = - 0.05133 \sqrt{P_1} A'\, y$$

A3.6.4 Oil bulk modulus effect

If the ram is at its centrol position there are equal oil volumes V_5 and V_6 at each side of the piston.

The bulk modulus of oil assumed to be 1.44×10^7 lbF/Ft^2, as used by Green & Crossley.

There is a negative rate of change of volume in each line, these being

$$- \frac{V_5}{N} \dot{P}_5 \quad \text{and} \quad - \frac{V_6}{N} \dot{P}_6$$

A3.6.5 Resultant ram flow equilibrium

For the line at pressure P_5

$$-A_R \dot{n} + 0.05133 \sqrt{P_1} A'\, y - V_5/N\, \dot{P}_5 = 0$$

For the line at pressure P_6

$$A_R \dot{n} - 0.05133 \sqrt{P_1} A'\, y - V_5/N\, \dot{P}_6 = 0$$

Since $V_5 = V_6$ and load pressure $p_L = p_5 - p_6$

the equations are combined

$$V_5/N\ \dot{p}_L + 1.267 \times 10^{-3}\ \dot{n} - 0.10266\sqrt{P_1}A'\ y = 0 \quad . \quad . \quad . \quad \text{(A3-12)}$$

APPENDIX 4

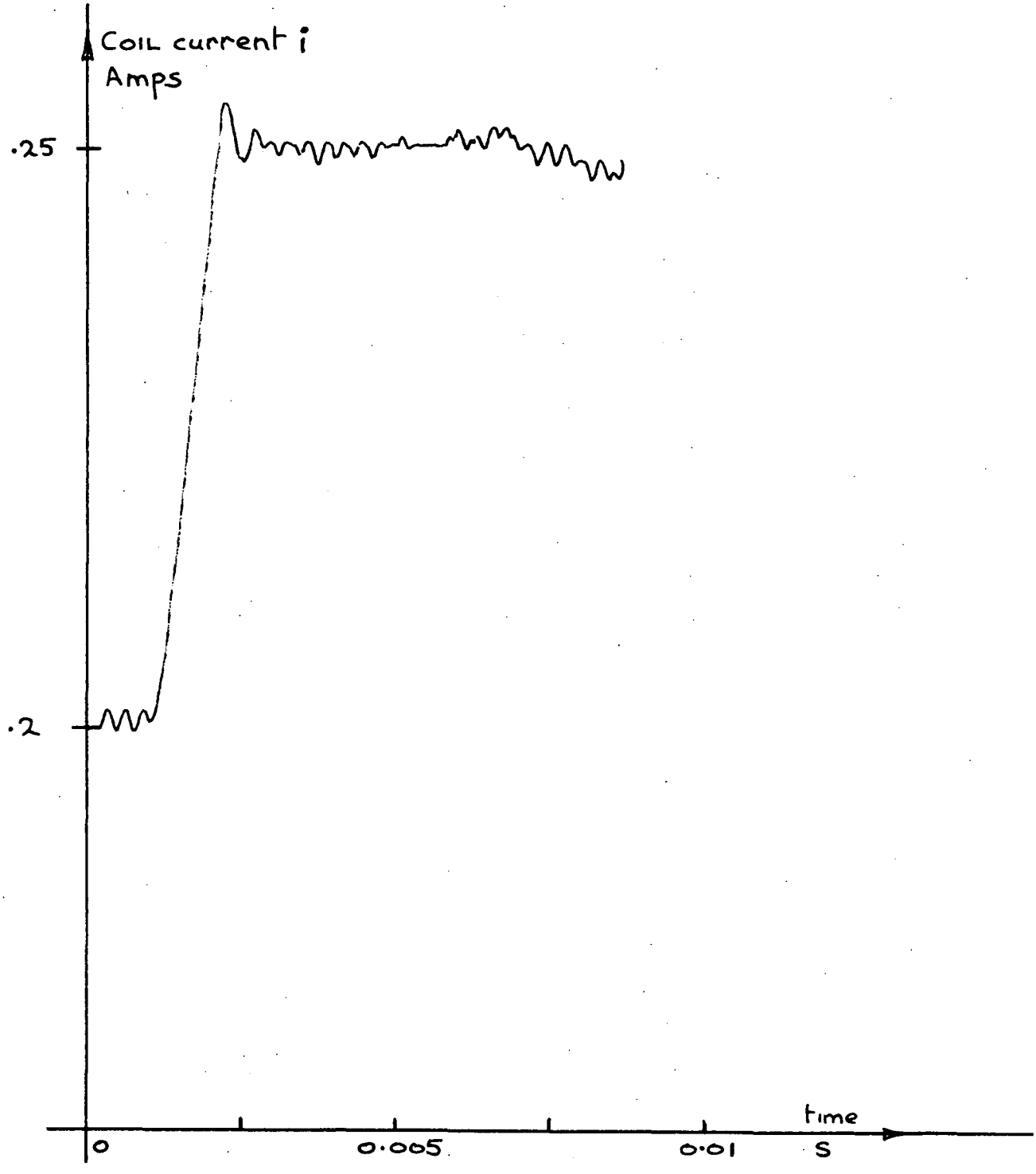

Current source step response Figure (A4-1)

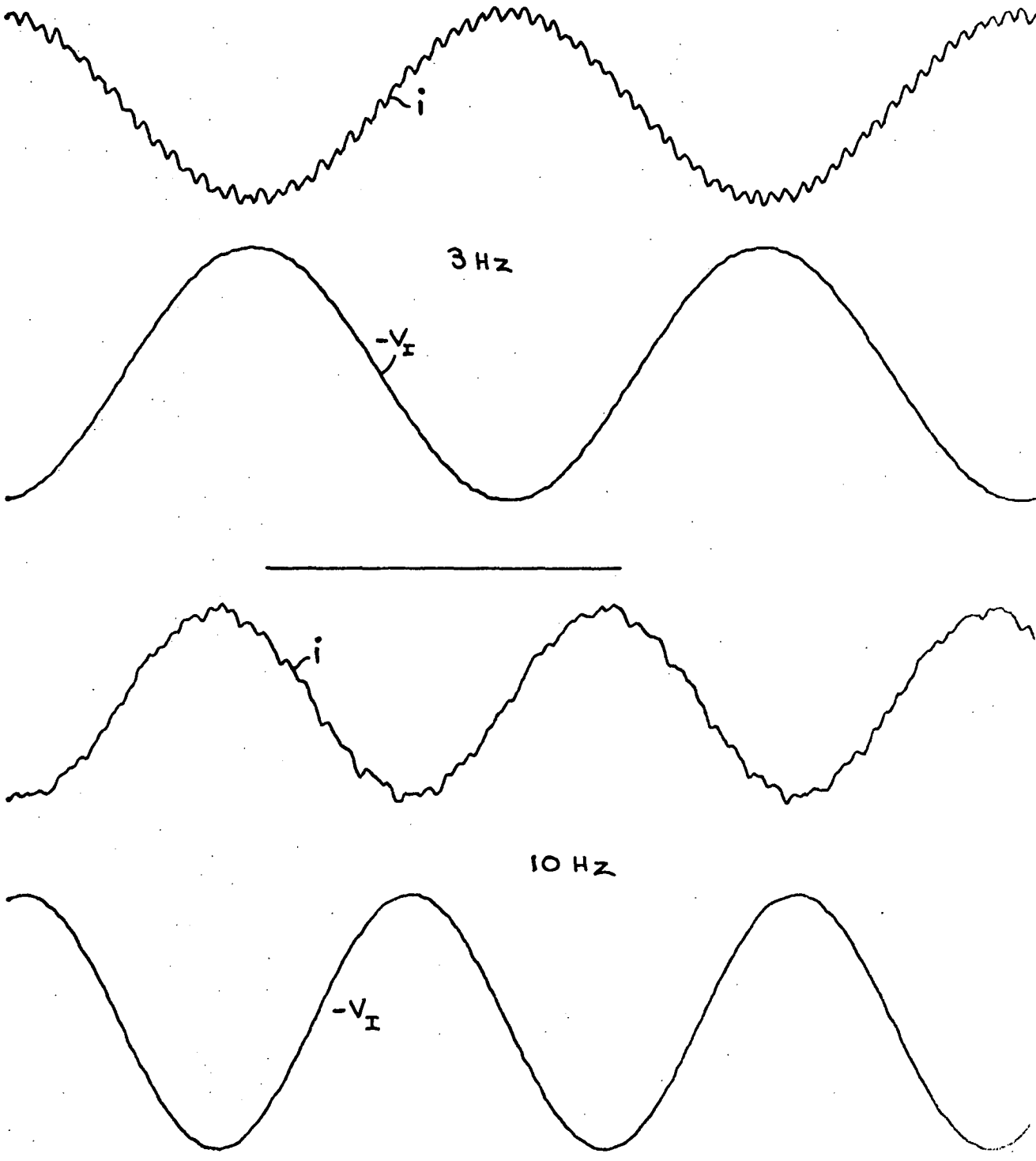

Current source frequency response Figure (A4-2)

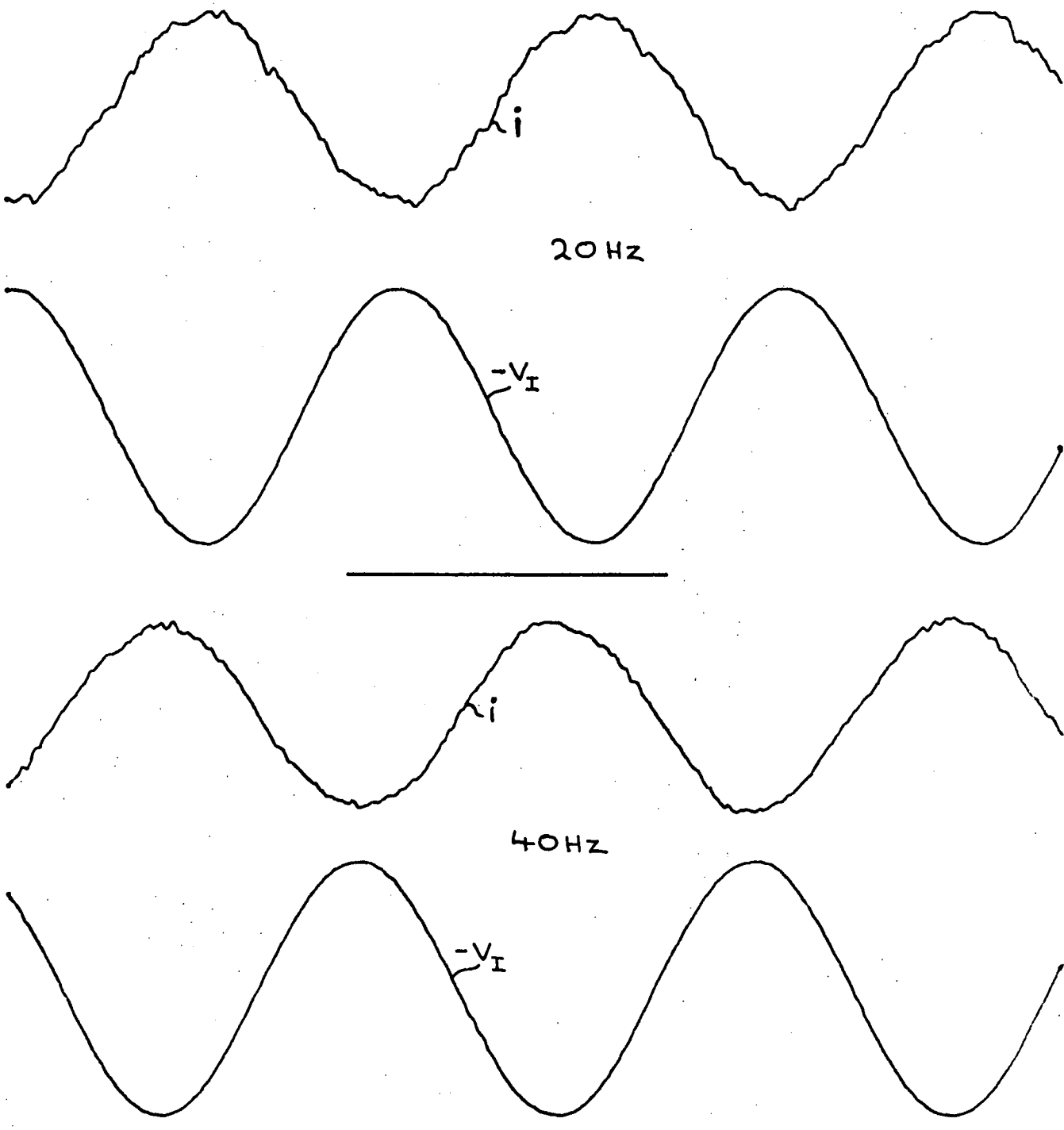

Current source frequency response Figure (A4-3)

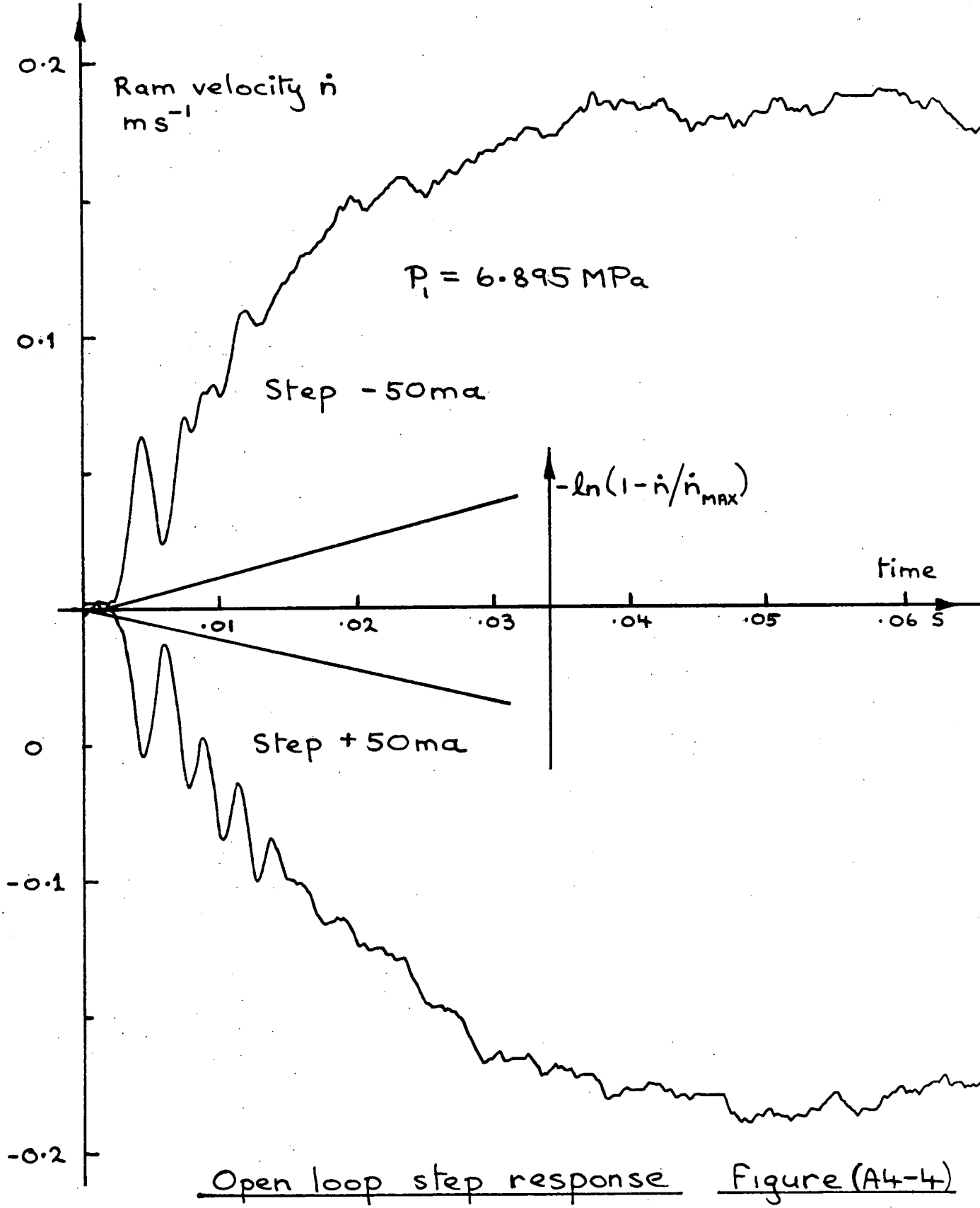

Open loop step response Figure (A4-4)

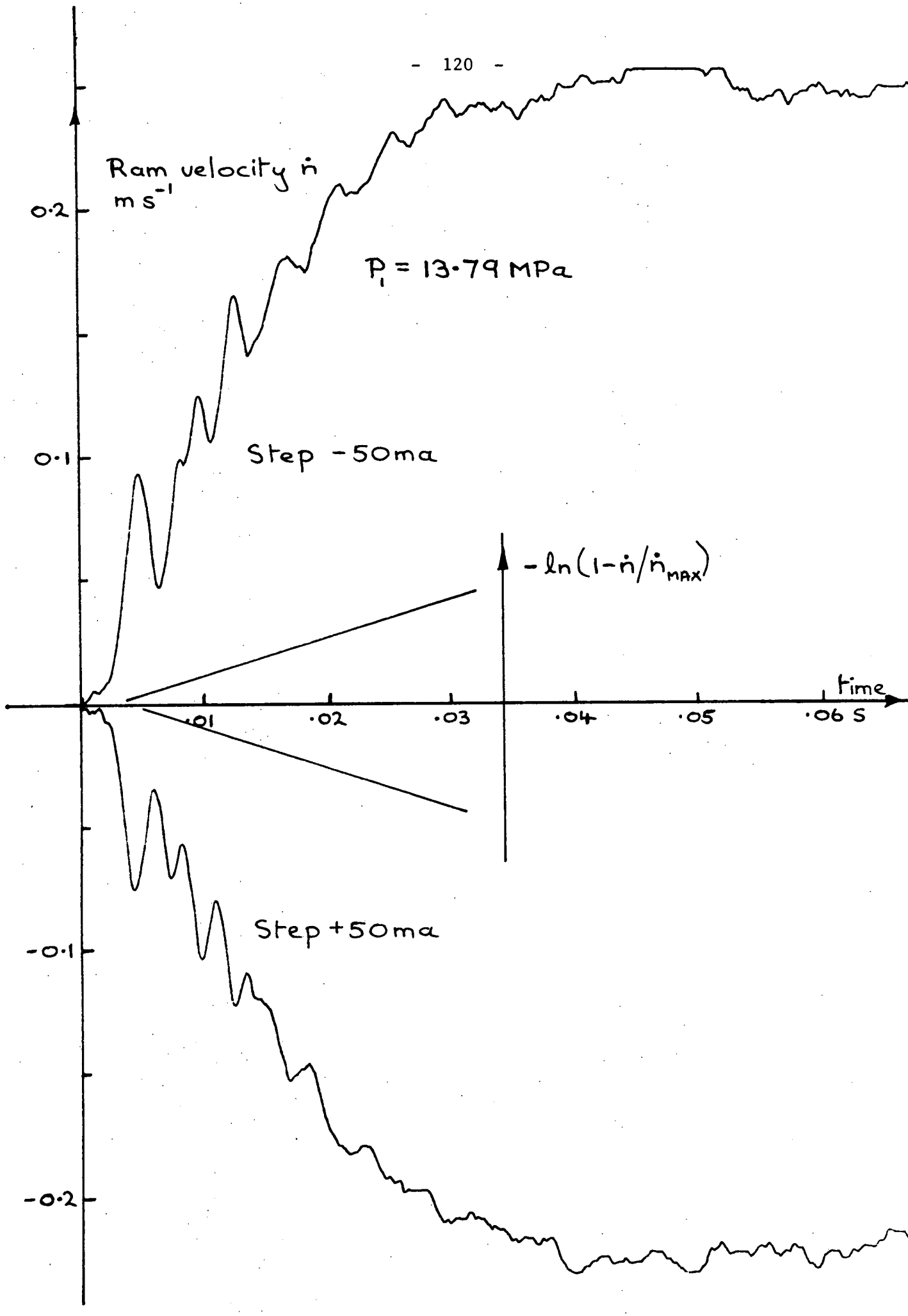

Open loop step response Figure (A4-5)

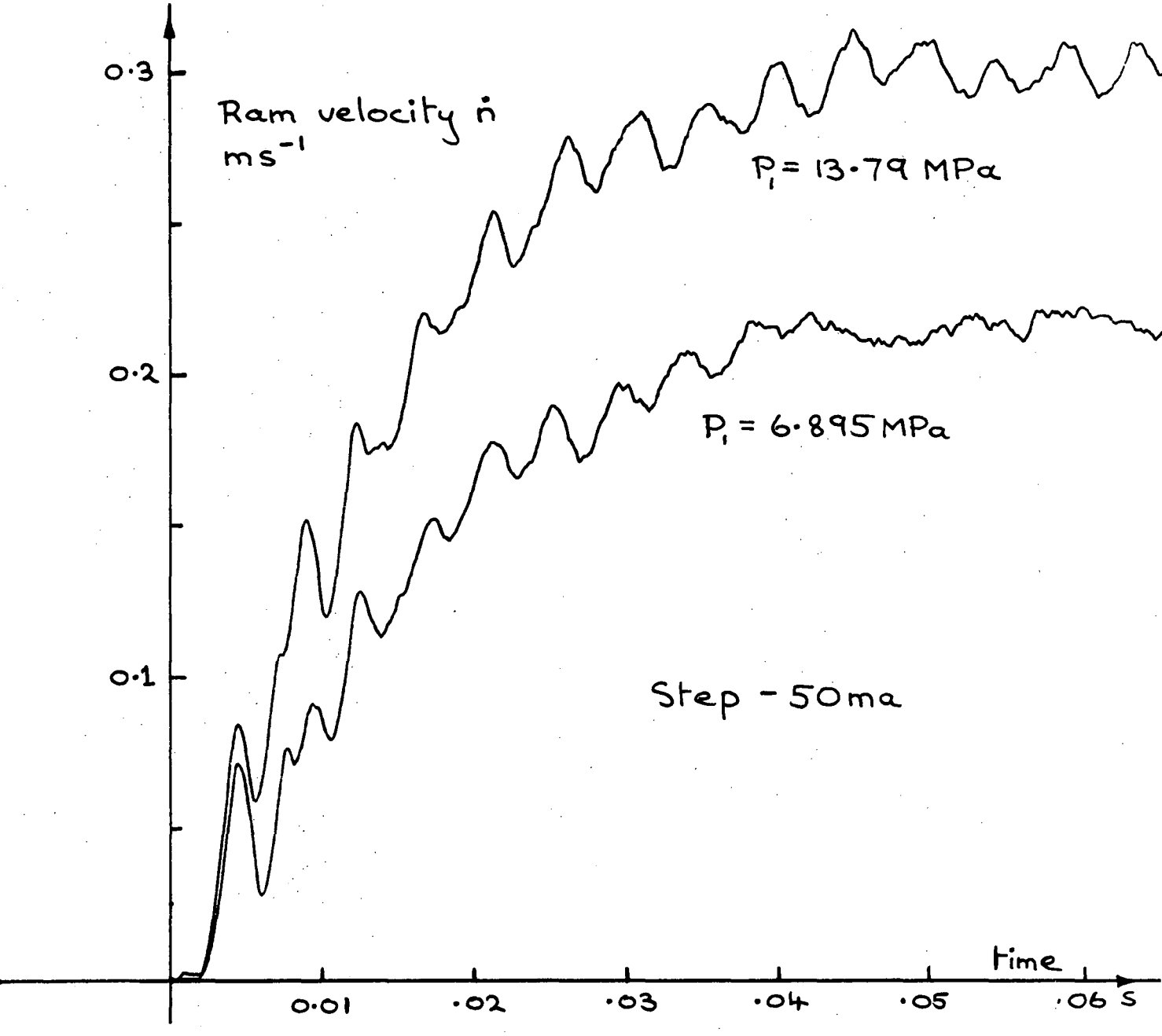

Open loop step response Figure (A4-6)

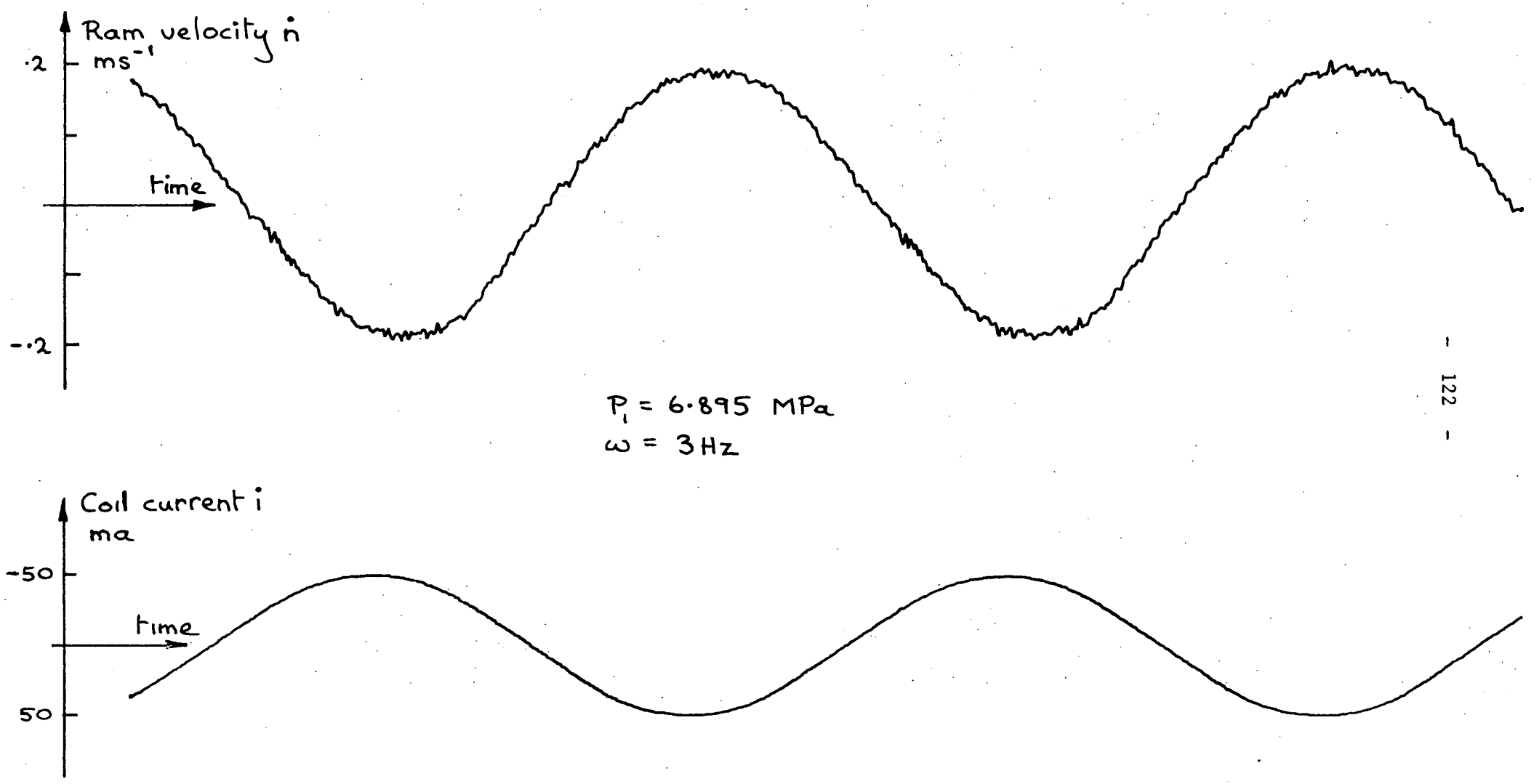

Servo-valve open-loop response Figure (A4-7)

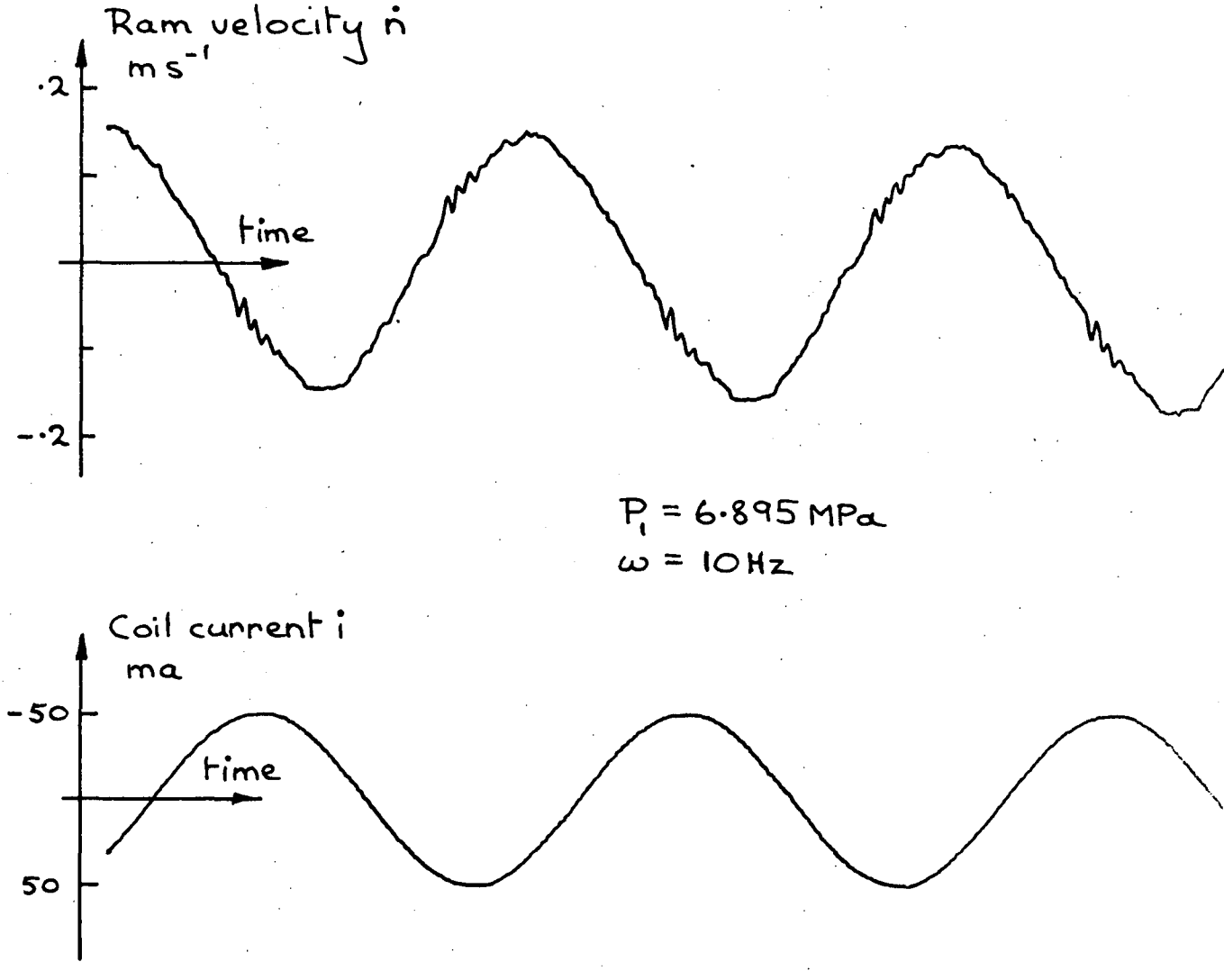

Servo-valve open-loop response Figure (A4-8)

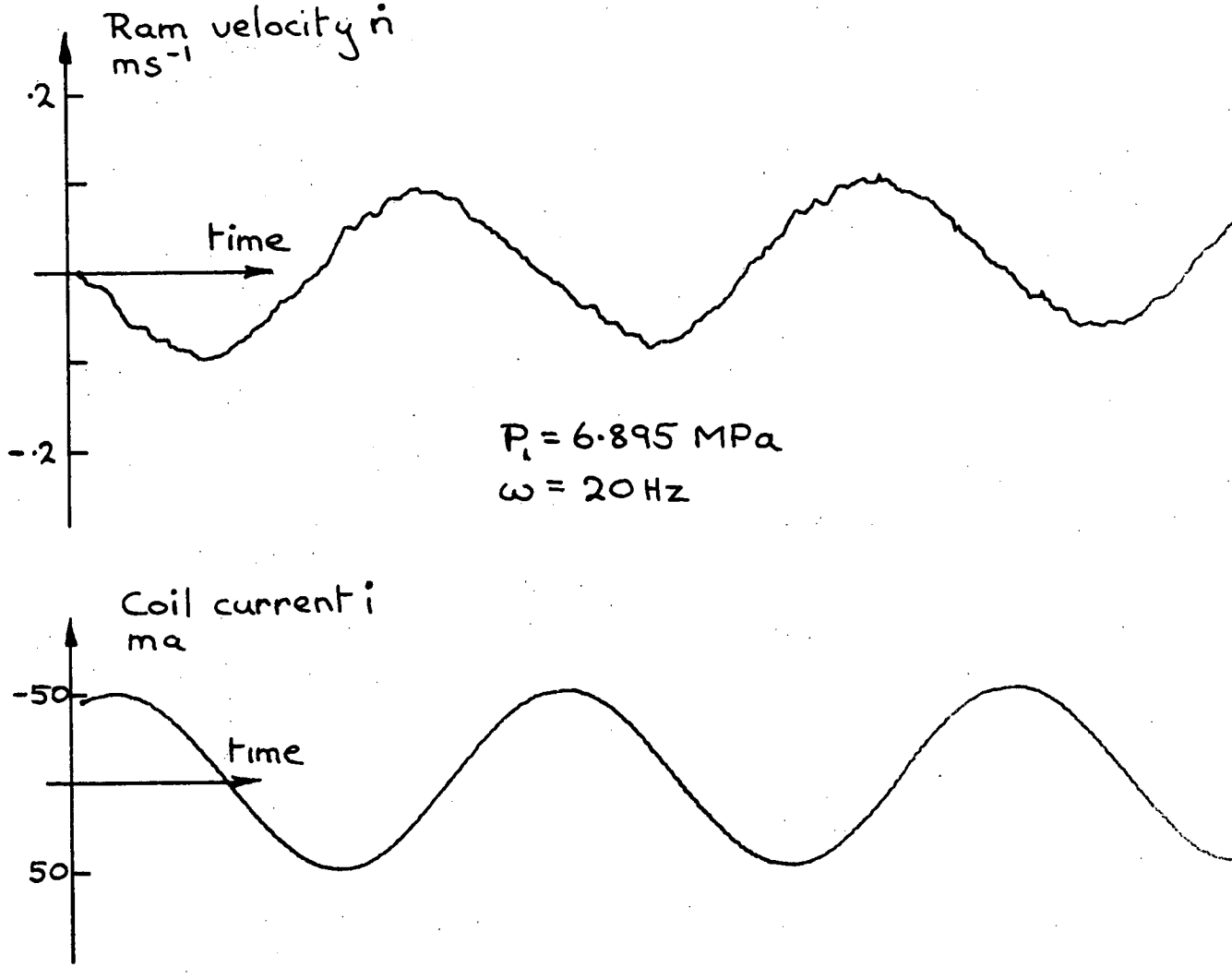

Servo-valve open-loop response Figure (A4-9)

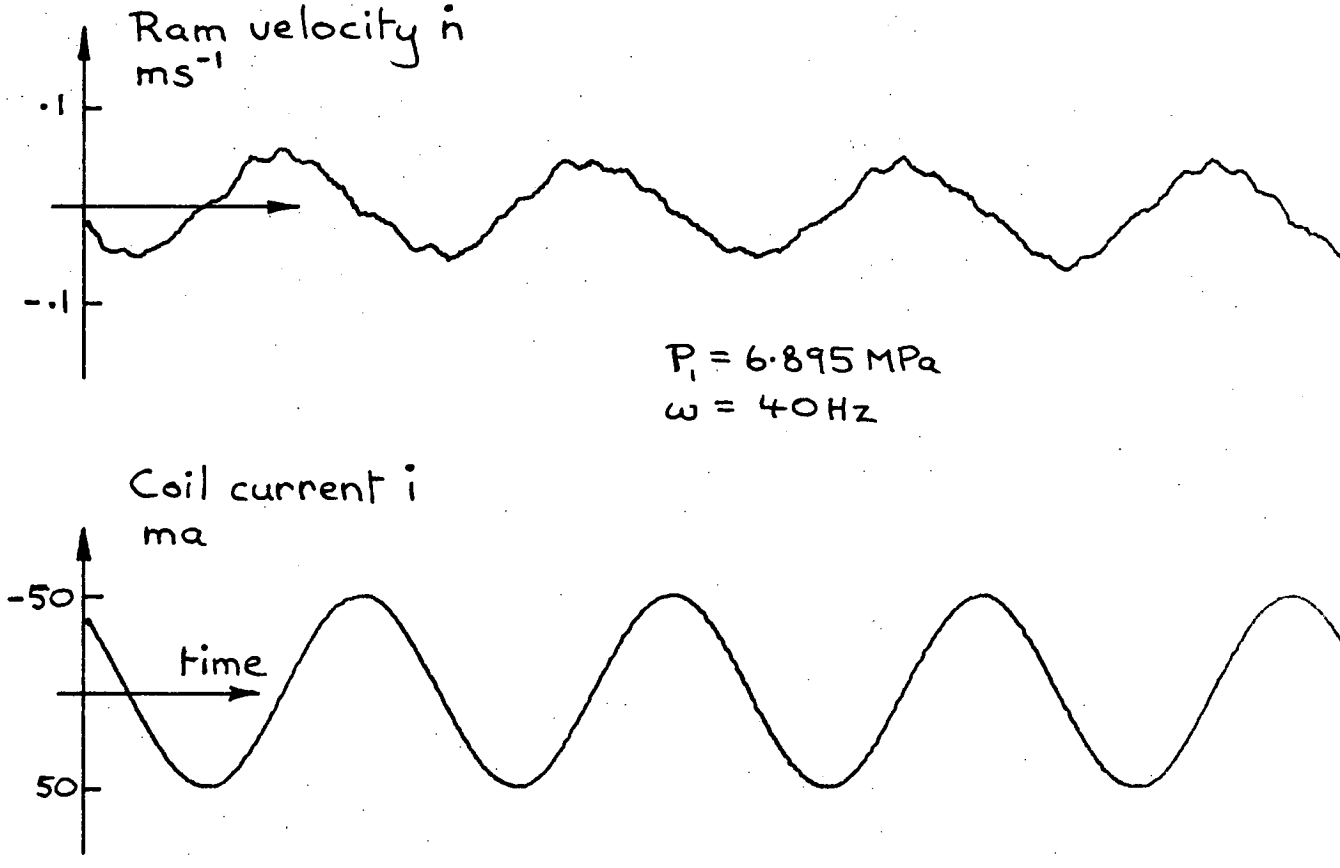

Servo-valve open-loop response Figure (A4-10)

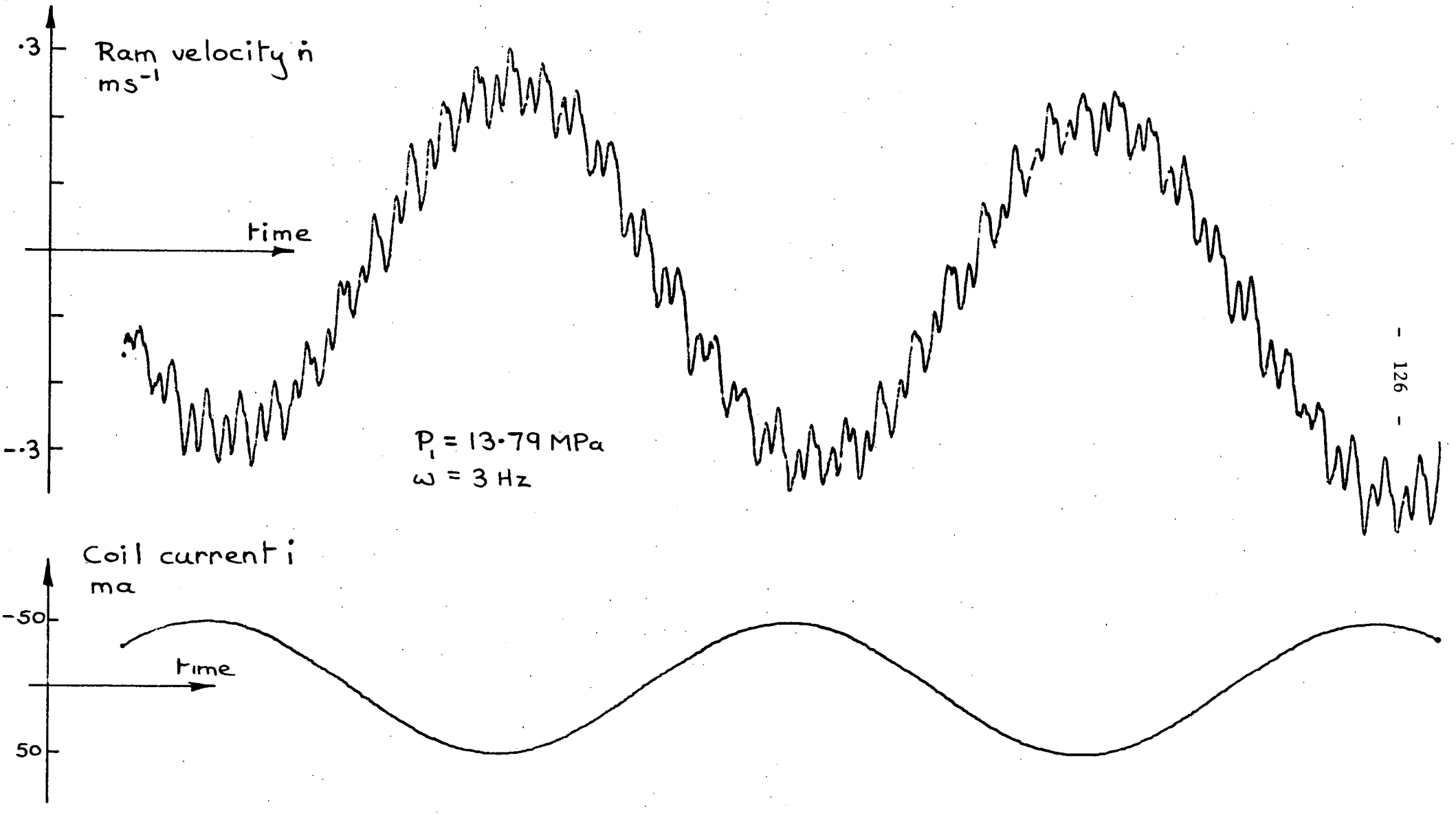

Servo-valve open-loop response Figure (A4-11)

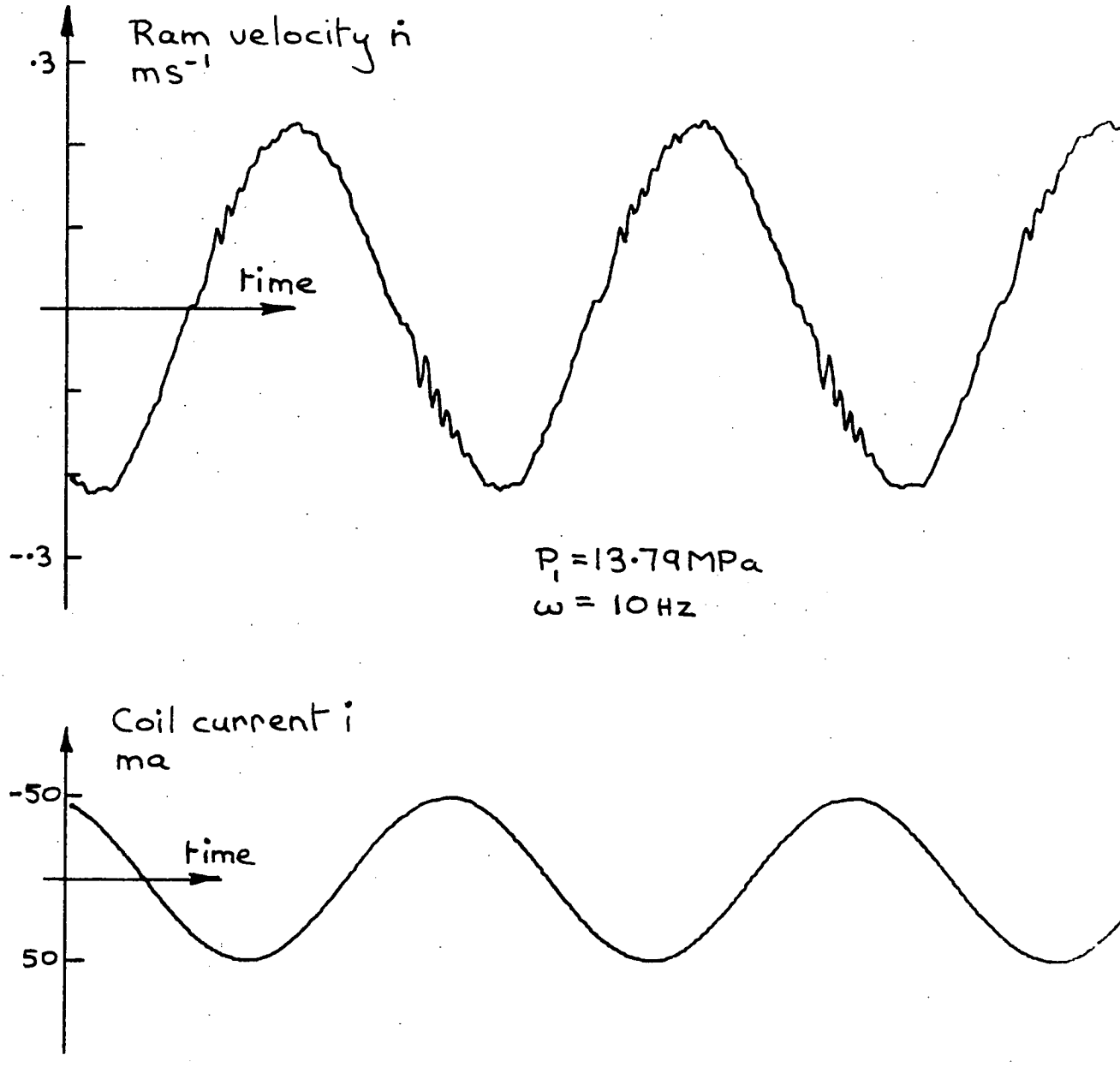

Servo-valve open-loop response Figure (A4-12)

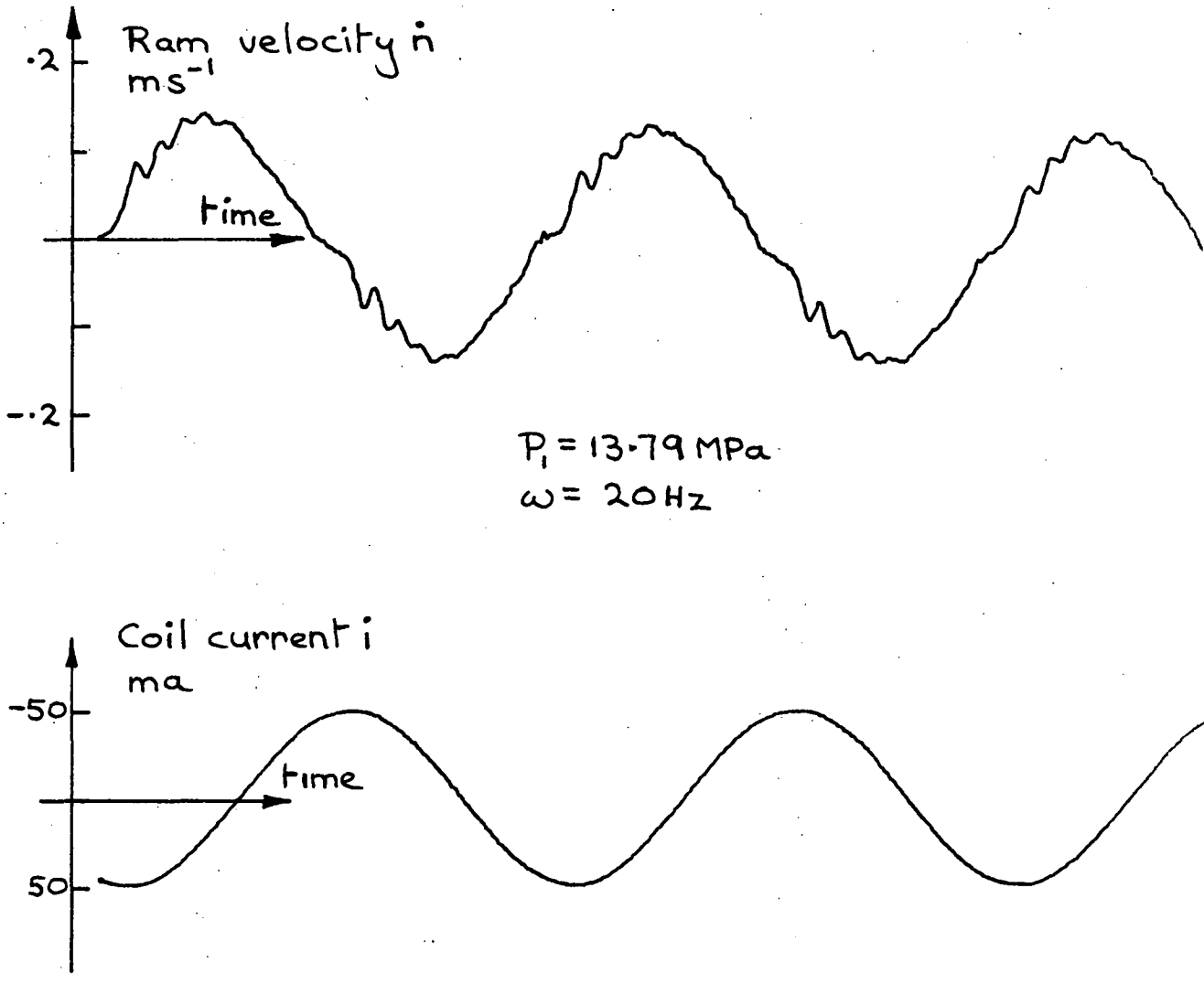

Servo-valve open-loop response Figure (A4-13)

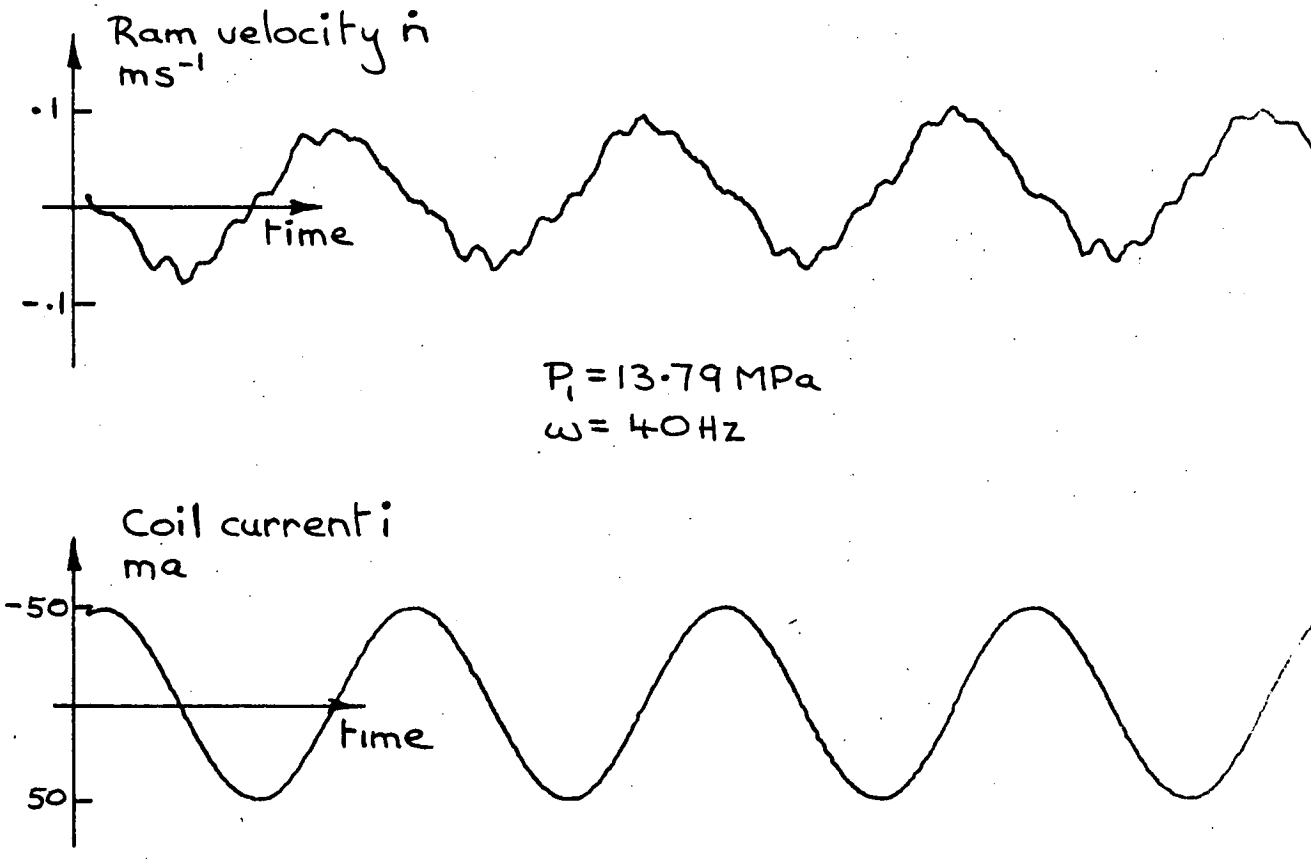

Servo-valve open-loop response Figure (A4-14)

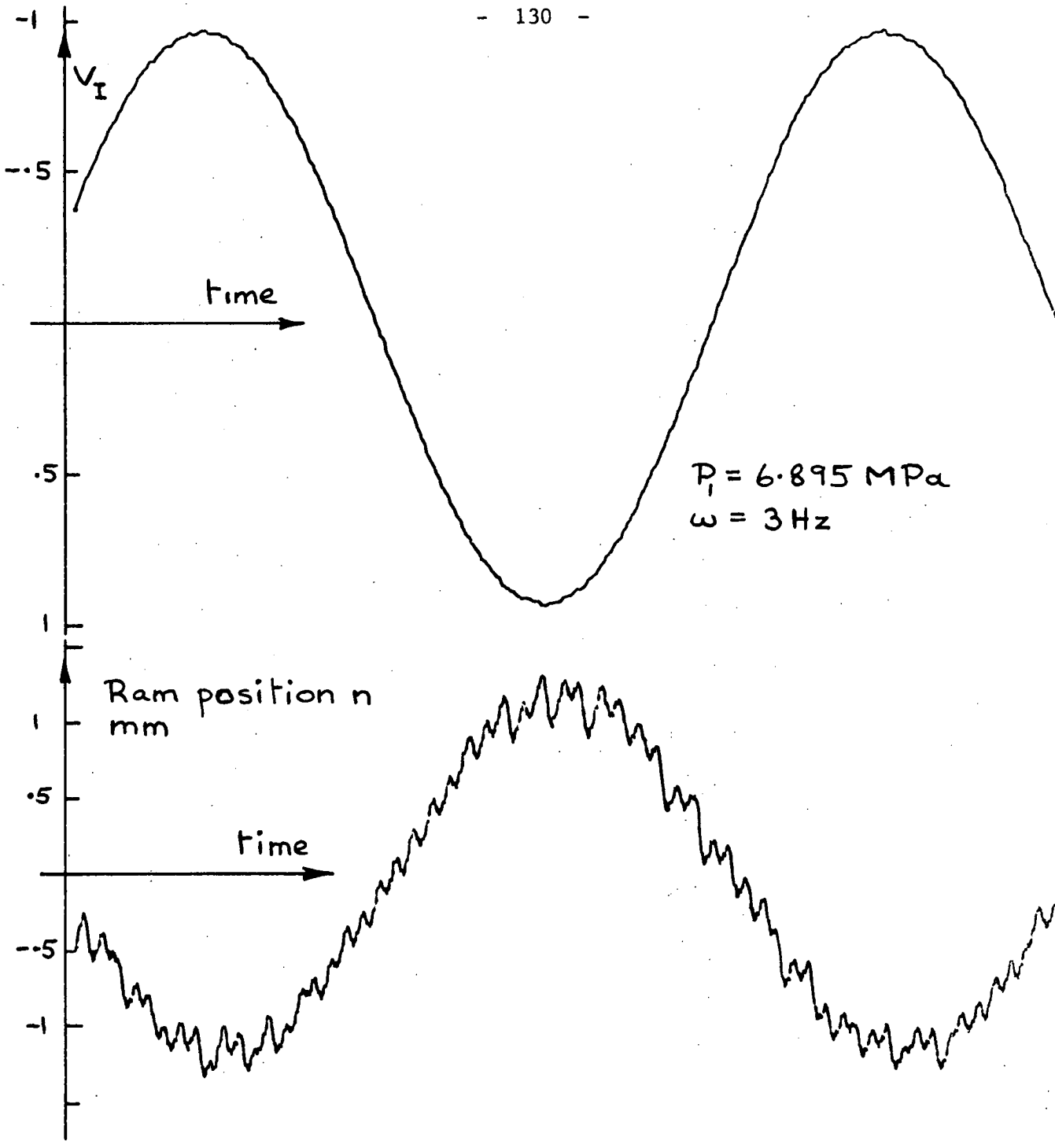

Servo-valve closed-loop response Figure(A4-15)

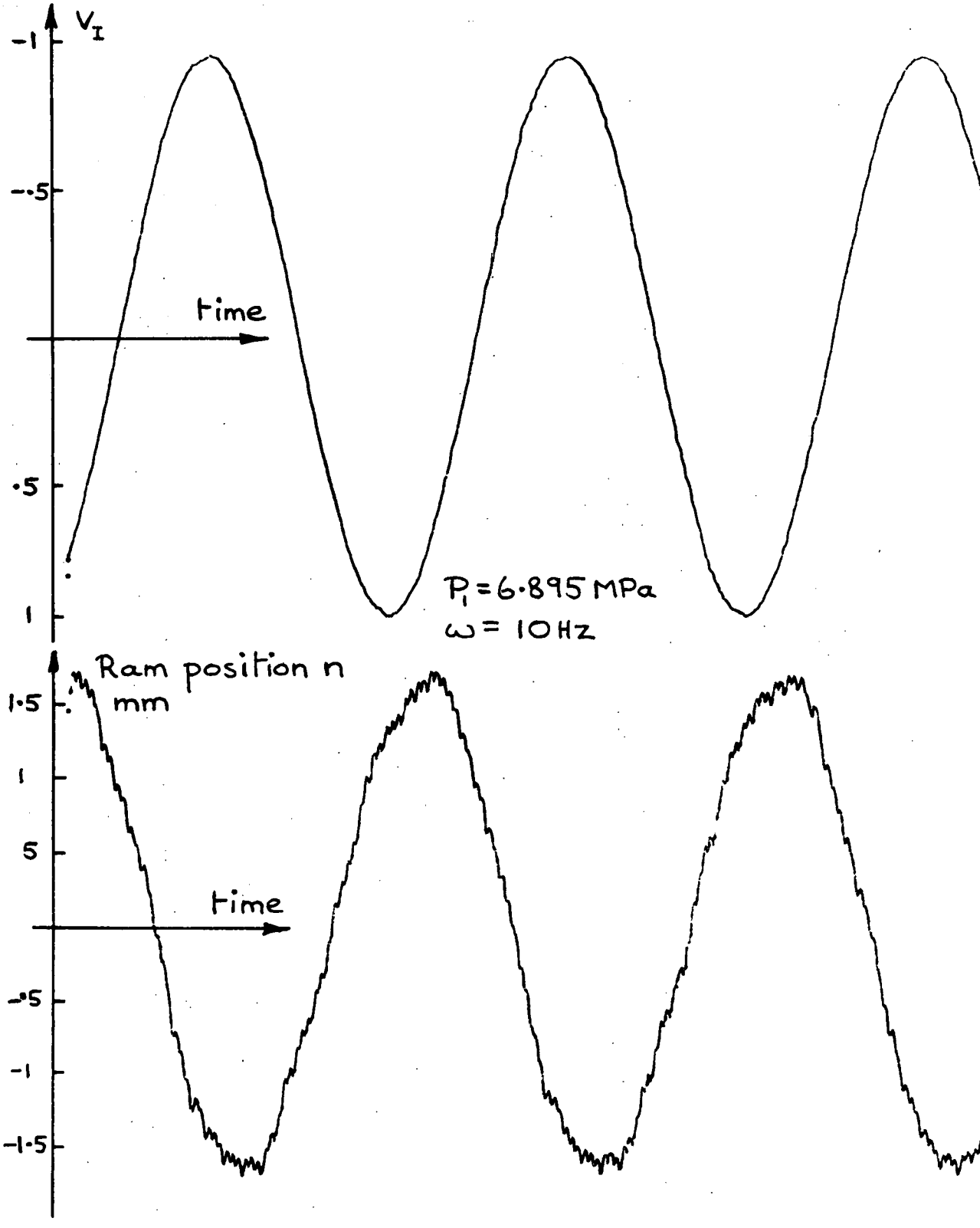

Servo-valve closed-loop response Figure(A4-16)

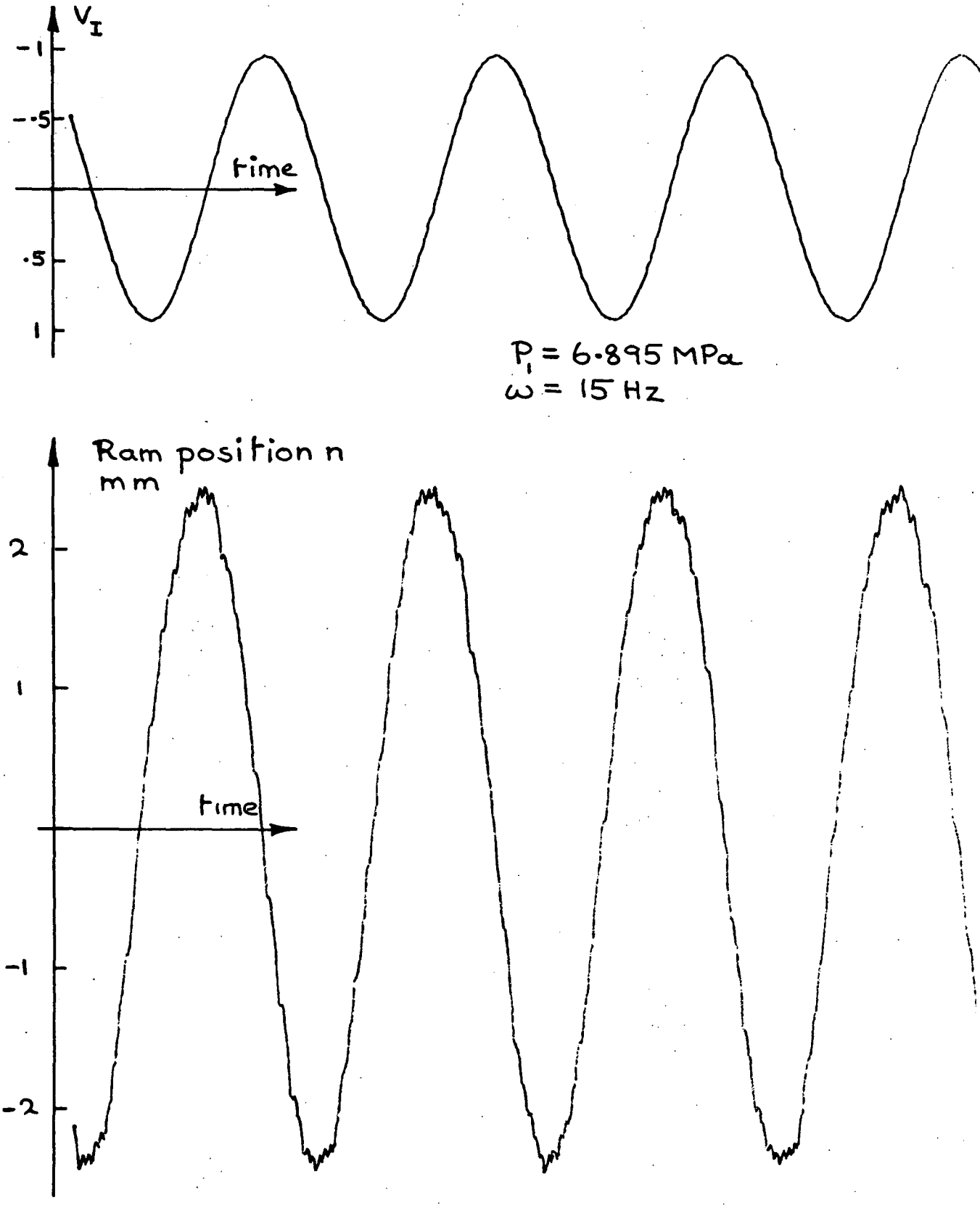

Servo-valve closed-loop response Figure (A4-17)

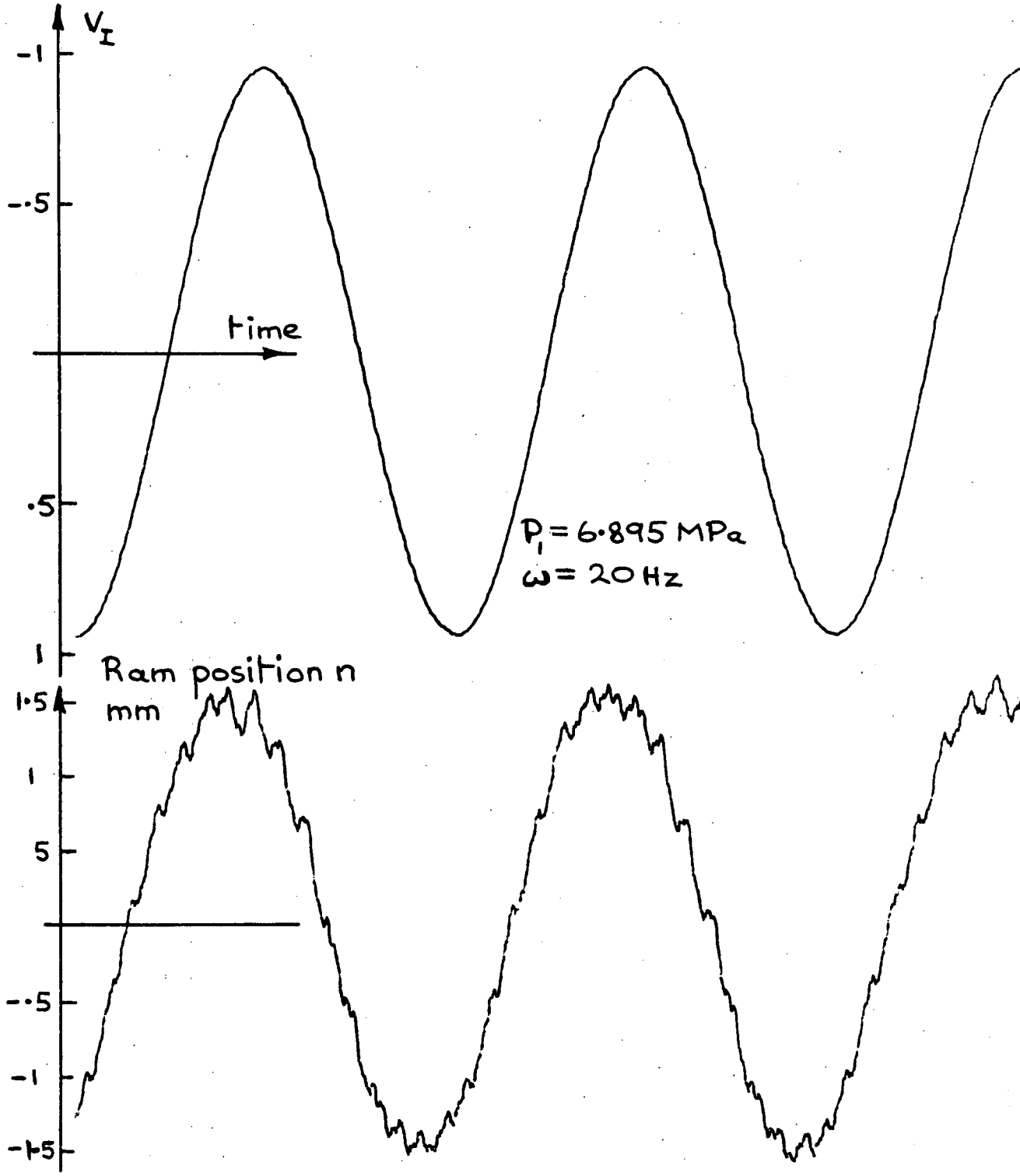

Servo-valve closed-loop response Figure(A4-18)

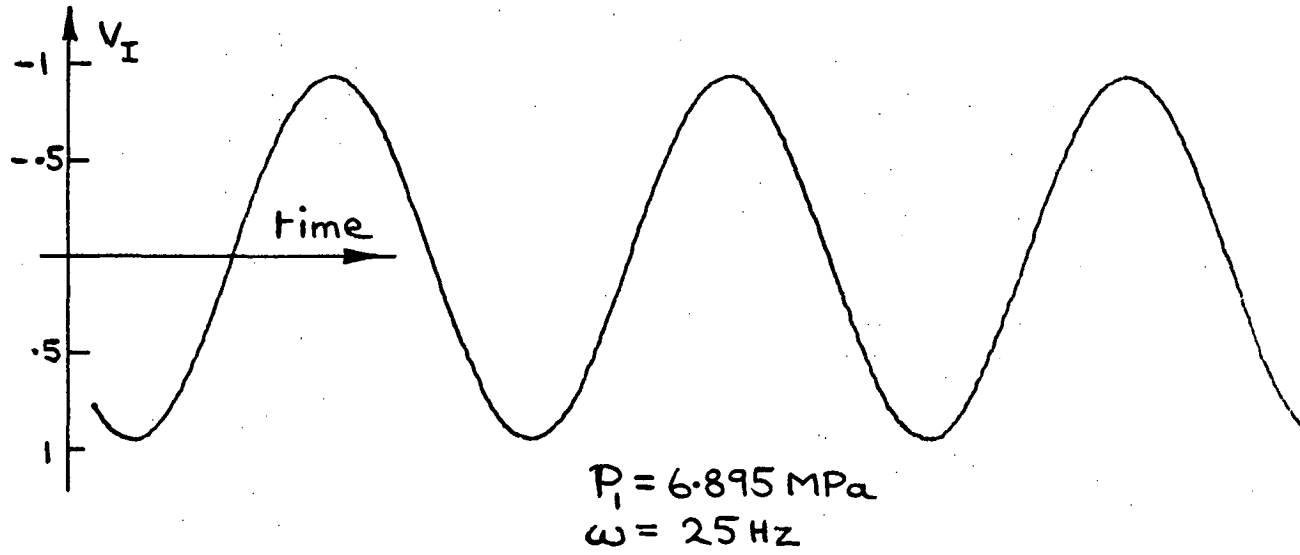

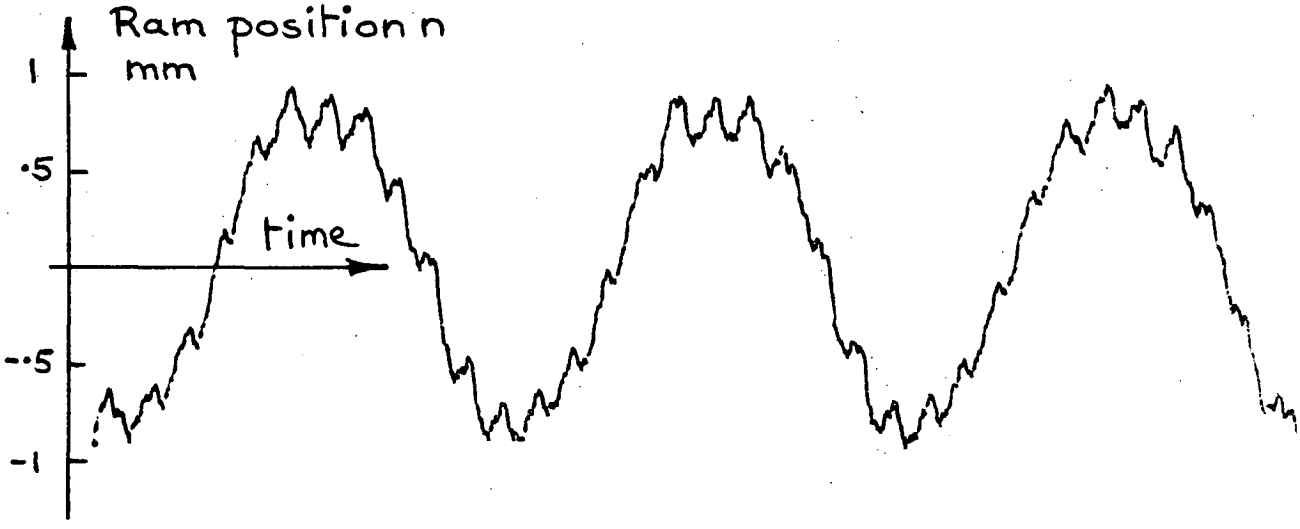

Servo-valve closed-loop response Figure (A4-19)

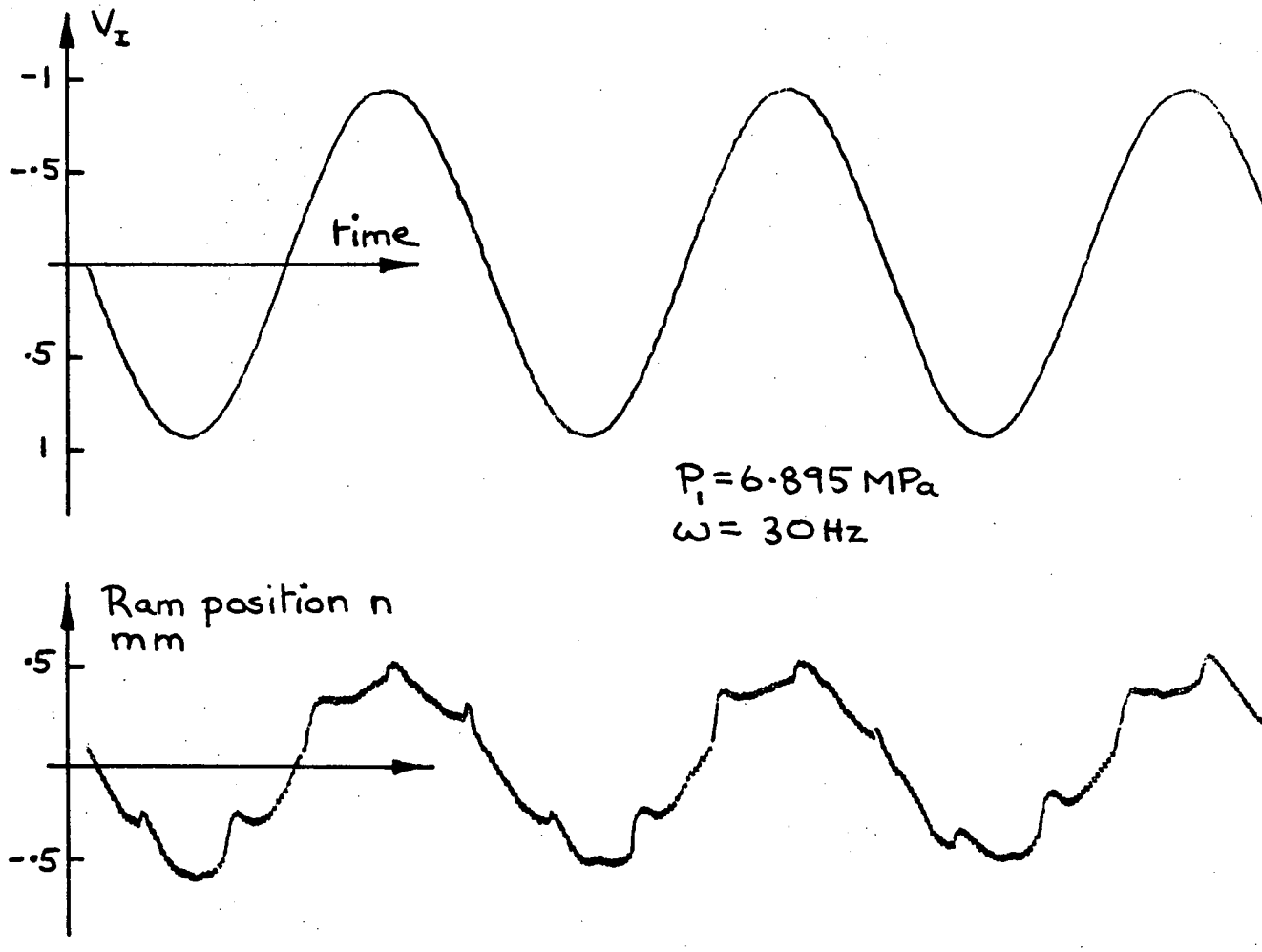

Servo-valve closed-loop response Figure(A4-20)

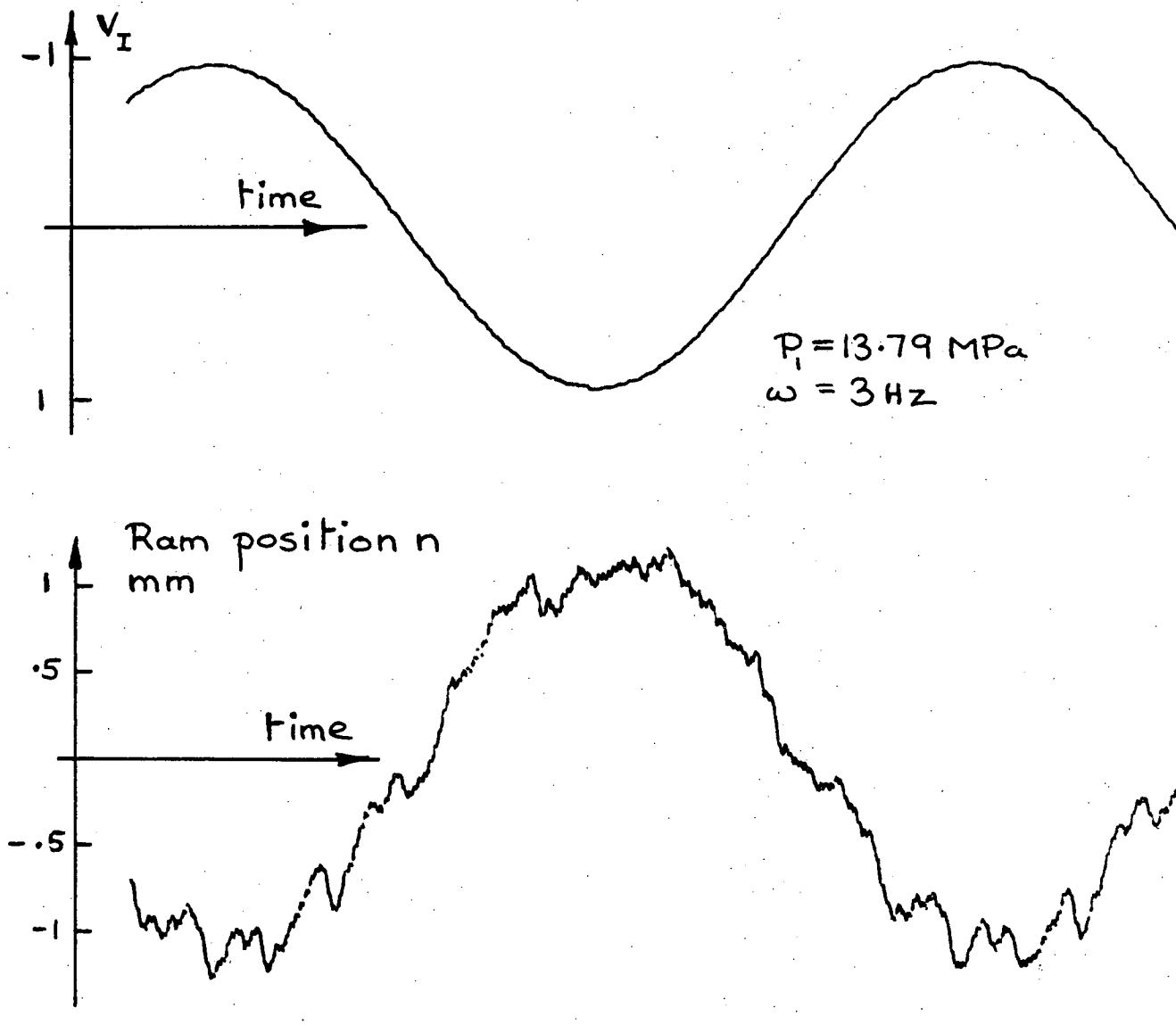

Servo-valve closed-loop response Figure(A4-21)

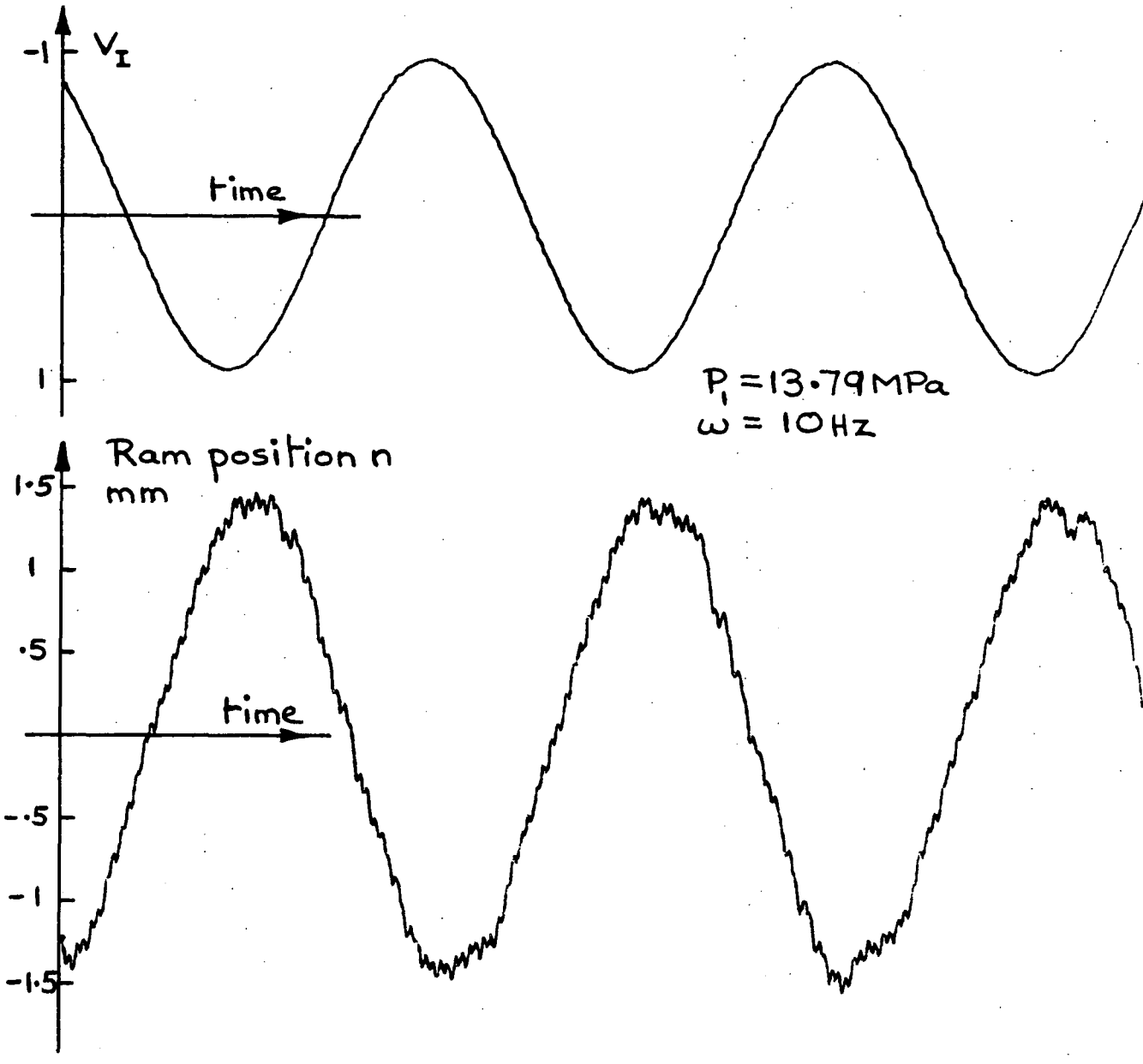

Servo-valve closed-loop response Figure (A4-22)

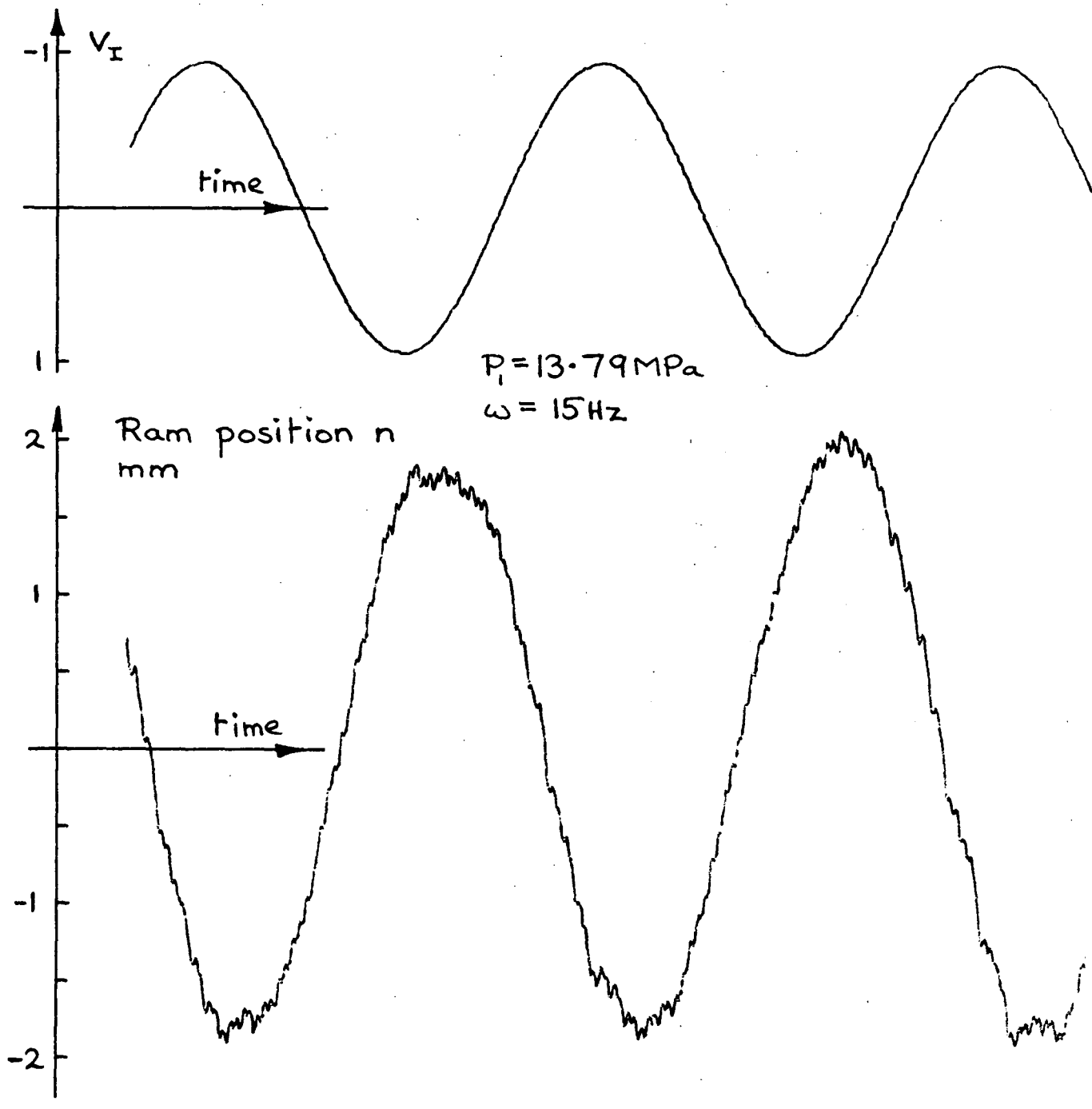

Servo-valve closed-loop response Figure (A4-23)

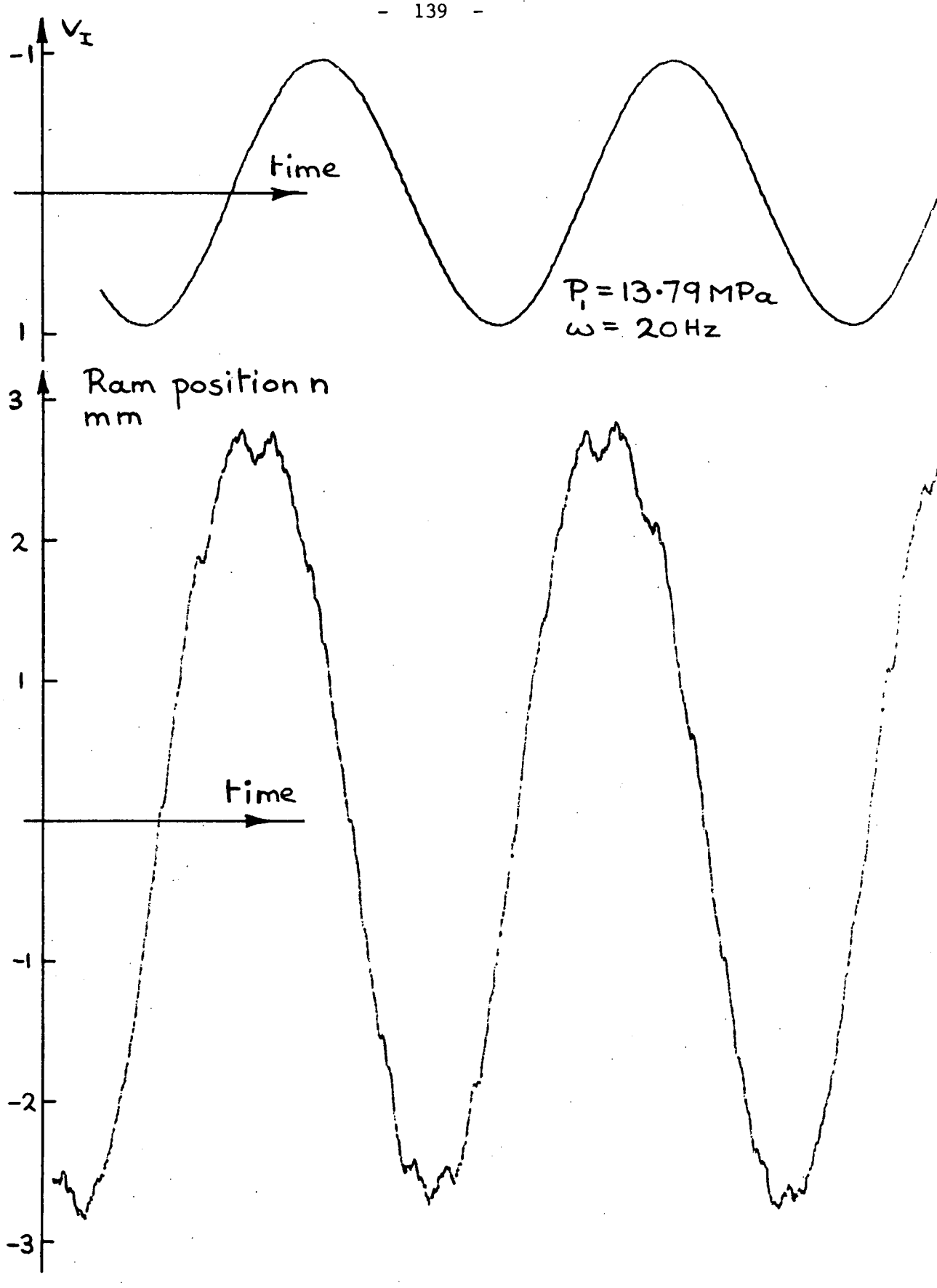

Servo-valve closed-loop response Figure (A4-24)

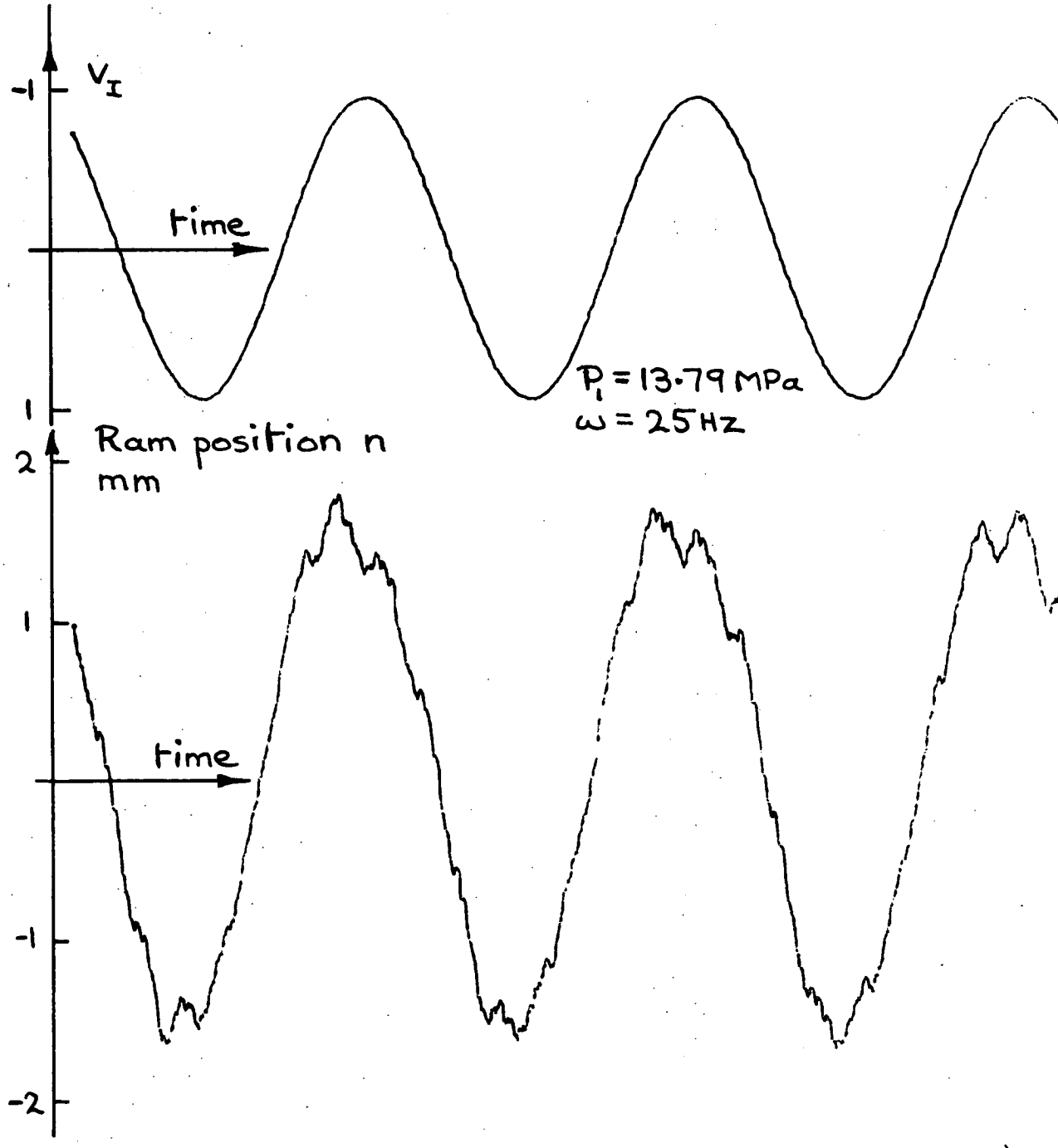

Servo-valve closed-loop response Figure(A4-25)

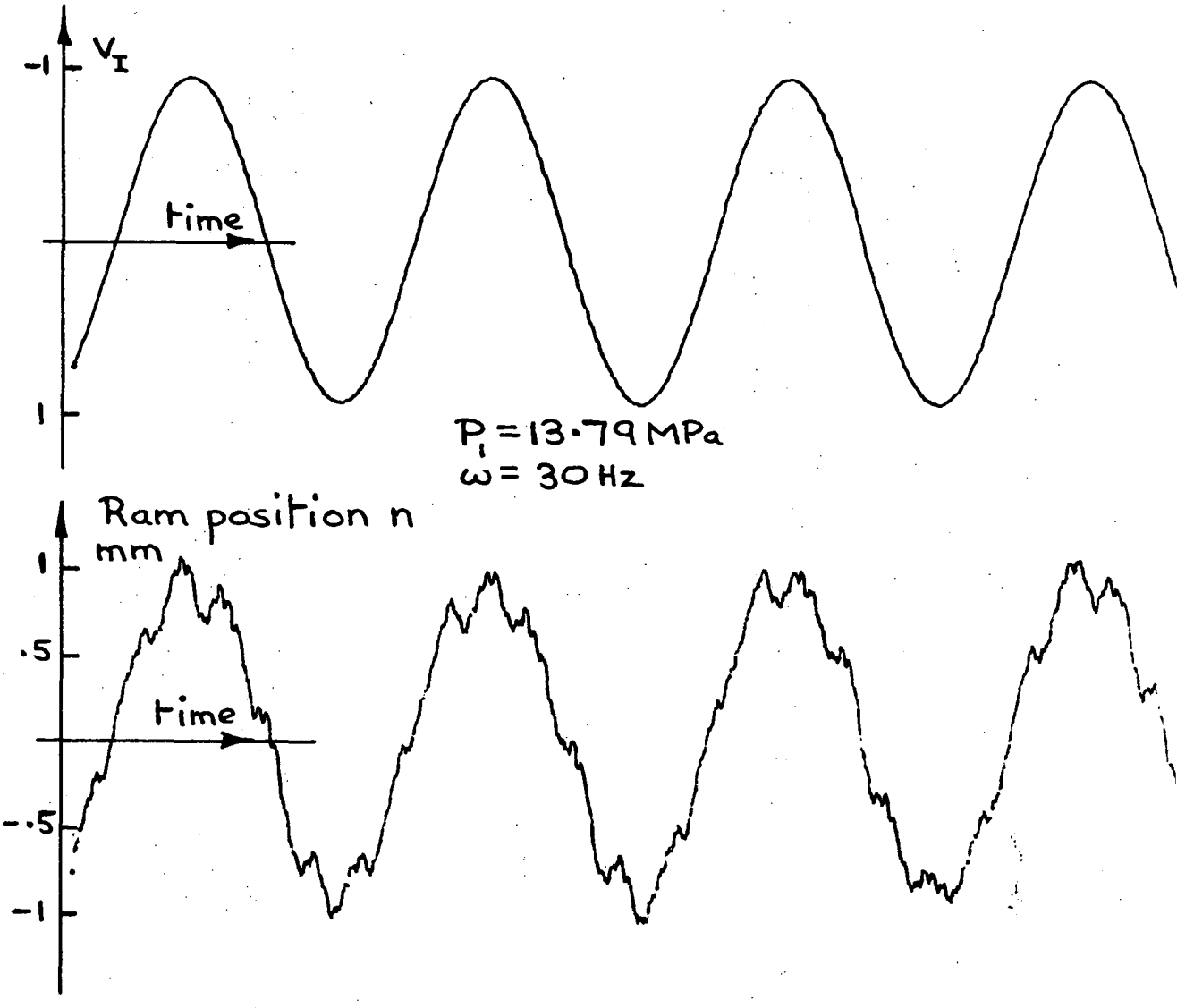

Servo-valve closed-loop response Figure(A4-26)

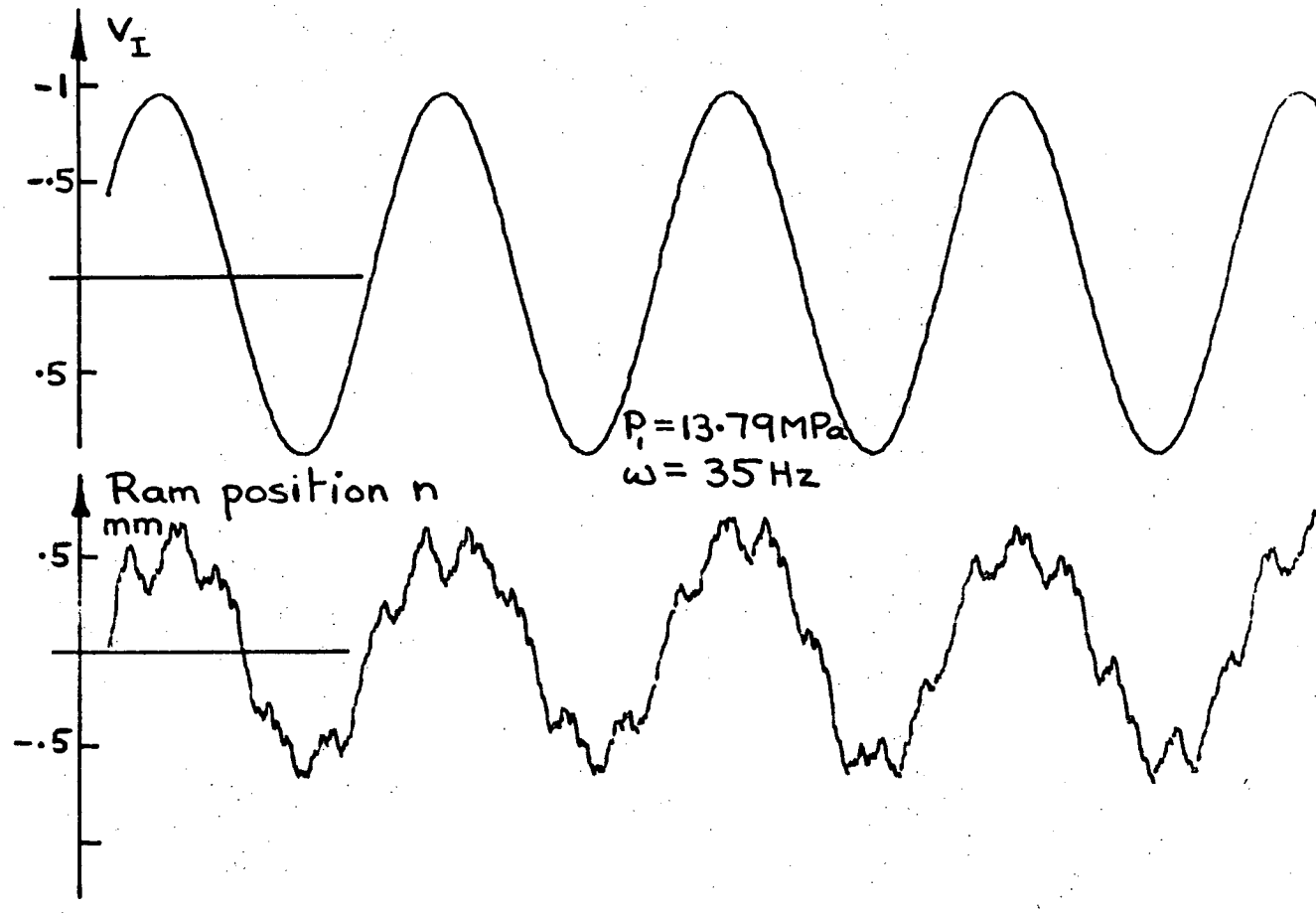

Servo-valve closed-loop response Figure(A4-27)

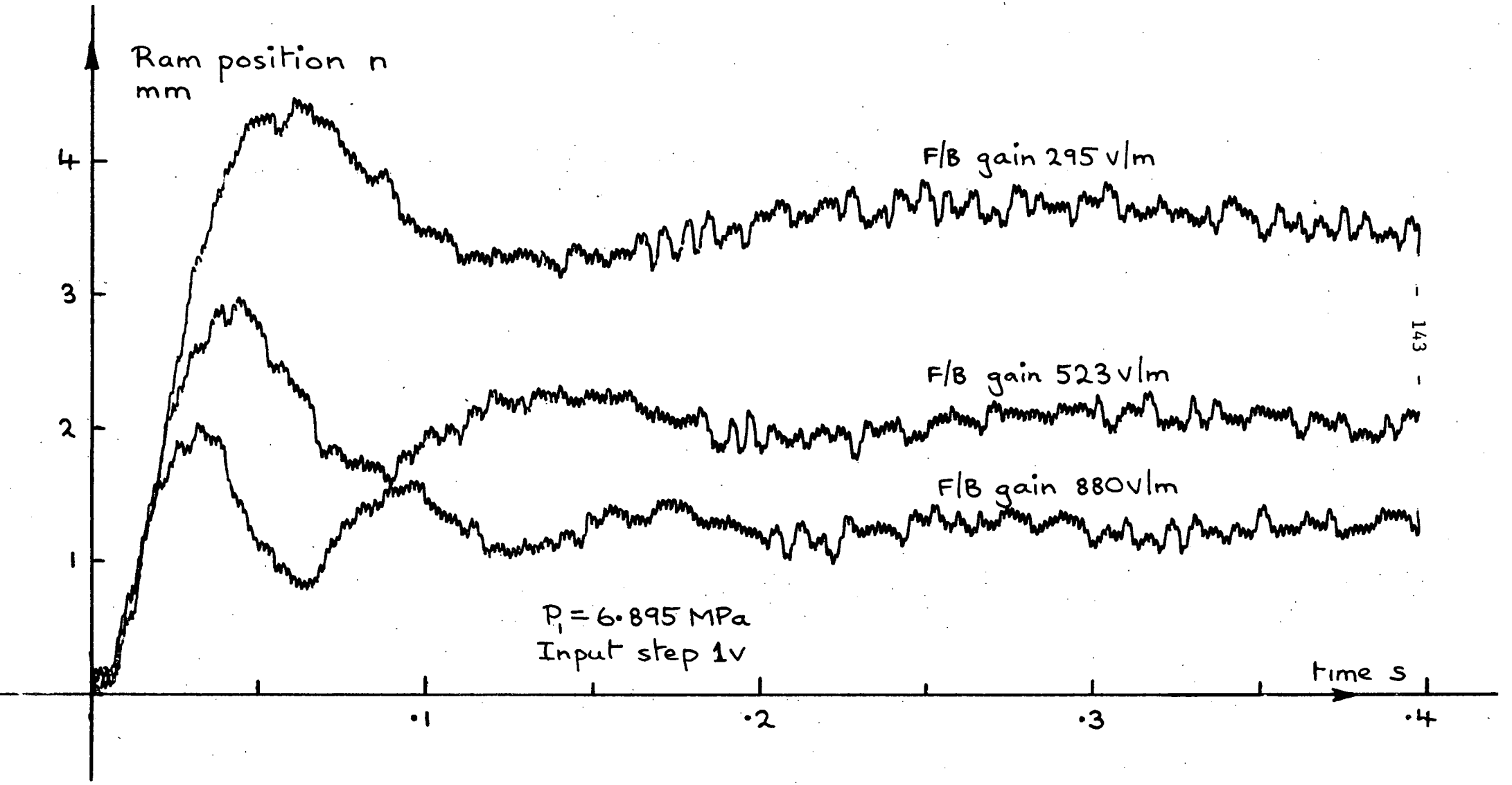

Servo-valve closed-loop step response Figure (A4-28)

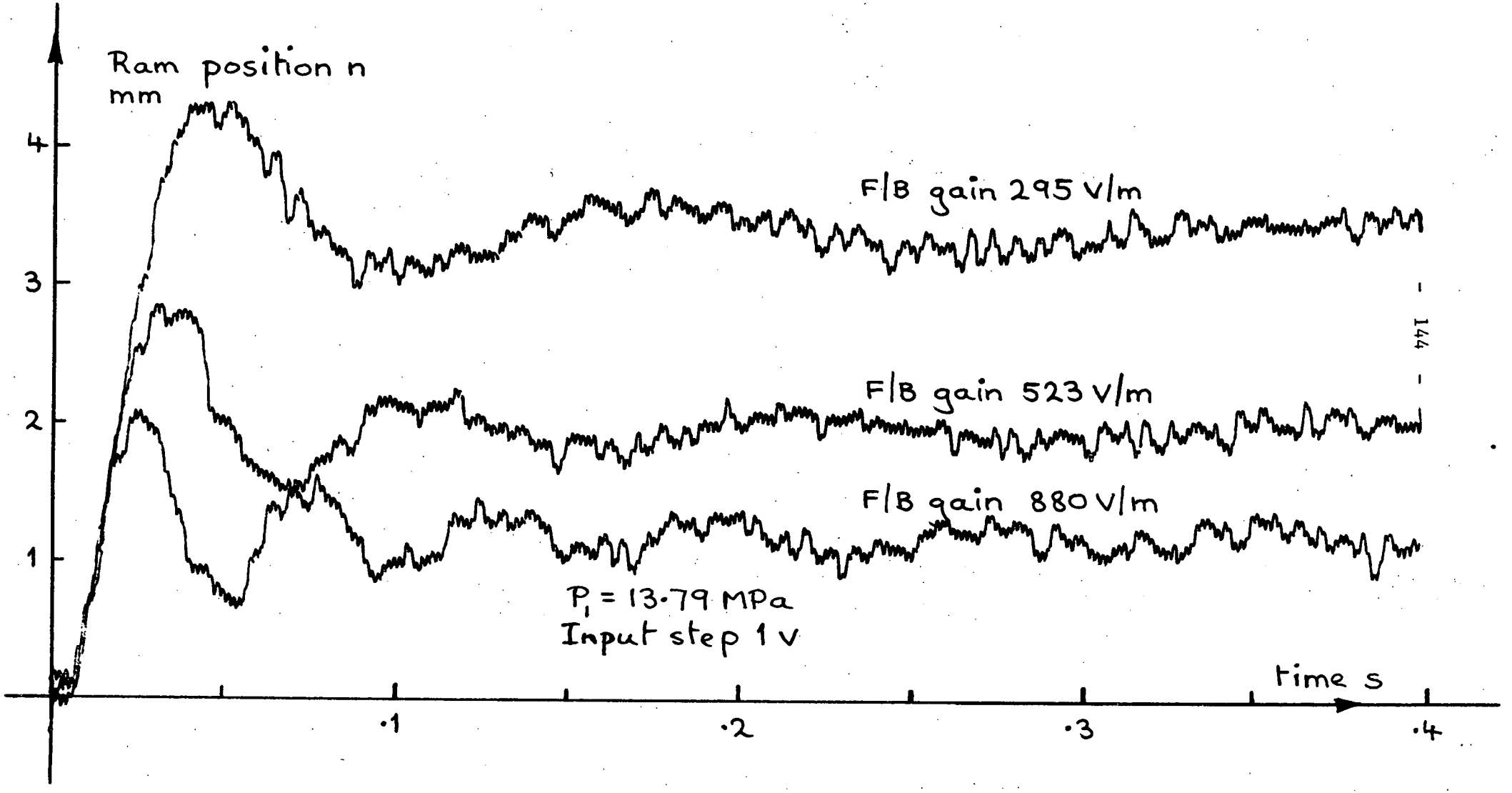

Servo-valve closed-loop step response Figure (A4-29)

PROGRAM 1 ~ FIDEL2.BA

```
10 PRINT"FIDEL2"
20 PRINT"DATA IN FOLL. ORDER, MATRICES BY ROWS"
30 PRINT"N=NO. OF EQNS, M=NO. OF INPUTS, T1=TIME INTVL, ";
32 PRINT"K1=NO.  OF T1 INTERVALS"
35 PRINT"N1=NO. OF TERMS SUMMED IN SUB1000, A MATRIX, "
40 PRINT"B MATRIX, X(0) MATRIX, U MATRIX (CONSTANTS)"
85 DIMA(7,7),A1(7,7),B(7,7),B1(7,7),C(7,7),D(7,7),X(7)
87 DIMX1(7),U(7)
90 PRINT"A MATRIX IS;"\READN,M,T1,K1,N1
100 FORI=1TON\FORJ=1TON\READA(I,J)\PRINTA(I,J),\NEXTJ
110 PRINT\NEXTI
115 PRINT"B MATRIX IS;"
120 FORI=1TON\FORJ=1TOM\READB(I,J)\PRINTB(I,J),\NEXTJ
130 PRINT\NEXTI
140 FORI=1TON\READX(I)\NEXTI
150 FORJ=1TOM\READU(J)\NEXTJ
160 PRINT"X(0) MATRIX IS;"
170 FORI=1TON\PRINTX(I)\NEXTI
180 PRINT"U MATRIX IS;"
190 FORI=1TOM\PRINTU(I)\NEXTI
210 T=T1\FORI=1TON\FORJ=1TON\B1(I,J)=A(I,J)\NEXTJ
220 NEXTI
230 FORI=1TON\C(I,I)=1\D(I,I)=T\NEXTI
240 PRINT"PRINTS 1 TO ";N1;"ON ENTERING THE E^AT LOOP"
245 L1=1\FORL=1TON1\PRINTL;
250 FORI=1TON\FORJ=1TON\C(I,J)=C(I,J)+B1(I,J)*T^L/L1
260 D(I,J)=D(I,J)+B1(I,J)*T^(L+1)/L1/(L+1)\NEXTJ
270 NEXTI
280 L1=L1*(L+1)\GOSUB1000\NEXTL
285 PRINT\PRINT"PHI MATRIX IS;"
290 FORI=1TON\FORJ=1TON\PRINTC(I,J),\NEXTJ
300 PRINT\NEXTI
330 FORI=1TON\FORJ=1TOM\FORD=1TON
340 A1(I,J)=D(I,D)*B(D,J)+A1(I,J)\NEXTD
350 NEXTJ
360 NEXTI
370 PRINT"DELL MATRIX IS;"
380 FORI=1TON\FORJ=1TOM\PRINTA1(I,J),\NEXTJ
382 PRINT\NEXTI
395 FORK=1TOK1\T=K*T1
400 FORI=1TON\FORJ=1TON\X1(I)=X1(I)+C(I,J)*X(J)\NEXTJ
410 NEXTI
420 FORI=1TON\X(I)=0\FORJ=1TON\X(I)=X(I)+A1(I,J)*U(J)\NEXTJ
430 X(I)=X(I)+X1(I)\X1(I)=0\NEXTI
434 PRINT"X MATRIX"\PRINTT,.001*T;"SEC"
440 FORJ=1TON\PRINTX(J),\IFJ>1THEN445\PRINTX(J)*.1\GOTO490
445 IFJ>2THEN450\PRINTX(J)/3\GOTO490
450 IFJ>3THEN455\PRINTX(J)/30\GOTO490
455 IFJ>4THEN460\PRINTX(J)/25\GOTO490
460 IFJ>5THEN465\PRINTX(J)*3\GOTO490
465 PRINTX(J)*.35
490 NEXTJ
500 NEXTK
510 STOP
1000 FORI=1TON\FORJ=1TON\FORD=1TON
1010 A1(I,J)=B1(I,D)*A(D,J)+A1(I,J)\NEXTD
1020 NEXTJ
1030 NEXTI
1040 FORI=1TON\FORJ=1TON\B1(I,J)=A1(I,J)\A1(I,J)=0\NEXTJ
1050 NEXTI
1060 RETURN\END
```

PROGRAM 2 ~ VALVE4W.BA

```
1000 PRINT"VALVE4W.BA BY K.CANEY"
1100 REMARK INPUT DATA
1110 A(1,2)=1\A(2,5)=1.777E-4\A(2,6)=-1.777E-5
1120 A(3,4)=1\A(4,3)=-7.668E6\A(4,4)=-3878\A(4,6)=8.926E-4
1130 A(5,0)=1.803E14\A(5,1)=-1.803E14\A(5,2)=-9.006E10
1140 A(5,5)=-5600\A(6,0)=-1.028E12\A(6,1)=1.079E12
1150 A(6,3)=-3.697E12\A(6,4)=-7.837E7\A(6,6)=-20.706
1160 N=6\T1=.00001
1165 A(6,0)=-3.184E12\A(5,0)=0
1180 PRINT"INPUT Z4(PRINT OUT INTERVAL).X(0)";\INPUTZ4,X(0)
1600 FORZ2=1TO2000\IFX1>0THEN1620
1610 A(6,1)=1.079E12\GOTO1650
1620 A(6,1)=-.976E12
1660 FORJ=1TO4\E(J)=0\F(J)=0\G(J)=0\H(J)=0
1665 K(J)=0\L(J)=0
1670 FORI=0TON\E(J)=T1*A(1,I)*X(I)+E(J)
1675 F(J)=T1*A(2,1)*X(I)+F(J)
1680 G(J)=T1*A(3,I)*X(I)+G(J)\H(J)=T1*A(4,I)*X(I)+H(J)
1685 K(J)=T1*A(5,I)*X(I)+K(J)\L(J)=T1*A(6,I)*X(I)+L(J)
1690 NEXTI
1700 IFJ=3THEN1760\IFJ=4THEN1770
1710 X(1)=X1+.5*E(J)\X(2)=X2+.5*F(J)\X(3)=X3+.5*G(J)
1712 X(4)=X4+.5*H(J)
1715 X(5)=X5+.5*K(J)\X(6)=X6+.5*L(J)
1720 GOTO1770
1760 X(1)=X1+E(J)\X(2)=X2+F(J)\X(3)=X3+G(J)\X(4)=X4+H(J)
1765 X(5)=X5+K(J)\X(6)=X6+L(J)
1770 NEXTJ
1780 X(1)=X1+(E(1)+2*E(2)+2*E(3)+E(4))/6\X1=X(1)
1790 X(2)=X2+(F(1)+2*F(2)+2*F(3)+F(4))/6\X2=X(2)
1800 X(3)=X3+(G(1)+2*G(2)+2*G(3)+G(4))/6\X3=X(3)
1810 X(4)=X4+(H(1)+2*H(2)+2*H(3)+H(4))/6\X4=X(4)
1812 X(5)=X5+(K(1)+2*K(2)+2*K(3)+K(4))/6\X5=X(5)
1813 X(6)=X6+(L(1)+2*L(2)+2*L(3)+L(4))/6\X6=X(6)
1815 Z3=Z3+1\IFZ3=Z4THEN1820\GOTO1840
1820 PRINTZ2*T1,X1,X3,X6,X(0)*A(6,0)\Z3=0
1840 NEXTZ2
3000 END
```

PROGRAM 3 ~ VALVE3W.BA

```
1000 PRINT"VALVE3W.BA BY K.CANEY"
1100 REMARK INPUT DATA
1110 A(1,2)=1\A(2,5)=3.554E-4\A(2,6)=-1.955E-4
1120 A(3,4)=1\A(4,3)=-7.668E6\A(4,4)=-3878\A(4,6)=8.926E-4
1130 A(5,0)=2.256E13\A(5,1)=-2.256E13\A(5,2)=-2.254E10
1140 A(5,5)=-3962\A(6,2)=5.134E8\A(6,3)=-3.6965E12
1150 A(6,4)=-7.837E7\A(6,6)=-20.706
1160 N=6\T1=.00001
1165 A(6,0)=-3.184E12\A(5,0)=0
1170 PRINT"INPUT Z4,X(0)";\INPUTZ4,X(0)
1630 FORZ2=1TO2000\IFSGN(0-X1)<0THEN1650
1640 A(6,1)=1.0789E12\GOTO1655
1650 A(6,1)=5.1308E10
1660 FORJ=1TO4\E(J)=0\F(J)=0\G(J)=0\H(J)=0
1665 K(J)=0\L(J)=0
1670 FORI=0TON\E(J)=T1*A(1,I)*X(I)+E(J)
1675 F(J)=T1*A(2,1)*X(I)+F(J)
1680 G(J)=T1*A(3,I)*X(I)+G(J)\H(J)=T1*A(4,I)*X(I)+H(J)
1685 K(J)=T1*A(5,I)*X(I)+K(J)\L(J)=T1*A(6,I)*X(I)+L(J)
1690 NEXTI
1700 IFJ=3THEN1760\IFJ=4THEN1770
1710 X(1)=X1+.5*E(J)\X(2)=X2+.5*F(J)\X(3)=X3+.5*G(J)
1712 X(4)=X4+H(J)*.5
1715 X(5)=X5+.5*K(J)\X(6)=X6+.5*L(J)
1720 GOTO1770
1760 X(1)=X1+E(J)\X(2)=X2+F(J)\X(3)=X3+G(J)\X(4)=X4+H(J)
1765 X(5)=X5+K(J)\X(6)=X6+L(J)
1770 NEXTJ
1780 X(1)=X1+(E(1)+2*E(2)+2*E(3)+E(4))/6\X1=X(1)
1790 X(2)=X2+(F(1)+2*F(2)+2*F(3)+F(4))/6\X2=X(2)
1800 X(3)=X3+(G(1)+2*G(2)+2*G(3)+G(4))/6\X3=X(3)
1810 X(4)=X4+(H(1)+2*H(2)+2*H(3)+H(4))/6\X4=X(4)
1812 X(5)=X5+(K(1)+2*K(2)+2*K(3)+K(4))/6\X5=X(5)
1813 X(6)=X6+(L(1)+2*L(2)+2*L(3)+L(4))/6\X6=X(6)
1815 Z3=Z3+1\IFZ3=Z4THEN1820\GOTO1830
1820 PRINTZ2*T1,X1,X3,X6,X(0)*A(6,0)\Z3=0
1830 NEXTZ2
3000 END
```

PROGRAM 4 ~ SERVO1.BA - PAGE1

```
1010 PRINT"SERVO1. BA"
1015 REMARK SPOOL STATIC CONDITION
1020 READ P1, C1, C2, C4, K1, K2, K4
1022 DATA144000, . 722, . 932, . 82, . 02, . 03, . 0625
1025 PRINT"INPUT PRESSURE P1"; \INPUTP\P1=P1*P
1030 P=ATN(1)*4\K1=(C1*P/4*(K1/12)^2*1. 098)^2
1040 K2=(C2*P/4*(K2/12)^2*1. 098)^2\K4=(C4*P/4*(K4/12)^2*1. 098)^2
1050 Q=(. 4836*P1-933. 39)/(. 4836/K4+1/K1+1/K2-. 5164/K1)
1060 P4=Q/K4+1\P2=P1-Q/K1\P3=P2-Q/K2\K1=. 5*SQR(K1/(P1-P2))
1070 K2=. 5*SQR(K2/(P2-P3))\K4=. 5*SQR(K4/(P4-1))
1075 K1=K1/1691\K2=K2/1691\K4=K4/1691\Q=SQR(Q)*. 3048^3
1085 P1=47. 88*P1\P2=47. 88*P2\P4=47. 88*P4\P3=47. 88*P3
1090 PRINT"Q, P1, P2, P3, P4←←M^3/S←←N/M^2"\PRINTQ, P1, P2, P3, P4
1100 X=Q/(13. 45E-6*(P3-P4)^. 475)\X=X^(1/. 7)
1105 REMARK SPOOL PERTN. CONSTANTS
1110 K3=13. 45E-6*(P3-P4)^. 475*. 7*X^(-. 3)*1. 41
1120 K5=13. 45E-6*X^. 7*. 475*(P3-P4)^(-. 525)
1130 PRINT"X="; X\PRINT"K1 TOK5"\PRINTK1, K2, K3, K4, K5
1140 REMARK FLAPPER VALVE PERTN. CONSTANTS
1150 K6=. 15056*X^. 4*1. 4*(P3-P4)^(. 95)
1160 K7=. 15056*X^1. 4*. 95*(P3-P4)^(-. 05)+1. 0261E-6
1195 PRINT"K6, 7, 8", K6, K7, K8
1220 DIMA(10, 14), A1(4, 4), B(4, 4), B1(4, 4), C(4, 4), D(4, 4), X(5)
1223 READN, M\DATA4, 1\PRINT"INP. T1, Z4"; \INPUTT1, Z4
1225 REMARK SCALING CONSTANTS\Y5=1\Y6=1\Y7=1\Y8=1
1230 FORI=0TON\FORJ=0TON\A(I, J)=0\NEXTJ
1236 NEXTI
1260 REMARK SET UP EQUATION MATRIX
1270 A(1, 1)=1\A(1, 5)=K1\A(2, 2)=-1\A(2, 5)=K2\A(2, 6)=-K2
1280 A(3, 4)=-1\A(3, 7)=K4\A(4, 3)=-1\A(4, 6)=K5\A(1, 13)=-K1
1290 A(4, 7)=-K5\A(4, 8)=K3\A(5, 1)=1\A(5, 2)=-1\A(5, 11)=1. 02E-4
1300 A(6, 2)=-1\A(6, 3)=1\A(6, 11)=1. 979E-4\A(5, 5)=-K8
1305 A(7, 3)=1\A(7, 4)=-1\A(7, 11)=. 959E-4
1310 A(8, 6)=K7\A(8, 7)=-K7\A(8, 8)=40818+K6\A(8, 9)=40512
1315 A(8, 14)=-42. 5\A(9, 6)=K7\A(9, 7)=-K7\A(9, 8)=K6-50091
1320 A(9, 12)=4528\A(9, 14)=-42. 5\A(10, 5)=1. 02E-4
1322 A(8, 12)=6382\A(9, 9)=4528\A(10, 6)=-1. 979E-4
1325 A(10, 7)=. 959E-4\A(10, 9)=1700\A(10, 10)=. 0705\A(10, 11)=2. 19
1350 GOTO1490
1470 FORI=1TO10\FORJ=1TO14\PRINTA(I, J), \NEXTJ
1480 PRINT\NEXTI
1490 Y1=9\Y2=10\Y3=14\Y4=Y1+1
1495 REMARK REDUCE EQUATION MATRIX
1500 FORJ=1TOY1\B=0
1505 FORI=1TOY2\IFA(I, J)=0THEN1540\C=A(I, J)
1510 FORK=JTOY3\A(I, K)=A(I, K)/C\NEXTK
1520 B=B+1\H(B)=I
1540 NEXTI
1550 FORI=1TOB\R1=B+1-I\R=H(R1)\S=H(1)
1560 FORK=JTOY3\A(R, K)=A(R, K)-A(S, K)\NEXTK
1570 NEXTI
1571 IFJ<40THEN1573\FORI=JTO10\FORK=J+1TO14\PRINTA(I, K), \NEXTK
1572 PRINT\NEXTI
1573 NEXTJ
```

SERVO1.BA PAGE 2

```
1574 REMARK COMP. RATE OF CHANGE OF ORIFICE AREA
1575 PRINT"INPUT I(MAX), W";\INPUTX1, W\A2=. 01\A3=0\A4=A(10, 12)
1577 U=7. 5E-5\N9=2*U/. 00635\GOSUB1584\B0=A1/U
1580 FORJ=1TO4\FORI=1TO10\N9=I*A2+A3\IFN9>2*U/. 00635THEN1582
1581 A1=B0\GOTO1586
1582 GOSUB1584\A1=A1/(N9*. 00635-U)\GOTO1586
1584 A1=ATN(SQR(4*N9-4*N9^2)/(1-2*N9))
1585 A1=. 00635^2/4*(A1-2*(1-2*N9)*SQR(N9-N9^2))\RETURN
1586 A(10, 12)=A4+(1. 25*P1*A1+1700)*A(10, 10)/. 0705
1587 X0=-A(10, 12)*N9*. 00635/A(10, 14)\IFX0>X1THEN1588\NEXTI
1588 A3=N9-A2\A2=. 1*A2\PRINT"J=";J, X0, A3\NEXTJ
1589 X1=0\X(0)=X0
1590 FORI=Y4TOY2\FORJ=Y4TOY3\PRINTA(I, J), \NEXTJ
1600 PRINT\NEXTI
1602 REMARK SET UP A MATRIX
1610 A(1, 1)=-A(10, 11)/A(10, 10)
1612 A(1, 2)=-A(10, 12)/A(10, 10)*Y6/Y5
1614 A(2, 1)=Y5/Y6\A(3, 2)=2*. 05133E13*SQR(P1)*A1*Y6/Y7/1. 313
1620 A(3, 4)=-1. 2668E10/1. 313*Y8/Y7
1625 A(4, 4)=-733/2. 2\A(4, 3)=. 6334E-3/2. 2*Y7/Y8
1630 A(1, 0)=-A(10, 14)/A(10, 10)/Y5
1635 FORI=1TON\FORJ=0TON\PRINTA(I, J), \NEXTJ
1636 IFN=4THEN1637\PRINT
1637 NEXTI
1638 FORI=0TON\PRINTX(I)\NEXTI
1639 REMARK RUNGE KUTTA ROUTINE
1640 FORZ2=1TO2000\T=Z2*T1
1660 FORJ=1TO4\E(J)=0\F(J)=0\G(J)=0\H(J)=0
1670 FORI=0TON\E(J)=T1*A(1, I)*X(I)+E(J)\F(J)=T1*A(2, I)*X(I)+F(J)
1680 G(J)=T1*A(3, I)*X(I)+G(J)\H(J)=T1*A(4, I)*X(I)+H(J)
1690 NEXTI
1700 IFJ=3THEN1760\IFJ=4THEN1770
1710 X(1)=X1+. 5*E(J)\X(2)=X2+. 5*F(J)\X(3)=X3+. 5*G(J)
1715 X(4)=X4+. 5*H(J)\T=Z2*T1+. 5*T1
1720 GOTO1770
1760 X(1)=X1+E(J)\X(2)=X2+F(J)\X(3)=X3+G(J)\X(4)=X4+H(J)
1765 T=Z2*T1+T1
1770 NEXTJ
1780 X(1)=X1+(E(1)+2*E(2)+2*E(3)+E(4))/6\X1=X(1)
1790 X(2)=X2+(F(1)+2*F(2)+2*F(3)+F(4))/6\X2=X(2)
1800 X(3)=X3+(G(1)+2*G(2)+2*G(3)+G(4))/6\X3=X(3)
1810 X(4)=X4+(H(1)+2*H(2)+2*H(3)+H(4))/6\X4=X(4)
1815 Z3=Z3+1\IFZ3=Z4THEN1820\GOTO1830
1820 PRINTINT(Z2*T1*1000+. 5)/1000, X1*Y5, X2*Y6, X3*Y7, X4*Y8\Z3=0
1830 NEXTZ2
1840 END
```

PROGRAM 5 ~ SERVO8.BA ~ PAGE 1

```
1010 PRINT"SERVO8. BA"
1015 REMARK SPOOL STATIC CONDITION
1020 READ P1, C1, C2, C4, K1, K2, K4
1022 DATA144000, . 722, . 932, . 82, . 02, . 03, . 0625
1025 PRINT"INPUT PRESSURE P1"; \INPUTP\P1=P1*P
1030 P=ATN(1)*4\K1=(C1*P/4*(K1/12)^2*1. 098)^2
1040 K2=(C2*P/4*(K2/12)^2*1. 098)^2\K4=(C4*P/4*(K4/12)^2*1. 098)^2
1050 Q=(. 4836*P1-933. 39)/(. 4836/K4+1/K1+1/K2-. 5164/K1)
1060 P4=Q/K4+1\P2=P1-Q/K1\P3=P2-Q/K2\K1=. 5*SQR(K1/(P1-P2))
1070 K2=. 5*SQR(K2/(P2-P3))\K4=. 5*SQR(K4/(P4-1))
1075 K1=K1/1691\K2=K2/1691\K4=K4/1691\Q=SQR(Q)*. 3048^3
1085 P1=47. 88*P1\P2=47. 88*P2\P4=47. 88*P4\P3=47. 88*P3
1090 PRINT"Q, P1, P2, P3, P4←←M^3/S←←N/M^2"\PRINTQ, P1, P2, P3, P4
1100 X=Q/(13. 45E-6*(P3-P4)^. 475)\X=X^(1/. 7)
1105 REMARK SPOOL PERTN. CONSTANTS
1110 K3=13. 45E-6*(P3-P4)^. 475*. 7*X^(-. 3)*1. 41
1120 K5=13. 45E-6*X^. 7*. 475*(P3-P4)^(-. 525)
1130 PRINT"X="; X\PRINT"K1 TOK5"\PRINTK1, K2, K3, K4, K5
1140 REMARK FLAPPER VALVE PERTN. CONSTANTS
1150 K6=. 15056*X^. 4*1. 4*(P3-P4)^(. 95)
1160 K7=. 15056*X^1. 4*. 95*(P3-P4)^(-. 05)+1. 0261E-6
1195 PRINT"K6, 7, 8", K6, K7, K8
1220 DIMA(10, 14), A1(4, 4), B(4, 4), B1(4, 4), C(4, 4), D(4, 4), X(5)
1223 READN, M\DATA4, 1\PRINT"INP. T1, Z4"; \INPUTT1, Z4
1225 REMARK SCALING CONSTANTS\Y5=. 03\Y6=. 001\Y7=115200\Y8=. 3
1228 Y5=1\Y6=1\Y7=1\Y8=1
1230 FORI=0TON\FORJ=0TON\A(I, J)=0\NEXTJ
1236 NEXTI
1260 REMARK SET UP EQUATION MATRIX
1270 A(1, 1)=1\A(1, 5)=K1\A(2, 2)=-1\A(2, 5)=K2\A(2, 6)=-K2
1280 A(3, 4)=-1\A(3, 7)=K4\A(4, 3)=-1\A(4, 6)=K5
1290 A(4, 7)=-K5\A(4, 8)=K3\A(5, 1)=1\A(5, 2)=-1\A(5, 11)=1. 02E-4
1300 A(6, 2)=-1\A(6, 3)=1\A(6, 11)=1. 979E-4
1305 A(7, 3)=1\A(7, 4)=-1\A(7, 11)=. 959E-4
1310 A(8, 6)=K7\A(8, 7)=-K7\A(8, 8)=40818+K6\A(8, 9)=40512
1315 A(8, 14)=-42. 5\A(9, 6)=K7\A(9, 7)=-K7\A(9, 8)=K6-50091
1320 A(9, 12)=4528\A(9, 14)=-42. 5\A(10, 5)=1. 02E-4
1325 A(10, 7)=. 959E-4\A(10, 9)=1700\A(10, 10)=. 0705\A(10, 11)=2. 19
1340 A(10, 12)=1700\A(8, 12)=6382\A(9, 9)=4528\A(10, 6)=-1. 979E-4
1350 GOTO1490
1470 FORI=1TO10\FORJ=1TO14\PRINTA(I, J), \NEXTJ
1480 PRINT\NEXTI
1490 Y1=9\Y2=10\Y3=14\Y4=Y1+1
```

```
1495 REMARK REDUCE EQUATION MATRIX
1500 FORJ=1TOY1\B=0
1505 FORI=1TOY2\IFA(I,J)=0THEN1540\C=A(I,J)
1510 FORK=JTOY3\A(I,K)=A(I,K)/C\NEXTK
1520 B=B+1\H(B)=I
1540 NEXTI
1550 FORI=1TOB\R1=B+1-I\R=H(R1)\S=H(1)
1560 FORK=JTOY3\A(R,K)=A(R,K)-A(S,K)\NEXTK
1570 NEXTI
1572 NEXTJ
1575 PRINT"INPUT I(MAX),W";\INPUTX0,W\A4=A(10,12)\X(0)=X0
1590 FORI=Y4TOY2\FORJ=Y4TOY3\PRINTA(I,J),\NEXTJ
1600 PRINT\NEXTI
1602 REMARK SET UP A MATRIX
1610 A(1,1)=-A(10,11)/A(10,10)
1612 A(1,2)=-A(10,12)/A(10,10)*Y6/Y5
1614 A(2,1)=Y5/Y6\A(3,2)=0
1620 A(3,4)=-1.2668E10/1.313*Y8/Y7
1625 A(4,4)=-733/2.2\A(4,3)=.6334E-3/2.2*Y7/Y8
1630 A(1,0)=-A(10,14)/A(10,10)/Y5
1635 FORI=1TON\FORJ=0TON\PRINTA(I,J),\NEXTJ
1636 IFN=4THEN1637\PRINT
1637 NEXTI
1638 FORI=0TON\PRINTX(I)\NEXTI
1639 REMARK RUNGE KUTTA ROUTINE
1640 U=7.5E-5\N9=2*U/.00635\GOSUB2000\B0=A1
1650 FORZ2=1TO9000\T=Z2*T1
1660 FORJ=1TO4\F(J)=0\H(J)=0\P2=P1-(X(3)*Y7)\GOSUB1970
1665 E(J)=X0*COS(W*T)*A(1,0)*T1-1.25*A*P2/Y5/.0705*T1
1667 G(J)=T1*.10266E13*SQR(P2)*A/Y7/1.313
1670 FORI=1TON\E(J)=T1*A(1,I)*X(I)+E(J)\F(J)=T1*A(2,I)*X(I)+F(J)
1680 G(J)=T1*A(3,I)*X(I)+G(J)\H(J)=T1*A(4,I)*X(I)+H(J)
1690 NEXTI
1700 IFJ=3THEN1760\IFJ=4THEN1770
1710 X(1)=X1+.5*E(J)\X(2)=X2+.5*F(J)\X(3)=X3+.5*G(J)
1715 X(4)=X4+.5*H(J)\T=Z2*T1+.5*T1
1720 GOTO1770
1760 X(1)=X1+E(J)\X(2)=X2+F(J)\X(3)=X3+G(J)\X(4)=X4+H(J)
1765 T=Z2*T1+T1
1770 NEXTJ
1780 X(1)=X1+(E(1)+2*E(2)+2*E(3)+E(4))/6\X1=X(1)
1790 X(2)=X2+(F(1)+2*F(2)+2*F(3)+F(4))/6\X2=X(2)
1800 X(3)=X3+(G(1)+2*G(2)+2*G(3)+G(4))/6\X3=X(3)
1810 X(4)=X4+(H(1)+2*H(2)+2*H(3)+H(4))/6\X4=X(4)
1815 Z3=Z3+1\IFZ3=Z4THEN1820\GOTO1825
1820 PRINTINT(Z2*T1*1000+.5)/1000,X1*Y5,X2*Y6,X3*Y7,X4*Y8\Z3=0
1825 NEXTZ2
1850 STOP
1970 N9=(ABS(X(2)*Y6)+U)/.00635\IFN9>2*U/.00635THEN2000
1980 A=B0/U*X(2)*Y6\RETURN
2000 A1=ATN(SQR(4*N9-4*N9^2)/(1-2*N9))
2010 A1=.00635^2/4*(A1-2*(1-2*N9)*SQR(N9-N9^2))
2020 A=A1*SGN(X(2))\RETURN
2500 END
```

/NAME SAMP3.PA PAGE1

PROGRAM 6

```
                /NAME SAMP3.PA
          6530  ADCL=6530
          6531  ADLM=6531
          6133  CLAB=6133
          6536  ADLE=6536
          6132  CLOE=6132
          6534  ADSK=6534
          6533  ADRB=6533
          6130  CLZE=6130
          6535  ADSE=6535
          6166  LOADY=6166
          6165  LOADX=6165
          6167  LOADZ=6167
          6153  LOADI=6153
          6162  MUTSW=6162
          6163  UP=6163
          6164  DOWN=6164
          6161  FLAG=6161
          0001  *1        /SAMPLE AT EQUAL INTERVALS
00001     5402            JMP I   2
00002     1200            SERVE               /GO TO SERVICE ROUTINE
          0020  *20       /VARIABLES
00020     0000  FLDCHK,    0
00021     0000  SAVEAC,    0
00022     0000  NEXT,      0
00023     0000  BUFFER,    0
00024     0000  NUMSAM,    0
00025     0000  LCOUNT,    0
00026     0000  NO,        0
00027     0000  COUNT,     0
00030     0000  XCRD,      0
00031     0000  ZEROI,     0
          0050  *50       /CONSTANTS
00050     0002  XINC,      2
00051     7737  STEPI,     -41       /.05AMP STEP
00052     7242  DISCNT,    -536
00053     6001  MCOUNT,    -1777
00054     7762  PCOUNT,    -16
00055     7716  FINE,      7716      /OVERFLOW EVERY 50 COUNTS
00056     1740  ENABLE,    1740
00057     0600  K600,      600
00060     0020  K20,       20
00061     0002  MXCHN2,    2
00062     0003  MXCHN3,    3
00063     0004  MXCHN4,    4
00064     0005  MXCHN5,    5
00065     0000  BUFSTRT,   0
00066     4000  K4000,     4000
00067     2000  K2000,     2000
          0200  *200
00200     7300  SAMPLE,    CLL       CLA
00201     7000              NOP
00202     7000              NOP
00203     6530              ADCL
00204     1053              TAD       MCOUNT
```

/NAME SAMP3.PA PAGE2

```
00205  3024          DCA     NUMSAM
00206  1065          TAD     BUFSTRT
00207  3010          DCA     10        /STORE CHN2 AT F2.A0+
00210  1065          TAD     BUFSTRT
00211  1067          TAD     K2000
00212  3011          DCA     11        /STORE CHN3 AT F2.A2000+
00213  1065          TAD     BUFSTRT
00214  1066          TAD     K4000
00215  3012          DCA     12        /STORE CHN4 AT F2.A4000+
00216  1065          TAD     BUFSTRT
00217  1066          TAD     K4000
00220  1067          TAD     K2000
00221  3013          DCA     13        /STORE CHN5 AT F2.A6000+
00222  7000          NOP
00223  1057          TAD     K600
00224  6536          ADLE              /EXT.STRT.TIMING ERROR
00225  1055          TAD     FINE      /INTERRUPT
00226  6133          CLAB              /SET FINE FREQY.CONTROL
00227  1056          TAD     ENABLE    /SET MODE 01,COURSE FQY
00230  6132          CLOE              /EXT.PERIPH.ENABLE,CLA
00231  7402          HLT
00232  6001          ION               /FOR TIMING ERROR
00233  7200          CLA
00234  6167          LOADZ             /+10V TO INITSE.INTEGR
00235  7200          CLA
00236  7604          LAS               /READ INIT.CURRENT
00237  3031          DCA     ZEROI     /FROM SR&DEPOSIT
00240  1031          TAD     ZEROI
00241  6153          LOADI             /LOAD INITIAL CURRENT
00242  5235          JMP     .-5       /INITIAL CURRENT LOOP
00243  7000  GONOW,   NOP               /TYPE 'G' TO START
00244  6001          ION
00245  7200          CLA
00246  1060          TAD     K20
00247  6130          CLZE              /START CLOCK
00250  1056          TAD     ENABLE    /SET NEGATIVE VOLTAGE TO
00251  6167          LOADZ             /ENABLE THE INTEGRATOR
00252  1031          TAD     ZEROI
00253  1051          TAD     STEPI
00254  6153          LOADI             /STEP THE CURRENT
00255  6221          CDF     20
00256  1061  NXTPT,  TAD     MXCHN2
00257  6531          ADLM              /SELECT MXCHN2
00260  6534          ADSK
00261  5260          JMP     .-1
00262  6533          ADRB              /READ CHN2
00263  3410          DCA I   10
00264  1062          TAD     MXCHN3
00265  6531          ADLM              /SELECT CHN3
00266  6534          ADSK
00267  5266          JMP     .-1
00270  6533          ADRB              /READ CHN3
00271  3411          DCA I   11
00272  1063          TAD     MXCHN4    /SELECT CHN4
00273  6531          ADLM
```

```
/NAME SAMP3.PA          PAGE3

00274   6534            ADSK
00275   5274            JMP     .-1
00276   6533            ADRB            /READ CHN4
00277   3412            DCA I   12
00300   1064            TAD     MXCHN5  /SELECT CHN5
00301   6531            ADLM
00302   6534            ADSK
00303   5302            JMP     .-1
00304   6533            ADRB            /READ CHN5
00305   3413            DCA I   13
00306   7000            NOP
00307   2024            ISZ     NUMSAM  /ALL SAMPLES TAKEN?
00310   5256            JMP     NXTPT   /NO←GET NEXT SAMPLE
00311   1060            TAD     K20     /YES←STOP SAMPLING
00312   6132            CLOE            /STOP CLOCK
00313   6002            IOF
00314   6201            CDF             /ALL SAMPLES OBTAINED
00315   7300            CLL     CLA
00316   7000            NOP
00317   7000            NOP
00320   7402            HLT
00321   7000            NOP
00322   4777'           JMS     CRO     /CRO DISPLAY ROUTINE
00323   7000            NOP
00324   7000            NOP
00325   7402            HLT
00326   7000            NOP
00327   4776'           JMS     DISXY   /OUTPUT TO PLOTTER
00330   7000            NOP
00331   7000            NOP
00332   7402            HLT
00333   7000            NOP
00334   7000            NOP
00335   7402            HLT
00376   0604
00377   0400
        0400    *400    /CRO DISPLAY ROUTINE
00400   0000    CRO,    0       /CRO DISPLAY ROUTINE
00401   7200            CLA
00402   3020            DCA     FLDCHK  /SET FIELDCHECK=0
00403   6221            CDF     20
00404   7200            CLA
00405   3022            DCA     NEXT    /NEXT=0
00406   1065            TAD     BUFSTRT
00407   3023            DCA     BUFFER
00410   6162            MUTSW
00411   6001            ION
00412   7200    START,  CLA
00413   1023            TAD     BUFFER
00414   3010            DCA     10
00415   1052            TAD     DISCNT
00416   3024            DCA     NUMSAM
00417   3030            DCA     XCRD    /SET XCRD=ZERO
00420   1410    DISPLAY,TAD I   10      /GET Y
00421   7040            CMA
```

/NAME SAMP3.PA PAGE4

```
00422  1377          TAD     (1000   /ZERO AT MIDDLE SCREEN
00423  6166          LOADY
00424  1030          TAD     XCRD    /GET X
00425  7040          CMA
00426  1376          TAD     (2000
00427  6165          LOADX
00430  1022          TAD     NEXT
00431  7440          SZA
00432  5242          JMP     AGAIN
00433  7200          CLA
00434  1030          TAD     XCRD
00435  1050          TAD     XINC
00436  3030          DCA     XCRD    /INCREMENT X
00437  2024          ISZ     NUMSAM  /END OF ONE PASS?
00440  5220          JMP     DISPLAY /NO
00441  5212          JMP     START   /YES LOOP AGAIN
00442  7200  AGAIN,  CLA
00443  3022          DCA     NEXT    /RESTORE NEXT TO 0
00444  6221          CDF     20      /SET DATA FIELD
00445  1023          TAD     BUFFER  /GET BUFFER START
00446  1376          TAD     (2000   /ALTER BUFFER START TO
00447  3023          DCA     BUFFER  /NEXT SECTION
00450  1020          TAD     FLDCHK
00451  7001          IAC
00452  3020          DCA     FLDCHK
00453  1020          TAD     FLDCHK
00454  1375          TAD     (-4     /AC >=0 IF FIELD 3
00455  7710          SPA     CLA     /CH. TO FIELD3
00456  5212          JMP     START   /NO<-STILL FIELD 2
00457  6231          CDF     30      /YES<-FIELD 3
00460  7200          CLA
00461  1020          TAD FLDCHK
00462  1374          TAD     (-10
00463  7440          SZA             /END DISPLAY
00464  5212          JMP     START   /DISLAY NEXT SECTION F3
00465  6002  INTRPT, IOF
00466  6162          MUTSW
00467  7300          CLA     CLL
00470  5600          JMP I   CRO
00574  7770
00575  7774
00576  2000
00577  1000
       0600  *600    /PLOTTER ROUTINE
       4200  WAIT=JMS WAITR
00600  0000  WAITR,  0               /WAIT ROUTINE
00601  6161          FLAG
00602  5201          JMP     .-1
00603  5600          JMP I   WAITR
00604  0000  DISXY,  0               /PLOTTER ROUTINE
00605  6163          UP              /PEN UP
00606  7200          CLA
00607  1065          TAD     BUFSTRT
00610  3023          DCA     BUFFER
00611  3020          DCA     FLDCHK
```

/NAME SAMP3. PA PAGE5

```
00612  7000          NOP
00613  7000          NOP
00614  6221          CDF     20
00615  7000          NOP
00616  7000          NOP
00617  7200  NEXSEC,  CLA
00620  7000          NOP
00621  7402          HLT             /SET MANUAL PEN UP
00622  7201          CLA     IAC     /START AT POINT2
00623  1023          TAD     BUFFER
00624  3010          DCA     10
00625  1410          TAD I   10
00626  7040          CMA
00627  1377          TAD     (1000
00630  6166          LOADY           /FIRST Y VALUE LOADED
00631  3030          DCA     XCRD    /SET XCRD TO ZERO
00632  7040          CMA
00633  1376          TAD     (2000
00634  6165          LOADX
00635  4200          WAIT            /FOR PEN UP
00636  7402          HLT
00637  6164          DOWN            /PEN DOWN
00640  7200          CLA             /SET AC=0
00641  1052          TAD     DISCNT  /DISP. SECCTN. SIZE
00642  3024          DCA     NUMSAM  /X COUNTER SET
00643  4200  LOOP,    WAIT            /FOR LAST MOVEMENT
00644  1410          TAD I   10      /GET Y
00645  7040          CMA
00646  1377          TAD     (1000
00647  6166          LOADY
00650  1030          TAD     XCRD
00651  1050          TAD     XINC
00652  3030          DCA     XCRD    /INCREMENT X
00653  1030          TAD     XCRD    /AND GET IT
00654  7040          CMA
00655  1376          TAD     (2000
00656  6165          LOADX
00657  2024          ISZ     NUMSAM  /COUNT POINTS
00660  5243          JMP     LOOP
00661  4200          WAIT            /FOR LAST MOVEMENT
00662  6163          UP              /PEN UP
00663  4200          WAIT
00664  7000          NOP
00665  7200          CLA
00666  2020          ISZ     FLDCHK
00667  1020          TAD     FLDCHK
00670  1375          TAD     (-4
00671  7710          SPA     CLA
00672  7410          SKP
00673  6231          CDF     30
00674  7200          CLA
00675  1023          TAD     BUFFER
00676  1376          TAD     (2000
00677  3023          DCA     BUFFER
00700  1020          TAD     FLDCHK

00701  1374          TAD     (-10
00702  7440          SZA
00703  5217          JMP     NEXSEC
00704  5604          JMP I   DISXY
```

/NAME SAMP3.PA PAGE 6

```
00774   7770
00775   7774
00776   2000
00777   1000
        1200    *1200     /SERVICE ROUTINE
01200   3021    SERVE,    DCA       SAVEAC   /SAVE AC
01201   6031              KSF                /SKIP ON KEYBOARD FLAG
01202   7410              SKP
01203   5216              JMP       KB       /KEYBOARD INTERRUPT
01204   6535              ADSE               /TIMING ERROR?
01205   5242              JMP       RETURN   /NO
01206   6530              ADCL               /TIMING ERROR ROUTINE
01207   7000              NOP
01210   7000              NOP
01211   7000              NOP
01212   7000              NOP
01213   7000              NOP
01214   7000              NOP
01215   7402              HLT
01216   6032    KB,       KCC                /CLEAR KEYBOARD FLAG
01217   6036              KRB                /READ INTO AC
01220   7000              NOP
01221   7000              NOP
01222   1377              TAD       (-307    /ASCII FOR 'G'
01223   7440              SZA                /IS IT 'G' FOR GONOW?
01224   7410              SKP                /NO←TRY 'N'
01225   5776'             JMP       GONOW    /IS 'G' START A RUN
01226   1375              TAD       (-7      /IS IT 'N'?
01227   7440              SZA
01230   7410              SKP                /NOT 'N'
01231   5236              JMP       NEXDIS   /YES 'N'-DISP. NXT. SECTN
01232   1374              TAD       (-5      /IS IS 'S'?
01233   7440              SZA                /YES STOP CRO DISPLAY
01234   5242              JMP       RETURN   /NO-KEY NOT 'S,G,N'
01235   5773'             JMP       INTRPT   /YES STOP CRO DISPLAY
01236   7201    NEXDIS,   CLA       IAC      /AC=1
01237   3022              DCA       NEXT     /NEXT=1-CRO DISP. TRIG.
01240   7000              NOP
01241   7410              SKP
01242   6007    RETURN,   CAF
01243   7200              CLA
01244   7000              NOP
01245   7000              NOP
01246   7000              NOP
01247   1021              TAD       SAVEAC   /GET AC
01250   6001              ION
01251   5400              JMP I     0
01373   0465
01374   7773
01375   7771
01376   0243
01377   7471
```

$